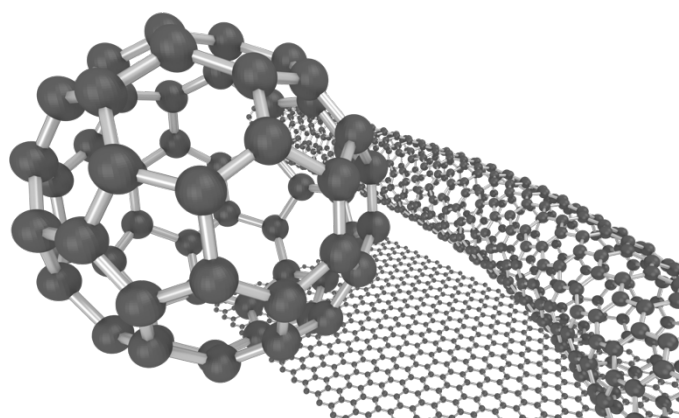


第 60 回記念 フラーレン・ナノチューブ・グラフェン 総合シンポジウム

The 60th Anniversary Fullerenes–Nanotubes–Graphene
General Symposium



講演要旨集 Abstracts

2021 年 3 月 1 日(月) ~ 3 日(水)
オンラインバーチャルシンポジウム
Online Virtual Symposium

主催 フラーレン・ナノチューブ・グラフェン学会
The Fullerenes, Nanotubes and Graphene Research Society

共催 ・ **後援**

日本化学会
名古屋大学 CIRFE

The Chemical Society of Japan
Center for Integrated Research of Future Electronics,
Nagoya University

協賛

日本物理学会
応用物理学会
高分子学会
電気化学会

The Physical Society of Japan
The Japan Society of Applied Physics
The Society of Polymer Science, Japan
The Electrochemical Society of Japan

GEMINI 超高安定性 干渉計

入力光から生成した2つのレプリカ間の時間遅延を制御。
比類のない安定性・精度・再現性を提供する究極の干渉計

主な特長

- 高感度、高スループット
- 高速スキャン(<1秒)
- コンパクト、低コスト
- 約1アト秒の安定性(2つのレプリカ間の光)
- スキャン範囲選択可能
- 高い振動耐性

アプリケーション

- 干渉計
- パルス対生成

検出パス内での導入例

- 時間/周波数 分解蛍光寿命測定
- ポンププローブ分光
- コヒーレントラマン分光

励起パス内での導入例

- 蛍光励起/発光マッピング
- 単一分子分析



Abstract of The 60th Anniversaries Fullerenes-Nanotubes-Graphene General Symposium

Sponsored by : The Fullerenes, Nanotubes and Graphene Research Society

Co-Sponsored by : The Chemical Society of Japan
Center for Integrated Research of Future Electronics, Nagoya University

Supported by : The Physical Society of Japan
The Japan Society of Applied Physics
The Society of Polymer Science, Japan
The Electrochemical Society of Japan

Date : March 1st (Mon.) –3rd (Wed.), 2021

Place : Online Virtual Symposium

Presentation Time : Special Lecture (25 min presentation + 5 min discussion)
Invited Lecture (10 min presentation + 5 min discussion)
General Lecture (10 min presentation + 5 min discussion)
Poster Preview (1 min presentation without discussion)

第 60 回記念フラーレン・ナノチューブ・グラフェン 総合シンポジウム 講演要旨集

主催 : フラーレン・ナノチューブ・グラフェン学会

共催・後援 : 日本化学会
名古屋大学未来エレクトロニクス集積研究センター

協賛 : 日本物理学会、応用物理学会、高分子学会、電気化学会

日時 : 2021 年 3 月 1 日 (月) ~ 3 月 3 日 (水)

場所 : オンラインバーチャルシンポジウム

発表時間 : 特別講演 (発表 25 分 + 質疑応答 5 分)
招待講演 (発表 10 分 + 質疑応答 5 分)
一般講演 (発表 10 分 + 質疑応答 5 分)
ポスタープレビュー (発表 1 分・質疑応答 なし)

展示団体御芳名（五十音順、敬称略）

テレダイн・ジャパン(株)

(株)日本レーザー

広告掲載団体御芳名（五十音順、敬称略）

オザワ科学(株)

(株)コロナ社

(株)セントラル科学貿易

テレダイн・ジャパン(株)

日本電子(株)

(株)日本レーザー

Contents

Timetable.....	i
Chairpersons	ii
Program.....	iii
Abstracts	
Special Lecture	1
Invited Lecture.....	8
General Lecture	15
Poster	46
Author Index	130

目次

早見表.....	i
座長一覧.....	ii
プログラム.....	iii
講演予稿	
特別講演	1
招待講演	8
一般講演	15
ポスター発表	46
発表索引.....	130

Timetable

March 1 (Mon)

08:50	Opening
09:00	Special lecture <i>Shintaro Sato</i>
09:30	Oral session <i>Carbon nanotubes:</i> - Transport property - Applications
10:15	Coffee break
10:30	Special lecture <i>Hisashi Sugime</i>
11:00	Invited lecture <i>Yan Li</i>
11:15	Oral session <i>Carbon nanotubes:</i> - Synthesis and growth
11:45	Poster preview
12:30	Lunch
13:45	Poster session
15:30	Coffee break
15:45	Special lecture <i>Jun Onoe</i>
16:15	Oral session <i>Fullerenes:</i> - Chemistry - Electronic structure - Optical property - Applications
17:15	Coffee break
17:30	Invited lecture <i>Yuya Shimazaki</i>
17:45	Oral session <i>Graphene and 2D materials:</i> - Electronic structure
18:00	Coffee break
18:15	Tutorial <i>Yoshihiro Iwasa</i>
(19:45)	

March 2 (Tue)

09:00	Special lecture <i>Jamie Warner</i>
09:30	Oral session <i>Graphene and 2D materials:</i> - Optical property - Electronic structure
10:00	Coffee break
10:10	NT21 Announcement
10:15	Invited lecture <i>Matteo Pasquali</i>
10:30	Invited lecture <i>Junichiro Kono</i>
10:45	Invited lecture <i>Kenji Yasuda</i>
11:00	Invited lecture <i>Yu Saito</i>
11:15	Oral session <i>Carbon nanotubes:</i> - Others
11:30	Poster preview
12:15	Lunch
13:30	Poster session
15:15	Coffee break
15:30	Award ceremony
16:00	Special lecture <i>Haruka Omachi</i>
16:30	Invited lecture <i>Esko Kauppinen</i>
16:45	Oral session <i>Carbon nanotubes:</i> - Applications - Chemistry <i>Others:</i> - Synthesis and growth - Chemistry
18:00	Banquet
(20:00)	

March 3 (Wed)

09:00	Special lecture <i>Takahiro Kondo</i>
09:30	Oral session <i>Graphene and 2D materials:</i> - Synthesis and growth - Others
10:15	Coffee break
10:30	Oral session <i>Carbon nanotubes:</i> - Applications - Optical property - Others
11:45	Poster preview
12:30	Lunch
13:45	Poster session
15:30	Coffee break
15:45	Special lecture <i>Takahiro Morimoto</i>
16:15	Oral session <i>Graphene and 2D materials:</i> - Applications - Electronic structure - Transport property
17:15	Closing (17:25)

Special lecture: 25 min (Presentation) + 5 min (Discussion)
 Invited lecture: 10 min (Presentation) + 5 min (Discussion)
 General lecture: 10 min (Presentation) + 5 min (Discussion)
 Poster preview: 1 min (Presentation)

座長一覧(Chairpersons)

3月1日(月)

(敬称略)

セッション	時間	座長
特別講演 (佐藤 信太郎)	9:00 ~ 9:30	大淵 真理
一般講演	9:30 ~ 10:15	平原 佳織
特別講演 (杉目 恒志)	10:30 ~ 11:00	野田 優
招待講演 (Yan Li)	11:00 ~ 11:15	
一般講演	11:15 ~ 11:45	丸山 隆浩
ポスターレビュー	11:45 ~ 12:30	Il Jeon 井ノ上 泰輝
特別講演 (尾上 順)	15:45 ~ 16:15	大野 雄高
一般講演	16:15 ~ 17:15	若林 知成
招待講演 (島崎 佑也)	17:30 ~ 17:45	宮田 耕充
一般講演	17:45 ~ 18:00	
チュートリアル (岩佐 義宏)	18:15 ~ 19:45	大野 雄高

3月2日(火)

セッション	時間	座長
特別講演 (Jamie Warner)	9:00 ~ 9:30	北浦 良
一般講演	9:30 ~ 10:00	
招待講演 (Matteo Pasquali)	10:10 ~ 10:30	丸山 茂夫
招待講演 (Junichiro Kono)	10:30 ~ 10:45	
招待講演 (安田 憲司)	10:45 ~ 11:00	中野 匡規
招待講演 (斎藤 優)	11:00 ~ 11:15	
一般講演	11:15 ~ 11:30	
ポスターレビュー	11:30 ~ 12:15	中西 勇介 岡田 光博
特別講演 (大町 遼)	16:00 ~ 16:30	藤ヶ谷 剛彦
招待講演 (Esko Kauppinen)	16:30 ~ 16:45	前田 優
一般講演	16:45 ~ 17:15	
一般講演	17:15 ~ 18:00	高井 和之

3月3日(水)

セッション	時間	座長
特別講演 (近藤 剛弘)	9:00 ~ 9:30	岡田 晋
一般講演	9:30 ~ 10:15	浦江
一般講演	10:30 ~ 11:45	千足 昇平
ポスターレビュー	11:45 ~ 12:30	小澤 大知 大塚 慶吾
特別講演 (森本 崇宏)	15:45 ~ 16:15	小久保 研
一般講演	16:15 ~ 17:15	長汐 晃輔

March 1 (Mon)

08:50~09:00 Opening

Graphene and 2D materials: Applications

09:00~09:30 Special lecture

1S-1 Growth and Application of Carbon nanotubes, Graphene, and Graphene Nanoribbons 1
**Shintaro Sato*

Carbon nanotubes: Transport property

09:30~09:45

1-1 Correlation between the thermal and mechanical properties of the high temperature thermal- treated carbon nanotube yarns 15
**Ryo Shikata, Yuho Shigeeda, Hirotaka Inoue, Hiroo Suzuki, Wataru Yajima, Tomohiro Nakagawa, Takeshi Nishikawa, Yoshifumi Yamashita, Yasuhiko Hayashi, Masaki Hada*

09:45~10:00

1-2 Unraveling Thermoelectric Dimensionless Figure-of-Merit of Aligned Single-Walled Nanotube Thin-Film 16
**Kan Ueji, Yota Ichinose, Yuya Matsuoka, Yohei Yomogida, Takashi Yagi, Junichiro Kono, Kazuhiro Yanagi*

Carbon nanotubes: Applications

10:00~10:15

1-3 Fabrication and characterization of oriented carbon nanotube/polymer composite films for high thermal conductivity 17
**Nikita Kumari, Maireyee Bhattacharya, Ryo Abe, Naofumi Okamoto, Manish Pandey, Masakazu Nakamura*

10:15~10:30 Coffee break

Carbon nanotubes: Synthesis and growth

10:30~11:00	Special lecture	
1S-2	14-cm-long carbon nanotube forest via in situ supplements of iron and aluminum vapor sources <i>*Hisashi Sugime, Toshihiro Sato, Rei Nakagawa, Tatsuhiko Hayashi, Yoku Inoue, Suguru Noda</i>	2
11:00~11:15	Invited lecture	
1I-1	What We Know about Single-Walled Carbon Nanotube Growth <i>*Yan Li</i>	8
11:15~11:30		
1-4	Effect of CO ₂ during annealing on formation of catalyst particles and growth of single-wall carbon nanotubes on substrates <i>*Mochen Li, Hisashi Sugime, Suguru Noda</i>	18
11:30~11:45		
1-5	Formation of Ultra-slender CNTs via Field Emission Discharge of CNT films <i>*Yahachi Saito, Koji Asaka</i>	19
11:45~12:30	Poster preview	
12:30~13:45	Lunch	
13:45~15:30	Poster session	

Fullerenes: Applications

☆ 1P-1	Formation of highly conductive N-type thermoelectric material by co-deposition of fullerene and cesium carbonate <i>*Tatsuma Izumi, Shinta Watanabe, Masato Nakaya, Jun Onoe</i>	46
---------------	---	----

Carbon nanotubes: Chemistry

☆ 1P-2	Chirality and helicity sorting of functionalized single-walled carbon nanotube <i>*Yui Konno, Michio Yamada, Yutaka Maeda</i>	47
☆ 1P-3	Diameter-based separation of SWNTs through their mechanical interlocking with nanorectangle <i>*Guoqing Cheng, Naoki Komatsu</i>	48

Carbon nanotubes: Transport property		
☆1P-4	Annealing Influence on Hall Measurement of Single-Walled Carbon Nanotube Thin Films <i>*Hiroki Date, Mika Nagatomo, Akari Kobayashi, Taiki Inoue, Takenori Fujii, Esko Kauppien, Shigeo Maruyama, Shohei Chiashi</i>	49
Graphene and 2D materials: Electronic structure		
☆1P-5	Theoretic Study of Anomalous Electric Polarization in Chiral Graphene Nanoribbons <i>*Daichi Obana, Katsunori Wakabayashi</i>	50
Graphene and 2D materials: Optical property		
☆1P-6	Bulk photovoltaic effect in WSe ₂ /black phosphorus heterostructure via symmetry engineering <i>*Yu Dong, Toshiya Ideue, Takatoshi Akamatsu, Ling Zhou, Sota Kitamura, Mao Yoshii, Masaru Onga, Yuji Nakagawa, Kenji Watanabe, Takashi Taniguchi, Junwei Huang, Takahiro Morimoto, Hongtao Yuan, Yoshihiro Iwasa</i>	51
Graphene and 2D materials: Others		
☆1P-7	Formation of self-assembled fibroin film on 2D materials <i>*Rio Takizawa, Yoshiki Nakamura, Kazunori Motai, Mirano Tsukiiwa, Chishu Honma, Yuhei Hayamizu</i>	52
Graphene and 2D materials: Synthesis and growth		
☆1P-8	Evaluating the degree of unintentional doping in CVD-grown MoS ₂ monolayer <i>*Hibiki Naito, Yusuke Nakanishi, Hong En Lim, Yoshiyuki Nonoguchi, Kenji Watanabe, Takashi Taniguchi, Takahiko Endo, Yasumitsu Miyata</i>	53
Graphene and 2D materials: Transport property		
☆1P-9	Zeeman-type spin-orbit interaction induced Ising ferromagnetism at a van der Waals interface <i>*Hideki Matsuoka, Masaki Nakano, Stewart Edward Barnes, Jun Ieda, Sadamichi Maekawa, Mohammad Saeed Bahramy, Bruno Kenichi Saika, Yukiharu Takeda, Hiroki Wadati, Yue Wang, Satoshi Yoshida, Kyoko Ishizaka, Yoshihiro Iwasa</i>	54
☆1P-10	Fabrication and transport properties of PN diodes based on chemically-doped few-layer WSe ₂ <i>*Shunta Suzuki, Hiroto Ogura, Yusuke Nakanishi, Hong En Lim, Takahiko Endo, Yoshiyuki Nonoguchi, Yasumitsu Miyata</i>	55

Fullerenes: Synthesis and growth

- 1P-11** Synthesis and Characterization of Lithium-Ion-Encapsulated [70]Fullerene $\text{Li}^+@C_{70}$: A New Ionic Endohedral Fullerene 56
**Daiki Kitabatake, Hiroshi Ueno, Kazuhiko Kawachi, Yasuhiko Kasama, Shinobu Aoyagi, Keijiro Ohshimo, Fuminori Misaizu*

Carbon nanotubes: Synthesis and growth

- 1P-12** Growth mechanism and handedness relation of one-dimensional van der Waals heterostructures 57
**Yongjia Zheng, Akihito Kumamoto, Rong Xiang, Kaoru Hisama, Keigo Otsuka, Yuta Sato, Taiki Inoue, Shohei Chiashi, Daiming Tang, Qiang Zhang, Anton Anisimov, Esko Kauppinen, Kazu Suenaga, Yuichiro Ikuhara, Shigeo Maruyama*
- 1P-13** Effect of hydrogen on the microplasma synthesis of carbon nanotubes 58
**Takashi Tsuji, Jaeho Kim, Hajime Sakakita, Guohai Chen, Kenji Hata, Don Futaba, Shunsuke Sakurai*

Carbon nanotubes: Transport property

- 1P-14** Thermal conductivity of C_{60} encapsulated single-walled carbon nanotubes thin films 59
**Rikuto Abe, Kan Ueji, Yohei Yomogida, Kazuhiro Yanagi*
- 1P-15** Thermal boundary resistance of aligned films of single-walled carbon nanotube using time-domain thermoreflectance method 60
**Atsuhiko Katagiri, Kan Ueji, Yuya Matsuoka, Junko Eda, Hitomi Okubo, Yohei Yomogida, Junichiro Kono, Takashi Yagi, Kazuhiro Yanagi*

Carbon nanotubes: Optical property

- 1P-16** Local Grafting of Polymer Radical on the Surface of Single-Walled Carbon Nanotubes and the Enhanced Photoluminescence in the Near-Infrared Region 61
**Yukiko Nagai, Kenta Nakamura, Tsuyohiko Fujigaya*

Carbon nanotubes: Applications

- 1P-17** Modeling and Optimization of Tensile Strength of CNT/HDPE Composites Using Response Surface Methodology 62
**Nao Otsuki, Masaru Sekido*
- 1P-18** Effects of deposition conditions on the states of Pt nanoparticles on carbon materials and their electrocatalytic properties toward methanol oxidation and CO poisoning 63
**Yuho Abe, Hironori Ogata*

1P-19	Scattering parameter analysis of self-aligned flexible carbon nanotube thin-film transistors <i>*Saya Ishimaru, Taiga Kashima, Hiromichi Kataura, Yutaka Ohno</i>	64
Graphene and 2D materials: Synthesis and growth		
1P-20	One-dimensional growth of WS ₂ by chemical vapor deposition <i>*Kazuma Shimogami, Misaki Kishibuchi, Hirotaka Inoue, Liu Zheng, Yasumitsu Miyata, Yasuhiko Hayashi, Hiroo Suzuki</i>	65
Graphene and 2D materials: Transport property		
1P-21	Gate-turning of carrier doping by oxygen molecule adsorption on MoS ₂ <i>*Takumi Yoshida, Kazuyuki Takai</i>	66
Graphene and 2D materials: Chemistry		
1P-22	Correlation between the amount of functional groups in graphene oxide and the catalytic activity in reduction of nitrobenzene <i>*Riku Kondo, Yoshiaki Matsuo, Kazuyuki Takai</i>	67
Graphene and 2D materials: Optical property		
1P-23	Comparison of light emission from different kinds of hBNs after UV or thermal treatments <i>*Yusuke Adachi, Kuniharu Takei, Takayuki Arie, Seiji Akita</i>	68
Graphene and 2D materials: Applications		
1P-24	Vibrational Spectra of Nucleotides at the Au Cluster attached to graphene nanopore in MD Simulation of a SERS Sensor <i>*Mohd Aidil Amin Bin Mohd Nasir, Tatiana Zolotoukhina</i>	69
1P-25	HER catalytic performance of Mo ₂ C/C composite films prepared by microwave-plasma CVD method <i>*Shunsuke Numata, Hironori Ogata</i>	70
Graphene and 2D materials: Others		
1P-26	Magnetizations and De Haas-van Alphen oscillations in the Dirac fermions <i>*Fenda Rizky Pratama, M. Shoufie Ukhtary, Riichiro Saito</i>	71
Others: Synthesis and growth		
1P-27	Synthesis of WTe ₂ nanowires by tellurization of tungsten oxide nanowires and origin of non-formation of tubular structure <i>*Mai Nagano, Yohei Yomogida, Hiromu Hamasaki, Kaori Hirahara, Yasumitsu Miyata, Kazuhiro Yanagi</i>	72

Others: Electronic structure

- 1P-28** Electronic structures of MoS₂ nanotube bundles 73
**Kaoru Hisama, Mina Maruyama, Shohei Chiashi, Shigeo Maruyama, Susumu Okada*

15:30~15:45 Coffee break

Fullerenes: Applications

15:45~16:15 Special lecture

- 1S-3** Low-dimensional C₆₀ polymers: Fundamental properties and their applications to environment and energy issues 3
**Jun Onoe*

Fullerenes: Chemistry

16:15~16:30

- 1-6** One-step direct oxidation of alkoxy to ketone for evaporable fullerene-fused ketone as efficient electron-transport materials 20
**Hao-Sheng Lin, Yue Ma, Rong Xiang, Sergei Manzhos, Il Jeon, Shigeo Maruyama, Yutaka Matsuo*

Fullerenes: Electronic structure

16:30~16:45

- 1-7** Quantum States of the Endohedral Fullerene Crystal [Li⁺@C₆₀]PF₆⁻ 21
**Hideo Ando, Yoshihide Nakao*

Fullerenes: Optical property

16:45~17:00

- 1-8** Anionic fluorinated Zn-porphyrin combined with Li⁺C₆₀ for long-lived photoinduced charge separation with low energy loss 22
**Kazuhira Miwa, Shinobu Aoyagi, Takahiro Sasamori, Hiroshi Ueno, Hiroshi Okada, Kei Ohkubo*

Fullerenes: Applications

17:00~17:15

- 1-9** Formation of high-performance P-type thermoelectric materials composed of fullerene molecules and molybdenum oxide nanoclusters 23
**Masato Nakaya, Shinta Watanabe, Jun Onoe*

17:15~17:30 Coffee break

Graphene and 2D materials: Optical property

17:30~17:45 Invited lecture

- 1I-2** Strongly correlated electrons in a moiré superlattice probed with exciton spectroscopy 9
**Yuya Shimazaki, Ido Schwartz, Kenji Watanabe, Takashi Taniguchi, Martin Kroner, Atac Imamoglu*

Graphene and 2D materials: Electronic structure

17:45~18:00

- 1-10** Energetics and electronic structure of corannulene-intercalated bilayer-graphene 24
**Mina Maruyama, Susumu Okada*

18:00~18:15 Coffee break

18:15~19:45 Tutorial

- 1T-1** **Yoshihiro Iwasa*

March 2 (Tue)

Graphene and 2D materials: Synthesis and growth

09:00~09:30 Special lecture

2S-1 Synthesis, structure, processing and electronic devices using 2D layered Noble Metal Dichalcogenides PdSe₂ and PtS₂ 4
**Jamie Warner*

Graphene and 2D materials: Optical property

09:30~09:45

2-1 Second harmonic generation in two-dimensional Janus TMDs 25
**Riichiro Saito, Nguyen Tuan Hung, M. Shoufie Ukhtary*

Graphene and 2D materials: Electronic structure

09:45~10:00

2-2 Geometric and electronic structures of a two-dimensional tetracoordinated C allotrope of fused pentagons 26
**Susumu Okada, Nguyen Thanh Cuong, Yanlin Gao, Mina Maruyama*

10:00~10:10 Coffee break

10:10~10:15 NT21 Announcement

10:15~10:30 Invited lecture

2I-1 Improved properties, increased production, and the path to broad adoption of carbon nanotube fibers 10
*Lauren W. Taylor, Oliver S. Dewey, Robert J. Headrick, Natsumi Komatsu, Nicolas Marquez Peraca, Geoff Wehmeyer, Junichiro Kono, *Matteo Pasquali*

Carbon nanotubes: Transport property

- 10:30~10:45 Invited lecture
- 2I-2** Ultrahigh-Conductivity Carbon Nanotube Fibers with Giant Thermoelectric Power Factor 11
*Natsumi Komatsu, Yota Ichinose, Oliver S. Dewey, Lauren W. Taylor, Mitchell Trafford, Yohei Yomogida, Geoff Wehmeyer, Matteo Pasquali, Kazuhiro Yanagi, *Junichiro Kono*

Graphene and 2D materials: Transport property

- 10:45~11:00 Invited lecture
- 2I-3** Stacking-engineered ferroelectricity in bilayer boron nitride 12
**Kenji Yasuda, Xirui Wang, Kenji Watanabe, Takahashi Taniguchi, Pablo Jarillo-Herrero*
- 11:00~11:15 Invited lecture
- 2I-4** Isospin Pomeranchuk effect in twisted bilayer graphene 13
**Yu Saito*

Carbon nanotubes: Others

- 11:15~11:30
- 2-3** In-situ TEM observation of laser induced carbon nanostructure growth 27
**Ryosuke Senga, Yung-Chang Lin, Sapna Sinha, Takeshi Kaneko, Norihiro Okoshi, Takeo Sasaki, Shigeyuki Morishita, Hidetaka Sawada, Kazu Suenaga*
- 11:30~12:15 Poster preview
- 12:15~13:30 Lunch
- 13:30~15:15 Poster session

Carbon nanotubes: Chemistry

- ☆2P-1** Dispersion of single-walled carbon nanotubes with commodity plastics PMMA 74
**Ayaka Demise, Tsuyoshi Ando, Hiroharu Ajiro, Tsuyoshi Kawai, Yoshiyuki Nonoguchi*

Carbon nanotubes: Applications

- ☆**2P-2** Cross-linking gelation of isomaltodextrin for the chromatographic separation of semiconducting carbon nanotubes 75
**Yuki Matsunaga, Jun Hirotsu, Yutaka Ohno, Haruka Omachi*

Carbon nanotubes: Others

- ☆**2P-3** self-aligned hybrid quantum structure of diamond nitrogen-vacancy center and carbon nanotube for electrical control of quantum states 76
**Haruki Uchiyama, Shigeru Kishimoto, Junko Ishi-Hayase, Yutaka Ohno*

Graphene and 2D materials: Synthesis and growth

- ☆**2P-4** Preparation of twisted bilayers by folding monolayer WS₂ 77
**Masahiko Kaneda, Yusuke Nakanishi, Hong En Lim, Takahiko Endo, Yasumitsu Miyata*

Graphene and 2D materials: Electronic structure

- ☆**2P-5** First-principles study of impurity states induced by a carbon or oxygen atom in h-BN monolayer 78
**Taishi Haga, Shuaishuai Yuan, Kirk H. Bevan, Susumu Saito*

Graphene and 2D materials: Transport property

- ☆**2P-6** Air-Stable, Efficient Electron Doping of Monolayer MoS₂ by Salt-Crown Ether Treatment 79
**Hiroto Ogura, Masahiko Kaneda, Yusuke Nakanishi, Yoshiyuki Nonoguchi, Jiang Pu, Mari Ohfuchi, Toshifumi Irisawa, Hong En Lim, Kazuhiro Yanagi, Takahiko Endo, Taishi Takenobu, Yasumitsu Miyata*
- ☆**2P-7** Detection of subband resonant tunneling in few-layer WSe₂/h-BN/p⁺-MoS₂ van der Waals junction 80
**Kei Takeyama, Rai Moriya, Shota Okazaki, Yijin Zhang, Satoru Masubuchi, Kenji Watanabe, Takashi Taniguchi, Takao Sasagawa, Tomoki Machida*

Graphene and 2D materials: Optical property

- ☆**2P-8** Optical induced Spin Current of Monolayer NbSe₂ 81
**Ren Habara, Katsunori Wakabayashi*
- ☆**2P-9** Intra-layer excitons trapped in moiré potential on monolayer-MoSe₂/NiPS₃ heterostructure 82
**Yan Zhang, Keisuke Shinokita, Yuhei Miyauchi, Kazunari Matsuda*

Graphene and 2D materials: Applications

- ☆**2P-10** Tuning Heat Flow Across Two-dimensional Layered van der Waals 83
Materials via Interfacial Mismatch and Coupling Engineering
**Wenyu Yuan, Kan Ueji, Takashi Yagi, Takahiko Endo, Hong En Lim,
Yasumitsu Miyata, Yohei Yomogida, Kazuhiro Yanagi*

Fullerenes: Chemistry

- 2P-11** Photoreaction of C₇₀ with Disilirane: Electronic Properties of Silylated 84
Adducts
**Shintaro Nishida, Masahiro Kako, Michio Yamada, Yutaka Maeda, Makoto
Furukawa, Takeshi Akasaka*

Fullerenes: Optical property

- 2P-12** Simulation and measurement of the infrared emission spectra of C₆₀ 85
**Tomonari Wakabayashi, Yutaka Mukai, Kaito Tanaka, Keisuke Fukumoto,
Miho Hatanaka, Takeshi Kodama*

Carbon nanotubes: Synthesis and growth

- 2P-13** Growth of single-walled carbon nanotubes on SiO₂/Si substrate and alumina 86
buffer layer by alcohol catalytic CVD method using Ir catalyst
**Daiki Yamamoto, Shu Kondo, Kamal Sharma, Takahiro Saida, Shigeya
Narituka, Takahiro Maruyama*
- 2P-14** Analysis of acetylene-induced growth acceleration of single-walled carbon 87
nanotubes by isotope labeling technique
**Akari Kobayashi, Ryoya Ishimaru, Keigo Otsuka, Taiki Inoue, Shohei
Chiashi, Shigeo Maruyama*

Carbon nanotubes: Transport property

- 2P-15** Fabrication and Efficiency Evaluation of Organic Photovoltaics using 88
Single-walled CNT of the Transparent Conductive Electrode
**Riku Hatamoto, Hao-Sheng Lin, Takeshi Hashimoto, Satoru Hashimoto,
Yutaka Matsuo*
- 2P-16** Thermoelectric properties of morphology-controlled single-walled carbon 89
nanotube alloys
**Yota Ichinose, Rikuto Abe, Kan Ueji, Yohei Yomogida, Kazuhiro Yanagi*

Carbon nanotubes: Optical property

- 2P-17** Gate-tuned high-harmonic generation in metallic single-walled carbon nanotubes and graphene 90
**Hiroyuki Nishidome, Kohei Nagai, Kento Uchida, Kenji Kawahara, Junko Eda, Hitomi Okubo, Yohei Yomogida, Hiroki Ago, Koichiro Tanaka, Kazuhiro Yanagi*
- 2P-18** Circular dichroism spectra on thin films of Helicity Selected Single-wall Carbon Nanotubes 91
**Yuuya Hosokawa, Yohei Yomogida, Kazuhiro Yanagi*

Carbon nanotubes: Applications

- 2P-19** Synthesis of Vertical-Aligned Carbon Nanotube / Al Composite Electrode for Li-ion Capacitor Cathode 92
**Masanori Hara, Ryo Kawachi, Takashi Banno, Masamichi Yoshimura*
- 2P-20** Observation of the UV-induced Photocurrent in PET sheet using CNT thin-film electrodes 93
**Satoru Suzuki, Taichi Nakamura, Takahiro Ishikawa, Teruaki Konishi, Tsuyoshi Hamano, Yutaka Ohno, Hiroshi Ajiki, Toshio Hirao, Satoshi Ishii*
- 2P-21** Relationship between van der Waals force and tensile strength of MWNT/polymer composites by Melt Blending 94
**Koichi Utsugi, Masaru Skido*

Graphene and 2D materials: Synthesis and growth

- 2P-22** Direct Growth of Graphene on GaN using Alcohol CVD 95
**Shohei Yabuta, Shinichiro Mouri, Tsutomu Araki*

Graphene and 2D materials: Electronic structure

- 2P-23** Elucidation of charge interactions between graphene and quantum dots 96
**Zen Inoue, Yasushi Ishiguro, Alexander Baranov, Igor Nabiev, Kazuyuki Takai*

Graphene and 2D materials: Transport property

- 2P-24** Transport Properties of two-dimensional n/p-doped Transition Metal Dichalcogenides prepared through a post-doping method 97
**Shaochun Zhang, Yuya Murai, Toshinori Shirafuji, Ryo Kitaura*

Graphene and 2D materials: Optical property

- 2P-25** Optical properties of Zn-porphyrin covalently bounded to MoS₂ and WS₂. 98
**Ruben Canton Vitoria, Ryo Kitaura*

Graphene and 2D materials: Applications

2P-26 Cationic Nitrogen Doped Graphene as p-type Dopant in PEDOT:PSS Hole-Transporters for Organic Solar Cells 99
**Takuhei Kaneko, Haosheng Lin, Sangwoo Chae, Takumi Yana, Nagahiro Saito, Yutaka Matsuo*

2P-27 Micro-patterning of graphite by Lithographic method 100
**Jianwei Fu, Genki Hirobe, Yasushi Ishiguro, Kazuyuki Takai*

Others: Optical property

2P-28 Phosphorescence excitation mapping of polyene molecules isolated in solid acetonitrile at 20 K 101
**Kaito Tanaka, Aoi Mineyama, Riku Ohnishi, Keisuke Fukumoto, Tomonari Wakabayashi*

15:15~15:30 Coffee break

15:30~16:00 Award ceremony

Carbon nanotubes: Applications

16:00~16:30 Special lecture

2S-2 Organic synthetic approaches to nanocarbon-based hybrid materials 5
**Haruka Omachi*

Carbon nanotubes: Synthesis and growth

16:30~16:45 Invited lecture

2I-5 FC-CVD synthesis of CNTs from methane for transparent conductor applications 14
**Esko Kauppinen, Qiang Zhang, Datta Sukanta, Hua Jiang*

Carbon nanotubes: Applications

16:45~17:00

2-4 Design and Fabrication of Carbon Nanotube-based Non-precious Metal Electrocatalysts with High ORR and OER Performances and their Applications 28
*Pandian Ganesan, Aleksandar Staykov, Hiroaki Shu, Mitsugu Uejima, *Naotoshi Nakashima*

Carbon nanotubes: Chemistry

17:00~17:15

- 2-5** Multifaceted approaches to quantitative surface characterization of as-grown and acid treated single-walled carbon nanotubes 29
**Kazufumi Kobashi, Yoko Iizumi, Kazutoshi Hirota, Naoki Shinomori, Kazuhiro Shimamoto, Yasumasa Koga, Takahiro Morimoto, Toshiya Okazaki*

Others: Synthesis and growth

17:15~17:30

- 2-6** Outstanding Performance of Single-digit Nanoparticle: 2.6nm Diamond Particle as the First Example 30
**Eiji Osawa, Ryoko Yamanoi, Shuichi Sasaki, Amanda Barnard*

Others: Chemistry

17:30~17:45

- 2-7** Solubilization and purification of carbon nanohorn aggregates using cyclodextrins as surfactants 31
**Hiroki Hanayama, Junya Yamada, Koji Harano, Eiichi Nakamura*

17:45~18:00

- 2-8** Visualizing outer surface functionalization of carbon nanohorn spherical aggregates by highly spatially resolved SEM-EDS 32
**Hideaki Nakajima, Takahiro Morimoto, Kazufumi Kobashi, Minfang Zhang, Ioanna Sideri, Nikos Tagmatarchis, Toshiya Okazaki*

18:00~20:00 Banquet

March 3 (Wed)

Graphene and 2D materials: Synthesis and growth

09:00~09:30 Special lecture

3S-1 Boron-based new two-dimensional materials: synthesis, characterization, and application 6
**Takahiro Kondo*

09:30~09:45

3-1 Self-assembly of metal-chalcogenide clusters into layered 2D materials 33
**Yusuke Nakanishi, Naoyuki Kanda, Zheng Liu, Motoki Aizaki, Mina Maruyama, Yanlin Gao, Susumu Okada, Yasumitsu Miyata*

09:45~10:00

3-2 Transmissible plasma evolved graphene: production and application 34
**Kamal Prasad Sharma, Aliza Khaniya Sharma, Daiki Yamamoto, Toru Asaka, Takahiro Maruyama*

Graphene and 2D materials: Others

10:00~10:15

3-3 Field-induced dynamics of Ne atom around graphene edges 35
**Yanlin Gao, Susumu Okada*

10:15~10:30 Coffee break

Carbon nanotubes: Applications

10:30~10:45

3-4 Foldable Perovskite Solar Cells Using Carbon Nanotube-Embedded Ultrathin Polyimide Conductor 36
**IL Jeon, Jungjin Yoon, Esko Kauppinen, Shigeo Maruyama, Philip Lee*

10:45~11:00

- 3-5** Highly Efficient Metal-Free Semi-Transparent Perovskite Solar Cells enabled by MoO₃-doped Transparent Carbon Nanotube Top Electrodes and Four-Terminal Perovskite Silicon Tandem Applications 37
**Seungju Seo, Il Jeon, Kosuke Akino, Ahmed Shawky, Hao-Sheng Lin, Hiroki Nagaya, Esko.I. Kauppinen, Rong Xiang, Yutaka Matsuo, Shigeo Maruyama*

11:00~11:15

- 3-6** Waveguide coupled cavity-enhanced light emission from individual carbon nanotubes 39
**Daiki Yamashita, Hidenori Machiya, Keigo Otsuka, Akihiro Ishii, Yuichiro K. Kato*

Carbon nanotubes: Optical property

11:15~11:30

- 3-7** Analytical Estimation of Quantum Emitters Formed in Air-Suspended Single-Walled Carbon Nanotubes 40
**Daichi Kozawa, Xiaojian Wu, Akihiro Ishii, Jacob Fortner, Keigo Otsuka, Rong Xiang, Taiki Inoue, Shigeo Maruyama, YuHuang Wang, Yuichiro K. Kato*

Carbon nanotubes: Others

11:30~11:45

- 3-8** Mechanical Vibration of Single-walled Carbon Nanotubes in a Water Using Finite Element Model 41
**Daisuke Miyashiro, Ryo Hamano, Hisao Taira, Kazuo Umemura*

11:45~12:30 Poster preview

12:30~13:45 Lunch

13:45~15:30 Poster session

Fullerenes: Applications

- ☆**3P-1** Control of optical absorption property of PbPc donor film for development of full-spectra organic photovoltaic cells 102
**Hayato Yoshizawa, Masahiro Kato, Masato Nakaya, Jun Onoe*

Carbon nanotubes: Synthesis and growth

- ☆**3P-2** Enhanced gas-phase synthesis of single-wall carbon nanotubes with methane as carbon source by preheating catalyst precursors 103
**Zihao Zhang, Itsuki Chikaarashi, Katsuya Namiki, Toshio Osawa, Hisashi Sugime, Suguru Noda*

Carbon nanotubes: Chemistry

- ☆**3P-3** Semiconducting carbon nanotube extraction enabled by cellulosic polymer wrapping 104
**Tomoko Yagi, Tsuyoshi Kawai, Yoshiyuki Nonoguchi*

Carbon nanotubes: Optical property

- ☆**3P-4** Investigation of water adsorption on vertically-aligned single-walled carbon nanotubes by Raman spectroscopy 105
**Masanori Bamba, Shu Sato, Taiki Inoue, Shigeo Maruyama, Shohei Chiashi*

Graphene and 2D materials: Synthesis and growth

- ☆**3P-5** Self-assembly of two-dimensional structures composed of tetrahedral molybdenum clusters 106
**Naoyuki Kanda, Zheng Liu, Motoki Aizaki, Mina Maruyama, Susumu Okada, Yanlin Gao, Hisanori Shinohara, Yasumitsu Miyata, Yusuke Nakanishi*

Graphene and 2D materials: Electronic structure

- ☆**3P-6** Theoretic Study on Raman Active Modes of SnS Thin Films 107
**Itsuki Yonemori, Sudipta Dutta, Kosuke Nagashio, Katsunori Wakabayashi*
- ☆**3P-7** Tuning electronic properties of graphene antidot lattices with truncated triangular holes: A First-principles study 108
**Yuta Taguchi, Susumu Saito*

Graphene and 2D materials: Transport property

- ☆**3P-8** Two-dimensional electron gas in laterally-assembled WTe atomic wires 109
**Hiroshi Shimizu, Jiang Pu, Zheng Liu, Hong En Lim, Yusuke Nakanishi, Takahiko Endo, Kazuhiro Yanagi, Taishi Takenobu, Yasumitsu Miyata*

Others: Synthesis and growth

- ☆**3P-9** High-yield synthesis of MoS₂ and MoSe₂ nanotubes 110
**Ryoga Tanaka, Yohei Yomogida, Yasumitsu Miyata, Kazuhiro Yanagi*

Fullerenes: Applications

- 3P-10** Preparation of bipyramidal gold nanoparticle-[C₆₀]fullerene nanowhisker composites and kinetics study for reduction of 4-nitrophenol 111
**Jeong Won Ko, Yeon A Son, Se Hwan Park, Weon Bae Ko*

Carbon nanotubes: Synthesis and growth

- 3P-11** Growth of single-walled carbon nanotubes using Ir catalyst prepared by dip-coating process 112
**Shu Kondo, Ai Misaki, Kamal Sharma, Takahiro Saida, Shigeoya Naritsuka, Takahiro Maruyama*
- 3P-12** Growth of hBN on CNT assemblies and their memristive behavior 113
**Misaki Kishibuchi, Kazuma Shimogami, Hiroataka Inoue, Kyohei Nasu, Tomohiro Nakagawa, Mitsuaki Maetani, Yuichiro Tanaka, Yasuhiko Hayashi, Hiroo Suzuki*
- 3P-13** Synthesis of high-density vertically aligned carbon nanotubes by suppressing migration of Fe using Fe/MoxOy catalyst 114
**Mitsuaki Maetani, Hiroataka Inoue, Tomohiro Nakagawa, Kyohei Nasu, Takeshi Nishikawa, Hiroo Suzuki, Yasuhiko Hayashi*

Carbon nanotubes: Chemistry

- 3P-14** Electrolyte effects on electrochemical doping of semiconducting carbon nanotube films 115
**Satoki Taniguchi, Tsuyoshi Kawai, Yoshiyuki Nonoguchi*

Carbon nanotubes: Transport property

- 3P-15** Visualization of thermal transports on bundled carbon nanotubes by monitoring phase transition of tin nanoparticles 116
**Hiromu Hamasaki, Takumi Kawase, Kaori Hirahara*

Carbon nanotubes: Optical property

- 3P-16** Excitonic photoluminescence properties of locally functionalized single-walled carbon nanotubes using cycloaddition modification 117
**Tomohiro Shiraki, Keita Hayashi, Tsuyohiko Fujigaya*

Carbon nanotubes: Applications

- 3P-17** Reflection and Absorption Properties of Microwave Absorbers Made by SWNT-Cellulose Composite Paper 118
**Weni Yulistia, Tetsu Mieno*
- 3P-18** Preparation of carbon nanotube/organic-inorganic hybrid aerogel composites 119
**Taiyo Shimizu, Takeo Yamada, Kenji Hata*

3P-19	CNT/HfO ₂ /CNT memristor with high on-off ratio for neuromorphic computing <i>*Adha Sukma Aji, Yutaka Ohno</i>	120
Graphene and 2D materials: Synthesis and growth		
3P-20	Synthesis and properties of carbon quantum dots using woody biomass. <i>*Takaki Yoda, Hironori Ogata</i>	121
Graphene and 2D materials: Chemistry		
3P-21	Effect of Defect Formation of Graphene on Proton Penetration Properties <i>*Tomohiro Fukushima, Takaha Komai, Kei Murakoshi</i>	122
Others: Electronic structure		
3P-22	Electronic properties of 1D transition-metal chalcogenides nanowires <i>*Nguyen Tuan Hung, Riichiro Saito</i>	123
Graphene and 2D materials: Optical property		
3P-23	Effect of iron ion beam irradiation on MoS ₂ fluorescence <i>*Takumi Hidaka, Tomoaki Nishimura, Kazuyuki Takai</i>	124
3P-24	Building of Platforms to Explore Transport Dynamics of Excitons and Trions in Monolayer Transition Metal Dichalcogenides <i>*Mengsong Xue, Yuya Murai, Shaochun Zhang, Toshinori Shirafuji, Ryo Kitaura</i>	125
Graphene and 2D materials: Applications		
3P-25	Spin current induced by edge plasmon on two-dimensional materials <i>*Yuan Tian, M. Shoufie Ukhtary, Riichiro Saito</i>	126
Others: Optical property		
3P-26	Molecular orbital calculations of small carbon molecules in the singlet and triplet states <i>*Keisuke Fukumoto, Riku Ohnishi, Kaito Tanaka, Tomonari Wakabayashi</i>	127
Others: Others		
3P-27	Effects of liquid phase oxidation of Nanodiamond surface on its water dispersibility and photo-absorption <i>*Takuma Tsuji, Kazuyuki Takai</i>	128
3P-28	Do Elementary Diamond Nanoparticles Aggregate in their Aqueous Colloidal Solutions by just Diluting with Pure Water? <i>*Masaya Nemoto, Shusuke Ando, Yuho Itabashi, Tomohito Obata, Daiki Ayai, Nagito Haga, Kaito Hiruta, Toshihiko Tanaka, Yasuhiro F. Miura, Tetsuya Aoyama, Kazunori Miyamoto, Atsuya Muranaka, Masanobu Uchiyama, Eiji Osawa</i>	129

15:30~15:45 Coffee break

Carbon nanotubes: Applications

15:45~16:15 Special lecture

3S-2 Characterization methods for the ensemble state of network structured nanomaterials 7
**Takahiro Morimoto*

Graphene and 2D materials: Applications

16:15~16:30

3-9 Co-self-assembly of probe and scaffold peptides on graphite surface toward functionalization of graphene biosensors 42
**Chishu Homma, Mirano Tsukiiwa, Yuhei Hayamizu*

16:30~16:45

3-10 Investigation of Schottky contact for transparent solar cell with monolayer WS₂ 43
**Xing He, Toshiro Kaneko, Toshiaki Kato*

Graphene and 2D materials: Electronic structure

16:45~17:00

3-11 Fabrication of Graphene/h-BN/graphene stacked mechanical resonator 44
**Kazuki Yasoshima, Taichi Inoue, Kuniharu Takei, Takayuki Arie, Seiji Akita*

Graphene and 2D materials: Transport property

17:00~17:15

3-12 p–n junction in graphene nanoribbon modified by periodically doped boron and nitrogen atoms 45
**Sake Wang, Md Shafiqul Islam, Nguyen T. Hung, Hongyu Tian, Ahmad R. T. Nugraha, Riichiro Saito*

17:15~17:25 Closing

特別講演
Special Lecture

1S – 1 ~ 1S – 3

2S – 1 ~ 2S – 2

3S – 1 ~ 3S – 2

Growth and Application of Carbon nanotubes, Graphene, and Graphene Nanoribbons

○Shintaro Sato^{1,2}

¹ *Fujitsu Laboratories Ltd., Atsugi 243-0197, Japan*

² *Fujitsu Limited, Atsugi 243-0197, Japan*

We work on growth of carbon nanotubes (CNTs), graphene, and graphene nanoribbons (GNRs), and their application to electronic devices, such as transistors, interconnects, and sensors. We explain some of our recent results here.

As for CNTs, we have been working on application of CNTs to interconnects [1, 2], and thermal interface materials (TIMs) [3]. In particular, we fabricated TIMs consisting of bundles of vertically aligned CNTs, where the density of CNTs was increased by a newly-developed compressing method [3]. The thermal resistance of the CNT-TIM was found to be as low as that of indium film [3]. Recently, we developed a flexible and adhesive CNT sheet consisting of bundles of vertically aligned CNTs and two laminate layers at both the ends of the CNTs, as shown in Fig. 1 [4]. The developed technology protects the carbon nanotubes themselves with a laminate layer, making them stable in shape and making cutting and handling easier.

We also work on bottom-up growth of armchair-edged graphene nanoribbons (AGNRs). The bandgap of AGNR can be controlled by its width; however, only AGNRs with bandgaps well above 1 eV have been reported so far. Recently, we have succeeded in growing AGNRs with 17 carbon-dimer lines (17-AGNRs) by polymerization and subsequent cyclodehydrogenation of precursor molecules on Au(111), as shown in Fig. 2 [5]. We found that, by scanning tunneling spectroscopy, 17-AGNRs have a bandgap of 0.2 eV on Au(111), which corresponds to a bandgap of 0.63 eV without the image charge effects of Au. This bandgap is about the same as that of Ge, and may be suitable for transistor applications.

This research was partly supported by JST CREST Grant Number JPMJCR15F1, Japan.

[1] M. Nihei, et al., *Jpn. J. Appl. Phys.* **44** 1626 (2005) [2] Y. Awano, et al., *Proc. IEEE* **98**, 2015 (2010) [3] D. Kondo, et al. 2017 *International Conference on Solid State Devices and Materials (SSDM)*, p.353 (2017) [4] <https://pr.fujitsu.com/jp/news/2020/04/17.html> [5] J. Yamaguchi, et al., *Commun. Mater.* **1**, 36 (2020).

Corresponding Author: S. Sato, Tel: +81-46-250-8832, Fax: +81-46-250-8235, E-mail: sato.shintaro@fujitsu.com



Fig. 1 Flexible and adhesive CNT sheet.

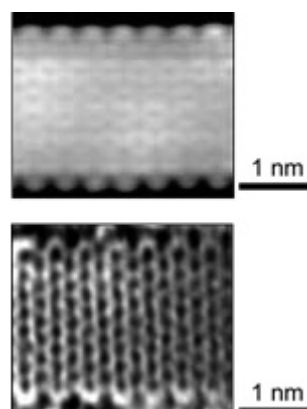


Fig. 2 (a) Scanning tunneling microscope image and (b) non-contact atomic force microscope image of 17-AGNR.

14-cm-long carbon nanotube forest via in situ supplements of iron and aluminum vapor sources

○Hisashi Sugime^{1*}, Toshihiro Sato², Rei Nakagawa², Tatsuhiro Hayashi³, Yoku Inoue³,
Suguru Noda^{1,2}

¹Waseda Research Institute for Science and Engineering, Waseda University

²Department of Applied Chemistry, Waseda University

³Department of Electronics and Materials Science, Shizuoka University

Growth of carbon nanotube (CNT) forests in large scale is one of the main challenges to utilize the attractive properties of CNTs in variety of applications. To date, several groups have reported the growth of centimeter-scale CNT forests, and the maximum length that has been reached is ~2 cm using an iron-gadolinium (Fe-Gd) catalyst on an aluminum oxide (Al₂O₃) support [1]. Nevertheless, with the conventional approaches, there seemed to exist a ceiling preventing growth that went beyond ~2 cm. Therefore, it is necessary to realize a method that achieves longer CNT forests while alleviating the growth termination which is mainly caused by the structural change of the catalyst nanoparticles [2].

In this work, a carbon nanotube forest with a length of 14 cm grew with an average growth rate of 1.5 μm s⁻¹ and a growth lifetime of 26 h (Fig. 1) [3]. Several key factors to realize this unprecedented long growth such as catalyst conditions, growth conditions in chemical vapor deposition, and reactor system were clarified. It was found that the combination of the catalyst system of iron/gadolinium/aluminum oxide (Fe/Gd/Al₂O_x) [4] and the in situ supplements of Fe and Al vapor sources at very low concentration was crucially important. A cold-gas system, where only the substrate is heated while keeping the gas at room temperature, was employed to suppress unnecessary reactions and depositions [5]. The long carbon nanotube forest enabled macroscopic measurements of the tensile and electrical properties of the carbon nanotube wires, and it gave several important insights for industrial applications of the carbon nanotubes in the future.

[1] W. Cho et al., *Carbon* **69**, 609 (2014). [2] H. Sugime et al., *ACS Appl. Mater. Interfaces* **6**, 15440 (2014). [3] H. Sugime et al., *Carbon* **172**, 772 (2021). [4] H. Sugime et al., *ACS Nano* **13**, 13208 (2019). [5] H. Sugime et al., *Carbon* **50**, 2953 (2012).

Corresponding Author: H. Sugime,
E-mail: sugime@aoni.waseda.jp

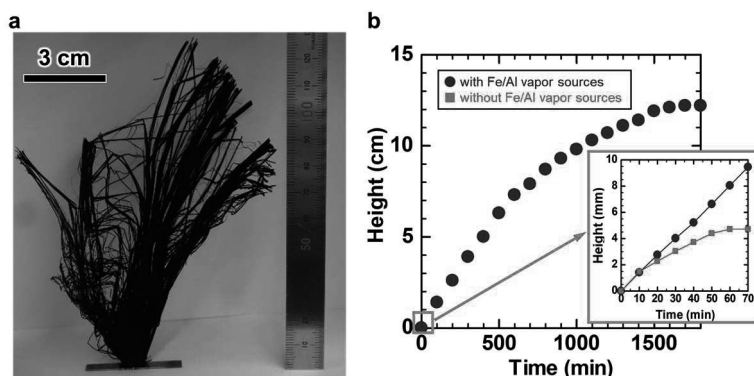


Fig. 1: (a) Pictures of the CNT forest after the growth for 32 h. (b) Growth curves of the CNT forests with and without Fe/Al vapor sources.

Low-dimensional C₆₀ polymers: Fundamental properties and their applications to environment and energy issues

Jun Onoe*

Department of Energy Science and Engineering, Nagoya University

Furo-cho, Chikusa-ku, Nagoya 464-8603, Japan

We have hitherto investigated the structures and properties of one- and two-dimensional (1D, 2D) C₆₀ polymers formed by electron- and photo-irradiation of pristine C₆₀ films, respectively [1, 2].

The 1D C₆₀ polymer has a periodic uneven-structure and exhibits a metal featuring Tomonaga-Luttinger liquids, and it is further interesting to note that the polymer shows Gaussian-curvature-induced geometrical effects on the electronic states [2–5], which has been theoretically predicted since 1950s. Recently, we have found that the nano-space in the 1D polymer film acts as a specific reaction field where CO₂ + H₂O reaction ($E_a = 2$ eV in gas phase) proceeds at room temperature to form carbonic ions (CO₃²⁻) when exposed to atmospheric air. This property can be applied to CO₂ immobilization and conversion to valuable compounds [6], which are important to solve environmental issues. On the other hand, the 2D polymer has a hexagonal structure via [2+2] dumbbell-type cross-linkage and exhibits a semiconducting character [7]. Recently, we have studied photo-irradiated C₆₀ film by using *in situ* STM and FT-IR [8], and applied it to organic thermoelectric materials that have been focused as energy-harvesting devices.

In this talk, I will introduce the details of the two latest topics described above.

Acknowledgments

The present two topics were partially supported by KAKENHI (18H01826) and NEDO (No.16101402-0).

References

- [1] J. Onoe *et al.*, “*Clusters and Nanomaterials: Theory and Experiment*” (Y. Kawazoe *et al* eds.), Springer, Chap. 6, pp.135–169 (2001) and references therein.
- [2] H. Shima and J. Onoe, “*The Role of Topology in Materials*” (S. Gupta and A. Saxena eds.), Springer, Chap. 3, pp.53–84 (2018) and references therein.
- [3] J. Onoe, “Interplay between topology-induced geometry and properties of nanocarbon materials” (**Keynote address**), *33rd Summer Conference on Topology and its Applications*, Bowling Green, KY, USA, July 17-20 (2018).
- [4] J. Onoe, “Riemannian geometric effects on electronic properties”, *HYOMEN KAGAKU* **34**, 38–43 (2013). [in Japanese]
- [5] For example, S. Matsutani, “Quantum mechanics of submanifolds IV”, *GENDAI SUGAKU* Issue **9**, 86–87 (2020). [in Japanese]
- [6] M. Nakaya *et al.*, *Adv. Sustain. Sys.*, 2000156 (2020). [**Press release**]
- [7] J. Onoe *et al.*, *J. Appl. Phys.* **96**, 443–445 (2004).
- [8] J. Onoe *et al.*, *AIP Adv.* **10**, 085212 (2020). [**Editor’s pick**]

*Corresponding Author: J. Onoe (E-mail: j-onoe@energy.nagoya-u.ac.jp)

Synthesis, structure, processing and electronic devices using 2D layered Noble Metal Dichalcogenides PdSe₂ and PtS₂

Jamie Warner ^{1,2}

¹ *Texas Materials Institute, The University of Texas at Austin, Austin, TX, US.*

² *Departure of Mechanical Engineering, The University of Texas at Austin, Austin, TX, US.*

2D materials have expanded well beyond graphene and the pursuit of new properties in stable monolayers is driving extensive research into various systems, primarily those that use metal-chalcogen bonding. Noble Metal Dichalcogenides (NMDs) are produced using Pt or Pd along with S, Se or Te atoms to form a new class of 2D layered materials with properties ranging from metallic to semi-metal and small band gap semiconductors [1]. The unique pentagonal crystal structure of PdSe₂, along with its rich Pd:Se phase diagram, makes it an interesting system to study defects and phase transformations into Pd₂Se₃ [2-4]. I will discuss our recent ways to synthesis Pd and Pt based NMDs using solution precursors and the resultant crystal structures that are grown directly on graphene and MoS₂ monolayers [3]. The understanding of the atomic structure will be given using annular dark field scanning transmission electron microscopy, with in-situ heating to drive phase transformations [4,6]. I will discuss how to directly process PdSe₂ thin films using focused laser irradiation, and the integration into nanoscale electronic devices [5]. The lateral and vertical epitaxy with other 2D transition metal dichalcogenides (TMDs), MoS₂ and WS₂, will be discussed (figure 1), along with device properties.

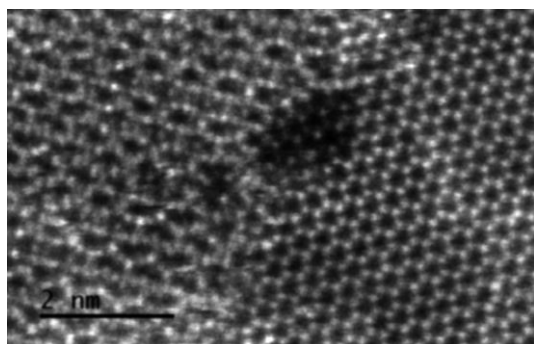


Figure 1. ADF-STEM image of the lateral interface of Pd₂Se₃ with MoS₂

- [1] E. Chen, W. Xu, J. Chen, *2D Layered Noble Metal Dichalcogenides (Pt, Pd, Se, S) for Electronics and Energy Applications*, **Materials Today Advances**, 7, 100076, (2020)
- [2] J. Chen, G. Ryu, S. Sapna, J. H. Warner, *Atomic Structure and Dynamics of Defects and Grain Boundaries in 2D Pd₂Se₃ Monolayers*, **ACS Nano**, 13, 8256-8264, (2019)
- [3] K. L. Tai, et al., *Phase Variations and Layer Epitaxy of 2D PdSe₂ Grown on 2D Monolayers by Direct Selenization of Molecular Pd Precursors*, **ACS Nano**, 14, 11677-11690, (2020)
- [4] G. H. Ryu, et al., *Striated 2D Lattice with Sub-nm Etch Channels by Controlled Thermally Induced Phase Transformations of PdSe₂*, **Advanced Materials**, 31, 1904251, (2019)
- [5] V. Shautsova, et al., *Direct Laser Patterning and Phase Transformation of 2D PdSe₂ Films for On Demand Device Fabrication*, **ACS Nano**, 13, 14162-14171, (2019)
- [6] G. H. Ryu, et al., *Thermally Driven Phase Transition of 2D Few-Layered 1T PtSe₂ into Ultrathin 2D Non-Layered PtSe Crystals*, **Chemistry of Materials**, 31, 9895-9903, (2019)

Corresponding Author: J. Warner

E-mail: Jamie.warner@austin.utexas.edu

Organic synthetic approaches to nanocarbon-based hybrid materials

○Haruka Omachi^{1,2}

¹ *Research Center for Materials Science, Nagoya University, Nagoya 464-8602, Japan*

² *Department of Chemistry, Graduate School of Science, Nagoya University, Nagoya, 464-8602, Japan.*

Owing to their high specific surface area, excellent electrical and mechanical properties, nanocarbon materials such as carbon nanotubes and graphene are widely utilized as the platforms of the hybrid materials for the electronic devices, rechargeable batteries and electrochemical catalysis. Although physical adsorption is commonly used as the simplest immobilization method to prepare hybrid materials, it is not suitable for the well-defined structural control and achieving long-term stability.

In this presentation, I will talk about the synthesis and fabrication of the nanocarbon-based hybrid materials by using approaches based on organic chemistry: (i) dehalogenative one-dimensional polymerization inside carbon nanotubes [1–3]; (ii) fabrication of carbon nanotube thin films for flexible transistor applications using a cross-linked amine polymer [4]; (iii) direct sulfur-functionalization of graphene oxide and immobilization of molecular clusters and battery applications [5].

[1] Nakanishi, Y.; Omachi, H.; Fokina, N. A.; Schreiner, P. R.; Kitaura, R.; Dahl, J. E. P.; Carlson, R. M. K.; Shinohara, H. *Angew. Chem., Int. Ed.* **2015**, *54*, 10802.

[2] Kinno, Y.; Omachi, H.; Nakanishi, Y.; Shinohara, H. *Chem. Lett.*, **2018**, *47*, 1022.

[3] Kinno, Y.; Omachi, H.; Shinohara, H. *Appl. Phys. Express*, **2020**, *13*, 015002.

[4] Matsumoto, K.; Ueno, K.; Hirotsu, J.; Ohno, Y.; Omachi, H. *Chem. Eur. J.*, **2020**, *26*, 6118.

[5] Omachi, H.; Inoue, T.; Hatao, S.; Shinohara, H.; Criado, A.; Yoshikawa, H.; Syrgiannis, Z.; Prato, M. *Angew. Chem., Int. Ed.* **2020**, *59*, 7836.

Corresponding Author: H. Omachi

Tel: +81-52-789-3660

Web: <https://sites.google.com/view/haruka-omachi/>

E-mail: omachi@chem.nagoya-u.ac.jp

Boron-based new two-dimensional materials: synthesis, characterization, and application

○Takahiro Kondo^{1,2}

¹ Department of Materials Science and Tsukuba Research Center for Energy Materials Science, Faculty of Pure and Applied Sciences, University of Tsukuba, Tsukuba 305-8573, Japan

² Materials Research Center for Element Strategy, Tokyo Institute of Technology, 226-8503, Japan

We have recently synthesized and characterized new two-dimensional materials of hydrogen boride (HB) [1] and boron monosulfide (BS) [2] sheets. HB sheets were synthesized by ion-exchange reaction between protons and magnesium cations in magnesium diboride (MgB_2) as shown in Fig. 1(a). HB sheets were then found to have catalytic activity as solid acid catalysts [3,4], hydrogen release function by the ultraviolet light irradiation [5], reductant property [6], and semimetal electronic structure [7], which is sensitive to the gas adsorption [8]. BS sheets (Fig. 1b and 1c) were prepared by the exfoliation of rhombohedral boron monosulfide (r-BS) synthesized at 5.5 GPa and 1873 K. BS sheets show larger band gap of 2.6 eV compared to that of r-BS (1.7 eV), which is consistent with theoretical prediction. In this talk, synthesis, characterization, and application of these HB and BS sheets will be presented.

Acknowledgement

This work was done with Mr. H. Nishino, Mr. R. Ishibiki, Mr. T. Goto, Mr. A. Fujino, Mr. H. Kusaka, Mr. R. Kawamura, Prof. T. Fujita, Dr. T. Tominaga, Dr. N. T. Cuong, Dr. S. Tominaka, Prof. M. Miyauchi, Prof. S. Iimura, Prof. A. Hirata, Dr. N. Umezawa, Prof. S. Okada, Prof. E. Nishibori, Dr. S. Ito, Prof. J. N. Kondo, Dr. T. Fujitani, Prof. I. Matsuda, Prof. J. Nakamura, Dr. T. Masuda, Dr. T. Taniguchi, Dr. K. Watanabe, Dr. M. Miyakawa, Prof. S. Saito, Dr. M. Toyoda, Prof. I. Hamada, Prof. A. Yamamoto, Dr. K. Horiba, and Prof. H. Hosono.

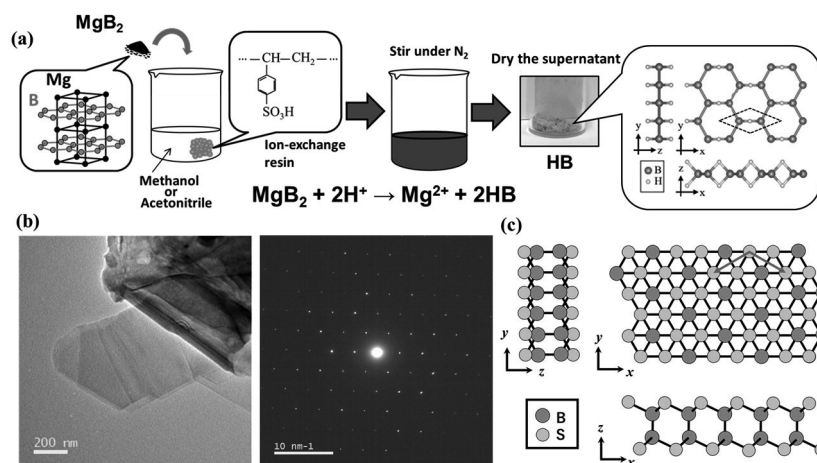


Fig. 1 (a) schematic of the synthesis method of HB sheets, (b) TEM image and diffraction pattern of BS sheets, (c) schematic structure of the BS sheet.

[1] H. Nishino, T. Fujita, N. T. Cuong, S. Tominaka, et al., *J. Am. Chem. Soc.* **139**, 13761 (2017).

[2] H. Kusaka, R. Ishibiki, et al., (to be submitted).

[3] A. Fujino, S. Ito, T. Goto, R. Ishibiki, J. Kondo, T. Fujitani, et al., *ACS Omega* **4**, 14100 (2019).

[4] A. Fujino, S. Ito, T. Goto, R. Ishibiki, J. Kondo, et al., *Phys. Chem. Chem. Phys.* Advanced publication (2021).

[5] R. Kawamura, N. T. Cuong, T. Fujita, et al., *Nat. Commun.* **10**, 4880 (2019).

[6] S. Ito, T. Hirabayashi, R. Ishibiki, R. Kawamura, T. Goto, et al., *Chem. Lett.* **49**, 789 (2020).

[7] I. Tateishi, N. T. Cuong, et al., *Phys. Rev. Materials* **3**, 024004 (2019).

[8] S. Tominaka, R. Ishibiki, A. Fujino, et al., *Chem* **6**, 406 (2020).

Corresponding Author: T. Kondo

Tel: +81-29-853-5934, Fax: +81-29-853-5934,

E-mail: takahiro@ims.tsukuba.ac.jp

Characterization methods for the ensemble state of network structured nanomaterials

Takahiro Morimoto

*CNT-Application Research Center, National Institute of Advanced Industrial Science and Technology
(AIST), Tsukuba 305-8565, Japan*

The networked and entangled structure is one important key feature for understanding the phenomenon in various devices and materials of carbon nanomaterials. Therefore, how to measure and control these structures are obviously important problem for the nano-carbon material research fields. In this session, I will present the two topics of our recent progress for developing unique characterization method based on the one-dimensional (1D) plasmon [1-3] and lock-in thermography (LIT) technique [4,5]. 1D plasmon resonance are useful for the CNT length and crystallinity characterization during short measurement time compare than the conventional AFM counting method. LIT method is also powerful tool for visualization the current density, which directly related to the bulk electrical properties. These methods promise to provide an important information, which complement conventional method.

CNTs show the strong absorption peak in the wavelength range from far-infrared to Tera-hertz region. This optical absorption phenomenon was firstly attracted as the mini-gap excitation as reported in the STM measurement [6]. For understanding this phenomenon, however, we carefully investigated the length dependent of these absorption peaks without changing on the diameters [1]. These results strongly indicate that the resonance spectra are originated from the plasmon resonance on the CNT length directions. In this time, I will present the recent progress on the length distribution, resonance confinement-controlled graphene devices, and various applications [7-10]. LIT are imaging method for the current density distribution via infrared radiation due to Joule heating, which has been originated from the local energy dissipation related nanoscale electron-phonon scattering. This means that we can obtain the useful information from a graveyard of energy, namely, “heat”. In another aspect, the conventional method based on a SPM technique has been needed some perturbation at the local position of samples. LIT method, however, is completely non-destructive and non-contact method. Therefore, LIT enable whole devices and material imaging with one shot accumulation during very short measurement time. I will also present the fundamental background and various related works with LIT technique [4,5,11].

- [1] T. Morimoto *et al.* ACS Nano, **8**, 9897 (2014).
- [2] T. Morimoto *et al.* Applied Physics Express, **8**, 055101 (2015).
- [3] T. Morimoto *et al.* Physical Review B, **93**, 195409 (2016).
- [4] T. Morimoto *et al.* Scientific Reports, **9**, 14572 (2019).
- [5] H. Nakajima *et al.* Science Advances, **5**, eaau3407 (2019).
- [6] M. Ouyang *et al.*, Science, **292**, 702-705 (2001).
- [7] T. Morimoto *et al.*, submitted (2021).
- [8] Xueli Wu *et al.*, Journal of Physical Chemistry C, **120**, 20419-20427 (2016).
- [9] Xueli Wu *et al.*, Applied Physics Express **10**, 055101 (2017).
- [10] N. Tajima *et al.*, Carbon **152**, 1-6 (2019).
- [11] Thanh Binh Nguyen Thi *et al.*, Carbon **153**, 136-147 (2019).

Corresponding Author: Takahiro Morimoto

Tel: +81-29-861-3804, Fax: +81-29-851-5425,

E-mail: t-morimoto@aist.go.jp

招待講演
Invited Lecture

1 I-1 ~ 1 I-2
2 I-1 ~ 2 I-5

What We Know about Single-Walled Carbon Nanotube Growth

Yan Li

College of Chemistry and Molecular Engineering, Peking University, Beijing 100871, China

Catalysts play important roles in CVD growth of single-walled carbon nanotubes (SWCNTs). The catalysts can maintain their crystalline structure or melt during the CVD process and consequently the SWCNT will grow through vapor-solid-solid (VSS) or vapor-liquid-solid (VLS) pathways. It is essential to understand how the diameter, chiral angle, or even the chirality of the resultant nanotubes are determined.

We found that the chiral angle distribution is very random when normal transition metal catalysts such as Cu, Fe, Co, and Ni. Then we choose metallic Co and intermetallic compound Co_7W_6 as typical catalysts and compared the growth processes of the two kind of catalysts by *in situ* studies. We studied the composition and structure of Co and Co_7W_6 nanocrystals in methane, carbon monoxide, and hydrogen at the temperature of 700–1100 °C by using environmental aberration-corrected transmission electron microscopy in combination with *in situ* synchrotron X-ray absorption spectroscopy. we directly present the structural and composition evolution of cobalt catalysts during the nucleation and growth of SWCNTs under carbon feeding. In the case of Co nanoparticles, the co-existence of cobalt and cobalt carbide was generally observed among the catalysts which are active in nucleating tubes. However, the structure and chemical composition of the Co_7W_6 nanocrystals were stable under the atmosphere of methane, carbon monoxide, and hydrogen at high temperature. The SWCNTs grown from Co_7W_6 nanocrystals also show smaller diameter than the catalysts. But the distribution of the tube diameters is discrete. The above observations reveal the difference in growth mechanism of the two types of catalysts.

We found by *in situ* observation that when Co is in molten state, the tubes grown via the VLS pathway always have similar diameter to the size of catalysts. However, the tubes grown from solid state Co nanoparticles always present smaller diameter than the catalysts and no structure-correlation. But SWCNTs grown with Co_7W_6 also showed smaller diameter than the catalyst particles. Nevertheless, the chiralities of the tubes are determined by the template effect of the catalysts, realizing chirality-specific growth of SWCNTs.

Corresponding Author: Yan. Li

Tel & Fax: +86-10-6275-6773

E-mail: yanli@pku.edu.cn

Strongly correlated electrons in a moiré superlattice probed with exciton spectroscopy

○Yuya Shimazaki¹, Ido Schwartz¹, Kenji Watanabe², Takashi Taniguchi², Martin Kroner¹,
Atac Imamoglu¹

¹ *Department of Physics, Institute for Quantum Electronics, ETH Zurich, Zurich 8093, Switzerland*
² *National Institute for Materials Science, Ibaraki 305-0044, Japan*

2D material moiré heterostructure constitute a novel platform to study many body physics of electrons and excitons. Transport study of twisted bilayer graphene revealed rich exotic phase of electrons including from Mott insulator state to superconductivity. On the other hand, optical spectroscopy study revealed the effect of moiré lattice potential on excitons in transition metal dichalcogenide (TMD) heterostructure, but the correlated phase of electrons has been elusive.

In this talk, I will present optical spectroscopy study of homo bilayer TMD moiré heterostructure, and report the observation of strongly correlated incompressible electronic state [1]. We utilized a boron nitride (hBN) encapsulated MoSe₂ / hBN (1L) / MoSe₂ heterostructure with top and bottom gates, which enable independent control of the chemical potential and the electric field. Tightly bound excitons in TMD interact with Fermi sea carriers by forming exciton-polaron, and we utilized the energy shift of exciton-polaron resonance to detect layer resolved charge configuration by optical means. In low electron density regime, we found periodic chemical potential dependence of carrier filling behavior indicating existence of moiré subband structure (Fig. 1). By analyzing interlayer charge transfer behavior between top and bottom MoSe₂ while tuning electric field, we figured out abrupt interlayer charge transfer happens at specific filling around 1 electron / moiré unit cell, evidencing the emergence of strongly correlated incompressible electronic state. In this incompressible state, we also observe emergence of new excitonic resonances from umklapp scattering, which is evidencing the emergence of charge order [2].

This highly tunable twisted MoSe₂ homo bilayer system separated by a monolayer hBN barrier with weak moiré potential, provides a promising platform for investigating strongly correlated Mott-Wigner physics.

[1] Y. Shimazaki *et al.* Nature, **580**, 472 (2020).

[2] Y. Shimazaki *et al.* arXiv:2008.04156 (2020).

Corresponding Author: Y. Shimazaki

Tel: +41-44-633-09-51,

E-mail: yuyas@phys.ethz.ch

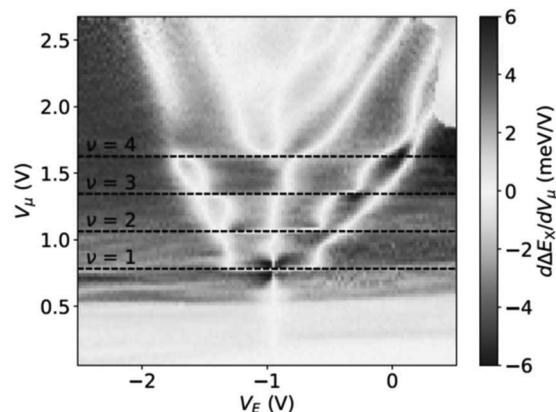


Fig. 1 Layer resolved periodic charge filling behavior revealed by excitonic charge sensing.

Improved properties, increased production, and the path to broad adoption of carbon nanotube fibers

Lauren W. Taylor¹, Oliver S. Dewey¹, Robert J. Headrick^{1,2}, Natsumi Komatsu³, Nicolas Marquez Peraca⁴, Geoff Wehmeyer⁴, Junichiro Kono^{3,5}, Matteo Pasquali^{1,2,5}

Departments ¹ Chemical and Biomolecular Engineering, ² Chemistry, ³ Electrical and Computer Engineering, ⁴ Mechanical Engineering, and ⁵ Materials Science and NanoEngineering
The Smalley-Curl Institute; The Carbon Hub, Rice University, Houston, Texas, USA

We report the latest properties of solution spun carbon nanotube fiber (SS-CNTF, [1]) and discuss them in the context of the overall field of CNTF, as well as the broader field of high-performance fibers. Using high aspect ratio, high purity carbon nanotubes (CNTs), we have produced neat SS-CNTF with an electrical conductivity of 10.9 MS/m, a tensile strength of 4.2 GPa, and a thermal conductivity of 390 W/m K [2]. We observe that electrical conductivity and strength of SS-CNTF have grown at $\sim 25\%$ yearly rate, i.e., they doubled every three years since the first reports in the mid-2000s [3]. This increase in properties has been due to improved CNT synthesis [4], understanding of the effect of CNT crystallinity and aspect ratio on the CNT phase behavior [5] and fiber properties [6]. Importantly, strength and conductivity scale linearly with CNT aspect ratio for highly crystalline CNTs (Raman G/D ratio > 50). Because the theoretical limits are an order of magnitude away from current properties, and the current results have been attained with $\sim 10 \mu\text{m}$ long CNTs, another doubling of properties could be achievable in 3 to 5 years. SS-CNTF would then be stronger than any other fiber material and as electrically and thermally conductive as most metals. Companies are driving up scale and lowering costs of CNT and CNTF production, with basic fiber-grade CNT material now available at $\sim 2,000$ \$/kg at the 100 Ton/yr scale and higher-quality CNT material at about 100x higher price and lower volume. If recent trends in properties, cost, and scale can be sustained for the next years, CNTF will be primed for large-scale market adoption.

- [1] N. Behabtu *et al.* Science, **339**, 182 (2013).
 [2] L. Taylor *et al.* Carbon, **171**, 689 (2021).
 [3] L. Ericson *et al.* Science, **305**, 1447 (2004).
 [4] B. Shukla *et al.* Chem. Commun., 3422– (2009).
 [5] D. Tsentlovich *et al.* Macromolecules, **49**, 681 (2016).
 [6] D. Tsentlovich *et al.* ACS Appl. Mater. Interfaces, **9**, 36189 (2017).
 [7] www.dexmat.com

Corresponding Author: M. Pasquali

Tel: +1 (713) 348-5830, Fax: +1 (713) 348-5478, E-mail: mp@rice.edu
 COI: M. P. is a co-founder and holds a financial interest in DexMat.

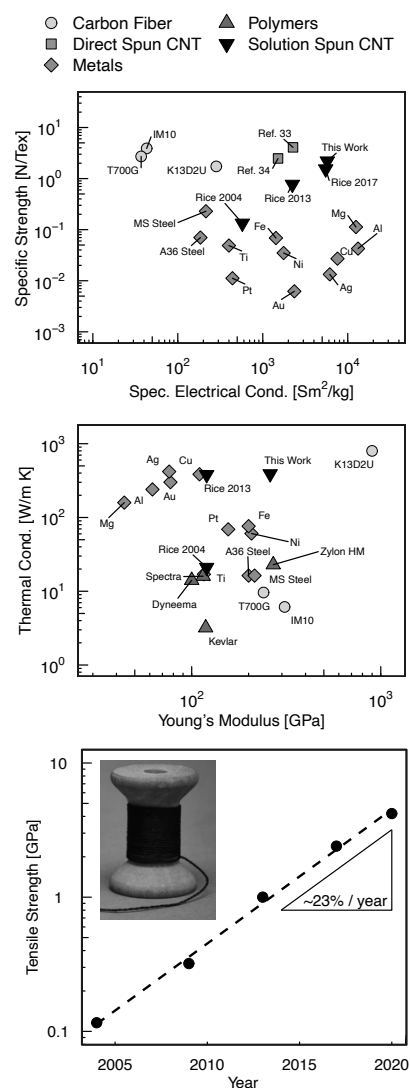


Fig. 1 (top) Specific strength and conductivity of high-performance materials. (middle) thermal conductivity vs. modulus of high-performance materials. (bottom) Learning curve of tensile strength vs. time for wet-spun CNT fibers [2]. Inset: a spool of DexMat's Galvorn™ CNTF yarn [7].

Ultrahigh-Conductivity Carbon Nanotube Fibers with Giant Thermoelectric Power Factor

Natsumi Komatsu,¹ Yota Ichinose,² Oliver S. Dewey,³ Lauren W. Taylor,³ Mitchell Trafford,³
Yohei Yomogida,² Geoff Wehmeyer,^{4,5} Matteo Pasquali,^{3,5,6,7} Kazuhiro Yanagi,² and
Junichiro Kono^{1,7,8}

¹Department of Electrical and Computer Engineering, Rice University, Houston, Texas, USA

²Department of Physics, Tokyo Metropolitan University, Tokyo 192-0372, Japan

³Department of Chemical and Biomolecular Engineering, Rice University, Houston, Texas, USA

⁴Department of Mechanical Engineering, Rice University, Houston, Texas, USA

⁵Carbon Hub, Rice University, Houston, Texas, USA

⁶Department of Chemistry, Rice University, Houston, Texas, USA

⁷Department of Materials Science and NanoEngineering, Rice University, Houston, Texas, USA

⁸Department of Physics and Astronomy, Rice University, Houston, Texas, USA

Thermoelectric (TE) materials can convert heat into electricity and vice versa, offering great potential for waste heat recovery and solid-state cooling. Carbon nanotubes (CNTs) are strong candidates for TE materials due to one-dimensional (1D) quantum confinement of charge carriers and their superb electrical and mechanical properties. Although semiconducting single-wall carbon nanotubes (SWCNTs) have been mainly studied, Ichinose *et al.* recently have shown that metallic SWCNTs can exhibit higher power factor when the Fermi energy is strategically tuned.^[1] Here, we studied the thermoelectric properties of aligned CNT fibers (Fig. 1a) with an ultrahigh electrical conductivity ($>10^6 \text{ Sm}^{-1}$)^[2,3] by varying the Fermi energy. When the Fermi energy was near the first van Hove singularity in the electronic density of states, the conductivity and Seebeck coefficient were enhanced simultaneously, resulting in a giant thermoelectric power factor value of $14 \pm 5 \text{ mWm}^{-1}\text{K}^{-2}$ (Fig. 1b), the highest value ever achieved for CNTs (Fig. 1c). These CNT fibers are also flexible, weavable, and large-scale, allowing us to fabricate a textile TEG with enough output power to drive a light-emitting diode. The unique combination of giant thermoelectric power factor, flexibility, and scalability in the CNT fibers promises an unprecedentedly diverse range of TE applications.

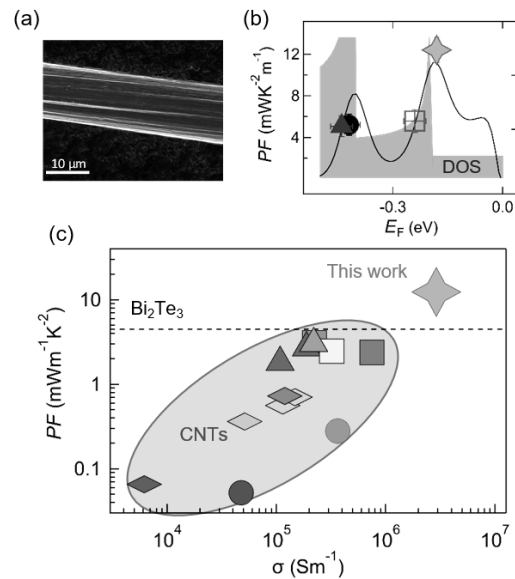


Fig. 1 (a) SEM image of the aligned CNT fiber. (b) The Fermi energy was tuned to optimize the power factor. (c) Giant power factor we found was higher than all previously reported values for CNTs.

[1] Y. Ichinose *et al.*, *Nano. Lett.* **19**, 7370 (2019).

[2] N. Behabtu *et al.*, *Science* **339**, 182 (2013).

[3] L. Taylor *et al.*, *Carbon* **171**, 689 (2021).

Corresponding Author: J. Kono

Tel: +1 (713) 348-2209, Fax: +1 (713) 348-3091,

E-mail: kono@rice.edu

Stacking-engineered ferroelectricity in bilayer boron nitride

○Kenji Yasuda¹, Xirui Wang¹, Kenji Watanabe², Takashi Taniguchi², Pablo Jarillo-Herrero¹

¹ *Department of Physics, Massachusetts Institute of Technology, Cambridge, Massachusetts 02139, USA.*

² *National Institute for Materials Science, Namiki 1-1, Tsukuba, Ibaraki 305-0044, Japan.*

Recent advances in van der Waals (vdW) assembly enabled the engineering of heterostructures with physical properties beyond the sum of those of the individual layers. One of the most representative examples is small-angle twisted bilayer graphene, whose flat band leads to a variety of emergent phenomena such as superconductivity and magnetism. In this talk, I will demonstrate that the vdW stacking can modify not only the electronic band structure but also the crystal symmetry, thereby enabling the design of ferroelectric materials out of non-ferroelectric parent compounds.

Figure 1a shows the crystal structure of bulk hexagonal boron nitride (BN). The adjacent layer is rotated by 180° (AA' stacking), and therefore, the bulk crystal is centrosymmetric. However, the crystal becomes ferroelectric when two BN sheets are stacked without rotation. The parallel-stacked BN takes the form of AB or BA stacking, which exhibits opposite out-of-plane electric polarization that reverses depending on the stacking order (Fig. 1b and c) [1]. We fabricate the parallel-stacked bilayer BN by “tear-and-stack” procedure and prove the polarization using piezoelectric force microscope and adjacently-stacked graphene sheet [2]. We observe a prominent hysteresis in the resistance of graphene, associated with the ferroelectric switching of parallel-stacked BN (Fig. 1d). The interfacial ferroelectricity persists to room temperature while keeping the high mobility of graphene. The ferroelectric polarization is stable for at least a month, paving the way for potential ultrathin nonvolatile memory applications [2-4].

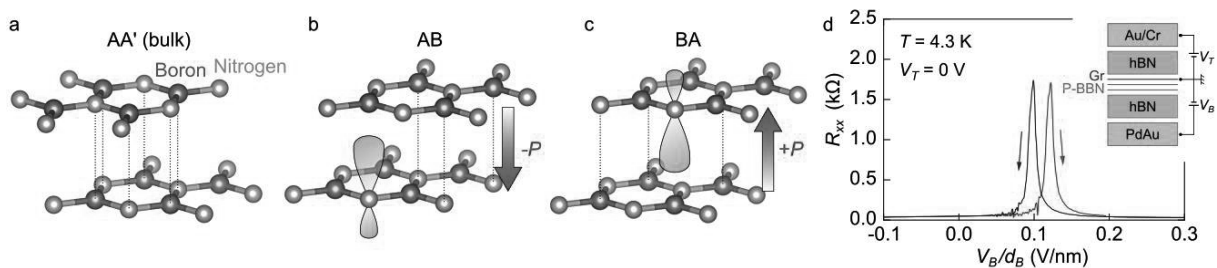


Fig. 1 a, Bulk form of hexagonal boron nitride, AA' stacking. b and c, Parallel-stacked boron nitride with AB and BA stacking. d, Resistance of graphene adjacent to the parallel-stacked boron nitride. The red and blue curves are forward and backward scan, respectively. The device schematics is illustrated in the inset.

[1] L. Li, M. Wu ACS Nano. 11, 6382–6388 (2017).

[2] K. Yasuda *et al.* arXiv:2010.06600

[3] M. V. Stern *et al.* arXiv:2010.05182

[4] C. R. Woods *et al.* arXiv:2010.06914

Corresponding Author: K. Yasuda

Tel: +1-617-460-1382

E-mail: yasuda@mit.edu

Isospin Pomeranchuk effect in twisted bilayer graphene

○Yu Saito¹

¹ *California NanoSystems Institute, University of California at Santa Barbara, CA 93106 USA*

In bilayer graphene rotationally faulted to 1.1 degrees, interlayer tunneling and rotational misalignment conspire to create a pair of low energy flat bands causing strongly correlated phenomena such as correlated insulating states [1], superconductivity [2], and ferromagnetism [3]. An emerging question in twisted bilayer graphene is the role and nature of isospin ferromagnetism [4,5]. In this talk, I will describe experiments probing the finite temperature phase diagram of isospin symmetry breaking in high quality twisted bilayer graphene using transport and thermodynamic measurements [6]. We find that low temperature transport at superlattice filling factor $\nu = -1$ shows no sign of a commensurate correlated phase, but a resistivity peak appears at a high temperature that resembles behavior observed near commensurate where the low temperature phase is a correlated insulator. Tilted field magnetotransport and direct measurements of the in-plane magnetic moment show that the resistivity peak near $\nu = -1$ is adiabatically connected to a metamagnetic phase transition at which the system develops finite isospin polarization. These data are suggestive of a Pomeranchuk-type mechanism, in which the entropy of disordered isospin moments in the ferromagnetic phase stabilizes it relative to the unpolarized Fermi liquid phase at elevated temperatures. Direct thermodynamic measurements of the entropy, S indeed find it to be large, $S \sim 1k_B$ per moiré unit cell, for $\nu \sim \pm 1$, and we find that a fraction of S is suppressed by an in-plane magnetic field consistent with an isospin contribution. In contrast to Helium-3, no discontinuities are observed in the thermodynamic quantities across this transition, implying that the magnetic transitions are continuous in nature. Our findings imply a small isospin stiffness, with implications for the nature of finite temperature transport as well as the mechanisms underlying isospin ordering and superconductivity in twisted bilayer graphene and related systems.

[1] Cao et al. *Nature* **556**, 80 (2018)

[2] Cao et al. *Nature* **556**, 43 (2018), Yankowitz et al. *Science* **363**, 1059 (2019).

Lu et al. *Nature* **574**, 653 (2019). Saito et al. *Nature Physics* **16**, 926 (2020)

[3] Shape et al. *Science* **165**, 605 (2019), Serlin et al. *Science* **367**, 900 (2020)

[4] Zondier et al. *Nature* **582**, 203 (2020)

[5] Saito et al. *Nature Physics* (2021)

[6] Saito et al. *Nature*, in press

Corresponding Author: Yu Saito

Tel: +1-805-202-9115

E-mail: yusaito@ucsb.edu

FC-CVD synthesis of CNTs from methane for transparent conductor applications.

Qiang Zhang, Datta Sukanta, Hua Jiang, Esko I. Kauppinen

*Department of Applied Physics, Aalto University School of Science, PO Box 15100,
FI-00076 Aalto, Espoo, FINLAND*

Due to scalability, low-cost and good control of carbon nanotube (CNT) synthesis, floating catalyst chemical vapor deposition (FC-CVD) keep attracting intense attention in both academic and industrial fields [1,2]. Especially, the CNT aerosol from FC-CVD can be directly deposited into transparent conducting films (TCFs) which are critical components of many optoelectronic devices that pervade modern technology [1]. Currently, one of the ideal models of high-performance CNT TCFs is the net-work containing long, straight, individual, high-quality single-wall CNTs (SWCNTs) [3]. Many efforts in FC-CVD have been devoted to increasing the conductivity of CNT TCFs based on this model. However, intrinsic nanotube collisions in the aerosol process of FC-CVD lead to a tread-off between yield and performance [3], because bundling increases when increasing the yield i.e. production rate, with the bundling decreasing film transmittance at the given sheet resistance. Here, we report TCFs of large-diameter CNTs from methane-based FC-CVD overcoming the performance–yield tradeoff. Based on the Fe-C-S system, the double-wall CNTs (DWCNTs) with a mean diameter of 4.15 nm and a mean bundle length of 20 μm have been produced into TCFs via FC-CVD. After gold chloride solution doping, the TCFs have an excellent performance of 42 ohm/sq sheet resistance at 90% transmittance. Unexpectedly, these high-performance DWCNTs films have an ultra-high yield i.e. production rate, being two orders of magnitude higher than that of SWCNT based TCFs with similar performance. Especially, these high-yield DWCNTs films contain ‘small’ bundles with around 50% of CNTs being individual, which is completely different from other FC-CVD results for SWCNTs produced at much lower yield. Moreover, the large-diameter DWCNTs will flatten at the junctions, which can provide a larger contact area between the tubes and reduce the contact resistance. These unique features of large-diameter CNTs in ‘small’ bundles are the key to obtain high-performance CNT TCFs with high yield. These results imply a new model with optimization windows for high-performance CNT TCFs with high yields and accordingly at reduced cost, and may accelerate the practical application of CNTs TCFs.

[1] Zhang, Qiang, et al. Topics in Current Chemistry, 99-128 (2019).

[2] Liao, Yongping, et al. Journal of the American Chemical Society 140.31 (2018).

[3] Mustonen, Kimmo, et al. Applied Physics Letters 107.14 (2015).

Corresponding Author: Esko I. Kauppinen

Tel: +358 40 509 8064 Fax: +358 9 2451 3517

E-mail: esko.kauppinen@aalto.fi

一般講演
General Lecture

1 - 1 ~ 1 - 10

2 - 1 ~ 2 - 8

3 - 1 ~ 3 - 12

Correlation between the thermal and mechanical properties of the high temperature thermal- treated carbon nanotube yarns

○Ryo Shikata¹, Yuho Shigeeda², Hirotaka Inoue², Hiroo Suzuki², Wataru Yajima¹, Tomohiro Nakagawa², Takeshi Nishikawa², Yoshifumi Yamashita², Yasuhiko Hayashi², Masaki Hada³

¹College Engineering Sciences, Tsukuba University, Tsukuba 305-8573, Japan

²Graduate School of Natural Science and Technology, Okayama University, Okayama 700-8530, Japan

³Tsukuba Research Center for Energy Material Science (TREMS), Tsukuba University, Tsukuba 305-8573, Japan

A carbon nanotube (CNT) exhibits extremely high thermal transport and physical properties. However, the properties of assembled CNTs, *e.g.*, CNT yarns, are significantly lower than those of a CNT due to the interfacial structure between the CNTs. In general, amorphous carbon (*a*-C) between the CNTs in dry-spun CNT yarns causes a decrease in the properties of CNT yarns. Thus, one of the key strategies to enhance the properties of assembled CNTs is to remove the interfacial *a*-C or to convert *a*-C into graphene by annealing. In our previous study, we have found that annealing can induce graphene from *a*-C in the interface between CNTs in CNT yarn [1,2]. The graphene formation can improve interaction at the interface between CNTs, which enhances the thermal conductivity of the CNT yarn. Due to the improvement of interfacial interaction, it also suggests that the mechanical strength of CNT yarns would be enhanced by annealing. In this study, we investigated the mechanical strength of CNT yarns after annealing at various temperatures. Figures 1 and 2 show the thermal conductivity and effective tensile strength of CNT yarns as a function of annealing temperature, respectively. The effective tensile strength is recalculated from the tensile strength using the effective cross-section of the CNT-yarns. Both the properties linearly increase above the annealing temperature of ~ 2000 K. The result suggests that the thermal transport and physical properties of assembled CNTs are simultaneously enhanced by the high-temperature annealing *via* the graphene formation and improvement of the interfacial interaction between the CNTs.

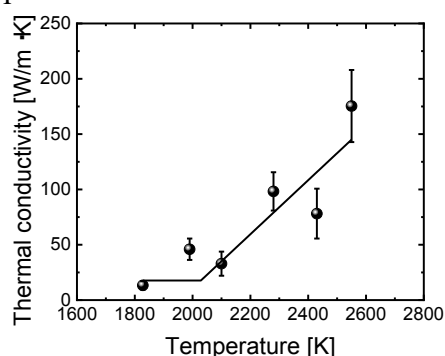


Fig. 1 Thermal conductivity of CNT yarns as a function of annealing temperature

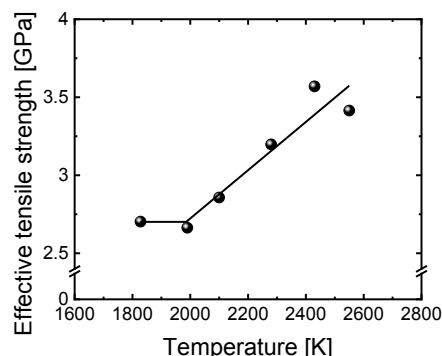


Fig. 2 Effective tensile strength of CNT yarns as a function of annealing temperature

[1] M. Hada et al., *ACS. Appl. Energy Mater.* **2**, 7700 (2019).

[2] M. Hada et al., *Carbon* **170**, 165 (2020).

Corresponding Authors: M. Hada, Y. Hayashi

Tel: +81-29-853-5289, +81-86-251-8230

E-mail: hada.masaki.fm@u.tsukuba.ac.jp, hayashi.yasuhiko@okayama-u.ac.jp

Unraveling Thermoelectric Dimensionless Figure-of-Merit of Aligned Single-Walled Nanotube Thin-Film

○Kan Ueji¹, Yota Ichinose¹, Yuya Matsuoka¹, Yohei Yomogida¹, Takashi Yagi², Junichiro Kono³, and Kazuhiro Yanagi¹

¹ Department of Physics, Tokyo Metropolitan University, Tokyo 192-0372, Japan

² National Metrology Institute of Japan, National Institute of Advanced Industrial Science and Technology, Tsukuba, Ibaraki 305-8563, Japan

³ Department of Electrical and Computer Engineering, Rice University, Houston, Texas 77005, United States

Evaluation of the dimensionless figure-of-merit: $ZT = (S^2\sigma T)/\kappa$, where S , T , σ , and κ denote the Seebeck coefficient, absolute temperature, electrical and thermal conductivities, respectively, is especially important for characterization of thermoelectric performance of materials. Recently, thermoelectric performance of thin film materials attracts a lot of interests, and a lot of studies have clarified the relationships among S , σ , and the electronic structures of materials. However, for thin-film systems, the understanding of the relationships between κ and σ has still been limited because evaluation of the thermal conductivity of thin films with systematically different doping levels is technically difficult. To overcome this problem, we have developed a unique time-domain thermoreflectance (TDTR, which is a pump-probe technique) method in which κ of nanoscale materials can be estimated *in situ* during electrolyte gating.^[1] In this study, we attempt to determine the ZT values of SWCNT thin-films with different doping levels using the electrolyte gating TDTR method.

Single-walled carbon nanotubes (SWCNTs) are promising candidates for enhancing the ZT value owing to their low-dimensionality.^[2] In this study, we employed aligned SWCNT films because the measurement directions of charge transport and heat flow become approximately identical (Fig. 1). To produce the aligned SWCNT films, dispersed SWCNTs with a surfactant in an aqueous solution were filtered with a membrane with a grating area at reduced pressure. The filtered aligned SWCNTs on the membrane were transferred onto a glass substrate with a patterned Au layer as an electrode and a TDTR transducer; S , σ , and κ were determined with the previously reported methods during electrolyte gating.^[1,3]

The maximal power factor ($S^2\sigma$) regarding the transverse intertube junction in the aligned SWCNT film with different doping level is approximately $56 \mu\text{W}/\text{mK}^2$ at room temperature. In addition, the thermal conductivity along the cross-plane direction (approximately $0.15 \text{ W}/\text{mK}$ at room temperature) is independent of the gate voltage. Therefore, ZT of the aligned SWCNT thin film is assumed to exceed 0.1, which is relatively high for flexible materials. The details of this study will be discussed in the presentation.

[1] K. Ueji *et al.*, *Appl. Phys. Lett.*, **117**, 133104 (2020).

[2] L. D. Hicks *et al.*, *Phys. Rev. B*, **47**, 16631 (1993)

[3] Y. Ichinose *et al.*, *Nano Lett.*, **19**, 7370 (2019)

Corresponding Author: K. Ueji (kueji@tmu.ac.jp) and K. Yanagi (yanagi-kazuhiro@tmu.ac.jp)

Tel: +81-42-677-2494.

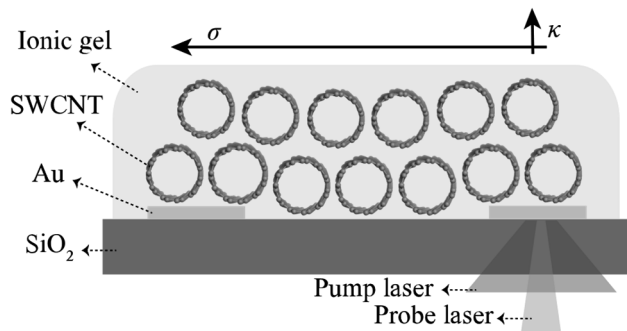


Fig. 1 Schematic measurement system for the ZT of aligned SWCNT film during electrolyte gating.

Fabrication and characterization of oriented carbon nanotube/polymer composite films for high thermal conductivity

°Nikita Kumari, Maireeye Bhattacharya, Ryo Abe, Naofumi Okamoto, Manish Pandey, Masakazu Nakamura

Division of Material Science, Nara Institute of Science and Technology, 8916-5 Takayama-cho, Ikoma, Nara 630-0192, Japan

Carbon nanotubes (CNTs) possessing unique chemical structure and uni-dimensionality, have been witnessing huge significant scientific research and development. Their exceptional mechanical, thermal, and electrical properties have qualified them for fabricating efficient, lightweight, portable, and flexible electronics [1]. Theoretical and simulation results predicted CNTs to have very high phonon-dominated thermal conductivity of thousands of $\text{W}\cdot\text{m}^{-1}\cdot\text{K}^{-1}$ [2]. However, so far reported thermal conductivity lags far behind from those values which is generally attributed to the difficulties in fabrication of ideally oriented CNT networks in CNT/polymer composite films, which is an essential requirement for planer heat transport in prospective vertically integrated flexible and wearable electronics. Thereby, facile techniques for orientated film fabrication are highly desirable to fully harness the inherent anisotropic properties of single CNTs for practical applications.

A new technique, for fabricating ribbon-shaped oriented CNT/polymer composite films using a programmable robotic dispenser, has been recently reported by our group [3]. It is hypothesized that, due to shear stress at the needle's inner wall, the CNTs get aligned parallel to it when the dispersion of CNT/polymer composite is dispensed. In the present work, the effect of various parameters on the CNT orientation was studied and optimized by fabricating the films under varying conditions and comparing the corresponding polarized-Raman spectra. Consequently, around four-fold enhancement in average CNT orientation (in terms of G-band ratio) in the film was achieved compared to the reference sample. Which further resulted in almost two times enhancement in the thermal diffusivity. The details of film fabrication with optimum CNT alignment by controlling the casting parameters where the streamlined orientation is preserved and their various characterization results will be discussed during the presentation.

This work was supported by JST CREST Grant Number JPMJCR18I3, Japan.

[1] Z. Han, Alberto Fina, *Prog. Polym. Sci.* **36**, 914 (2011).

[2] T. Ji *et al.* *Composites: Part A* **91**, 351 (2016).

[3] Pandey *et al.* *Appl. Phys. Express* **13**, 065503 (2020).

Corresponding Author: M. Nakamura

Tel:+81-743-72-6031; Fax:+81-743-72-6047; E-mail:mnakamura@ms.naist.jp

Effect of CO₂ during annealing on formation of catalyst particles and growth of single-wall carbon nanotubes on substrates

Mochen Li¹, Hisashi Sugime¹, Suguru Noda^{1, 2*}

¹ Waseda Research Institute for Science and Engineering, Waseda University, 3-4-1 Okubo, Shinjuku-ku, Tokyo 169-8555, Japan

² Department of Applied Chemistry, Waseda University, 3-4-1 Okubo, Shinjuku-ku, Tokyo 169-8555, Japan

In this research, the effects of CO₂ during annealing on formation of catalyst particles and growth of single-wall carbon nanotubes (SWCNTs) on substrates were investigated systematically. The Fe (1 nm)/AlO_x (15 nm) catalyst sputter-deposited on SiO₂/Si substrates showed prolonged catalyst lifetime and yielded taller SWCNT forests of higher areal mass and better alignments when annealed under 10 vol% H₂/Ar without CO₂ than with 1 vol% CO₂. Detailed analysis showed the catalyst maintained dense Fe layer and constant surface content of Fe after annealing without CO₂ for 5-30 min while Fe diffused into AlO_x support layer quickly when annealed with CO₂. These results indicated that the added/residual oxidant could partially oxidize Fe and increase its solubility in AlO_x. Therefore, our research emphasized the importance of maintaining a highly reductive atmosphere at the annealing stage to achieve active catalyst particles with higher number density and longer lifetime.

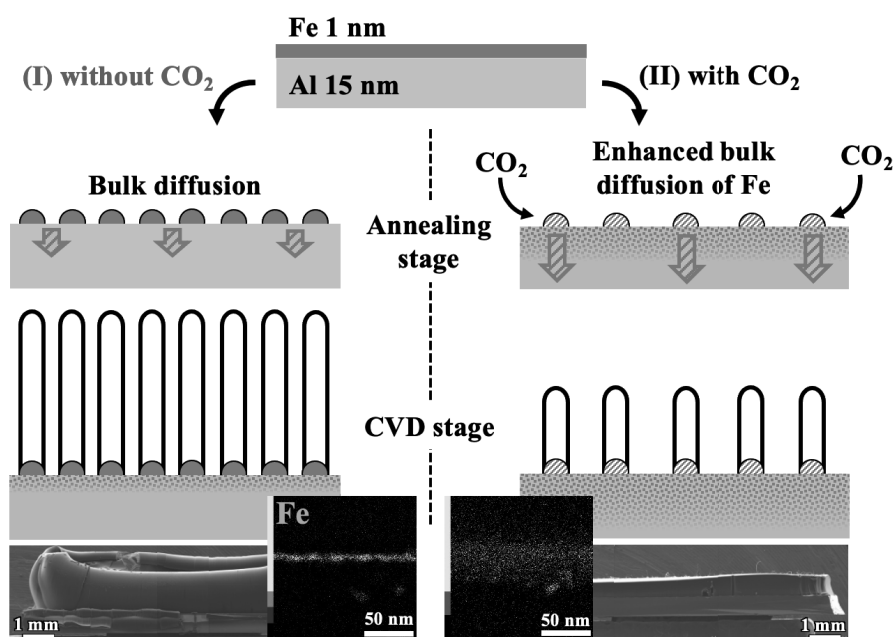


Fig. 1. The effects of CO₂ during annealing on the formation of catalyst particles and growth of SWCNTs. Schematic is shown with side-view scanning electron microscope (SEM) images of the resulting SWCNT forests and elemental maps of the catalyst layer by scanning transmission electron microscope-energy dispersive spectroscopy (STEM-EDS).

Corresponding Author: S. Noda

Tel: +81-03-5286-2769, Fax: +81-03-5286-2769, E-mail: noda@waseda.jp

Formation of Ultra-slender CNTs via Field Emission Discharge of CNT films

○Yahachi Saito¹ and Koji Asaka²

¹ Toyota Physical and Chemical Research Institute, Nagakute-city 480-1192, Japan

² Department of Applied Physics, Nagoya University, Nagoya 464-8603, Japan

A few years ago, we reported a new method to produce long linear carbon chains (LCCs) encapsulated in single-wall carbon nanotubes (SWCNTs) by using field emission (FE)-induced discharge of CNT films [1, 2]. Subsequent scrutiny of the CNT films subjected to the FE-discharge revealed the presence of ultra-slender SWCNTs with diameters of about 0.4 nm, which were absent before the FE-discharge. In the present report, Raman spectroscopy and transmission electron microscopy (TEM) study on the CNT films showing the formation of ultra-slender SWCNTs via FE-discharge is presented.

CNT films used for the FE experiment were pieces cut from a mat of eDIPS CNT (Meijo Nano Carbon). Figures 1 (a) and (b) show Raman spectra of the CNT film before and after the FE discharge, respectively. Comparison between the two radial-breathing mode (RBM) regions reveals that new peaks with high frequencies over ca. 280cm^{-1} are apparently observed after the discharge experience. High-frequency RBM peaks at 511, 565 and 664cm^{-1} are tentatively assigned to (4,3), (5,1) and (5,0) with diameters 0.49, 0.44 and 0.37nm, respectively. Figure 2 shows a TEM picture showing the presence of ultra-slender SWCNTs with diameters 0.43 and 0.45nm. These ultra-slender SWCNTs correspond to the ultimately thin nanotubes which are thermodynamically stable [3]. This report shows a new route to form ultra-slender CNTs.

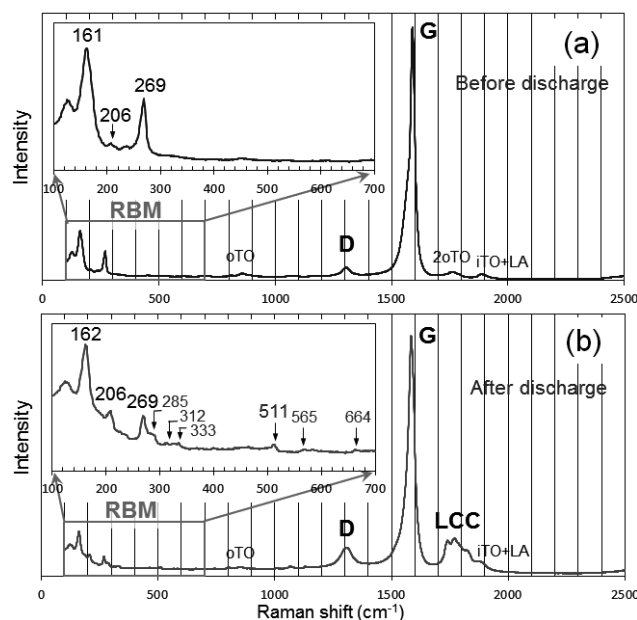


Fig. 1. Raman spectra of CNT films. 785nm excitation.

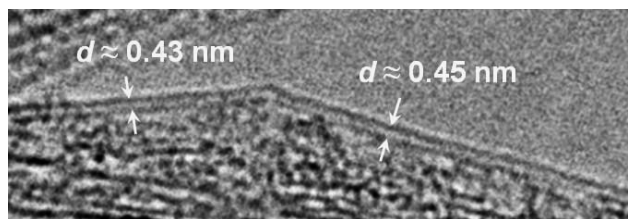


Fig. 2. TEM picture.

[1] S. Toma, K. Asaka, M. Irita and Y. Saito, *Surf. Interface Anal.* **51**, 131 (2019).

[2] K. Asaka, S. Toma, and Y. Saito, *e-J. Surf. Sci. Nanotech.* **18**, 159 (2020).

[3] S. Sawada and N. Hamada, *Solid State Comm.* **83**, 917 (1992)

Corresponding Author: Y. Saito

Tel: +81-561-57-9516, Fax: +81-561-63-6302,

E-mail: ysaito@toyotariken.jp

One-step direct oxidation of alkoxy to ketone for evaporable fullerene-fused ketone as efficient electron-transport materials

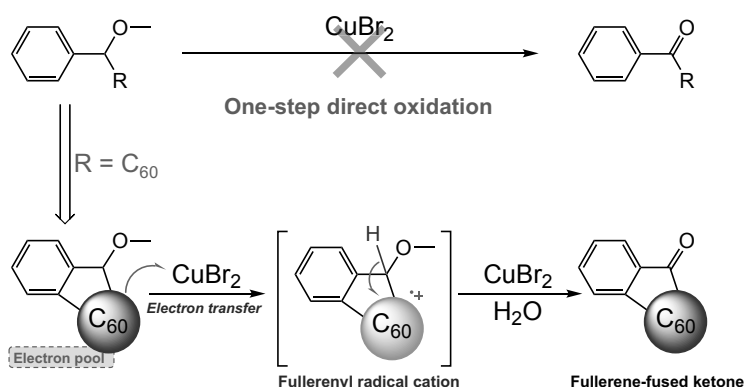
○Hao-Sheng Lin,¹ Yue Ma,² Rong Xiang,¹ Sergei Manzhos,³ Il Jeon,¹ Shigeo Maruyama¹,
Yutaka Matsuo^{1,2*}

¹ Department of Mechanical Engineering, The University of Tokyo, Tokyo 113-8656, Japan

² Hefei National Laboratory for Physical Sciences at the Microscale, University of Science and Technology of China, 96 Jinzhai Road, Hefei, Anhui 230026, China

³ Centre Énergie Matériaux Télécommunications, Institut National de la Recherche Scientifique, 1650 boulevard Lionel-Boulet, Varennes QC J3X1S2 Canada.

Oxidation reactions, such as the direct oxidation of alcohols to aldehydes or ketones, are among the most critical and fundamental transformations in organic synthesis. However, the oxidation methods are limited when alcohols are protected/functionalized with an alkyl group to form the alkoxy structure, which is mainly



attributed to high activation energy barrier for directly converting the alkoxy group to ketone structure. Consequently, the one-step direct oxidation of alkoxy to ketone has yet to be presented. Fullerene, a well-known intrinsically electron-deficient molecule, is prone to accept electrons affording the reduced fullerene anion species for versatile functionalizations. With our interest in exploring the classical organic chemistry reaction under assistance of fullerene, and also inspired by the recent studies on fullerene radical cation ($C_{60}^{+\bullet}$) mediated reaction, we conceived that $C_{60}^{+\bullet}$ should be feasible for the one-step oxidation of alkoxy group to ketone through the electron transfer activation. Herein, we report a copper (II) bromide promoted one-step direct oxidation of alkoxy to ketones with the aid of an oxidizable fullerene pendant. Distinct from the unfavourable energy barrier in direct oxidation of alkoxy group to ketone, fullerene pendant serves as an electron pool for facilitating the electron transfer from the alkoxy structure to oxidant. Mechanistic studies indicate that the fullerene assisted one-step oxidation involves two critical steps: 1) electron transfer from C_{60} to $Cu[II]$ affords $C_{60}^{+\bullet}$, and 2) the generated $C_{60}^{+\bullet}$ attracts electron density from the neighbouring C–H bond, contributing to the further electron transfer from the alkoxy structure to the fullerene cage. Meanwhile, obtained fullerene-fused ketones are fabricated to the electron-transport layers through thermally deposition, which provides the photovoltaic devices with uniformly pin-hole free electron-transport films. The reaction presented herein not only provides an understanding on one-step oxidation of alkoxy group to ketone, but also access the high-quality electron-transport layers through thermally evaporation.

Corresponding Author: Y. Matsuo

Tel: +81-3-5841-6408

E-mail: matsuo@photon.t.u-tokyo.ac.jp

Quantum States of the Endohedral Fullerene Crystal $[\text{Li}^+@C_{60}]\text{PF}_6^-$

○Hideo Ando¹, Yoshihide Nakao²

¹ Faculty of Science, Yamagata University, Yamagata 990-8560, Japan

² Faculty of Life Science, Kyushu Sangyo University, Fukuoka 813-8503, Japan

Endohedral fullerene $\text{Li}^+@C_{60}$ is an ideal porous system for studying the quantized nuclear motion of Li^+ under (sub)nanoscale confinement. Using $\text{Li}^+@C_{60}$ crystallized together with various anions and solvents, Aoyagi *et al.* have clarified that the anions and solvents around the C_{60} cage exterior can substantially affect the distribution of Li^+ [1, 2]. Zhang *et al.* have theoretically revealed that an extremely small cage distortion ($\sim 10^{-3}$ Å) may completely alter the Li^+ wave function [3]. Although recent papers have pointed out the importance of the electronic polarization of the C_{60} cage induced by the nearby ions [4, 5], it has yet to be clarified what intermolecular interactions (de)localize and (de)stabilize the Li^+ wave function of interest.

Focusing on the $[\text{Li}^+@C_{60}]\text{PF}_6^-$ crystal, we developed a model potential energy function that fits a highly-accurate post-Hartree-Fock energy surface for the Li^+ motion. Using the Fourier grid Hamiltonian method, we calculated 803 lowest energy wave functions of Li^+ . The ground state is nearly two-fold degenerate, and its wave functions are mostly localized under two C_6 rings (Fig. 1), near the disorder sites of Li^+ in the X-ray crystal structure [2]. The wave functions are slightly delocalized under six C_6 rings, each of which is contacted by a negatively charged F atom.

We decomposed the potential energy function into four intermolecular interaction energy functions: the quasi-classical electrostatic, exchange repulsion, polarization, and dispersion ones. These functions helped clarify that the shell-shaped adsorbent potential in the cage interior is formed chiefly by the exchange repulsion and the polarization attraction, both of which are strongly dependent on the cage distortion. The relative stabilities among the potential wells underneath the individual ring centers are primarily determined by the exchange repulsion and the electrostatic interaction. Moreover, it turns out that the ground-state wave functions of Li^+ gain substantial polarization stabilization (-21.36 kcal/mol) and somewhat electrostatic and dispersion stabilization (-0.49 , -0.71 kcal/mol) due to their off-centering in the cage. Beyond the common picture of Li^+ moving in a classical electrostatic field, our approach can deepen the understanding of the Li^+ wave function confined in various polarizable nanopores.

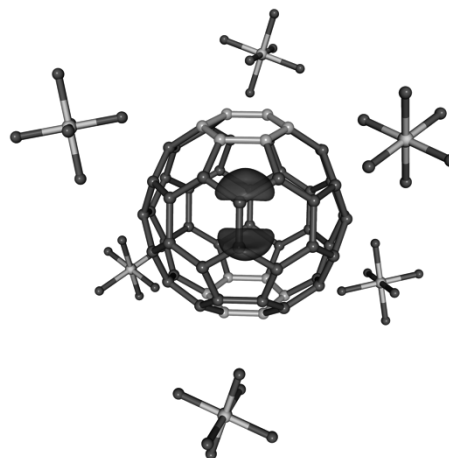


Fig. 1 Isosurfaces of a ground-state wave function of Li^+ in $[\text{Li}^+@C_{60}]6\text{PF}_6^-$ model.

[1] S. Aoyagi *et al.* Nat. Chem., **2**, 678 (2010).

[2] S. Aoyagi *et al.* J. Phys. Soc. Jpn., **85**, 094605 (2016).

[3] M. Zhang *et al.* J. Phys. Chem. A, **112**, 5478 (2008).

[4] G. Raggi, A. J. Stace and E. Bichoutskaia, Phys. Chem. Chem. Phys., **16**, 23869 (2014).

[5] V. V. Chaban and E. E. Fileti, Phys. Chem. Chem. Phys., **17**, 15739 (2015).

Corresponding Author: H. Ando

Tel: +81-23-628-4564, Fax: +81-23-628-4567,

E-mail: ando@sci.kj.yamagata-u.ac.jp

Anionic fluorinated Zn-porphyrin combined with $\text{Li}^+\text{@C}_{60}$ for long-lived photoinduced charge separation with low energy loss

○Kazuhira Miwa¹, Shinobu Aoyagi¹, Takahiro Sasamori², Hiroshi Ueno^{3,4},
Hiroshi Okada^{5,6,7}, Kei Ohkubo⁸

¹Department of Information and Basic Science, Nagoya City University, Nagoya, 467-8501, Japan

²Division of Chemistry, Faculty of Pure and Applied Sciences, and Tsukuba Research Center for Energy Materials Sciences (TREMS), University of Tsukuba, Tsukuba, 305-8571, Japan

³Frontier Research Institute for Interdisciplinary Sciences, Creative Interdisciplinary Research Division, Tohoku University, Sendai, 980-8578, Japan

⁴Department of Chemistry, Graduate School of Science, Tohoku University, Sendai, 980-8578, Japan

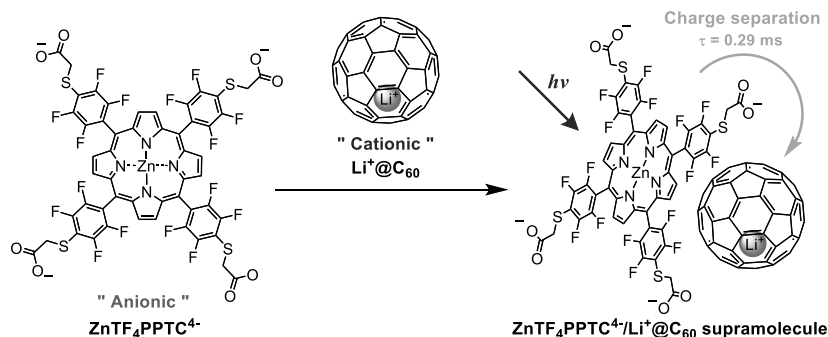
⁵Fukamatsugumi Co., Ltd. Sendai, 981-0931, Japan

⁶Idea International Co., Ltd. Sendai, 981-0922, Japan

⁷Center for Fundamental and Applied Research of Novel Nanocarbon Derivatives, Center for Key Interdisciplinary Research, Tohoku University, Sendai, 980-8578, Japan

⁸Institute for Advanced Co-Creation Studies, Open and Transdisciplinary Research Initiatives, Osaka University, Suita, 565-0871, Japan

A donor-acceptor supramolecular complex consisting of a cationic lithium endohedral [60]fullerene ($\text{Li}^+\text{@C}_{60}$) and an anionic *meso*-tetrakis(sulfonatophenyl) zinc porphyrin (ZnTPPS^{4-}) generates a long-lived photoinduced charge-separated (CS) state with a lifetime of 0.30 ms in benzonitrile at 300 K.^[1] To reduce the energy loss associated with relaxation from the lowest singlet excited state to the CS state, we designed and synthesized an anionic *meso*-tetrakis(4-carboxymethylthio-2,3,5,6-tetrafluorophenyl) zinc porphyrin ($\text{ZnTF}_4\text{PPTC}^{4-}$) to form a supramolecular complex with higher oxidation potential. The energy level of the CS state of the supramolecular $\text{ZnTF}_4\text{PPTC}^{4-}/\text{Li}^+\text{@C}_{60}$ complex determined by electrochemical measurements is at 0.94 eV, which is much higher than that of a supramolecular complex using ZnTPPS^{4-} at 0.55 eV. Time-resolved transient absorption spectroscopy demonstrates that $\text{ZnTF}_4\text{PPTC}^{4-}/\text{Li}^+\text{@C}_{60}$ generates a long-lived CS state with a lifetime of 0.29 ms in a binary solvent of acetonitrile and chlorobenzene.



[1] K. Ohkubo *et al.* Chem. Commun., **48**, 4314 (2012).

Corresponding Author: S. Aoyagi (aoyagi@nsc.nagoya-cu.ac.jp)

Formation of high-performance P-type thermoelectric materials composed of fullerene molecules and molybdenum oxide nanoclusters

○Masato Nakaya¹, Shinta Watanabe¹, Jun Onoe¹

¹ Department of Energy Science and Engineering, Nagoya University, Aichi, 464-8603, Japan

Organic thermoelectric conversion devices have attracted a great deal of attention as a power source for wearable devices that are one of key technologies in sustainable society. Fullerene (C₆₀) film is one of possible candidates for high-performance thermoelectric materials because of its giant Seebeck coefficient (S) of -110 mV/K at room temperature (RT) [1]. For application of the C₆₀ film to the practical thermoelectric devices, it is indispensable to improve a very low electrical conductivity (σ of *ca.* $10^{-5} \Omega^{-1}\text{cm}^{-1}$) of the C₆₀ film. In addition, since the C₆₀ film exhibits a large N-type S value (< 0), a large P-type S value (> 0) should be emerged for C₆₀-based films, because practical thermoelectric devices have a π -type structure composed of a sequential array of P- and N-type thermoelectric materials. In this study, we have demonstrated that the P-type thermoelectric films can be formed by co-deposition of C₆₀ and molybdenum oxide (MoO₃).

All experiments were carried out in an ultrahigh vacuum chamber. C₆₀•MoO₃ composite films were formed by co-deposition of C₆₀ and MoO₃ (supply ratio: $x = \text{MoO}_3/\text{C}_{60}$) on mica substrates at RT. The σ of the composite films were evaluated by four-probe measurement. To evaluate S of the films, a micro-gap electrode array was formed by depositing titanium (Ti) atoms on the composite films. The value of S ($-\Delta V/\Delta T$) was obtained from a thermoelectromotive force (ΔV) between adjacent Ti electrodes with a temperature difference (ΔT), using a microprobe S measurement system [2].

Fig. 1 shows change in the σ (□) and S (○) of the C₆₀•MoO₃ composite films as a function of the x . The σ increased with x drastically and monotonically. On the other hand, the S increased steeply at a small value of x and thereafter decreased rapidly with increasing x . The maximum value of S was obtained to be *ca.* 95 mV/K, which is a large P-type S value when compared to conventional thermoelectric materials. Scanning tunneling spectroscopy and first-principles calculations indicate that the local hole doping into the highest occupied molecular orbital (HOMO) of C₆₀ takes place *via* the charge transfer from C₆₀ to MoO₃ nanoclusters. We will also discuss the details of the present work in association with the power factor ($PF = S^2\sigma$) at this talk.

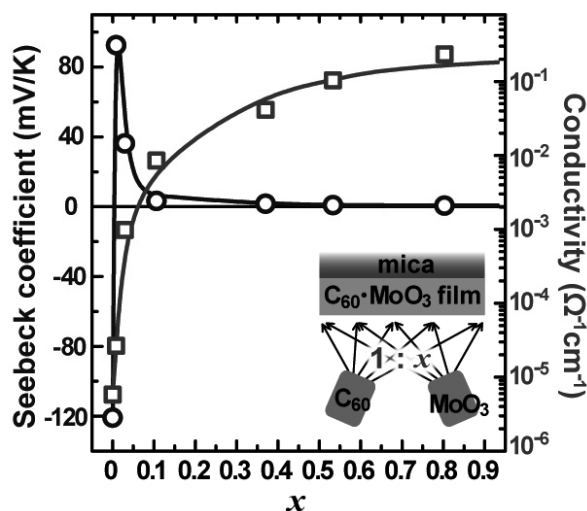


Fig. 1. Plot of the S (open circles) and σ (open squares) of C₆₀•MoO₃ films as a function of x .

[1] H. Kojima *et al.* *Mater. Chem. Front.* **2**, 1276 (2018).

[2] M. Nakaya *et al.*, ACSIN-14 & ICSPM26, 23F09, Oct. 21-25 (2018).

Corresponding Author: M. Nakaya

Tel: +81-52-789-3785, Fax: +81-52-789-3785,

E-mail: m-nakaya@energy.nagoya-u.ac.jp

Energetics and electronic structure of corannulene-intercalated bilayer-graphene

○Mina Maruyama, Susumu Okada

Department of Physics, University of Tsukuba, Ibaraki 305-8577, Japan

Graphite intercalation compounds (GICs) are representative examples of van der Waals heterocomplexes consisting of host graphene layers and guest layers consisting of atoms or molecules [1]. GICs basically show unusual electronic properties owing to charge transfer between the host and guest layers. In addition to the electronic properties, guest intercalants confined in two-dimensional nano-spacing between graphene layers possess unique arrangement and conformations those are hardly observed in their bulk phases. In our previous work, intercalating bowl-shaped hydrocarbon sumanene induces electron and hole doping on bilayer graphene, even though the complex is comprised of carbon atoms. Furthermore, molecular conformation of sumanene between graphene layers changes from bowl to flat by applying vertical pressure of 1 GPa. Following our previous work, in this work, we investigate energetics and electronic structure of corannulene-intercalated bilayer-graphene by using density functional theory.

Corannulene ($C_{20}H_{10}$) is the other bowl shaped hydrocarbon molecule consisting of a pentagon and five hexagonal rings (Figure 1a). Energy differences between bowl and flat conformations of corannulene are summarized in Table I. An isolated corannulene with a bowl conformation is more stable than that with a flat conformation of which energy difference is 435 meV. This energy difference substantially decreases by inserting corannulene into the interlayer spacing of bilayer graphene (Fig. 1b). The calculated energy difference is 65 meV, indicating that corannulene undergoes conformation change between bilayer graphene under the vertical pressure of 140 MPa. We also found that electron and hole doping occurs on graphene layers when the corannulene has bowl conformation.

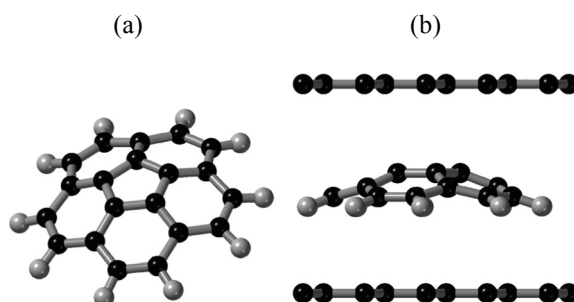


Fig. 1 Geometric structures of (a) corannulene molecule and (b) corannulene-intercalated AA stacking bilayer-graphene with bowl shaped conformation.

Table 1. Energy difference between bowl and flat conformation of corannulene.

	mol.	mol. on monolayer	GIC with AA stack.
Energy [meV]	435	265	65

[1] M. S. Dresselhaus & G. Dresselhaus, *Adv. Phys.* **30**, 130 (1981).

Corresponding Author: M. Maruyama

Tel: +81-29-853-5921, Fax: +81-29-853-5924,

E-mail: mmaruyama@comas.frsc.tsukuba.ac.jp

Second harmonic generation in two-dimensional Janus TMDs

○Riichiro Saito, Nguyen Tuan Hung, M. Shoufie Ukhtary,

Department of Physics, Tohoku University, Sendai 980-8578, Japan

We discuss second harmonic generation (SHG) in Janus two-dimensional (2D) transition metal dichalcogenides (TMDs). The 2D Janus TMD is defined by a TMD in which the two chalcogenide layers within the TMD consist of different elements such as S-Mo-Se [1, 2]. Because of a broken symmetry in the monolayer Janus TMD, an intrinsic vertical-dipole moment exists, which is important for SHG even for a 2D material [3]. Recent experimental work shows six-fold rotational symmetry for the SHG intensity as a function of emission angle [4]. Here, using the symmetry analysis, we explain the origin of the six-fold rotational symmetry. Further, in order to evaluate the efficiency of SHG, we calculate the non-linear susceptibility, $\chi^{(2)}$, by using the first-principles calculations as a function of incident light frequency. The first-principles calculations are performed by using Quantum ESPRESSO and Yambo packages. Since Janus SHG is a two-dimensional material, the so-called phase-matching condition is not needed for SHG generation. Thus, it is convenient to fabricate the SHG devices for any wavevectors. We would like to discuss the possible geometry for enhancing the SHG intensity.

Reference:

- [1] V.V. Thanh, N. D. Van, D. V. Truong, R. Saito, N. T. Hung, Appl. Surf. Sci, 526, 146730, (2020)
- [2] K. Zhang et al., JACS, 142, 17499 (2020)
- [3] M. Zhao et al., Light: Science & Applications, 5, e16131 (2016).
- [4] K. Zhang et al., unpublished.

Geometric and electronic structures of a two-dimensional tetracoordinated C allotrope of fused pentagons

○Susumu Okada, Nguyen Thanh Cuong, Yanlin Gao, Mina Maruyama

Department of Physics, University of Tsukuba, Tsukuba 305-8571, Japan

Hydrocarbon molecules are building block for constructing nanocarbon network materials. Numerous nanocarbon materials have been synthesized on metal surfaces and in solution under the controlled manners. Indeed, graphene nanoplates or nanoribbons have been synthesized from planar polycyclic hydrocarbons. In addition, non-planar hydrocarbons, such as triptycene and tetraphenylmethane, also form non-planar nanocarbon materials. In this work, we theoretically designed a two-dimensional covalent network of fused pentagons by polymerizing spiro[4.4]nonatetraene, using the density functional theory with the generalized gradient approximation. As shown in Fig. 1, the allotrope has a layered structure with rippling owing to sp^3 C atom located at the vertex of fused pentagon. The calculated total energy of the network is 0.619 eV/atom with respect to that of graphene, indicating that the network is relatively high total energy among known C allotropes. However, first-principles molecular dynamics simulation corroborated the thermal stability of this C allotrope up to 2000K. Interestingly, this C allotrope has a Dirac lines above the Fermi level by 1eV at the Brillouin zone boundary. We further investigated the electronic structures of nanoribbons derived from this allotrope and found that the ribbon with zigzag edges possesses edge localized mode as the case of graphene nanoribbons with zigzag edges.

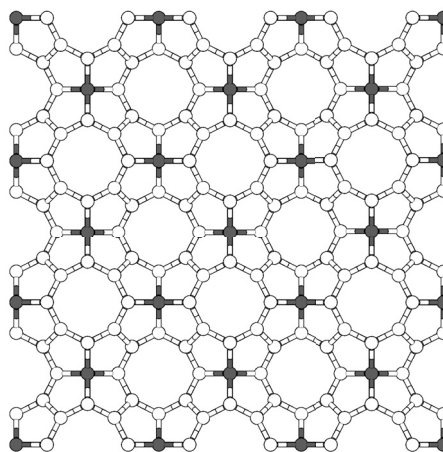


Fig.1 Geometric structure of 2D covalent network of fused pentagons. White and gray circles denote sp^2 and sp^3 C atoms, respectively.

Corresponding Author: Susumu Okada
TEL: +81-29-853-5921, FAX: +81-29-853-5924
E-mail: sokada@comas.frsc.tsukuba.ac.jp

In-situ TEM observation of laser induced carbon nanostructure growth

○Ryosuke Senga¹, Yung-Chang Lin¹, Sapna Sinha¹, Takeshi Kaneko², Norihiro Okoshi², Takeo Sasaki², Shigeyuki Morishita², Hidetaka Sawada² and Kazu Suenaga¹

¹ Nanomaterial research institute, AIST, Tsukuba 305-8565, Japan

² JEOL Ltd., Akishima, Tokyo 196-8558, Japan

Various methods have been used to synthesize carbon nanomaterials, such as laser ablation, arc discharge, and chemical vapor deposition, and it is now possible to control their structures, such as the diameter and number of layers of carbon nanotubes, with high precision. The growth mechanism of carbon nanomaterials has also been discussed for many years, and various models have been proposed both experimentally and theoretically [1-4]. However, it is still unclear what happens to the catalytic metal in the initial stage of growth process and how the chirality and number of layers are determined, because there are few examples that directly observe the precipitation of carbon atoms on metal catalysts.

In this study, using a laser irradiation system (LuminaryTM Micro) in a transmission electron microscope (TEM) developed by JEOL Ltd. and IDEs, Inc., we have succeeded in directly observing the formation of tube- or onion-shaped carbon nanostructures around metal particles activated by laser ablation. The technique enables in-situ TEM observation while irradiating a laser beam parallel to the electron beam onto a sample. By controlling the laser power, it is possible to minimize the vibration and drift of the sample and keep high spatial resolution during the laser irradiation.

In our experiment, we prepared ferrocene nanoclusters deposited on a lacey carbon film by vacuum deposition. When the sample was irradiated with a laser at a wavelength of 577 nm with an output power of 50 mW, the ferrocene decomposed instantly to form iron particles. Then, the iron particles randomly moved on the carbon film while changing their shape, forming tube-like structures along their path under the continuous square wave (1kHz~5kHz) laser irradiation. The surface of the iron particles repeatedly alternated between spherical and faceted in the process. Interestingly, the graphitic structures formed most likely at the faceting moment, suggesting a correlation between the tube chirality and facet orientation. This method, which enables direct observation of physical phenomena and chemical reactions induced by a laser in atomic scale, would be a promising candidate for a paradigm shift in a wide range of fields, including photochemistry and -biology, as well as materials science.

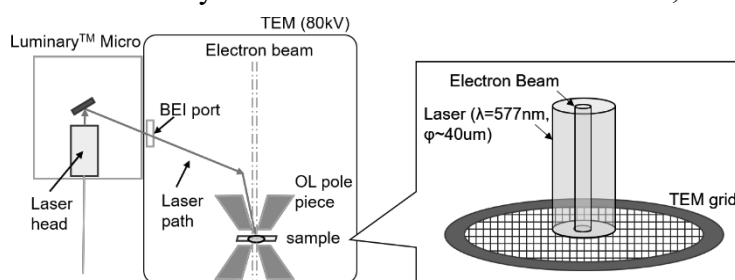


Fig.1 Schematic of the laser irradiation system in TEM (LuminaryTM Micro). The center of the electron beam and the laser are adjusted to be the same.

[1] S. Iijima, *Materials Science and Engineering: B* **19**, 172 (1993)

[2] H. Zhu *et al.*, *Small* **1**, 1180 (2005)

[3] H. Yoshida *et al.*, *Nano Letters* **8**, 2082 (2008)

[4] M. Kumar and Y. Ando, *Journal of Nanoscience and Nanotechnology* **10**, 3739 (2010)

Corresponding Author: R. Senga

Tel: +81-29-862-6518 E-mail: ryosuke-senga@aist.go.jp

Design and Fabrication of Carbon Nanotube-based Non-precious Metal Electrocatalysts with High ORR and OER Performances and their Applications

Pandian Ganesan¹, Aleksandar Staykov¹, Hiroaki Shu², Mitsugu Uejima²,
Naotoshi Nakashima¹

¹International Institute for Carbon Neutral-Energy Research (WPI-I2CNER), Kyushu University, Fukuoka, Japan; ²Nihon Zeon Corporation, Chiyoda-ku, Tokyo

In recent years, a sustainable and low-carbon emission energy chain has attracted much attention. Toward the goal, the development of non-precious metal electrocatalysts for fuel cells, water splitting and batteries with high performance, durability, and scalability is a strong social demand for the next-generation eco-friendly energy society[1]. Recently, we have focused on i) nanocarbons /iron phthalocyanine (II) hybrids with well-defined nanostructures that show excellent efficiency and durability for oxygen reduction reaction (ORR)[2,3], and ii) decorating unoxidized-carbon nanotubes with homogeneous Ni-Co-spinel nanocrystals that show superior performance for oxygen evolution (OER) and oxygen reduction reactions[4].

In this study, we have designed and synthesized a new $(\text{Fe}_3\text{NiS}_{8-\delta})^{-4+\delta}$ carbon nanotube (CNT) hybrid electrocatalyst and revealed that their catalyst shows a very high OER (1.55 V at 10 mA/cm²) and ORR ($E_{1/2} = 0.82$ V vs RHE) performances. Based on the analyses by in situ XRD, *in situ* electrochemical FT-IR, transmission electron microscopy (TEM) and computer simulations, such a high performance is derived from the sulfur vacancies[5]. Based on the obtained superior ORR and OER performance and durability of the catalyst, we used this material as a cathode material for the Zn-air battery and found that the battery acts as a rechargeable Zn-air battery with high performance.

References

- [1] N. Nakashima (Editor), “Nanocarbons for Energy Conversion-Supramolecular Approach-”, Springer, **2018**, pp. 1-564.
- [2] J. Yang, J. Tao, T. Isomura, H. Yanagi, I. Moriguchi, N. Nakashima, *Carbon*, **2019**, *145*, 565-571.
- [3] J. Yang, F. Toshimitsu, T. Fujigaya, N. Nakashima, *J. Mater. Chem. A*, **2017**, *5*, 1184-1191
- [4] J. Yang, T. Fujigaya, N. Nakashima, *Sci. Rep.*, **2017**, *7*, art.no.45384.
- [5] P. Ganesan, A. Staykov, H. Shu, M. Uejima, N. Nakashima, *ACS Appl. Energy Mater.* **2020**, *3*, 10961-10975.

Corresponding Author: N. Nakashima

Tel: +81-92-802-6745, Fax: Tel: +81-92-802-6745, E-mail:
nakashima.naotoshi.614@m.kyushu-u.ac.jp

Multifaceted approaches to quantitative surface characterization of as-grown and acid treated single-walled carbon nanotubes

○Kazufumi Kobashi¹, Yoko Iizumi¹, Kazutoshi Hirota², Naoki Shinomori², Kazuhiro Shimamoto², Yasumasa Koga², Takahiro Morimoto¹, Toshiya Okazaki¹

¹ National Institute of Advanced Industrial Science and Technology, Tsukuba 305-8565, Japan

² Sumika Chemical Analysis Services, Ltd., Osaka 541-0043, Japan

The surfaces of an individual carbon nanotube (CNT) and its bundle have been analyzed over a few decades to utilize the excellent properties. In recent years, understanding the macroscale surfaces created by large number of CNTs is getting requisite in the academic and industrial fields. Diverse analytical methods have so far provided the averaged or localized data, however the quantitative characterization from a multifaceted aspect remains challenging.

Here, we propose multifaceted approaches to quantitatively characterize the macroscale surfaces of CNTs by 11 different analytical methods (Raman, far and mid IR, TEM, Boehm titration, TGA, weight change, TPD/MS, EGA/MS, XPS, SEM/EDS). Our characterization is based on the averaged, localized, mapped [1] data of surface functional groups, and revealed the kind, amount, distribution of both as-grown and acid treated, single-walled CNTs. In addition to the analysis of functional groups, interestingly the adsorbed water on the surfaces was quantified, which we believe important to understand CNTs surfaces.

A comparison between as-grown and functionalized CNTs can present a good example to understand the surfaces. We selected Zeonano SG101 as single-walled CNTs with high carbon purity (>99 wt%). To achieve a homogeneous functionalization without severely disrupting CNTs, the powder was exfoliated in viscous liquid of glycerol at rt by stir bar [2] before acid treatment with 22 wt% H₂SO₄ aqueous solution and KMnO₄ at 80°C for 2h. The acid treated CNTs mainly possessed carboxylic acid (13 wt%) and hydroxy (6 wt%) groups in the total functional groups (41 wt%). The adsorbed water increased by the acid treatment and reached up to ~20 wt%. Furthermore, based on the obtained results, the plausible chemical structure of the acid treated CNTs can be drawn (Figure). Taken together, our findings indicate an importance to analyze the macroscale CNTs surfaces in a multiple manner, and can be applied to understand surfaces of nanocarbon materials.

[1] H. Nakajima *et al.*, *Nanoscale* **11**, 21487 (2019).

[2] K. Kobashi *et al.* *ACS Appl. Nano Mater.*, **3**, 1391 (2020).

Corresponding Author: K. Kobashi

Tel: +81-29-861-4874,

E-mail: kobashi-kazufumi@aist.go.jp

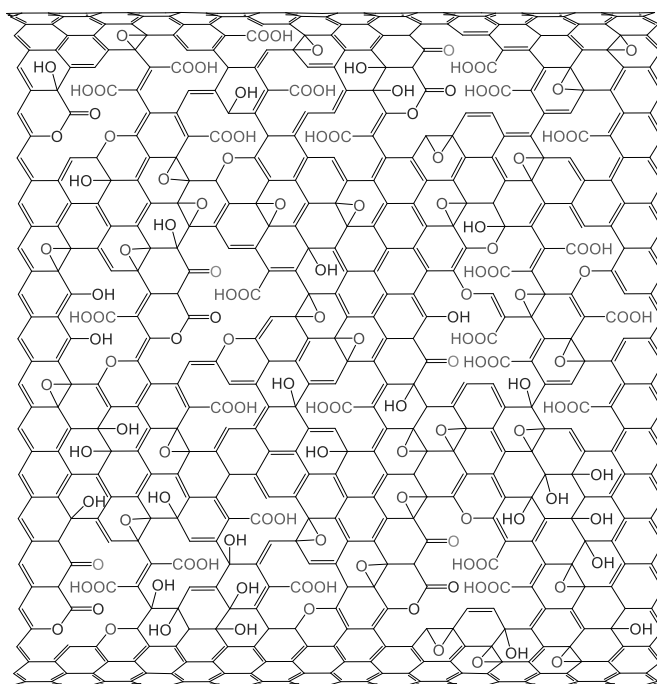


Figure Chemical structural model for the sidewalls of acid treated single-walled CNTs.

Primary Particles of Detonation Nanodiamond: The Only Scalable, Single Nano-sized and Well-Characterized Carbon Particle

○Eiji Ōsawa¹, Ryoko Yamanoi¹, Shuichi Sasaki¹, and Amanda Barnard²

¹ NanoCarbon Res. Inst., AREC, Shinshu University, Ueda, Nagano 386-8567, Japan.

² Research School of Computer Science, ANU College Engineering and Computer Science, The Australian National University, Canberra ACT 2601, Australia.

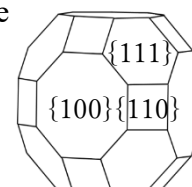
PRODUCTION

Detonation nanodiamonds (DND) were discovered by Danilenko in 1964, in the form of micron-sized and extremely tight agglomerates. The interparticle bonding resisted all attempts to break until 2005, when attrition milling using water as medium was found effective to reach its primary particles (PP) [1]. The nature of agglomeration was found Coulombic attraction between surface charges of neighboring particles [2]. Among the known methods of producing carbon nanoparticles [3], the detonation-milling method is at the moment considered the best in terms of simplicity, efficiency and scalability. Thus, we now have a stable colloidal solution of a standard material for nanotechnology.

IDENTIFICATION

Conventional DLS method gave 2.6 ± 0.5 nm as the average diameter of PPDND. This diameter coincides with those reported for the first nanodiamonds isolated from Allende meteorites in 1987 [4]. Based on these pieces of evidence we suspect that the presently prevailing commercial nanodiamonds of 4~5 nm in diameter [3] are likely dominated by the dimers. The {111} facets of PPDND are considered graphitized, according to our calculations of all possible models of real sizes, and based on the translucent but extremely dense black color of the colloidal solution. Enormous strain generated by this phase transition caused amorphization of the top layer(s) of core diamond. Our calculations indicate that core diamond in PPDND comprises only 60% of the total carbon atoms.

Shapes are estimated almost entirely by computation. With the aid of surface transformation map involving all metamorphic forms (to be displayed in the talk), three intermediate structures (A is the most likely) were identified as dominating in the detonation mixture.



A

One remarkable aspect of PPDND is that it dissolves well in water and many other organic solvents including DMSO. While such a behavior may look unusual for diamond having as many as 1,700 carbon atoms, Petit noted exceptionally strong hydration towards the surface of PPDND [5]. It is likely that other single-nano particles having isomorphic crystal systems may behave more or less similarly with their extremely active surfaces. Properties of single-nano particles could be entirely unique compared to conventional chemical materials.

[1] A. Krueger *et al.*, *Carbon*, **2005**, 43, 1772. [2] A. Barnard *et al.*, *J. Mater. Chem.* **2008**, 18, 4038. [3] 'Ultrananocrystalline Diamond, 2nd Edition,' O. A. Shenderova & D. M. Gruen (eds.), Elsevier, Amsterdam, 2012, pp. 558. [4] R. S. Lewis *et al.*, *Nature*, **1987**, 325, 160. [5] T. Petit *et al.*, *J. Phys. Chem. C*, **2017**, 121, 5185.

Corresponding Author: E. Ōsawa

Tel: +81-268-75-8381, E-mail: osawa@nano-carbon.jp

Solubilization and purification of carbon nanohorn aggregates using cyclodextrins as surfactants

○Hiroki Hanayama¹, Junya Yamada¹, Koji Harano¹, Eiichi Nakamura¹

¹ Department of Chemistry, The University of Tokyo, Tokyo 113-0033, Japan

Solubilization of graphitic nanomaterials is of great importance for their application in materials science. Surfactants with a polar head and nonpolar tails reduced the interfacial tension through non-specific hydrophobic or π - π interactions between the tails and the surface of nanocarbons. The hydrophobicity of surface is affected not only by chemical properties of the surface itself but also by the surface roughness. For example, the spiked structure increases the hydrophobicity of surface as discussed by Cassie, Wenzel, and others known as superhydrophobicity [1]. Therefore, we considered that cyclodextrins (α -, β - and γ -CDs), cyclic saccharides made from six to eight glucose units, site-selectively functionalized tips of the spikes by mimicking hemimicelle structure of surfactant and reduced hydrophobicity of the spiked surface. Here, we reported the efficient solubilization of carbon nanohorn aggregates (NHa), which are spherical particles of 50–150 nm in diameter bearing spikes of tapered-shape carbon nanotubes, with only 1 wt% of CDs via tip-cognitive binding in water [2], while conventional surfactants require excess amount for solubilization due to non-selective functionalization [3]. Tip-selective binding enabled purification of NHa by removing graphitic ball-shaped impurities without spiked surface as a precipitate. The binding of CDs to the tips of NHa was visually confirmed by using single-molecule atomic-resolution real-time electron microscopic analysis (SMART-EM) [4], and the analysis also revealed that CDs recognized the tip larger than cavity size via rim binding mode other than conventional cavity binding mode. A gram-scale purification was achieved by using α -CD, which was easily removed from NHa by washing with water. The purified NHa was successfully utilized in further amination reaction.

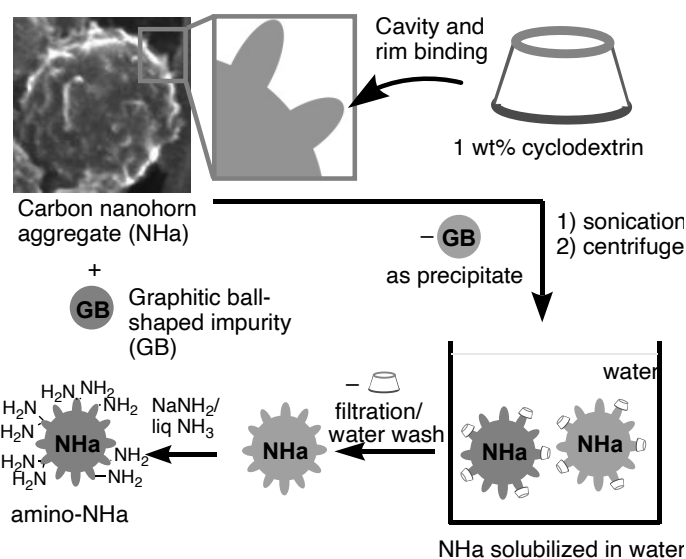


Fig. 1. Solubilization and purification of NHa by binding of CDs to the tip of NHa followed by amination reaction.

[1] A. Lafuma, D. Quéré, *Nat. Mater.*, **2**, 457–460 (2003). [2] H. Hanayama, J. Yamada, K. Harano, E. Nakamura, *Chem. Asian. J.*, **15**, 1549–1552 (2020). [3] M. Zhang, M. Yudasaka, J. Miyazaki, J. fan, S. Iijima, *J. Phys. Chem. B*, **109**, 22201–22204 (2005). [4] E. Nakamura, *Acc. Chem. Res.*, **50**, 1281–1292 (2017).

Corresponding Author: E. Nakamura, K. Harano

Tel: +81-3-5841-4369, Fax: +81-3-5841-4370,

E-mail: nakamura@chem.s.u-tokyo.ac.jp, harano@chem.s.u-tokyo.ac.jp

Visualizing outer surface functionalization of carbon nanohorn spherical aggregates by highly spatially resolved SEM-EDS

Hideaki Nakajima¹, Takahiro Morimoto¹, Kazufumi Kobashi¹, Minfang Zhang¹,
Ioanna K. Sideri², Nikos Tagmatarchis², and Toshiya Okazaki¹

¹National Institute of Advanced Industrial Science and Technology, Tsukuba 305-8565, Japan

²National Hellenic Research Foundation, Athens 11635, Greece

Single-walled carbon nanohorns (CNHs) exhibit a great potential for diverse applications such as gas storage, catalyst support, and drug carrier. Although chemical functionalization of CNHs is key approach for enhancing the dispersibility and handling in solution, they inherently form robust spherical “dahlia-type” aggregates (Fig. 1a) which may prevent chemical reactivity. Theoretical and experimental studies have identified spatial information related to the functional groups on each tubule. However, the overall characteristics of dahlia aggregates remain unclear. Here, we successfully visualize the site-selective chemical functionalization in CNH dahlia-type aggregates by using a highly spatially-resolved energy dispersive X-ray spectrometry (EDS) analysis in scanning electron microscopy (SEM) [1]. The differences of the degree of functionalization between the outer surface and the inner core of individual dahlia aggregates is quantitatively discussed.

Figure 1(b) shows a schematic of SEM-EDS measurement setup. Highly sensitive X-ray detection and drift-free EDS operation enable us to image light elements with a sufficient spatial resolution of < 10 nm [2]. CNH sample was synthesized from graphite targets by CO₂ laser ablation and was chemically modified with aniline derivative *tert*-butyl 2-(2(2-(4-aminobenzamido)-ethoxy)ethoxy)ethyl carbamate.

Figure 1(c) indicates the analytical result of N atomic concentration that derives from the covalently added functional groups on CNHs. The spatial distribution of functional groups is clearly obtained. Especially, the N concentration is higher at fringe of the individual dahlia structure. This result suggests that functionalization of CNHs selectively occurs on the outer surface of the dahlia-type aggregate. The detailed analysis about the degree of functionalization and mechanism of chemical modification in CNHs will be discussed in the symposium.

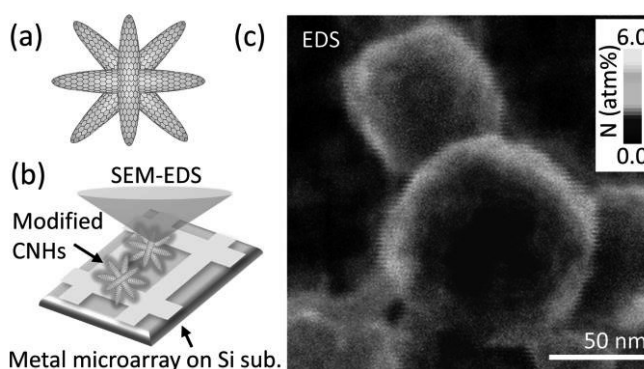


Figure 1. (a) Schematic of a spherical dahlia-type aggregate of CNHs and (b) highly spatially resolved SEM-EDS setup. (c) Analytical results of N atomic concentration image superimposed on SEM image.

Acknowledgments: This work was supported by a project (JPNP16010) commissioned by the New Energy and Industrial Technology Development Organization (NEDO).

[1] H. Nakajima *et al.*, *J. Phys. Chem. C* **124**, 25142 (2020). [2] H. Nakajima *et al.*, *Nanoscale* **11**, 21487 (2019).

Corresponding Author: Toshiya Okazaki

Tel: +81-29-861-4173 / E-mail: toshi.okazaki@aist.go.jp

Self-assembly of metal-chalcogenide clusters into layered 2D materials

○Yusuke Nakanishi^{1,*}, Naoyuki Kanda^{1,2}, Zheng Liu³, Motoki Aizaki², Mina Maruyama⁴, Yanlin Gao⁴, Susumu Okada⁴, and Yasumitsu Miyata¹

¹ Department of Physics, Tokyo Metropolitan University, Tokyo 192-0397, Japan.

² Department of Chemistry, Nagoya University, Nagoya 464-8603, Japan.

³ National Institute of Advanced Industrial Science and Technology (AIST), Nagoya 463-8560, Japan

⁵ Department of Physics, University of Tsukuba, Tsukuba 305-8571, Japan

Two-dimensional (2D) layered materials exhibit unique Re: Decision on manuscript NCOMMS-20-50288-T electronic, optical, and structural properties markedly different from those of 3D materials. Over the last decade, there has been a significant advance in investigating 2D materials that consist of one or a few atomic layers, and researchers started paying attention to a variety of 2D layers. Molecular clusters of transition metal chalcogenides (TMCs) are promising building blocks for the self-assembly of 2D molecular layers *via* chemical cross-linking. Depending on their morphology and dimensionality, the 1D and 3D solids composed of TMC clusters display versatile electronic states ranging from Mott insulator, conductor, to superconductor [1, 2]. Similarly, the Chemical and structural diversity of TMC clusters would greatly expand the functional scope of 2D materials.

In this work, we report the self-assembly of layered 2D structures comprising TMC clusters bridged by Cl atoms, including the realization of isolated monolayers by using nano-test-tubes (Fig. 1). Two kinds of characteristic layered structures were confirmed by atomic-level transmission electron microscopy. We also found the possibility that these layered materials would exhibit strong PL emission. Detailed discussion will be presented in the conference.

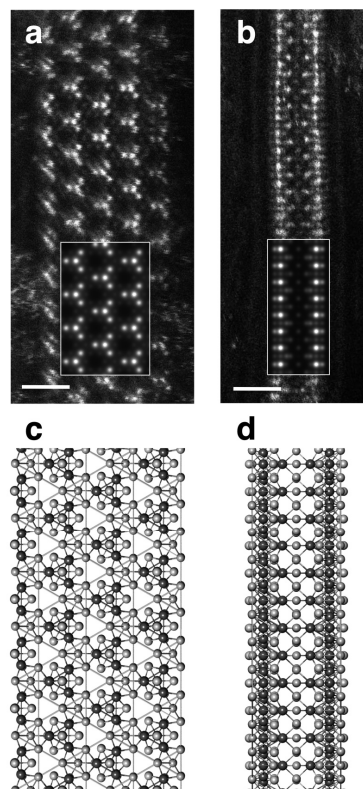


Fig 1 HAADF-STEM images of 2D structures comprising Mo₄S₄ clusters inside carbon nanotubes viewed from b) surface and c) cross section, and c, d) the corresponding schematics.

[1] R. Pocha *et al.*, Chem. Mater. **12**, 2882 (2000); C. Vaju *et al.*, Microelectron. Eng. **85**, 2430 (2008); M. M. Abd-Elmeguid *et al.*, Phys. Rev. Lett. **93**, 126403 (2004)

[2] N. Kanda, **Y. Nakanishi** *et al.*, Nanoscale **12**, 17185 (2020); N. Kanda, **Y. Nakanishi** *et al.*, Nano Lett. **19**, 4845 (2019); H. E. Lim, **Y. Nakanishi** *et al.*, Nano Lett. **21**, 243 (2021)

Corresponding Author: Y. Nakanishi

Tel: +81-42-677-2498

E-mail: naka24ysk@tmu.ac.jp

Transmissible plasma evolved graphene: production and application

- Kamal P Sharma^{1,2}, Aliza K. Sharma¹, Daiki Yamamoto¹, Toru Asaka³, Takahiro Maruyama^{1,2}
¹Department of Applied Chemistry, ²Nanomaterials Research Center, Meijo University
³Department of Life Science and Applied Chemistry, Nagoya Institute of Technology

The chemical vapour deposition (CVD) of carbon feedstock onto a catalyst surface, carbon species that are excited by a plasma, and high-energy laser irradiation of carbon surfaces are important methods for graphene production [1-3]. Among them, plasma enhanced CVD (PECVD) utilizing microwave, surface wave, or radio frequency (rf) plasma has been realized as promising techniques for graphene synthesis at low temperature and with short processing time [4]. However, for most CVD and PECVD techniques, time-consuming transfer and chemical treatment processes are essential to produce graphene for subsequent applications. Here, we propose a simple technique to produce suspended graphene which address these issues and termed as transmissible plasma evolved graphene (TPEG) based on its formation process [5].

For TPEG production, commercially available TEM microgrids with amorphous carbon (a-C) membranes were utilized, onto which Co plasma produced from Co target in a pulsed arc plasma deposition system (APD-2S, Advance Riko) was exposed (**Figure 1(a)**). Each arc pulse is triggered by a surface flashover from a trigger electrode to the cathode surface (trigger duration $\sim 10 \mu\text{s}$) and the discharge voltage between cathode and anode was varied, which affects mainly the density of metal plasma. As produced TPEG was analyzed by OM, Raman spectroscopy, XPS, AFM, and TEM.

Figure 1(b) shows the Co plasma utilized with biased voltage of 140V (3 pulses) or more produced the TPEG and high quality TPEG was produced at 170V (**Figure 1(c)**). As produced TPEG was comprised of 3 to 12 layers with interlayer distance of 0.34 nm (**Figure 1(d)**), and is of uniform quality throughout the suspended part of a-C as seen in G-band map (**Figure 1(e)**). Besides graphene production in both time and energy efficient ways, this technique could be used to produce heterostructures (**Figure 1(f)**), and would serve as graphene grids for TEM characterization.

Acknowledgement: This work was supported in part by Private University Research Branding Project from the Ministry of Education, Culture, Sports, Science and Technology (MEXT), Japan.

- [1] Li, X. et al., Science 324, 1312 (2009).
 [2] Jacov, M. V. et al., Nano Lett. 15, 5702 (2015).
 [3] Lin, J. et al. Nat. Commun. 5, 5714 (2014).

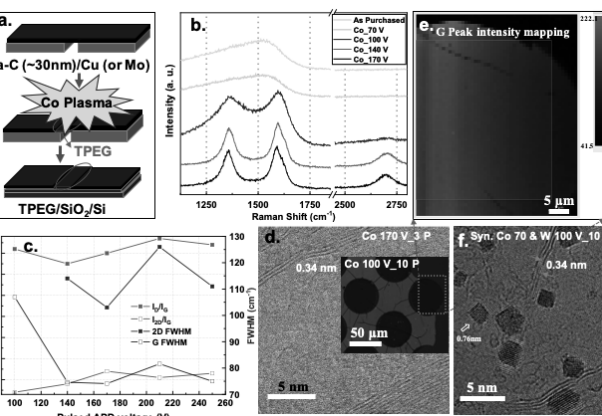


Figure 1. (a) Schematics diagram showing TPEG formation, (b) Raman spectra of TPEG at different biased voltage for Co target, and (c) qualitative analysis of Raman spectra. (d) HRTEM image of as formed TPEG. Inset is OM image of TPEG/SiO₂/Si. (e) Raman map of G-peak intensity as indicated in inset to (d). (f) HRTEM image of as formed TPEG with 0D and 1D materials.

Corresponding Author: takamaru@meijo-u.ac.jp (T.M.), kamalprasads@gmail.com (K.P.S.)

Field-induced dynamics of Ne atom around graphene edges

○Yanlin Gao, Susumu Okada

Department of Physics, Graduate School of Pure and Applied Sciences, University of Tsukuba, Tsukuba, 305-8571, Japan

Graphene has been extensively studied in both fundamental and applied sciences, because of its unusual geometric and electrical properties making it an emerging material for wide applications. The electronic properties of graphene are sensitive to its edge structures. Thereby, the edge structure characterization of graphene is very important. Field ion microscope (FIM) is one of microscopic techniques providing the atomic-resolution image of nanomaterials, such as the protrusions of surface, edges, and tips. Rare gas atoms around these surfaces and edges of nanomaterials are ionized and then bounced under the strong positive electric field, forming atomic-resolution images on the screen. These images reflect the atomic structures of these target nanomaterials. Although, the FIM can provide the atomic-resolution images of carbon nanomaterials, microscopic dynamics of rare-gas atoms around the carbon nanostructures under the positive electric field is not addressed to date. Thus, in this work, we aim to theoretically investigate the microscopic dynamics of Ne around the graphene edges to give theoretical insight into the field ion microscope, based on the density functional theory combined with the effective screening medium method [Fig. 1]

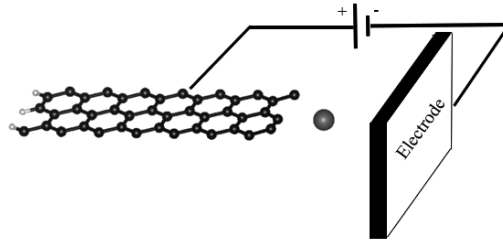


Fig.1. A structural model to simulate Ne atom around the graphene edges under the positive electric field. Gray, red, and white balls indicate C, Ne, and H atoms, respectively.

Our calculations showed that the dynamics of Ne atom depends on its initial positions with respect to the graphene edge shape. The Ne atom is attracted to the edge atomic sites of graphene, when it initially is located above the graphene edges with both zigzag and armchair edges. From the side of the zigzag edge, Ne also moves toward to the graphene because of the electrostatic interaction between Ne and edge states. In contrast, Ne is rapidly accelerated toward to the counter electrode when it initially is located aside the armchair edge.

Foldable Perovskite Solar Cells Using Carbon Nanotube-Embedded Ultrathin Polyimide Conductor

Il Jeon¹, Jungjin Yoon², Esko I. Kauppinen³, Shigeo Maruyama⁴, Philp Lee⁵

¹Department of Chemical Materials, Pusan National University, Busan 46241, Republic of Korea

²Department of Materials Science & Engineering, Pennsylvania State University, USA

³Department of Applied Physics, Aalto University School of Science, Aalto FI-00076, Finland

⁴Department of Mechanical Engineering, School of Engineering, The University of Tokyo, Tokyo 113-8656, Japan

⁵Department Photo-Electronic Hybrids Research Center, Korea Institute of Science and Technology (KIST), Seoul 02792, Republic of Korea

Recently, foldable electronics technology has become the focus of both academic and industrial research. The foldable device technology is distinct from flexible technology, as foldable devices have to withstand severe mechanical stresses such as those caused by an extremely small bending radius of 0.5 mm. To realize foldable devices, transparent conductors must exhibit outstanding mechanical resilience, for which they must be micrometer-thin, and the conducting material must be embedded into a substrate. Here, a single-walled carbon nanotubes–polyimide (SWNT-PI) composite film with a thickness of 7 μm is synthesized and used as a foldable transparent conductor in perovskite solar cells. During the high-temperature curing of the carbon nanotubes-embedded polyimide conductor, the carbon nanotubes are stably and strongly *p*-doped using MoO_x , resulting in enhanced conductivity and hole transportability (Figure 1). The ultrathin foldable transparent conductor exhibits a sheet resistance of $82 \Omega \text{ sq.}^{-1}$ and transmittance of 80% at 700 nm, with a maximum-power-point-tracking-output of 15.2% when made into a foldable solar cell (Figure 2). The foldable solar cells can withstand more than 10,000 folding cycles with a folding radius of 0.5 mm. Such mechanically resilient perovskite solar cells are unprecedented; further they exhibit the best performance among the carbon-nanotube-transparent-electrode-based flexible solar cells.

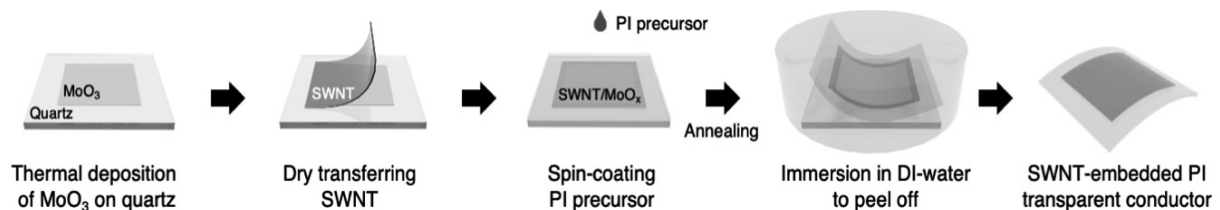


Fig. 1 Schematic illustration of the fabrication process of SWNT–PI ultrathin conductors.

Corresponding Author: I. Jeon
Tel: +82 (0)51 510 2682,
E-mail: il.jeon@spc.oxon.org

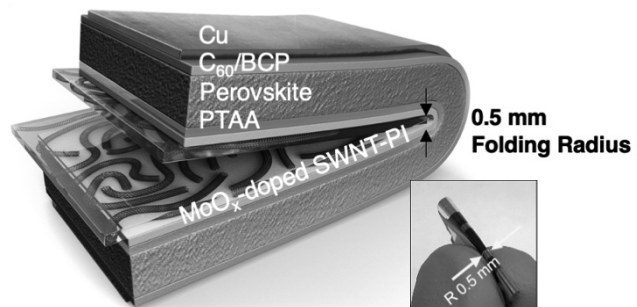


Fig. 2 Illustration and picture of the foldable perovskite solar cells

Highly Efficient Metal-Free Semi-Transparent Perovskite Solar Cells enabled by MoO₃-doped Transparent Carbon Nanotube Top Electrodes and Four-Terminal Perovskite Silicon Tandem Applications

Seungju Seo¹, Il Jeon^{1,2}, Kosuke Akino¹, Ahmed Shawky^{1,3}, Hao-Sheng Lin¹, Hiroki Nagaya¹, Esko I. Kauppinen⁴, Rong Xiang¹, Yutaka Matsuo^{1,5}, and Shigeo Maruyama^{1,*}

1. Department of Mechanical Engineering, School of Engineering, The University of Tokyo
2. Department of Chemistry Education, Graduate School of Chemical Materials, Institute for Plastic Information and Energy Materials, Pusan National University, 63-2 Busandaehak-ro, Busan 46241, South Korea.
3. Nanomaterials and Nanotechnology Department, Advanced Materials Division, Central Metallurgical R&D Institute (CMRDI), P.O. Box 87 Helwan, Cairo 11421, Egypt
4. Department of Applied Physics, Aalto University School of Science
5. Department of Chemical System Engineering, Nagoya University, Furo-Cho, Chikusa-ku, Nagoya, 464-8603, Japan.

ABSTRACT

Organic-inorganic lead halide perovskite solar cells (PSCs), since the first report in 2009, have outpaced all other photovoltaic technologies with the high power conversion efficiency (PCE), low material cost and simple solution processing. Now the certified PCE in the laboratory scale reads over 25%. However, the maximum PCE still remains limited to ~ 33% according to the theoretical Shockley-Queisser (SQ) for a single junction cell. To break this theoretical radiative limit, tandem structures, where perovskite absorbers are combined with other narrower band gap materials have been developed to expand the absorption spectral range. Among various combinations with top perovskite cell, thanks to excellent spectral responsivity in the near-infrared region as well as commercialization in the market, the silicon solar cell (SiSC) has been the most successful pair with the perovskite absorber, achieving the highest PCE of 29.15% to date. In terms of device configuration, they are either mechanically stacked, known as four-terminal tandem (4T) or monolithically integrated, known as two-terminal tandem (2T) with a perovskite top cell.

Advantages of the 4T configuration include that the top and bottom cells are only optically coupled while electrically independent, allowing each subcell to be processed and optimized independently. In contrast, the 2T solar cells are subject to close current and voltage matching between subcells. This requires careful optical design of the structures and precise control of absorption layer thickness within tens of nanometers, thus limiting the band gap combinations for the perovskite top cell. This makes 4T solar cells more favorable to the change of spectral and temperature changes.

To achieve high PCE in perovskite-silicon tandem solar cells (PSiSCs), transparent electrode in semi-transparent PSCs with minimum parasitic optical loss is crucial. So far, transparent conductive oxide (TCO) electrodes such as indium tin oxide (ITO), indium zinc oxide (IZO), and Al-doped zinc oxide (AZO) have been dominantly used. However, they are usually deposited by a high-cost vacuum process magnetron sputtering, where high energetic particles often damage the underlying organic contact and perovskite absorbers. In addition, TCO usually needs oxygen gas flow during sputtering and post annealing above 100C after deposition

to obtain high optical transmittance and electrical conductivity, but this additional process can degrade the sublayers as oxygen and heat is detrimental to perovskite absorber. Ultra-thin metal layers and metal nanowires could be the choice to replace the TCO electrodes because of modest process, but not favorable considering their reflective nature and metal-migration-induced device degradation.

Recently, single-walled carbon nanotubes (CNTs) as a top transparent electrode in semi-transparent PSCs has been reported to achieve high PCE in PSiSCs. In addition, it drastically reduces the fabrication cost as it can be easily deposited onto devices by a simple mechanical transfer. Despite such advantages, there are two factors limiting the PCE of the CNT top electrode-based semi-transparent PSCs that need to be addressed: (1) the unfavorable work function of the CNTs with respect to the active perovskite layer, leading to loss in open-circuit voltage (V_{oc}), (2) lower conductivity than the TCO counter parts, limiting the fill factor (FF) and short-circuit current (J_{sc}).

Here, we address those three issues by engineering the CNT top transparent electrode. We tuned the work function of CNT transparent electrodes and hole selectivity by thermally depositing MoO_3 under vacuum, without damaging underneath perovskite layers. Using photoelectron yield spectroscopy, X-ray photoelectron spectroscopy, absorbance and raman spectroscopy, we determine the necessary MoO_3 thickness to efficiently dope the CNT top electrode and study underlying doping mechanism between CNTs and MoO_3 to achieve highly efficient CNT top electrode-based PSCs. As a result, 70% transparent (at a wavelength of 550nm) CNT films with 8nm MoO_3 layer led to the highest PCE of 20.25% with a J_{sc} of 23.09 mA / cm², V_{oc} of 1.162V, and FF of 0.755 in PSCs. The obtained PCE, V_{oc} and FF were not only the highest among the values reported from CNT electrode-based PSCs, but also higher than that of metal electrode-based control devices. Furthermore, we investigate charge extraction dynamics from perovskite absorber to CNT transparent electrodes upon MoO_3 hole doping on CNTs using photoluminescence and impedance spectroscopy. Finally, 4T CNT-laminated PSCs / Silicon was simulated from optical transmittance of top perovskite subcell.

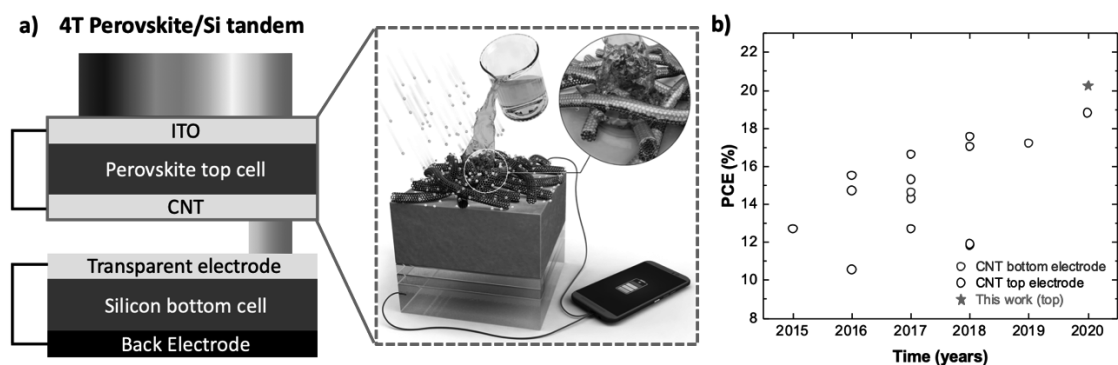


Figure 1 a) Schematics of the four-terminal perovskite-Si tandem solar cell with CNT-top-electrode-based semi-transparent perovskite solar cell. b) Efficiency table of CNT-based perovskite solar cells.

Corresponding Author: Prof. Shigeo Maruyama (maruyama@photon.t.u-tokyo.ac.jp)

Waveguide coupled cavity-enhanced light emission from individual carbon nanotubes

○D. Yamashita¹, H. Machiya^{2,3}, K. Otsuka², A. Ishii^{1,2} and Y. K. Kato^{1,2}

¹*Quantum Optoelectronics Research Team, RIKEN Center for Advanced Photonics, Saitama 351-0198, Japan*

²*Nanoscale Quantum Photonics Laboratory, RIKEN Cluster for Pioneering Research, Saitama 351-0198, Japan*

³*Department of Electrical Engineering, The University of Tokyo, Tokyo 113-8656, Japan*

Carbon-nanotube-based photonic devices have potential applications in the framework of on-chip optical communications. Single-walled carbon nanotubes (CNTs) exhibit telecom-band light emission at room temperature and they can be directly grown onto silicon substrates, which is favorable in terms of compatibility with silicon photonics. Recently, integration of CNTs with microcavities and waveguides has been demonstrated [1-4], but the deposition of CNTs has been performed by using solution processes. To harness the unique optical properties of CNTs such as single photon emission, it is important to isolate individual CNTs and eliminate contamination during the solution-based processes.

Here, individual CNT telecom-wavelength emitters are integrated onto a microcavity and a waveguide. Using finite-difference time-domain simulations, we have designed an air-mode photonic crystal nanobeam cavity with one thin end mirror for guiding the light into the waveguide. CNTs are grown on a SiO₂/Si substrate and transferred on the cavities through an all-dry process ensuring cleanliness of CNTs and devices. We characterize the devices using two geometries: a top detection configuration that measures light emission from CNTs on a nanobeam cavity, and a side detection configuration that collects light emission coupled to the waveguide. The nanobeam cavity with a small mode volume enhances light emission from a chirality-identified single CNT. The cavity-coupled light propagates into the waveguide and is emitted from the waveguide facet with a sharp linewidth and a large off-resonance rejection.

This work is supported in part by JSPS (KAKENHI JP19J00894, JP20H02558, JP20J00817, JP20K15137, JP20K15199), MIC (SCOPE 191503001), MEXT (Nanotechnology Platform JPMXP09F19UT0078) and RIKEN (Incentive Research Project). D.Y., H.M. and K.O. are supported by the JSPS Research Fellowship. The finite-difference time-domain simulations were performed using the HOKUSAI BigWaterfall supercomputer at RIKEN. We acknowledge the Advanced Manufacturing Support Team at RIKEN for technical assistance.

[1] F. Pyatkov, V. Fütterling, S. Khasminkskaya, B. S. Flavel, F. Hennrich, M. M. Kappes, R. Krupke, and W. H. P. Pernice, *Nat. Photonics* **10**, 420 (2016).

[2] A. Noury, X. L. Roux, L. Vivien, and N. Izard, *Nanotechnology* **26**, 345201 (2015).

[3] T. H. C. Hoang, E. Durán-Valdeiglesias, C. Alonso-Ramos, S. Serna, W. Zhang, M. Balestrieri, A.-S. Keita, N. Caselli, F. Biccari, X. L. Roux, A. Filoramo, M. Gurioli, L. Vivien, and E. Cassan, *Opt. Lett.* **42**, 2228 (2017).

[4] N. Higuchi, H. Niiyama, K. Nakagawa, and H. Maki, *ACS Appl. Nano Mater.* **3**, 7678 (2020).

Corresponding Author: Yuichiro K. Kato

Tel: +81-48-462-1449

Web: <http://katogroup.riken.jp>

E-mail: yuichiro.kato@riken.jp

Analytical Estimation of Quantum Emitters Formed in Air-Suspended Single-Walled Carbon Nanotubes

○Daichi Kozawa¹, Xiaojian Wu², Akihiro Ishii^{1,3}, Jacob Fortner², Keigo Otsuka³, Rong Xiang⁴, Taiki Inoue⁴, Shigeo Maruyama^{4,5}, YuHuang Wang^{2,6}, Yuichiro K. Kato^{1,3}

¹ *Quantum Optoelectronics Research Team, RIKEN Center for Advanced Photonics*

² *Department of Chemistry and Biochemistry, University of Maryland, College Park*

³ *Nanoscale Quantum Photonics Laboratory, RIKEN Cluster for Pioneering Research*

⁴ *Department of Mechanical Engineering, The University of Tokyo*

⁵ *Energy NanoEngineering Laboratory, National Institute of Advanced Industrial Science and Technology (AIST)*

⁶ *Maryland NanoCenter, University of Maryland, College Park*

Single-walled carbon nanotubes (SWCNTs) realize single-photon emission simultaneously at room temperature and in the telecom range suitable for the practical use [1]. Air-suspended nanotubes provide an ideal platform for a quantum emitter that exhibiting bright photoluminescence (PL). While the precise estimation of emitter density plays a key role to evaluate the quality of the single photon sources, the quantitative analysis in the air-suspended system is lacking. We here determine the defect density by comparing the PL intensity change in functionalization obtained from experiments with simulations. A theoretical model based on a one-dimensional diffusion equation is developed to describe the exciton density profile and PL intensity in pristine and functionalized tubes. We find that the PL intensity is more sensitive to the introduction of defects in the air-suspended tubes than typical solution-processed tubes because only the trapping E_{11} excitons at defects contribute to the quenching in the former. The defect density increases as the tube diameter decreases which is consistent with previously reported diameter-dependent reactivity model [2].

Acknowledgments

This work was supported in part by RIKEN (Special Postdoctoral Researcher Program), MIC (SCOPE 191503001), JSPS (KAKENHI JP15H05760, JP18H05329, JP20K15112, JP20K15137, JP20H02558), and MEXT (Nanotechnology Platform JPMXP09F19UT0077). We thank the Advanced Manufacturing Support Team at RIKEN for technical assistance.

References

- [1] X. He, N. F. Hartmann, X. Ma, Y. Kim, R. Ihly, J. L. Blackburn, W. Gao, J. Kono, Y. Yomogida, A. Hirano, T. Tanaka, H. Kataura, H. Htoon, and S. K. Doorn, *Nat. Photonics* **11**, 577 (2017).
 [2] D. Kozawa, X. Wu, A. Ishii, J. Fortner, K. Otsuka, R. Xiang, T. Inoue, S. Maruyama, Y-H. Wang, Y. K. Kato, Manuscript in preparation (2021).

Corresponding Author: Y. K. Kato

Tel: +81-48-462-1449

Web: <http://katogroup.riken.jp/>

E-mail: yuichiro.kato@riken.jp

Mechanical Vibration of Single-walled Carbon Nanotubes in a Water Using Finite Element Model

○Daisuke Miyashiro^{1,2}, Ryo Hamano¹, Hisao Taira³, Kazuo Umemura¹

¹ *Department of Physics, Graduate School of Science, Tokyo University of Science, 1-3 Kagurazaka, Shinjuku-ku, Tokyo, Japan.*

² *ESTECH CORP., 2-7-31 Fukuura, Kanazawa-ku, Yokohama, Japan*

³ *Faculty of Education, Hokkaido University of Education, Sapporo, Hokkaido 002-8502, Japan*

There are studies to apply the excellent mechanical properties of single-walled carbon nanotubes (SWCNTs) as a nanomechanical resonator. Assuming mass measurement of biomolecules by them, long SWCNTs have a problem that it is difficult to measure the basic vibrations due to the influence of water damping. While the molecular dynamics (MD) method can perform precise calculations at the molecular level, it requires a huge amount of calculation time for applying to mechanical vibration of long SWCNTs. On the other hand, there are studies on vibrational analysis of long SWCNTs using the finite element (FE) method. However, there are few studies of FE method for SWCNTs in a water. Therefore, we analyzed the mechanical vibration taking into account the damping according to the length of SWCNT in a water using FE method.

The FE model of SWCNTs used for vibration analysis was created in the range of 25 to 200 nm. In this model, a six-membered ring network was formed by expressing covalent bonds between carbons with beam elements. The properties of these beam elements were defined according to the beam elements diameter of 0.147 nm, length of 0.142nm and the Young's modulus of 5.49 TPa. The effect of water on SWCNTs loaded the mass of water molecules on their carbon atoms and defined structural damping according to SWCNTs length [1]. The analysis solver used the commercial MSC Nastran.

We verified the validity of the FE model by static analysis and investigated the mechanical vibration of SWCNTs by frequency response analysis under the conditions that SWCNTs are in a vacuum and water. The Young's modulus of SWCNTs obtained by static analysis is approximately 1.0 TPa, which is in agreement with the studies reported in the experiment. In a vacuum state, the natural frequency of bending vibration in SWCNTs by FE method longer than 25nm can be represented by Bernoulli-Euler beam theory. In the water case, we have clarified that the natural frequency of bending vibration in SWCNTs were reduced by about 60% compared with the vacuum case. In particular, SWCNTs longer than 100 nm are more affected by water damping. These results mean that the present method is useful for analyzing the mechanical vibration of SWCNTs in a water.

[1] D. Miyashiro *et al.* Compos. Part C, **2**, 100028 (2020).

Co-self-assembly of probe and scaffold peptides on graphite surface toward functionalization of graphene biosensors

○Chishu Homma¹, Mirano Tsukiiwa¹, Yuhei Hayamizu¹

¹*Department of Materials Science and Engineering, School of Materials and Chemical Technology, Tokyo Institute of Technology, 2-12-1 Ookayama, meguroku, Tokyo, Japan*

Graphene, one of the most typical 2D materials, has a high carrier mobility and specific surface area and is used in various electronics fields. Due to its unique properties, graphene is expected to be applied as a biosensor^[1]. In graphene biosensors, probe biomolecules are immobilized on graphene surface. To achieve higher sensitivity, it is necessary to develop a way of their non-covalent immobilization. In this study, we focused on peptides that adsorb and self-assemble on graphene surfaces^[2] and attempted to use self-assembling peptides as molecular scaffolds to immobilize bioprobes in a non-covalent manner.

Two types of peptides were designed: (1) a scaffold peptide, which is adsorbed on the graphene surface, and (2) a probe peptide, which has an amino acid sequence beyond the scaffold peptide that is expected to interact with target molecules. It has been reported that this sequence forms an oriented β -sheet structure and is able to maintain uniform nanostructures even after washing with deionized water^[3]. AFM observation showed that the probe peptide was stably anchored to the peptide membrane (Fig 1). By varying the ratio of the scaffold peptide to the probe peptide from 0 to 100%, the self-assembled structure on the graphene surface changes.

[1] Y. Ohno, et al.; J. Am. Chem. Soc., 2010, 132 (51), 18012–18013

[2] Khatayevich, Dmitriy, et al. Langmuir, 2012, 28, 23, 8589-8593.

[3] Li, P. et al. ACS Appl. Mater. Interfaces 2019, 11, 20670-20677.

Corresponding Author: Y. Hayamizu

Tel: +81-03-5734-3651

E-mail: honma.c.aa@m.titech.ac.jp

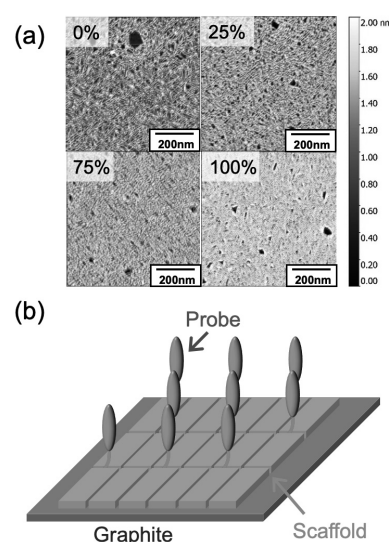


Fig 1. (a) AFM images of co-self-assembled peptides on graphite at different ratios of probe peptide. (b) Schematic diagram of co-self-assembled structure

Investigation of Schottky contact for transparent solar cell with monolayer WS₂

○X. He¹, T. Kaneko¹, and T. Kato^{1,2}

¹Graduate School of Engineering, Tohoku University, Sendai 980-8579, Japan

²JST-PRESTO

Layered transition metal dichalcogenide (TMD) is known as a true 2D material with excellent semiconducting properties. TMD is one of the most attractive materials for future transparent and flexible optoelectrical devices due to their atomically thin structure, band gap in visible light range, and high optical transparency. Those merits of TMD have not been applied for transparent and flexible solar cell, which is attracted intense attention as a next-generation energy harvesting technology. Recently, we have developed a new fabrication process of TMD-based solar cell [1]. In our process, Schottky type device configuration is utilized, which can be simply formed by asymmetrically contacting electrodes and TMD (Fig. 1(a)). The power conversion efficiency clearly depended on the work function difference between two electrodes (ΔWF), and a higher efficiency could be obtained with higher ΔWF (Pd-Ni). Based on the optimizations of electrodes and distance, the power conversion efficiency (PCE) can be reached up to 0.7 %, which is the highest value for solar cell with similar TMD thickness [1].

In order to achieve higher efficiency, it is important to investigate the detailed contact between TMD and electrodes. Thin metal (M_x) deposited ITO and pure ITO were used as Schottky and Ohmic electrode, respectively. Monolayer WS₂ was used as a suspended channel between each electrode. Schottky barrier height (SBH) was measured by photocurrent line scan through the channel under different bias conditions for various devices.

The SBH of $M_x = Au, Ag, Cu$ increase with WF of M_x/ITO (Fig.1(b)), which can be explained with traditional band model. Although higher SBH can be expected with Ni by following this trend, the SBH of Ni was lower than that of Cu. This can be explained by difference of Fermi level pinning effect. The Fermi level pinning factor (S), i.e. weakness of Fermi level pinning effect, is known to be sensitive to the binding energy between metal and channel material. Ni is known to have higher binding energy than that of other metals such as Au, Ag, and Cu. Thus, Ni should show smaller S and lower SBH than other metals, which is consistent with our results (Fig. 1(b)). Based on these investigations, we successfully revealed the most suitable M_x (Cu) for Schottky electrode in TMD-based solar cell, which has relatively higher WF and weaker pinning effect, resulting in higher SBH and PCE. This finding is essential for understanding the contact between TMD and electrodes, and further improvement of the device performance can be expected.

[1] T. Akama, W. Okita, R. Nagai, C. Li, T. Kaneko, and T. Kato, *Sci. Rep.* **7**, 11967 (2017).

Corresponding Author: Toshiaki Kato

Tel: +81-22-795-7046, Fax: +81-22-263-9225, E-mail: kato12@ecei.tohoku.ac.jp

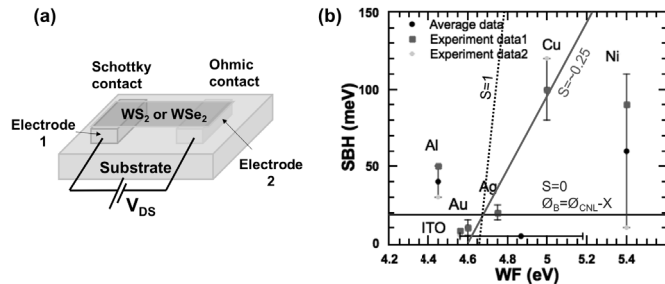


Fig.1. (a) Typical device structure used in this study. (b) Plot of SBH as a function of the WF of thin metal modified ITO.

Fabrication of Graphene/h-BN/graphene stacked mechanical resonator

○Kazuki Yasoshima¹, Taichi Inoue¹, Kuniharu Takei¹, Takayuki Arie¹, Seiji Akita¹

¹Department of Physics and Electronics, Osaka Prefecture University, Sakai 599-8531, Japan

Atomically thin materials are expected as elements for nano-electro-mechanical resonator (NEMR) because of their unique electrical and mechanical properties. In addition, stacked 2D materials have also applied to NEMRs, which is expected for exploiting mechanical effects of heterojunction and interlayer interactions.[1] Here, we investigate the resonance properties of graphene/h-BN/graphene trilayer NEMR.

Sample fabrication process is as follows. First, we transferred CVD grown monolayer-graphene as bottom layer on the electrodes on n⁺-Si/SiO₂ substrate followed by transferring CVD grown multilayer h-BN (~3 nm thick, Graphene super-market, USA) on the graphene. Finally, CVD grown monolayer-graphene as top layer was transferred on the h-BN. All transfer process was performed by using polymethyl methacrylate. To fabricate suspended structure, SiO₂ layer underneath of the stacked layer was etched using buffered HF. Figure 1 shows a scanning electron microscope image of thus prepared sample, which is a drum type resonator with a typical diameter of 6 μm. Note that the top layer graphene was electrically floating. Resonance properties of graphene/hBN/graphene NEMR were evaluated by using frequency-modulation (FM) down mixing method[2] with modulation frequency $f_{mod} = 670$ Hz under the vacuum of $\sim 10^{-3}$ Pa as shown in Fig. 2.

Figure 3 shows a grayscale plot of drain source current I_{ds} as a function of gate voltage V_{gs} (x-axis) and frequency (y-axis). The white area corresponds to larger vibration amplitude and indicates resonance of the trilayer NEMR. At $V_{gs} > 0$, the resonance frequency is first decreased from 6.8 MHz to 6.3 MHz with increasing V_{gs} , which is caused by electrical softening effect. Further application of V_{gs} induces the monotonous increase of the resonance frequency because of the increase of the tension of the stacked layer. Thus, we have successfully fabricate the graphene/hBN/graphene NEMR.

References: [1] T.Inoue *et al.* 2D Materials, **5**, 045022 (2018).

[2] V. Sazanova *et al.* Nature **431**, 284 (2004).

Corresponding Author: K. Yasoshima

Tel: +81-90-8113-7597,

E-mail: yasoshima-4@pe.osakafu-u.ac.jp

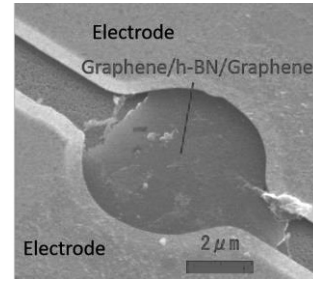


Fig. 1 SEM image of the device
 $\sim 10^{-3}$ Pa

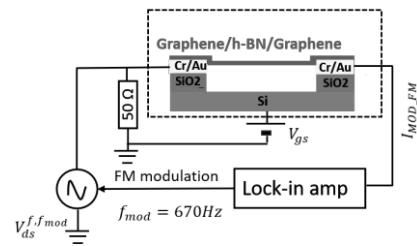


Fig. 2 Measurement setup.

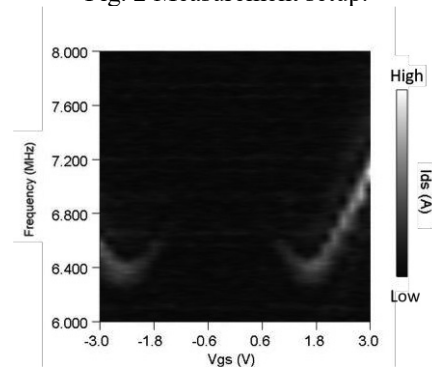


Fig. 3 Gray scale plot of resonance curve as a function of gate voltage V_{gs} .

p–n junction in graphene nanoribbon modified by periodically doped boron and nitrogen atoms

○Sake Wang¹, Md Shafiqul Islam¹, Nguyen T. Hung¹, Hongyu Tian², Ahmad R. T. Nugraha³,
Riichiro Saito¹

¹ *Department of Physics, Tohoku University, Sendai 980-8578, Japan*

² *School of Physics and Electronic Engineering, Linyi University, Linyi 276005, China*

³ *Research Center for Physics, LIPI, Tangerang Selatan 15314, Indonesia*

Graphene nanoribbon (GNR) is a one-dimensional graphene nanostructure whose electronic property depends on edge geometry, ribbon width, chemical doping, and crystallographic symmetry. According to the edge geometry, there are two categories of GNRs, namely, armchair GNRs (AGNRs) and zigzag GNRs. In particular, the energy band gaps of AGNRs are known to be inversely proportional to the ribbon width [1]. Due to such a gap tunability, the AGNRs are considered beneficial for electronic device applications. Moreover, the energy band gaps of AGNRs are sensitive to the chemical doping and doping position in the GNR.

A bottom-up approach of substitutional impurity for GNR using a well-defined precursor molecule was reported useful to fabricate atomically-precise doped GNRs [2]. The experiments [3] indicate that nowadays the periodic and precise doping of boron (B) or nitrogen (N) atoms can be experimentally achieved. However, the extensions of the nanoelectronics applications of the synthesized materials are not yet investigated. Therefore, by employing the B-doped p-type and N-doped n-type GNRs, we could construct a p–n junction theoretically, which is important for designing an integrated circuit.

We expect that the periodic doping of electron acceptors or donors will induce delocalized impurity-induced subbands, where physical properties are fundamentally different from an impurity level in the conventional semiconductor physics. Therefore, combining density functional theory, Wannier function basis set, and nonequilibrium Green's function, we explore electronic transport properties of a p–n junction in which the p (n)-side is based on periodically B (N)-doped AGNR. We consider practical devices with various smooth potential profiles of the depletion region. The I–V curves demonstrate a rectification effect behavior in the p–n junction, while slowly changing potential profile near the p–n junction would suppress the current. However, for the bias voltage between 0 and 0.3 V, since only the impurity bands contribute to the transmission, the electrical current is robust against the change of the smoothness of potential profile because the delocalization of the wave function for the impurity band cannot recognize the change of smoothness of potential profile. We also discuss the validity of our results at room temperature. The findings suggest that the doped AGNR could have potential nanoelectronics applications.

[1] Y.-W. Son, M. L. Cohen, and S. G. Louie, *Phys. Rev. Lett.* **97**, 216803 (2006).

[2] J. Cai *et al.* *Nature* **466**, 470 (2010).

[3] E. Carbonell-Sanromà *et al.* *Nano Lett.* **17**, 50 (2017); S. Kawai *et al.* *Nat. Commun.* **6**, 8098 (2015).

Corresponding Author: S. Wang

Tel: +81-22-795-7754, Fax: +81-22-795-6447,

E-mail: sake@flex.phys.tohoku.ac.jp

ポスター発表
Poster Preview

1P-1 ~ 1P-28

2P-1 ~ 2P-28

3P-1 ~ 3P-28

Formation of highly conductive N-type thermoelectric material by co-deposition of fullerene and cesium carbonate

○Tatsuma Izumi¹, Shinta Watanabe¹, Masato Nakaya¹, Jun Onoe¹

¹ Department of Energy Science and Engineering, Nagoya University, Aichi 464-8603, Japan

Fullerene (C₆₀) film exhibits a giant Seebeck coefficient (S) of -110 mV/K at room temperature (RT) [1], thus being one of candidates for novel flexible thermoelectric materials. Our goal is to fabricate high-performance thermoelectric conversion devices with a π -type structure composed of a sequential array of P- and N-type C₆₀-based films. We recently found that the composite film formed by co-deposition of C₆₀ and molybdenum oxide (MoO₃) shows a giant P-type S of +40 mV/K and an electrical conductivity (σ) greater by 10² times than that of pristine C₆₀ films [2]. Although the pristine C₆₀ film has the giant N-type S as described above, it shows a very low σ of ca. 10⁻⁶ $\Omega^{-1}\text{cm}^{-1}$. In this study, we aim to form a highly conductive N-type C₆₀-based film by co-deposition of C₆₀ and cesium carbonate (Cs₂CO₃).

All experiments were carried out in an ultrahigh vacuum chamber. C₆₀·Cs₂CO₃ composite films were formed by co-deposition of C₆₀ and Cs₂CO₃ on a natural mica substrate at RT. The σ of the composite films thus formed was evaluated by four-probe measurement. In order to evaluate S , a micro-gap electrode array was formed by depositing titanium (Ti) atoms on the composite film. The value of S ($-\Delta V/\Delta T$) was obtained from a thermoelectromotive force (ΔV) between adjacent Ti electrodes with a temperature difference (ΔT), using a microprobe S measurement system [2].

Figure 1 shows the temporal ΔT (top) and ΔV (bottom) between adjacent Ti electrodes. Since the ΔV was obtained to be a positive value, the C₆₀·Cs₂CO₃ composite film exhibits a N-type thermoelectric property ($S < 0$). Figure 2 shows the σ - $|S|$ plot for C₆₀·Cs₂CO₃ composite films formed by various molar ratios (x) of Cs₂CO₃ to C₆₀. The σ of the composite films drastically increased with x , and became greater by 10⁶ times than that of the pristine C₆₀ film. This may be due to the electron transfer from Cs₂CO₃ to C₆₀. However, the S remarkably decreased with increasing x , which is unpreferable to improve the thermoelectric conversion efficiency. We will discuss the trade-off relationship between S and σ .

[1] H. Kojima *et al.*, Mater Chem. Front., **2**, 1276 (2018).

[2] T. Kawai *et al.*, ACSIN-14, 23P128, Oct. 21-25, 2018.

Corresponding Author: Jun Onoe

Tel: +81-52-789-3784

E-mail: j-onoe@energy.nagoya-u.ac.jp

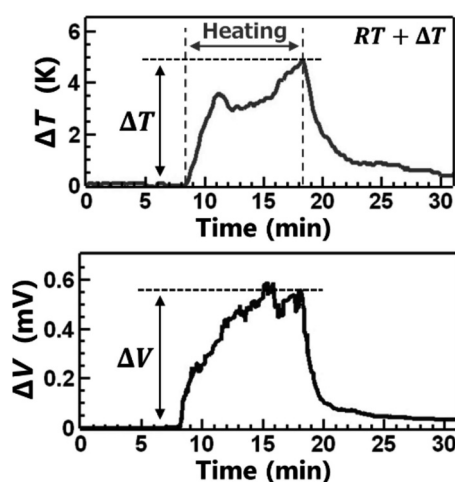


Fig. 1 Temporal ΔT and ΔV between adjacent Ti electrodes on the C₆₀·Cs₂CO₃ composite film.

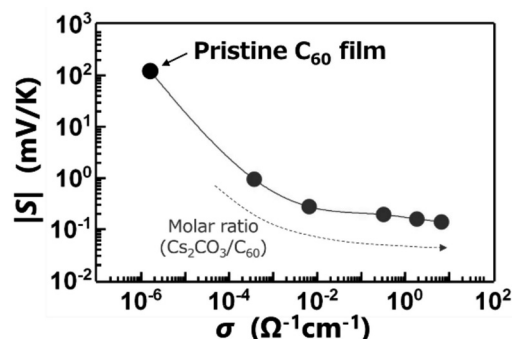


Fig. 2 The σ - $|S|$ plot of the C₆₀·Cs₂CO₃ composite films.

Chirality and helicity sorting of functionalized single-walled carbon nanotube

○Yui Konno, Michio Yamada, Yutaka Maeda

Department of Chemistry, Tokyo Gakugei University, Tokyo 184-8501, Japan

Single-walled carbon nanotubes (SWNTs) have attracted attention as nanocarbon materials with semiconductor or metallic properties. These properties depend on the diameter and the chiral angle of SWNTs. In practical applications of SWNTs as optoelectronic devices, it is important to separate SWNTs to improve their performance. The chirality sorting of SWNTs has been widely discovered with several methods such as ion-exchange chromatography [1], density gradient ultracentrifugation (DGU) [2], gel chromatography [3], and aqueous two-phase extraction (ATPE) [4]. The chemical functionalization of SWNTs has been extensively studied to increase their dispersibility and add new functions. Recent studies had clarified that oxidation, arylation, and alkylation reactions are effective to modulate local electronic structures of SWNTs [5]. As a result, new photoluminescence (PL) is observed from functionalized SWNTs efficiently depending on the addenda. We have previously investigated the alkylation and oxidation of SWNTs and revealed that the functionalization of (6,5) SWNTs selectively induced new PL peaks in a wide range from 1092 nm to 1268 nm, depending on the reagents used [5-7]. However, these studies had been conducted using the SWNTs mixture. The separation of SWNTs is also effective as functionalization to improve their intrinsic properties and performance in applications. For this purpose, we conducted the separation of functionalized SWNTs by gel chromatography [8].

SWNTs was functionalized using 1,2-bis(bromomethyl)benzene, which induced red-shifted PL at ~1230 nm, as in previous report. The gel chromatography method using a Sephacryl gel and three surfactants (sodium dodecyl sulfate (SDS), sodium cholate (SC), and sodium deoxycholate (DOC)), reported by Kataura and co-workers, was applied to the separation of the functionalized SWNTs due to the high efficiency of a separation of unfunctionalized SWNTs [9]. The separation of SWNTs was performed by a stepwise increase of DOC concentration in the mobile phase (0.5 wt% SC and 0.5 wt% SDS aqueous solution). (6,5) and (11,-5) SWNTs were eluted even after functionalization at DOC concentrations of 0.029 and 0.0315 wt%, respectively. The functionalized (6,5) and (11,-5) SWNTs exhibited the mirror-image CD spectra, similar to those of unfunctionalized SWNTs.

PL measurement of SWNTs at various concentrations provided evidence for the concentration quenching of E_{11} PL due to the reabsorption. On the other hand, smaller concentration quenching of the red-shifted PL peak was observed in the functionalized SWNTs. In addition, the concentration quenching of both SWNTs and functionalized SWNTs decreased after the separation.

1) Zeng, M. *et al. Nature* **2009**, 460, 250-253. 2) Kappes, M. M. *et al. J. Phys. Chem. C* **2009**, 113, 14628-14632. 3) Kataura, H. *et al. Nat. Commun.* **2011**, 2, 309. 4) Zeng, M. *et al. Adv. Mater.* **2014**, 26, 2800-2804. 5) Wang, Y. H. *et al. Nat. Rev. Chem.* **2019**, 3, 375-392. 6) Maeda, Y. *et al. Nanoscale* **2016**, 8, 16916-16921. 7) Maeda, Y. *et al. RSC Adv.* **2019**, 9, 13998-14003. 8) Maeda, Y. *et al. J. Phys. Chem. C* **2020**, 124, 21886-21894. 9) Kataura, H. *et al. Carbon*, **2018**, 132, 1-7.

Corresponding Author: Y. Maeda
Tel: +81-42-329-7512
E-mail: ymaeda@u-gakugei.ac.jp

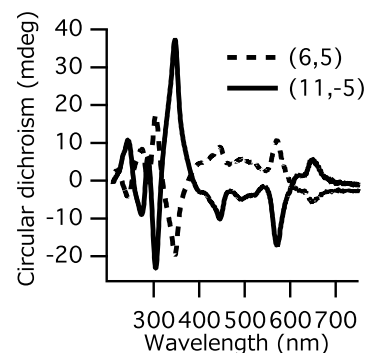


Fig. CD spectra of the functionalized SWNTs after the separation.

Diameter-based separation of SWNTs through their mechanical interlocking with nanorectangle

○ Guoqing Cheng, and Naoki Komatsu

Graduate School of Human and Environmental Studies, Kyoto University, Kyoto 606-8501, Japan

Although mechanical interlocking of SWNTs has attracted considerable attention [1], it has not been used for separating SWNTs. In this work, a new host molecule named “nanorectangle” connecting two nanocalipers by metal was designed, synthesized, and employed for separating SWNTs. After HiPCO SWNTs were sonicated in 2-propanol followed by centrifugation, the resulting extract showed the red shift in the absorption of nanorectangle (Fig. 1a), indicating its complexation with SWNTs. The mechanical interlocking of nanorectangle was observed in TEM, where two anthracenes attached on the both faces of SWNT (Fig 1b). After removal of host molecule through demetallization, the resulting SWNTs were analyzed by Raman and absorption spectroscopies, revealing the diameter enrichment around 0.9 nm (Fig. 1c). Such high selectivity was also confirmed with (6,5) and (7,6)-CoMoCAT SWNTs. As compared with nanocalipers [2], the better selectivity was observed toward the smaller diameters (Fig. 1c).

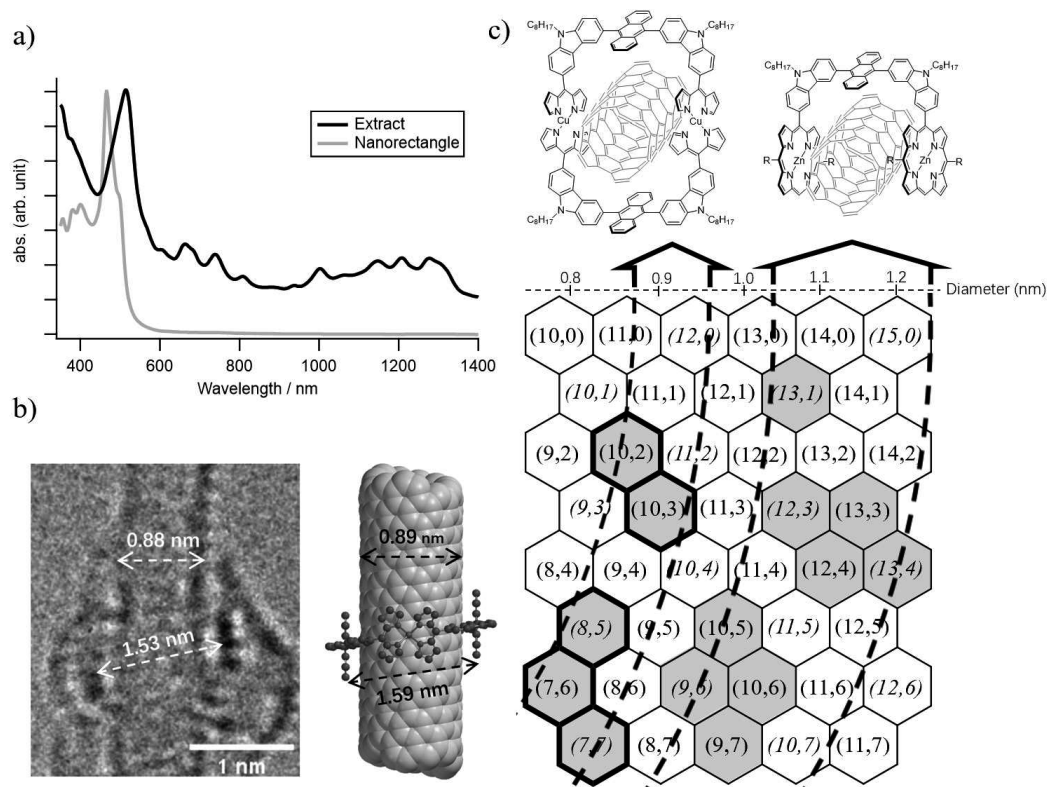


Fig.1 a) Absorption spectra of nanorectangle and SWNT extract. b) TEM image and model structure (alkyl chains are omitted) of SWNT wrapped with nanorectangle. c) Schematic structures of nanorectangle and nanocalipers complexed with SWNTs and their (n,m) selectivity in the map.

[1] B. Balakrishna, M. von Delius *et al. Angew. Chem. Int. Ed.*, **59**, 18774 (2020).

[2] G. Liu, N. Komatsu *et al. J. Am. Chem. Soc.* **135**, 4805 (2013).

Corresponding Author: Naoki Komatsu, Tel: +81-75-753-6833, E-mail: komatsu.naoki.7w@kyoto-u.ac.jp

Annealing Influence on Hall Effect Measurement of Single-Walled Carbon Nanotube Thin Films

○Hiroki Date¹, Mika Nagatomo¹, Akari Kobayashi¹, Taiki Inoue², Takenori Fujii³, Esko I. Kauppien⁴, Shigeo Maruyama¹, and Shohei Chiashi¹

¹ Department of Mechanical Engineering, The University of Tokyo, Tokyo 113-8656, Japan

² Department of Applied Physics, Osaka University, Osaka 565-0871, Japan

³ Cryogenic Research Center, The University of Tokyo, Tokyo 113-0032, Japan

⁴ Department of Applied Physics, Aalto University, Aalto FI-00076, Finland

Single-walled carbon nanotubes (SWCNTs) are one-dimensional materials in which graphene is rolled up into a cylindrical shape and they are expected to be applied in various industrial fields because of their high mechanical strength and electrical / thermal conductivity. Many studies have been conducted on the electrical conductivity of SWCNTs. While each individual SWCNTs have a very high electrical conductivity [1], macroscale SWCNT materials such as yarns and films, which are composed of bundled SWCNTs, have low electrical conductivity [2]. The doping effects of molecules in the air on the electrical conductivity of SWCNTs were also studied [3]. However, the origin of the low electrical conductivity is unknown and the yarn or thin films with high electrical conductivity have not been obtained. Therefore, in this study, in order to clarify the carrier properties, the electrical conductivity of SWCNT thin films [4] with different densities (i.e. different light transmittance) transferred on or suspended over the substrate was analyzed taking into account the adsorption effect. The device for measurement is shown in Fig. 1. The resistance change was measured in a vacuum in the temperature range from room temperature to 400 K, and then the magnetic field response of the Hall resistance was measured at 300 K. It was found that the resistance increased with increasing temperature, and activation energy obtained from the temperature dependence of the resistance rise rate suggested that water molecule desorption increased the electrical resistance (Fig. 2). Furthermore, the magnetic field response of the Hall resistance revealed that the carriers are holes and that the Hall resistance shows a non-linear change with respect to the magnetic field (Fig. 3). The non-linearity is thought to be due to the existence of two types of carriers with different mobilities or the one-dimensionality of SWCNTs [5].

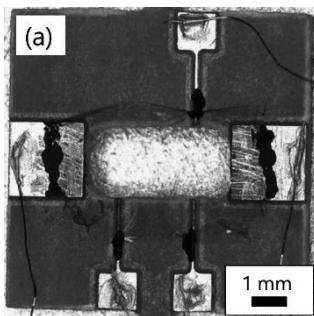


Fig. 1 Hall measurement device with suspended SWCNT thin film.

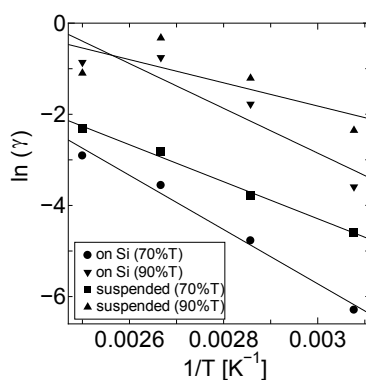


Fig. 2 Temperature dependence of the rate of the electrical resistance increase due to desorption.

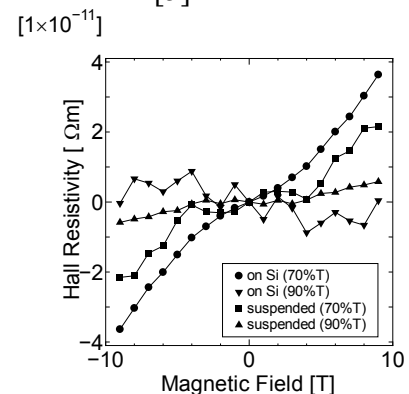


Fig. 3 Magnetic field dependence of Hall resistivity.

[1] T.W. Ebbesen *et al.*, Nature, **382**, 54 (1996). [2] N. Behabtu *et al.*, Science, **339**, 182 (2013).

[3] P.G. Collins *et al.*, Science, **287**, 1801 (2000). [4] A.G. Nasibulin *et al.*, ACS Nano, **5**, 3214 (2011).

[5] M.L. Roukes *et al.*, Phys. Rev. Lett., **59**, 3011 (1987).

Corresponding Author: S. Chiashi E-mail: chiashi@photon.t.u-tokyo.ac.jp

Theoretic Study of Anomalous Electric Polarization in Chiral Graphene Nanoribbons

Daichi Obana¹, Katsunori Wakabayashi¹

¹ *Department of Nanotechnology for Sustainable Energy, School of Science and Technology, Kwansei Gakuin University, Gakuen 2-1, Sanda 669-1337, Japan*

Zigzag graphene nanoribbons (ZGNR) have partial flat bands at the Fermi energy owing to topological edge states (TES), which can be associated with the finite Zak phase of bulk wave function in graphene [1]. TES are robust to weak perturbations, and provide a perfectly conducting channel [2]. The presence of finite Zak phase Z for bulk wave functions induces the electronic polarization with $P = \frac{e}{2\pi} Z$ at the graphene edge. Here, e is an elementary charge. Since TES are attributed to the electronic polarization, anomalously sensitive electric polarization to electric field is expected [3]. In armchair nanoribbon, the electric polarization has a very weak electric field dependence as shown fig. 1. However, the electric polarization value increases abruptly in other nanoribbon.

In this work, we calculated the electronic polarization of chiral graphene nanoribbons subjected to transverse electric field. We focus on the chiral angle dependence of electronic polarization under the infinitesimal transverse electric field for several different nanoribbons. Here, the chiral angle θ is measured from the axis parallel to the armchair edge, i.e., $\theta = 0^\circ$ corresponds to armchair nanoribbons and $\theta = 30^\circ$ corresponds to zigzag nanoribbons. The angle between 0° and 30° represents the

chiral nanoribbons. We confirmed that the electronic polarization linearly increases with increase of the chiral angle and saturates with the value of $e/6$. This saturation value is originated from the fact that the partial flat bands extend over the $1/3$ region of 1st BZ of ZGNR.

In conclusion, it is clearly confirmed that electronic polarization has strong chiral angle dependence, which originates from the topological properties of graphene.

[1] P. Delplace, et al., Phys. Rev. B **84**, 13 (2011). [2] K. Wakabayashi, et al., PRL **99**, 036601 (2007). [3] Y. Aihara, et al., Phys Rev. Res. **2**, 033224 (2020).

Corresponding Author: K. Wakabayashi (E-mail: waka@kwansei.ac.jp)

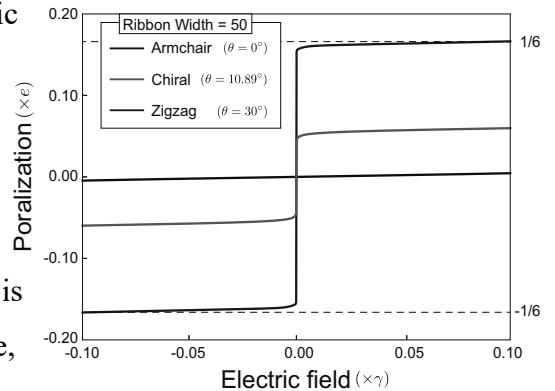


Fig. 1 Electric field dependence on electronic polarization of graphene nanoribbons. γ represents the nearest-neighbor hopping energy between carbon atoms.

Bulk photovoltaic effect in WSe₂/black phosphorus heterostructure via symmetry engineering

○Yu Dong¹, Toshiya Ideue¹, Takatoshi Akamatsu¹, Ling Zhou², Sota Kitamura¹, Mao Yoshii¹, Masaru Onga¹, Yuji Nakagawa¹, Kenji Watanabe³, Takashi Taniguchi⁴, Junwei Huang², Takahiro Morimoto¹, Hongtao Yuan², Yoshihiro Iwasa^{1,5}

¹ *Quantum-Phase Electronics Center (QPEC) and Department of Applied Physics, The University of Tokyo, Tokyo 113-8656, Japan*

² *College of Engineering and Applied Sciences & National Laboratory of Solid-State Microstructures, Nanjing University, Nanjing, China*

³ *Research Center for Functional Materials, National Institute for Materials Science, 1-1 Namiki, Tsukuba 305-0044, Japan*

⁴ *International Center for Materials Nanoarchitectonics, National Institute for Material Science, 1-1 Namiki, Tsukuba 305-0044, Japan*

⁵ *RIKEN Center for Emergent Matter Science (CEMS), Wako, Saitama 351-0198, Japan*

Symmetry plays an important role in condensed matter physics. It is determined by the crystal structure in bulk materials, while symmetry of two-dimensional (2D) systems can be artificially modified. For instance, bulk crystals of 2H type transition metal dichalcogenide (TMDC) have the inversion symmetry, but once it is exfoliated to monolayer form. The inversion symmetry is broken, resulting in peculiar optical and transport properties, which give rise to the concept of valleytronics [1]. Another recent example is the TMDC nanotubes. When TMDC is rolled into a tubular structure, it becomes a chiral and polar system, despite the nonpolar nature of the 2D TMDCs. As a result, we have observed a relatively large bulk photovoltaic effect, which is absent in nonpolar carbon nanotubes [2]. These examples exhibit that both the linear and nonlinear properties can be controlled by the manipulation of symmetry in nanostructures. In other words, nanomaterials are a fruitful platform of symmetry engineering, which might bring about novel functionalities [3].

In this poster presentation, we report symmetry engineering in van der Waals heterostructures. Specifically, we focus on the emergence of in-plane polar structure at the heterointerfaces of nonpolar 2D materials. The combination we have chosen is the monolayer WSe₂ and multilayer black phosphorus. Both materials are nonpolar, but polarization is created in their heterointerface. The emergence of polarity is intuitively understood as breaking rotational symmetry by combination of two lattice with three-fold and two-fold rotational symmetry. The polarity was probed by the observation of bulk photovoltaic effect [4]. Interestingly, the polar direction is rotated by twisting the alignment angle between Wse2 and black phosphorus. We will present detailed experimental results in the poster.

[1] J. R. Schaibrey *et al.* Nat. Rev. Mater., **1**, 160555 (2016).

[2] Y. J. Zahng *et al.* Nature, **570**, 349 (2019).

[3] T. Ideue and Y. Iwasa, Annu. Rev. Condens. Matter Phys., in press.

[4] T. Akamatsu *et al.* submitted for publication.

Corresponding Author: T. Ideue

Tel: +81-03-5841-6822, Fax: +81-03-5841-6822,

E-mail: ideue@ap.t.u-tokyo.ac.jp

Formation of self-assembled fibroin film on 2D materials

○Rio Takizawa¹⁾, Yoshiki Nakamura¹⁾, Kazunori Motai¹⁾, Mirano Tsukiiwa¹⁾,
Chishu Honma¹⁾, Yuhei Hayamizu¹⁾

¹⁾ School of Materials and Chemical Technology Department of Materials Science and Engineering,
Tokyo Institute of Technology, 2-12-1 Ookayama, meguroku, Tokyo, Japan

Silk fibroin is a protein which is a main component of silk. Silk fibroin is one of the most widely used natural materials for biomedical applications due to its excellent mechanical properties and biocompatibility. It is known that fibroins self-assemble into an ordered fibrils with a β -sheet structure, and their composition and self-assembled structure can be changed by genetic modification. The assembled structure can be used for bioelectronics with nanomaterials. Biosensors using 2 dimensional (2D) nanomaterials, such as graphene and MoS₂, are widely researched and expected to be high-performance, high-sensitivity sensors due to their atomically-flat surface, high specific surface area, and excellent electrical properties. For biosensor applications, it is important to create a surface that does not react with biomolecules other than the target molecule. At the same time, it is essential to fix biomolecules that bind to the target substance on the surface of the two-dimensional material. Fibroin can be a good candidate for this sake due to the mechanical stability of its self-assembled structures. However, to date, no research has been conducted on the self-assembly of fibroins on the surface of 2D nanomaterials. In this study, we aimed to use fibroins as a molecular scaffold and evaluated the self-assembly of fibroin on the surface of 2D materials.

Fibroin was produced by genetically modified bacteria [1]. Substrates of graphite and MoS₂ were exfoliated by the mechanical exfoliation method and transferred onto silicon wafers. 50 μ L of aqueous fibroin solution dissolved in MilliQ water or phosphate-buffer (PB) was dropped onto the substrate and allowed to stand at room temperature for 1 hour. Then, the aqueous solution was blown off by nitrogen gas and vacuum-dried overnight. The surface morphology of fibroins was then evaluated at the nanoscale using atomic force microscopy (AFM). We evaluated both substrates prepared with fibroin solutions in water and PB.

Figure 1 shows the AFM images of the self-assembled structures of fibroin when using 0.5 and 20 μ g / mL of fibroin solution. From the AFM images, the structure was observed to be linear. Also, the thickness of the film was found to be uniform, about 1.5 nm. Uniform films were formed in both pure water and PB as well, and the coverage increased with increasing concentration. Besides, when the washing resistance was checked using pure water and PB solution under the condition of high coverage, it was found that there was no significant change in the coverage in both cases. Thus, fibroin is expected to be one of the candidates as a molecular scaffold for future biosensor applications using 2D nanomaterials.

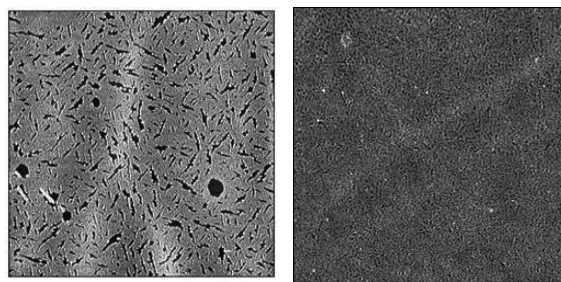


Fig. 1 AFM images of silk fibroin with 0.5 μ g / mL pure water (left) and 20 μ g / mL PB (right). Image size is 2x2 μ m

[1] Magaz, Adrián, *et al.* Advanced healthcare materials, 7.23 (2018): 1800308.

Corresponding Author: Y. Hayamizu

Tel: +81-3-5734-3651

E-mail: takizawa.r.ae@m.titech.ac.jp

Evaluating the degree of unintentional doping in CVD-grown MoS₂ monolayer

○Hibiki Naito¹, Yusuke Nakanishi¹, Hong En Lim¹, Yoshiyuki Nonoguchi²,
Takahiko Endo¹, Kenji Watanabe³, Takashi Taniguchi³, and Yasumitsu Miyata¹

¹Department of Physics, Tokyo Metropolitan University, Hachioji, 192-0397, Japan

²Faculty of Materials Science and Engineering, Kyoto Institute of Technology, Kyoto 606-8585, Japan

³National Institute for Materials Science, 1-1 Namiki, Tsukuba, 305-0044, Japan

Monolayer MoS₂ has been studied intensively because of its superior semiconducting properties and excitonic optical responses. Generally, monolayer MoS₂ is known to behave as an n-type semiconductor [1], due to the unintentional electron doping, which probably caused by the presence of lattice defects such as sulfur vacancies [2]. To explore the intrinsic physical properties and their potential in electronic devices, it is essential to develop a sophisticated growth technique that produces high quality samples with suppressed unintentional doping. For this purpose, we have investigated the growth and optical properties of various TMDC monolayers grown by chemical vapor deposition (CVD) [3]. However, it is still difficult to evaluate the unintentional doping of as-grown samples.

In this work, we have investigated the degree of electron doping for CVD-grown monolayer MoS₂ by studying its photoluminescence (PL) after chemical de-doping treatments. The samples were grown on SiO₂, sapphire, and hBN surfaces by CVD. Electron de-doping was conducted by spin-coating the butanol solution of different AgTFSI concentrations on the samples [4]. For monolayer MoS₂ grown on SiO₂ and sapphire surfaces, a blue shift and PL intensity increase were observed with the increase of AgTFSI concentration from 0.5 to 1 mM. In contrast, for the MoS₂ grown on hBN, the PL intensity remains unchanged up to 0.2 mM, but decreases with a concentration beyond. A longer PL lifetime (~150 ps) is observed in the as-grown MoS₂ on hBN compared to the on SiO₂. These results indicate that the unintentional doping of MoS₂ can be suppressed by selecting appropriate growth substrate. The present results provide a basis for the growth of high-quality samples and understanding the intrinsic optical properties of TMDC atomic layers.

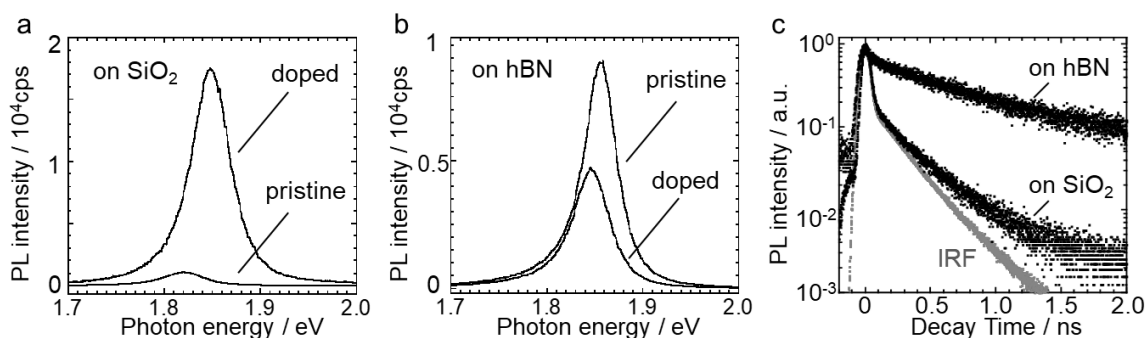


Fig.1. PL spectra of the CVD-grown monolayer MoS₂ synthesized on (a) SiO₂/Si and (b) hBN before and after doping with 1 mM AgTFSI solution. (c) Time-resolved PL decay profiles of the as-grown monolayer MoS₂ on SiO₂ and on hBN.

[1] B. Radisavljevic *et al.*, Nat. Nanotechnol **6**,147–150 (2011) [2] Wu Zhou *et al.*, Nano Lett **13**,2615–2622 (2013)
[3] Y. Kobayashi *et al.*, ACS Nano **13**,7527–7535 (2019) [4] Y. Nonoguchi *et al.*, Sci. Tech. Adv. Mater. **19**,581–587(2018)

Corresponding Author: Y. Miyata, Tel: 042-677-2508, E-mail: [ymiyata@tmu.ac.jp](mailto:y Miyata@tmu.ac.jp)

Zeeman-type spin-orbit interaction induced Ising ferromagnetism at a van der Waals interface

Hideki Matsuoka,¹† Masaki Nakano,^{1,2} Stewart Edward Barnes,³ Jun'ichi Ieda,⁴ Sadamichi Maekawa,^{2,5} Mohammad Saeed Bahramy,¹‡ Bruno Kenichi Saika,¹ Yukiharu Takeda,⁶ Hiroki Wadati,⁷ Yue Wang,¹ Satoshi Yoshida,¹ Kyoko Ishizaka,^{1,2} Yoshihiro Iwasa,^{1,2}

¹*Quantum-Phase Electronics Center and Department of Applied Physics, the University of Tokyo*

²*RIKEN Center for Emergent Matter Science (CEMS)*

³*Department of Physics, University of Miami*

⁴*Advanced Science Research Center, Japan Atomic Energy Agency*

⁵*Kavli Institute for Theoretical Sciences (KITS), University of Chinese Academy of Sciences*

⁶*Materials Sciences Research Center, Japan Atomic Energy Agency*

⁷*Graduate School of Material Science, University of Hyogo*

†*Present address: RIKEN Center for Emergent Matter Science (CEMS)*

‡*Present address: School of Physics and Astronomy, University of Manchester*

A van der Waals (vdW) heterostructure provides an indispensable material platform in modern condensed-matter researches. There, weak interlayer bonding nature ensures formation of an atomically abrupt heterointerface beyond fundamental constraint imposed by lattice matching condition, while strong electronic coupling enables creation of an emergent electronic ground state that is missing in individual materials. The most studies on the vdW heterostructures have been made by the top-down approach, exfoliation, pick-up, and dry-transfer. On the other hand, the bottom-up approach by MBE has remained almost totally undeveloped, probably due to difficulties in fabrication of high-enough quality samples. However, MBE should enable fabrication of a few layer samples even for hardly-cleavable materials as well as thermally-metastable compounds, and therefore, the MBE-based approach should be in principle extremely powerful and important for broadening the scope of vdW heterostructures.

Here we fabricated vdW heterostructures by MBE, where a new type of 2D magnet, vanadium selenide epitaxial thin film¹, was incorporated. The result demonstrates a new type of magnetic proximity effect mediated by Zeeman spin-orbit interaction of NbSe₂ across the vdW interface, which significantly impacts the magnetic properties of a neighboring 2D ferromagnet. In the presentation, we will show transport properties of those magnetic heterostructures, and discuss the interface proximity effect on 2D magnetism.

[1] M. Nakano *et al*, *Nano Lett.* **12**, 8806-8810 (2019).

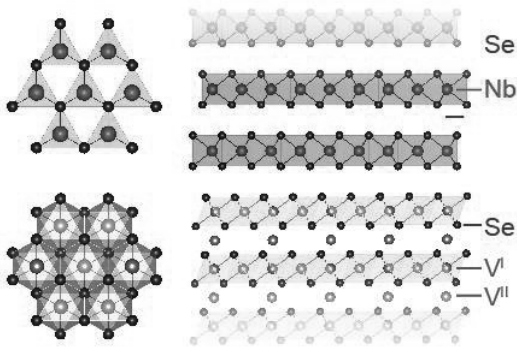


Fig. 1. The crystal structures for NbSe₂ (top) and V₅Se₈ (bottom).

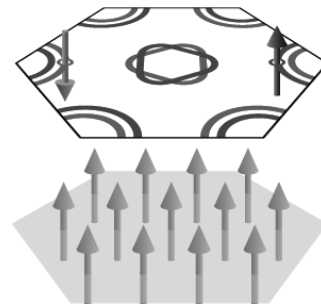


Fig. 2. The schematic of spin splitting bands in NbSe₂ (top) and the ferromagnetism in V₅Se₈ (bottom).

Fabrication and transport properties of PN diodes based on chemically-doped few-layer WSe₂

○Shunta Suzuki¹, Hiroto Ogura¹, Yusuke Nakanishi¹, Hong En Lim¹, Takahiko Endo¹,
Yoshiyuki Nonoguchi², Yasumitsu Miyata¹

¹Department of Physics, Tokyo Metropolitan University, Hachioji, 192-0397

²Faculty of Materials Science and Engineering, Kyoto Institute of Technology, Kyoto, 606-8585

Atomically-thin transition metal dichalcogenides (TMDCs) have attracted attention because their superior electrical properties and potential applications in electronics. In particular, TMDC-based PN junctions are expected to be useful for future light emitting devices and tunneling field effect transistors. Among the various reported techniques, chemical doping provides a facile way to fabricate a PN junction on a single TMDC layer. For example, such TMDC-based PN junction was realized by treating WSe₂ with diazonium salt and diethylenetriamine [1]. As high doping efficiency and long-term stability are oftentimes concerned in these chemically treated devices, we recently found that KOH and benzo-18crown, an n-type dopant, is a well-match to serve the above purposes [3]. In this study, we have fabricated the PN diodes based on few-layer WSe₂ using crown ether and AgTFSI as dopants and have investigated their transport properties.

Few-layer WSe₂ was grown on Si/SiO₂ substrates using chemical vapor deposition (CVD). In/Au electrodes were then deposited on the sample to fabricate the devices. Electron and hole doping of WSe₂ was conducted by spin coating of a solution of KOH and benzo-18crown and AgTFSI [3,4], respectively. I_d - V_{sd} curves show that both dopants can effectively increase electrical conductivity of the WSe₂ devices even in air, and carrier types of each device are confirmed by gate voltage dependence (Fig.1a). A rectification property is observed for the WSe₂ grain which was treated in parts with these dopants (Fig. 1b,c), implying the formation of a PN junction. Detailed fabrication process and transport properties of the devices will be further discussed in this presentation.

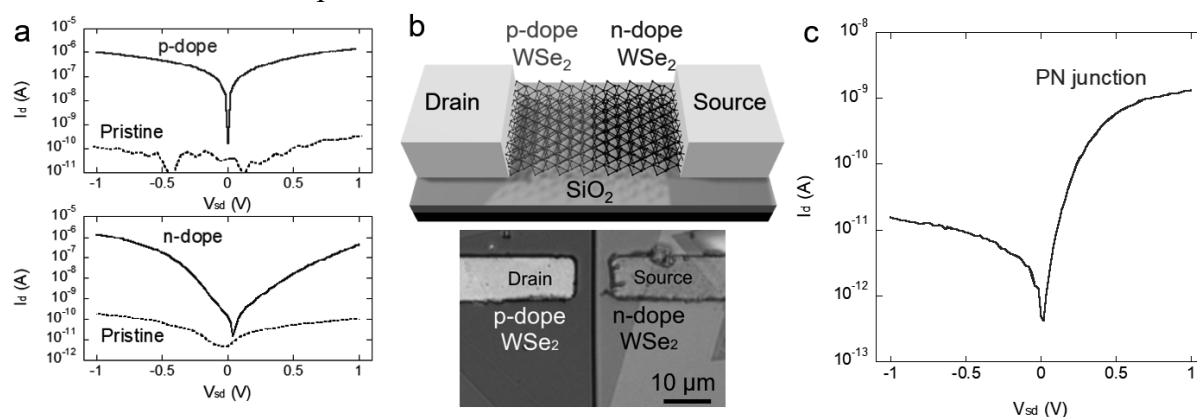


Fig.1 (a) I_d - V_{sd} curves of the p- and n-type doped WSe₂ device fabricated using AgTFSI and KOH & Benzo-18crown, respectively. (b) Schematic and optical images and (c) I_d - V_{sd} curve of a WSe₂ PN diode created with the dopants used in (a).

[1] H. G. Ji *et al.* *Adv. Mater.*, 31, 1903613 (2019). [2] Y. Nonoguchi *et al.* *Adv. Funct. Mater.*, 26, 3021 (2016).
[3] H. Ogura *et al.* *60th FNTG symposium*. [4] B. Xu *et al.* *ChemSusChem*, 7, 3252 (2014).

Corresponding Author: Y. Miyata, Tel: +81-42-677-2508, E-mail: miyata-yasumitsu@tmu.ac.jp

Synthesis and Characterization of Lithium-Ion-Encapsulated [70]Fullerene $\text{Li}^+\text{@C}_{70}$: A New Ionic Endohedral Fullerene

○Daiki Kitabatake,¹ Hiroshi Ueno,^{1,2} Kazuhiko Kawachi,^{3,4}
Yasuhiko Kasama,^{3,4} Shinobu Aoyagi,⁵ Keiji Ohshimo,¹ Fuminori Misaizu^{1,4}

¹ Department of Chemistry, Graduate School of Science, Tohoku University

² The Frontier Research Institute for Interdisciplinary Sciences, Tohoku University

³ Idea International Co. Ltd.

⁴ New Industry Creation Hatchery Center, Tohoku University

⁵ Department of Information and Basic Science, Nagoya City University

Inserting a small chemical species into fullerenes is a fascinating method to endow them with unique characteristic properties. Previously, a powerful method to access alkali metal encapsulated fullerenes, so-called “plasma implantation”, was developed, which enabled us to achieve scalable synthesis of lithium-ion encapsulated [60]fullerene $\text{Li}^+\text{@C}_{60}\text{X}^-$, a stable ionic form of lithium-encapsulated fullerene.^[1] In addition to the study of the properties of $\text{Li}^+\text{@C}_{60}$ arising from its ionic nature, it is important to unveil those of other “metal-ion-encapsulated” fullerenes.^[2]

In this work, we synthesized lithium-ion-encapsulated [70]fullerene ($\text{Li}^+\text{@C}_{70}$) as PF_6^- and TFSI^- ($\text{TFSI}^- = \text{bis}(\text{trifluoromethanesulfonyl})\text{imide}$) salts using our improved plasma shower method followed by previously developed oxidative purification process. ^7Li , ^{13}C , and ^{19}F NMR spectra clearly confirmed the encapsulation of Li^+ in defectless C_{70} cage and its diamagnetic ion-pair structure with the TFSI^- anion (Fig. 1). Further structural information and basic properties of the novel material will be presented at the symposium.

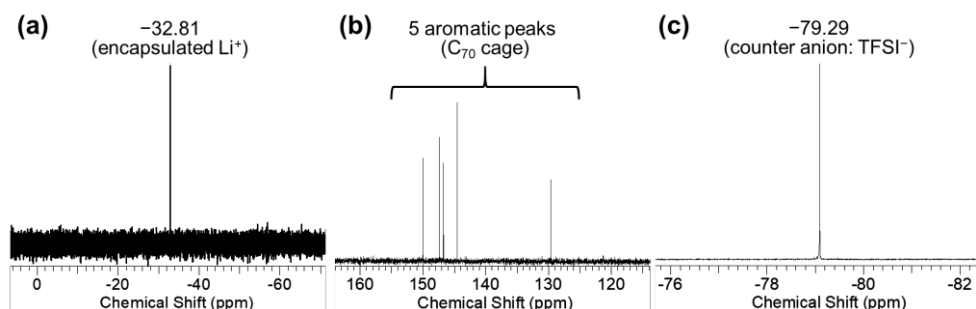


Fig. 1. (a) ^7Li , (b) ^{13}C , (c) ^{19}F NMR spectra of $\text{Li}^+\text{@C}_{70}\text{TFSI}^-$ measured in CD_2Cl_2 . $\text{LiCl}/\text{D}_2\text{O}$ (0 ppm) and $\text{C}_6\text{H}_5\text{CF}_3/\text{CDCl}_3$ (-62.61 ppm) were used as external standards for ^7Li and ^{19}F NMR, respectively.

[1] Aoyagi, S. *et al. Nature Chem.* **2010**, *2*, 678.

[2] Matsuo, Y. *et al. Endohedral Lithium-Containing Fullerenes: Preparation, Derivatization, and Application*; Springer: Singapore, 2017.

Corresponding Author: H. Ueno, Tel: +81-22-795-7645, E-mail: hiroshi.ueno.d5@tohoku.ac.jp

Growth mechanism and handedness relation of one-dimensional van der Waals heterostructures

Yongjia Zheng¹, Akihito Kumamoto², Rong Xiang¹, Kaoru Hisama¹, Keigo Otsuka¹, Yuta Sato³,
Taiki Inoue^{1,7}, Shohei Chiashi¹, Daiming Tang⁴, Qiang Zhang⁵, Anton Anisimov⁶, Esko
Kauppinen⁵, Kazu Suenaga⁸, Yuichiro Ikuhara², Shigeo Maruyama¹

¹ Department of Mechanical Engineering, The University of Tokyo, Tokyo 113-8656, Japan

² Institute of Engineering Innovation, The University of Tokyo, Tokyo 113-8656, Japan

³ Nanomaterials Research Institute, National Institute of Advanced Industrial Science and Technology (AIST),
Tsukuba 305-8565, Japan

⁴ International Center for Materials Nanoarchitectonics (WPI-MANA), National Institute for Materials Science
(NIMS), Namiki 1-1, Tsukuba 3050044, Japan

⁵ Department of Applied Physics, Aalto University School of Science, Espoo 15100, FI-00076 Aalto, Finland

⁶ Canatu Ltd., Helsinki FI - 00390, Finland

⁷ Department of Applied Physics, Osaka University, Osaka 565-0871, Japan

⁸ The Institute of Scientific and Industrial Research (ISIR-SANKEN), Osaka University, Mihogaoka 8-1, Ibaraki,
Osaka 567-0047, Japan

Recently, we presented one-dimensional (1D) van der Waals (vdW) heterostructure that includes single-walled carbon nanotubes (SWCNTs), boron nitride nanotubes (BNNTs) and molybdenum disulfide (MoS₂) [1]. The shell-by-shell growth of this heteronanotube is different from conventional growth of 1D homo-material nanotubes where multiple walls are formed simultaneously from a nanoparticle. Therefore, nucleation and crystal growth behaviors on these highly curved surfaces are of fundamental research interest. Here we present a comprehensive and thorough characterization on the formation process of BN layer on SWCNT surface. This is achieved by combining transmission electron microscopy (TEM) approach with the direct growth of 1D vdW heterostructures on TEM grid. This combination allows heterostructures to keep in the most intrinsic morphology, and many structure details can be clearly visualized. Furthermore, their crystal relationship and handedness correlation were also investigated.

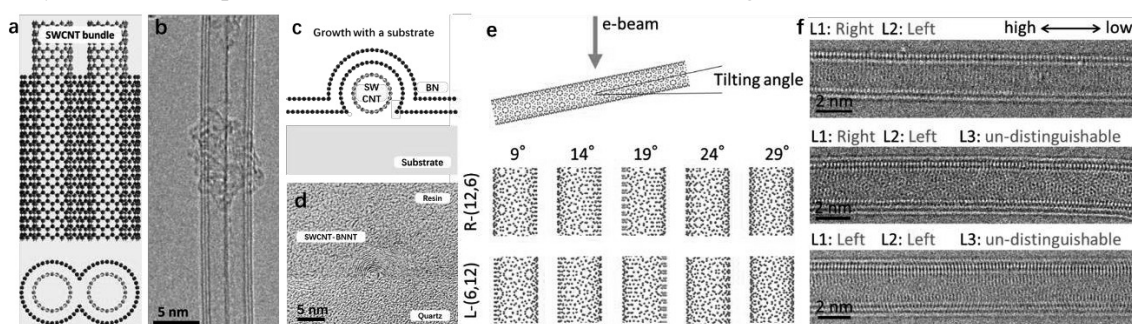


Fig. 1: (a) Atomic model of a BN coated bundle consisting of two SWCNTs, and its cross-section view. (b) TEM image for this bundle situation. (c) Atomic model of a BN coated SWCNT on a flat substrate as the second situation. (d) Specimen based on the second situation made by a focused-ion-beam (FIB) system for TEM characterization. (e) Schematic illustration of identifying the handedness of inner SWCNT or outer BNNT under TEM measurement. (f) representative TEM images of three SWCNT-BNNT heterostructures having different handedness combinations.

[1] R. Xiang *et al.*, *Science*, **367**, 537 (2020).

Corresponding Author: S. Maruyama

Tel: +81-3-5841-6421,

Fax: +81-3-5841-6983,

E-mail: maruyama@photon.t.u-tokyo.ac.jp

Effect of hydrogen on the microplasma synthesis of carbon nanotubes

○Takashi Tsuji¹, Jaeho Kim², Hajime Sakakita², Yoshiki Shimizu^{3,4}, Guohai Chen¹, Kenji Hata¹, Don N. Futaba¹, Shunsuke Sakurai¹

¹*CNT-Application Research Center, National Institute of Advanced Industrial Science and Technology (AIST), Ibaraki 305-8565, Japan*

²*Innovative Plasma Processing Group, Research Institute for Advanced electronics and Photonics, National Institute of Advanced Industrial Science and Technology (AIST), Ibaraki 305-8568, Japan*

³*Nanomaterials Research Institute, National Institute of Advanced Industrial Science and Technology (AIST), Tsukuba, Ibaraki 305-8565, Japan*

⁴*AIST-UTokyo Advanced Operando-Measurement Technology Open Innovation Laboratory (OPERANDO-OIL), National Institute of Advanced Industrial Science and Technology (AIST), Kashiwa, Chiba 227-8589, Japan*

The importance of hydrogen for the synthesis of carbon nanotubes (CNTs) is well known as it has been well documented in the literature. Its role spans the reduction and formation of the catalyst nanoparticle as well as additional functions, such as etching of disordered carbon and defect healing, during the graphitic precipitation process. Across the diverse techniques approaches to synthesize CNTs, hydrogen has been reported to play slightly different roles in promoting, or inhibiting, growth.

Recently, we have reported a mini-synthesis system composed of a microplasma reactor as the primary energy source [1, 2]. This reactor was shown to efficiently grow highly crystalline single and double wall CNTs at exceptionally high growth rates. Within this approach, we also found hydrogen to be critically important in increasing the yield and purity of the growth CNTs, but our investigation revealed that hydrogen served a different role. As the hydrogen content increased from zero to 5%, visible changes in the color and shape of the plasma were apparent. Optical emission spectroscopy of the plasma demonstrated that hydrogen increased the temperature through dissociation and recombination induced from the absorption of the plasma energy. In doing so, hydrogen essentially shifted the decomposition of the reactant gases from a solely electron-driven process to one including a thermally driven component. As such, this supported the appropriate order of reactions which are necessary to support CNT synthesis, (specifically, catalyst precursor decomposition, catalyst nanoparticle formation, carbon feedstock decomposition, and CNT nucleation and growth) and led to an increase in CNT growth and reduced disordered carbon particles. Combined with transmission electron microscopy evaluation, we propose a model describing the driving mechanism of our mini-synthesis system. These results not only indicate the multifaceted role which hydrogen can contribute to the synthesis of CNTs, but also that while electron-driven processes can effectively dissociate reactance processes, they do not necessarily support the necessary series of reactions for CNT synthesis for mixed (catalyst and carbon) precursors.

[1] T. Tsuji *et al.* Abstracts of the 59th Fullerene-Nanotubes-Graphene General Symposium (2020).

[2] T. Tsuji *et al.* Carbon 173, 448 (2021).

Corresponding Author: T. Tsuji

Tel: +81-29-861-0254, Fax: +81-29-861-4851

E-mail: takashi.tsuji@aist.go.jp

Thermal conductivity of C₆₀ encapsulated single-walled carbon nanotubes thin films

Rikuto Abe, Kan Ueji, Yohei Yomogida, Kazuhiro Yanagi

Department of Physics, Tokyo Metropolitan University, Tokyo 192-0397, Japan

Encapsulation of molecules and inorganic materials into the hollow core of single walled carbon nanotubes (SWCNTs) is one of techniques to tune the physical properties of SWCNTs, and to fabricate novel one-dimensional materials. Regarding the control of thermal conductivity, κ , of SWCNTs by C₆₀ encapsulation, previous studies reported that the encapsulation of C₆₀ into SWCNTs slightly enhanced the κ in their bucky paper form [1], but a recent study revealed that in a single bundle of SWCNTs the reduction of κ in a single bundle by encapsulation of C₆₀ is observed due to the formation of phononic band gap [2]. Thus, whether the encapsulation of C₆₀ can enhance or reduce the κ is not clear. In this study, we measured the κ of SWCNT thin films with thickness of approximately 100 nm, and evaluated the influence of the encapsulation of C₆₀ on the thin film thermal conductivity. We prepared C₆₀@SWCNTs by a conventional vapor phase method [3], and then we measured the thermal conductivity of thin films of C₆₀@SWCNTs by time-domain thermal reflectance (TDTR) method at room temperature [4]. Fig. 1 shows the TDTR signals of SWCNTs and C₆₀@SWCNT thin films. The TDTR signals were almost identical between SWCNTs with and without C₆₀, indicating that no significant changes on thermal flow. The κ values of SWCNT and C₆₀@SWCNTs are determined to be $(2.7 \pm 0.3) \times 10^{-1}$ and $(2.0 \pm 0.3) \times 10^{-1}$ W/mK, respectively. There was a slight decrease of κ by encapsulation of C₆₀, but not so significant, indicating the thermal boundary resistance between tube-tube contacts would dominantly contribute the heat flow in the thin films.

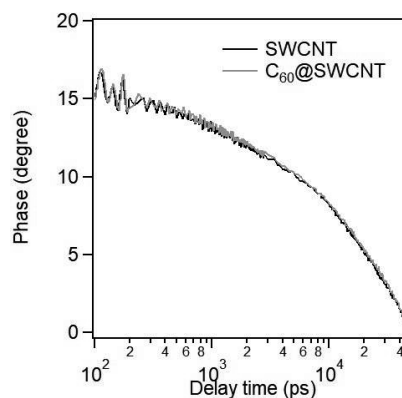


Fig. 1 TDTR signals of thin films of SWCNTs and C₆₀@SWCNTs

[1] Vavro et al., Appl. Phys. Lett. 80, 1450 (2002) [2] Kodama et al., Nat materials.,10,1038 (2017)
 [3] M. Kawai et al. J.Am.Chem.Soc., 134, 9545 (2012) [4] Ueji et al., JJAP 58, 128006 (2019)

Corresponding Author: K. Yanagi, E-mail: yanagi-kazuhiro@tmu.ac.jp

Thermal boundary resistance of aligned films of single-walled carbon nanotube using time-domain thermoreflectance method

○Atsuhiko Katagiri¹, Kan Ueji¹, Yuya Matsuoka¹, Junko Eda¹, Hitomi Okubo¹, Yohei Yomogida¹, Junichiro Kono² Takashi Yagi³ and Kazuhiro Yanagi¹

¹Department of physics, Tokyo Metropolitan University, Hachioji, Tokyo 192-0397, Japan

²Department of Electrical and Computer Engineering, Rice University, Houston, TX 77005, U.S.A.

³National Metrology Institute of Japan, National Institute of Advanced Industrial Science and Technology, Tsukuba, Ibaraki, 305-8563, Japan

Understanding of thermal flow through inter-tube junctions between single-walled carbon nanotube (SWCNT) is important to obtain optimal thermal conductivity for thin-film device using SWCNT. Several theoretical simulations mentioned that a thermal resistance of inter-tube junction depends on the angle between the axes of the contacted nanotubes [1-2], and then it is required to experimentally clarify such characters for the thermal managements of the SWCNT thin films. Recently, a method to fabricate aligned SWCNT films with large area has been developed. In this study, we investigate the effect of the stacking angle on a thermal boundary resistance between two aligned SWCNT films by a time-domain thermoreflectance (TDTR) method.

First, we prepare a membrane where the grooved structures were artificially formed, and then we fabricated the aligned SWCNT thin-film by filtration under vacuum controlled system. [3] During the filtration, the filtration area was controlled by Si rubber. This technique enables us to prepare uniform, thick and aligned thin film with good reproducibility (Figure a). Finally, the aligned film was transferred and stacked onto the Au substrate with controlled angles between the aligned direction of the films, and then we evaluated the thermal boundary resistance at the interfaces between the stacked films by TDTR. Figure b shows experimental TDTR signals for the samples (1-layer, 2-layer with different stacking angles). One dimensional heat conduction model suggested that the thermal boundary resistance at the interface where the stacking angle is 90° is higher than that at the interface where its angle is 0°. The detailed of the thermal boundary resistance will be presented in the poster.

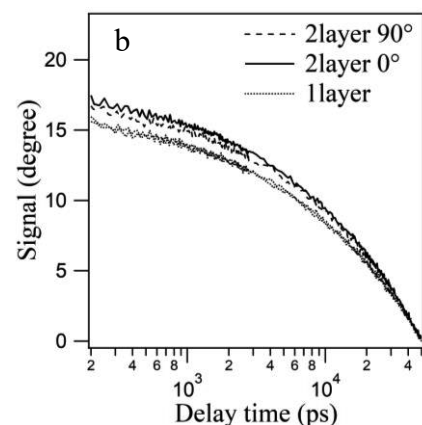
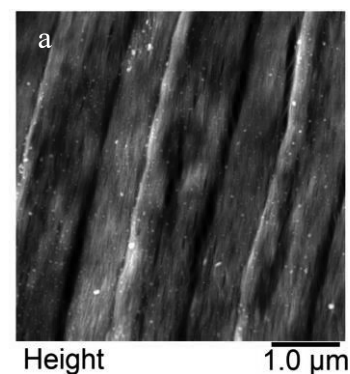


Figure: AFM images of SWCNT film prepared using the Si rubber (a) and angle dependence of TDTR signal Which measure 2layer SWCNT (b).

References: [1] Evans *et al. Appl. Phys. Lett.* **100**, 261908 (2012)

[2] Hu *et al. J. Appl. Phys.* **114**, 224308 (2013) [3] He *et al. Nat. Nanotechnol.* **11**, 1 (2016)

Corresponding Author: K. Yanagi Tel: +81-42-677-2809 E-mail: yanagi-kazuhiro@tmu.ac.jp

Local Grafting of Polymer Radical on the Surface of Single-Walled Carbon Nanotubes and the Enhanced Photoluminescence in the Near-Infrared Region

○Yukiko Nagai¹, Kenta Nakamura¹, Tsuyohiko Fujigaya^{1,2,3}

¹Department of Applied Chemistry, Graduate School of Engineering, Kyushu University, 744 Motoooka, Fukuoka 819-0395, Japan. ²WPI ICNER, Kyushu University. ³Center for Molecular Systems, Kyushu University.

Photoluminescence (PL) of single-walled carbon nanotubes (SWCNTs) in the near-infrared (NIR) region (E_{11} emission) is attractive, especially for bioimaging and biosensing *in vivo*. In this study, we achieved brighter NIR emission of SWCNTs compared with E_{11} emission by polymer grafting on the SWCNT surface, which generates emissive sp^3 defects through local chemical functionalization of the polymer radical in the interior of surfactant (SDS)-dispersed SWCNTs (**Fig. 1**) [1]. The locally functionalized SWCNTs (lf-SWCNTs) show new PL assignable to E_{11}^* and E_{11}^{2*} emission at longer wavelength (>1100 nm) than E_{11} emission (<1100 nm) [2], which is preferable to avoid the strong autofluorescence from the body.

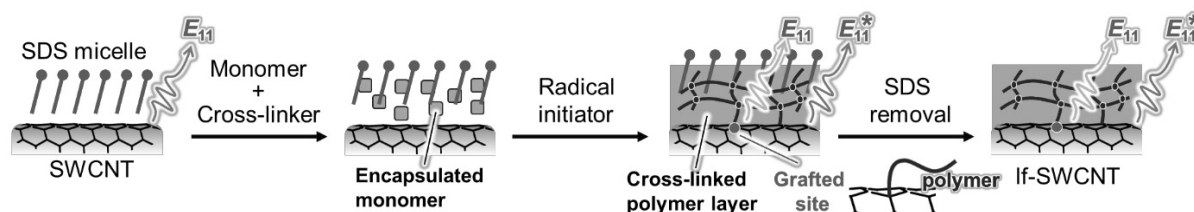


Fig. 1 Scheme of synthesis of lf-SWCNTs by polymer grafting.

Recently, we have developed a unique emulsion polymerization method to coat SWCNT surface with a cross-linked polymer by radical polymerization around the SWCNTs called carbon nanotube (CNT) micelle polymerization [3]. It was found that the radical initiator concentration and polymerization time strongly affected the E_{11}^* and E_{11}^{2*} emission intensities, and as polymerization progresses, E_{11}^* and E_{11}^{2*} emission became brighter, while E_{11} emission became darker (**Fig. 2**). At the optimum condition, the E_{11}^* emission intensity was about 6 times brighter than the initial E_{11} emission.

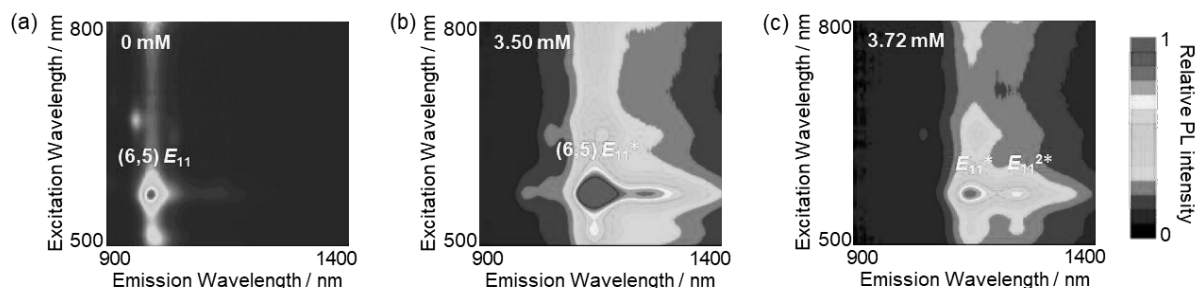


Fig. 2 Two-dimensional PL counterplots of SWCNTs after CNT micelle polymerization using (a) 0 mM, (b) 3.50 mM and (c) 3.72 mM of radical initiator.

[1] Y. Nagai and T. Fujigaya *et al.*, *ACS Appl. Nano Mater.* **3**, 8840 (2020). [2] Y. Wang *et al.*, *Nat. Chem.* **5**, 840 (2013). [3] T. Fujigaya *et al.*, *RSC Adv.* **4**, 6318 (2014).

Corresponding Author: T. Fujigaya

Tel: +81-92-802-2842, Fax: +81-92-802-2842, E-mail: fujigaya.tsuyohiko.948@m.kyushu-u.ac.jp

Modeling and Optimization of Tensile Strength of CNT/HDPE Composites Using Response Surface Methodology

○Nao Otsuki¹, Masaru Sekido²

¹ *Division of Production System and Design Engineering, National Institute of Technology, Sendai College, Natori 981-1239, Japan*

² *Department of Materials and Environmental Engineering, National Institute of Technology, Sendai College, Natori 981-1239, Japan*

CNTs are considered as the ideal reinforcement fillers for the composites material due to their light weight, high aspect ratio, and outstanding mechanical properties. In previous study we have studied the tensile strength of CNT/high density polyethylene(HDPE) composites prepared by Melt Blending and found that tensile strength of CNT/HDPE was increased with the weight ratio of CNT [1]. Tensile strength of composites depends on crystallinity of matrix and dispersibility of filler in matrix as well. Crystallinity of matrix varies with the injection pressure. The increase of screw speed will produce higher shear stress on the mixture and better dispersion of filler in matrix [2].

In this study we have studied the effects of weight ratio of CNT, injection pressure, and screw speed on tensile strength of CNT/HDPE composites to optimize the preparation conditions. Samples were prepared with different compositions of CNT(0, 2.5, 5.0 wt%) at different injection pressure(10, 12, 14 bar) and screw speed(100, 150, 200 rpm). The mathematical model have been developed by Response Surface Methodology(RSM). The adequacy of the developed model is tested using the analysis of variance(ANOVA).

[1] Atsushi Onodera *et al.*, The 54th fullerenes-Nanotubes-Graphene General Symposium, 1P-11(2018)

[2] Ruey Shan Chen *et al.*, International Conference on Agricultural, Ecological and Medical Science, Malaysia, 45-47(2015)

Corresponding Author: N. Otsuki

Tel: +81-22-381-0329, Fax: +81-22-381-0329

E-mail: a1912608@sendai-nct.jp

Effects of deposition conditions on the states of Pt nanoparticles on carbon materials and their electrocatalytic properties toward methanol oxidation and CO poisoning

○Yuho Abe¹ and Hironori Ogata^{1,2}

¹ *Department of Chemical Science and Technology, Hosei University*

² *Research Center for Micro-Nano Technology, Hosei University*

E-mail: hogata@hosei.ac.jp

A direct methanol fuel cells(DMFCs), which is a type of solid oxide fuel cell(SOFC), is expected as a next generation energy supply source. DMFCs are one of the most promising transportable power sources which can be used in mobiles, laptops, and small power generation. The basic operation principle of DMFCs involves methanol oxidation and oxygen reduction on the precious metal catalysts, which are carbon supports as well as catalyst particle size and shape plays a dominant role in the electrochemical performance for fuel cells. The most important advantage of DMFCs over other types of fuel cells is that methanol can integrate effectively with transmission and distribution systems that already exist. However, there are technological challenges for the commercialization of DMFCs that remain unsolved [1,2,3]. The basic operation principle of DMFCs involves methanol oxidation and oxygen reduction on the precious metal catalysts, which are loaded on the support surfaces. As is well-known, the dispersion of Pt-based nanoparticles on carbon supports as well as catalyst particle size and shape plays a dominant role in the electrochemical performance for fuel cells. We have explored the electrocatalytic properties of Pt-based nanoparticles supported on the carbon materials by one-step electrodeposition [4]. In this study, we investigated CO stripping in addition to the operations performed in the past. In the liquid phase reduction method, the concentration was changed, and in the electrodeposition method, the effect of support due to changes in the applied voltage and application time was investigated. Especially, we selected the electrodeposition method and the liquid phase reduction method as the loading of Pt nanoparticles on single walled carbon nanotubes (SWNTs) composite materials and compared the dispersion state of Pt nanoparticles on the nanocarbon materials and the oxygen reduction reaction activities. The surface state of SWNTs, the loading state of Pt nanoparticles and the catalytic properties of electrode were investigated using TEM, XPS, and cyclic voltammogram (CV).

The detailed results will be presented.

References:

- [1] N. Pongpichyakul *et al.*, *Springer Nature*, **50**, 51-62 (2019).
- [2] S.K.Kamarudin *et al.*, *Applied Catalysis B: Environmental*, Elsevier, **262**, 118217 (2019)
- [3] I. Martinalou *et al.*, *International Journal of Hydrogen Energy*, Elsevier, **34**, 6902-6916 (2009)
- [4] Zhipeng Wang, Mao Shoji and Hironori Ogata, *Appl. Surf. Sci.*, **259**, 219-224 (2012).

Corresponding Author: H.Ogata

Tel: +81-42-387-6229, Fax: +81-42-387-6229,

E-mail: hogata@hosei.ac.jp

Scattering parameter analysis of self-aligned flexible carbon nanotube thin-film transistors

○Soya Ishimaru¹, Taiga Kashima¹, Hiromichi Kataura², and Yutaka Ohno^{1,3}

¹*Department of Electronics, Nagoya University, Nagoya 464-8603, Japan*

²*Nanomaterials Research Institute, National Institute of Advanced Industrial Science and Technology 305-8565, Japan*

³*Institute of Material and Systems for Sustainability, Nagoya University, Nagoya 464-8601, Japan*

Scattering- (S -) parameter analysis is powerful technique to characterize the operation speed of transistors and to clarify the causes of excess delay. We apply S -parameter analysis to the self-aligned flexible CNT TFTs [1] to show the effect of the self-aligned structure on the operation speed enhancement. The equivalent circuit analysis is also carried out the extract device delay parameters.

We fabricated CNT TFTs with a bottom gate structure by the (a) self-align and (b) conventional processes (Fig. 1). Semiconducting CNTs purified by the gel-chromatography were used as the channel. S -parameter measurements were carried out by using a vector network analyzer (Keysight, E5061B) at frequencies up to 10 MHz. The open and through calibrations were performed in order to remove the impact of the parasitics associated with the measurement setup and contact pads.

Figure 2 shows the current gain cutoff frequencies (f_T) and maximum oscillation frequencies (f_{max}) evaluated from S -parameters various channel length (L_{ch}) at V_{DS} of -5 V and V_{GS} of -3 V. The f_T and f_{max} were enhanced by a factor of about 10 by introducing the self-aligned structure. High f_T and f_{max} over 10 MHz were obtained for the self-aligned device of $L_{ch} = 5 \mu\text{m}$. The equivalent circuit analysis based on the measured S -parameters shows that the contact resistance at the source and drain electrodes becomes the dominant cause of delay with reducing L_{ch} less than $10 \mu\text{m}$.

[1] S. Ishimaru *et al.*, *The 59th Fullerenes-Nanotubes-Graphene General Symposium*, 3P-16

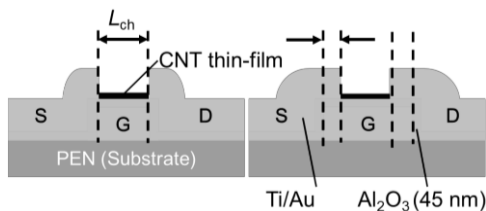


Fig.1 Device structure.

(a) Self-aligned, (b) conventional.

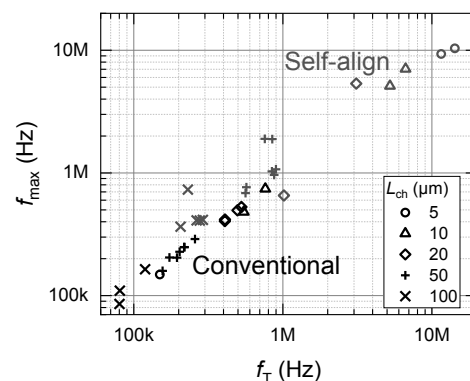


Fig. 2 f_{max} versus f_T .

Corresponding Author: Yutaka Ohno, Phone: +81-52-789-5387, E-mail: yohno@nagoya-u.jp

One-dimensional growth of WS₂ by chemical vapor deposition

○Kazuma Shimogami¹, Misaki Kishibuchi¹, Hiroataka Inoue¹, Liu Zheng², Yasumitsu Miyata³,
Yasuhiko Hayashi¹, Hiroo Suzuki¹

¹Graduate School of Natural Science and Technology, Okayama University, Okayama
700-8530, Japan

²Innovative Functional Materials Research Institute, National Institute of Advanced Industrial
Science and Technology (AIST), Tsukuba 305-8565, Japan

³Department of Physics, Tokyo Metropolitan University, Hachioji 192-0397, Japan

Transition metal dichalcogenides (TMDCs) are potential candidates for the next-generation optoelectronics device such as photodetectors, light-emitting diodes, and solar cells due to its superior optoelectronic properties and flexibility. The optoelectronic properties of TMDCs are sensitive to their crystal structures such as number of layers, crystal phase, defect density, and presence of edges. Because the dimension of the crystal is also an impactful factor, the dimension control from 3D to 2D (multilayer to monolayer) has been studied well, showing the significant increase of photoluminescence (PL) intensity. In contrast to such studies from 3D to 2D, much less study has been conducted on downscaling from 2D to 1D. The structure control from 2D to 1D is possible to allow us to investigate novel optoelectronic physics and applications derived from quantum confinement effect and presence of edges.

The two strategies for the synthesis of 1D-TMDC can be considered. One is a top-down, and the other is a bottom-up process. The top-down approach by the conventional lithography technique is frequently used, but there is a great advantage in the bottom-up process in terms of the cleanness of the surface and edge.

In this research, we have investigated the growth of 1D-WS₂ by chemical vapor deposition (CVD), which is a bottom-up process. The cold-wall CVD system with the infrared gold image furnace was established for TMDC growth. The solution of Na₂WO₃ was employed as a W source for WS₂ and deposited on SiO₂/Si substrates. The vapor of (t-C₄H₉)₂S₂ was introduced to a CVD chamber as an S source. From the systematic investigation of CVD growth, we found that the fiber-like materials can be grown with a relatively low (t-C₄H₉)₂S₂ supply (Fig. 1(a)). The atomic force microscopy (AFM) revealed that the fibers are around 3 nm in thickness, which is relatively thicker than monolayer WS₂. The fibers showed both almost the same Raman and PL peaks as monolayer WS₂ (Fig. 1(b)). The transmission electron microscopy (TEM) observations revealed the presence of W_xO_y nanowires in the sample. These results suggest that the 1D-WS₂ could be formed on the CVD-grown W_xO_y nanowire.

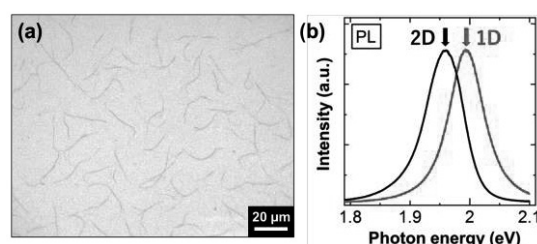


Fig. 1. (a) Optical microscope image of 1D-WS₂. (b) PL spectra of 1D- and 2D-WS₂.

Corresponding Author: H. Suzuki

Tel: +81-86-251-8133

E-mail: hiroo.suzuki@okayama-u.ac.jp

Gate-turning of carrier doping by oxygen molecule adsorption on MoS₂

○T. Yoshida¹, K. Takai^{1,2}

¹Department of Chemical Science and Technology, Hosei University, Tokyo 184-8584, Japan

²Graduate school of Science and Engineering, Hosei University, Tokyo 184-8584, Japan

2D-materials are susceptible to adsorbents from the ambient environment because all constituent atoms are present on the surface. For example, MoS₂, which is one of the 2D-materials is known to be hole-doped when oxygen molecules are adsorbed [1]. There are two types of adsorption of molecules: physical adsorption and chemisorption. In the case of chemisorption involving charge transfer, the adsorption rate differs depending on the charge state of the host substance. Previous studies have shown that upshifting the Fermi energy (E_F) of graphene increases the characteristic rate of charge transfer in oxygen molecule adsorption [2]. In this study, the E_F of MoS₂ was modulated by applying gate voltage (V_G) during oxygen exposure, and the adsorption characteristics were investigated by the electron transition.

MoS₂-FET was fabricated after mechanical exfoliation of 1L-sample on a 285 nm SiO₂ / Si substrate. The electric conductivity was measured after exposure of oxygen gas applying V_G .

Fig. 1 shows the V_G dependence of the source-drain current I_{SD} when exposed to oxygen ($V_G = 0$ V). Hole doping by oxygen molecule adsorption progresses as the exposure time (t) increases. **Fig. 2** shows the t dependence of the shift of threshold voltage ΔV_{TH} from that at $t = 0$ when exposed to oxygen gas at $V_G = -60$, 0, and +60 V. The hole doping by oxygen gas adsorption gradually shows a tendency to saturate. In addition, the relaxation time when $V_G = +60$ V was applied and exposed to oxygen gas was shorter than that of $V_G = -60$ V. These results indicate that the adsorption of oxygen molecules depends on the charge state of MoS₂ as the host substance.

[1] Y. Minakawa, T. Umehara, and K. Takai, The 58th FNTG (2020),

[2] Y. Sato, K. Takai, and T. Enoki, Nano Lett., 11, 8 (2011),

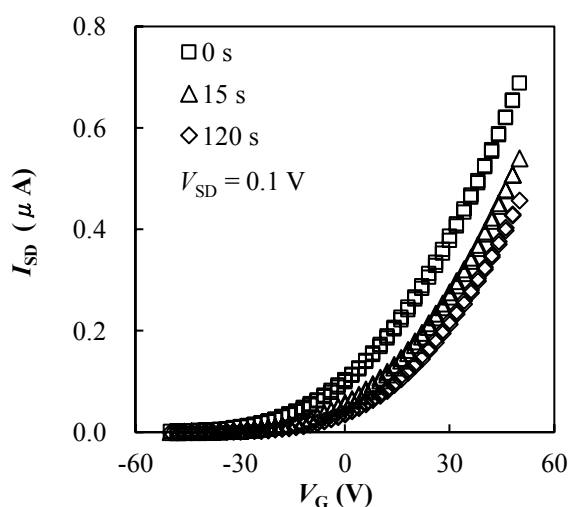


Fig. 1 V_G dependence of I_{SD} for 100Pa O₂ adsorption

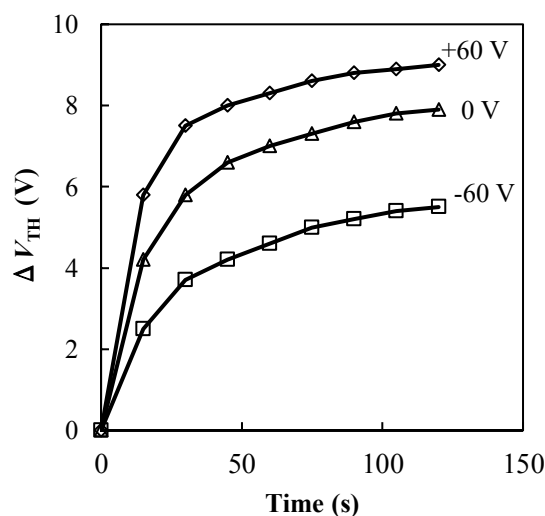


Fig. 2 Exposure time dependence of ΔV_{TH}

Corresponding Author: Kazuyuki Takai
 Tel: +81-42-387-6138, Fax: +81-42-387-7002
 E-mail: takai@hosei.ac.jp

Correlation between the amount of functional groups in graphene oxide and the catalytic activity in reduction of nitrobenzene

○Riku Kondo¹, Yoshiaki Matsuo², Kazuyuki Takai¹

¹Dept. of Appl. Chem., Hosei Univ., ² Dept. of Appl. Chem., Univ. of Hyogo.

Graphene oxide (GO) has oxygen-containing functional groups such as epoxy-, carboxyl- and hydroxyl groups. GO is mainly synthesized by the Brodie (BGO) and the Hummers (HGO) methods [1, 2] in which different oxidizing agents are used. Our group found that the ratio of quantities of each kinds of oxygen-containing functional groups depends on the oxidation methods greatly, suggesting that the catalytic activity of GO depends on the synthesis methods of GO [3]. Indeed, we reported HGO exhibits the higher catalysis in a dehydrogenative coupling reaction to obtain N-benzylidenebenzylamine from benzylamine [4], although GO could partially acts as an oxidant rather than a catalyst in the reaction. Recently, a catalysis of GO in the reduction of nitrobenzene was reported [5].

In this study, we precisely determined the quantity of each acidic functional groups in HGO and BGO by Boehm titration and investigated the correlation between the amount of functional groups in graphene oxide and the catalytic activity in reduction reaction of nitrobenzene.

GO was synthesized by oxidation of natural graphite using concentrated sulfuric acid and potassium permanganate followed by the modified Hummers method [2], and using potassium chlorate and fuming nitric acid according to the Brodie method. The Boehm method based on neutralization titration was used to determine the quantity of acidic functional groups. Hydrogenation reaction of nitrobenzene was performed by adding BGO or HGO sample as a catalyst to nitrobenzene and heating at 60 °C for 2 h to synthesize aniline.

The amount of acidic functional groups of different strengths in GO calculated from the amount of HCl (aq) added until reaching the equivalent point obtained from the titrations. The total amount of acidic functional groups, strongly, moderately acidic groups in HGO and BGO are 9 mEq/g and 5 mEq/g, 6 mEq/g and 3 mEq/g, 3 mEq/g and 2 mEq/g, respectively. Almost no weak acid group were found in both of HGO and BGO.

In the hydrogenation reaction of

nitrobenzene, the yield was about 5 times larger for HGO catalyst than that for BGO catalyst. HGO has more total acidic functional groups than that of BGO, as well as the more localized states at the Fermi level [3]. Both of them would be responsible for the higher catalysis of HGO.

Table 1 Reduction of Nitrobenzene with HGO and BGO

Catalyst	Nitro-benzene (mmol)	Temperature (°C)	H ₂ gas pressure (MPa)	Time (h)	Relative yield (%)	Conversion rate (%)
--	0.5	130	1.5	2	0	99.9
BGO	0.5	130	1.5	2	1	99.8
BGO	0.5	130	1.5	19	21	99.5
HGO	0.5	130	1.5	2	5	99.2

[1] B. C. Brodie, *Philos. Trans. R. Soc. London*, **149**, 249–259 (1859).

[2] W.S. Hummers et al, *J. Am. Chem. Soc.* 80 1339-1339 (1958), [3] K.Tajima, et al., *Polyhedron*, **136**, 155-158 (2017), [4] R. Kondo FNTG Symposium (2020), [5] M. Ahmad, et al *Org. Lett.* 21, 8164-8168 (2019).

Corresponding Author: Kazuyuki TAKAI

E-mail: takai@hosei.ac.jp

Comparison of light emission from different kinds of hBNs after UV or thermal treatments

○Yusuke Adachi, Kuniharu Takei, Takayuki Arie, Seiji Akita

Department of Physics and Electronics, Osaka Prefecture University, Sakai 599-8531, Japan

Hexagonal boron nitride (hBN) is getting attention as an important component in the field of quantum communication technology because it acts as single-photon emitters (SPEs). However, the light emission is not high enough to adopt in practical devices. Here, in improving the emission intensity of SPEs, we investigate the light emission from different kinds of hBNs treated with thermal [1] or UV ozone[2] treatments.

Samples examined here are flakes-power, exfoliated from bulk crystal and CVD grown hBNs purchased from “2D semiconductors, USA”. The samples are transferred on SiO₂/Si substrate. In the case of thermal treatment, the samples were annealed for 30 min at 700, 800, 850 or 900 °C in Ar gas at atmospheric pressure. For UV treatment, the samples were first annealed at 120 °C followed by UV ozone irradiation for 30, 45, 60 or 75 min.

For flakes-power hBN, we compare the thermal and UV ozone treatments. The photoluminescence (PL) of hBN under the irradiation of LED light with the center wavelength of 530 nm was brightest at 850°C (Fig.1(a)) taken using the fluorescence microscope. In the case of UV treatment, The PL intensity was brightest over 60 min treatment (Fig.1(b)). Comparing Fig.1(a) with Fig.1(b), they show almost equivalent emission intensities. The UV ozone treatment without high temperature treatment is beneficial for the fabrication of practical devices.

Next, we investigated the difference of kinds of hBNs after UV ozone treatment for 60 min. The PL intensity of CVD-hBN was highest. Figure 1(c) shows a PL spectrum using 532 nm laser from CVD-hBN measured at room temperature. The clear peak around 570 nm was observed corresponding to the zero phonon line.[1] This implies that the CVD-hBN has more appropriate defects for light emission than that for other types.

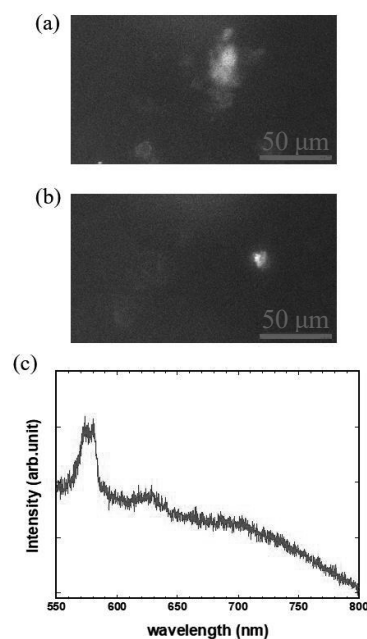


Fig.1: (a) PL image of the flakes-power hBN in high-temperature annealing at 850°C when irradiated 530 nm light. (b) PL image of hBN bulk in UV ozone treatment for 60 min. (c) The PL spectrum of CVD hBN excited by 532 nm laser after UV ozone treatment for 60 min.

References

- [1] T. T. Tran *et al.*, Nat. Nanotechnol. **11**, 37 (2016).
 [2] C. Li *et al.*, Nanophotonics **8**, 2049 (2019).

Corresponding Author: Y. Adachi

Tel: +81-72-254- 9261, E-mail: adachi-4@pe.osakafu-u.ac.jp

Vibrational Spectra of Nucleotides at the Au Cluster attached to graphene nanopore in MD Simulation of a SERS Sensor

○Mohd Aidil Amin Bin Mohd Nasir¹, Tatiana Zolotoukhina¹

¹ Department of Mechanical Engineering, University of Toyama, Toyama 930-8555, Japan

Sensing and analysis of protein structure and DNA sequences and epigenetic modifications are essential for the understanding of the mechanism of cell functions and the development of diseases. The surface-enhanced Raman scattering (SERS) nanoprobe has opened a way to identify molecular structures in a label-free way and investigate mechanisms of interaction with the environment in biomolecules with the high sensitivity and specificity of their fingerprint-like spectra. As current Raman scanners rely on multiple spectra acquisitions, the use of nanoparticle agglomerates provides sufficient enhancement for the single-molecule measurements [1]. Development of the SERS spectroscopy promotes work on DNA and protein identification at a single oligomer resolution and with respect to interactions [2-3].

The study of the vibrational spectra of the nucleotides in the dynamic interaction with the Au nanoparticles (NP) located close to (grown on) graphene nanopore combines (1) translocation localization by graphene nanopore and (2) nucleotide interaction enhancement by Au NP. The spectral maps of the nucleotides were obtained by molecular dynamics (MD) simulation with LJ interaction between components. The spectra of various bonds were evaluated in reaction coordinates for DNA nucleotides and in Cartesian ones for Au NP. Spectra at the interaction with the Au NP helps to select a transient COM velocity of nucleotide passing along the cluster and at the edge of the graphene pore. We test the nucleotide-graphene-NP system to understand whether the LJ interaction with Au NP at the translocation time can influence the changes in the transient spectra calculated by MD. The frequencies that can serve as markers of the corresponding Au – nucleotide interaction are evaluated.

The simulation methods can create spectral libraries for vibrations of molecular species vs. different types of interaction to specify the interaction's type and strength.

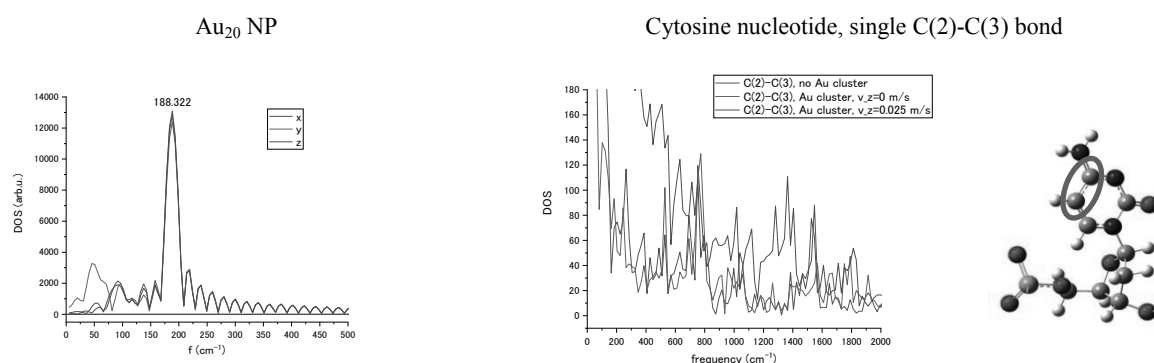


Fig1 Vibrational spectra of the tip atoms of Au₂₀ nanoparticle and Cytosine C-C ring bond marked on the right panel.

- [1] L. M. Almealmadi, S. M. Curley, N. A. Tokranova, S. A. Tenenbaum & I. K. Lednev, *Sci. Reports*, **9**, 12356 (2019).
 [2] T. Zolotoukhina, M. Yamada and S. Iwakura., *Proceedings of IECEB2020*, 035671 (2020)
 [3] D. Macdonald, E. Smith, K. Faulds, D. Graham, *Analyst*, **145**, 1871-1877 (2020).

Corresponding Author: T. Zolotoukhina

Tel: +81-76-445-6739, Fax: +81-76-445-6739, E-mail: zolotu@eng.u-toyama.ac.jp

HER catalytic performance of Mo₂C/C composite films prepared by microwave-plasma CVD method

○Shunsuke Numata¹ and Hironori Ogata^{1,2}

¹ Department of Chemical Science and Technology, Hosei University

² Research Center for Micro-Nano Technology, Hosei University

Electrocatalytic water splitting is one of the suitable methods for hydrogen production. However, this process relies on the electrocatalysis of the hydrogen evolution reaction (HER).

It is well known that Pt-based electrocatalysts show high current density at low overvoltages and are efficient HER electrocatalysts. However, since they are rare and expensive, transition metal carbide (TMC) such as molybdenum carbide has been proposed as an alternative to Pt, and much research has been done so far. It has been reported that the penetration of carbon atoms into the transition metal lattice increases the density of d-band electrons at the Fermi level, leading to Pt-like properties. In addition, it has been reported that HER and conductivity are improved by synthesizing TMC using nanocarbon materials [1].

Microwave-plasma chemical vapor deposition (MPCVD) method is one of the methods that use plasma generated by microwave.

The MPCVD method has the advantages of high power density and controllable parameters. Due to these advantages, it is possible to produce high quality molybdenum carbides. [2]

In this study, we prepared Mo₂C / C composite films by directly laminating a nanocarbon materials on a molybdenum substrate by a microwave plasma chemical vapor deposition (MPCVD) method and investigated the possibility of application to a catalyst electrode for HER. Fig. 1 shows the C 1s XPS spectrum of the fabricated material. This result means that molybdenum carbide and nanocarbon are produced. Detailed experimental results about the performance of the catalyst electrode for HER will be reported at the meeting.

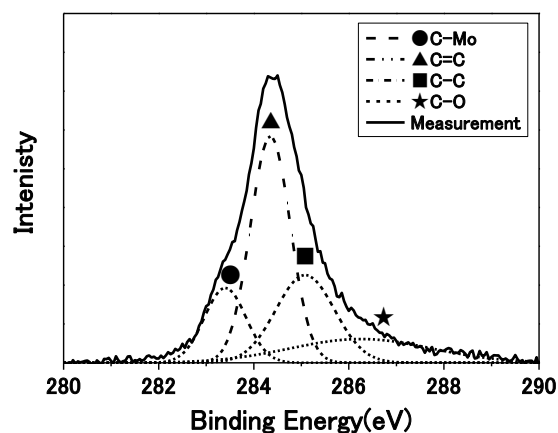


Fig. 1 C 1s XPS spectrum of prepared material

[1] Dezhi Wang *et al.*, *ACS Sustainable Chem Eng*, **6**, 13995 (2018).

[2] Hongyang Zhao *et al.*, *Journal of Applied Physics*, **123**, 053301 (2018).

Corresponding Author: H. Ogata

E-mail: hogata@hosei.ac.jp

Magnetizations and De Haas-van Alphen oscillations in the Dirac fermions

◦F. R. Pratama¹, M. Shoufie Ukhtary¹, Riichiro Saito¹

¹*Department of Physics, Tohoku University, Sendai 980-8578, Japan*

Graphene and related two-dimensional (2D) materials are known to possess intrinsic orbital diamagnetism (OD) [1, 2], which is originated from the coalescence of the Dirac fermions at the valence bands to the zeroth Landau levels (LLs) in the presence of an external magnetic field B . A method to calculate the OD χ is by applying the Euler-Maclaurin formula for the thermodynamic potential Ω and by using the relation $\chi = -(\partial^2 \Omega / \partial^2 B)_{B=0}$, as employed by Landau [3] to show the OD in metals. In the context of the Dirac materials, the method is used to calculate the Fermi energy dependence of χ in gapped graphene [4], MoS₂ [5], and the Weyl semimetals [6]. However, the magnetization M as a function of B and temperature T cannot be calculated by using the Euler-Maclaurin formula, because $M = -(\partial \Omega / \partial B)$ diverges due to the infinite number of the LLs when we calculate Ω . If we consider only the LLs from the conduction bands, such divergence would not appear but it is not well-justified approximation.

In this study [7], we analytically calculate $\Omega(B, T)$ for strong- B /low- T and weak- B /high- T limits with the method of zeta function regularization, in order to avoid the divergence in the expression of $M(B, T)$. Our formulas reproduce the experimental observation of M of graphene as a function of B for several values T [8], which was fitted into a Langevin function [8] (see Fig. 1). Moreover, we generalize the result by including the effect of band-gap and impurity scattering on M and χ . We found that in the presence of impurity, χ of graphene follows a scaling law. In the case of a gapped Dirac fermions, a large band-gap in MoS₂ gives a smaller but more robust magnetization with respect of T and impurity. In the doped systems, we show that the opening of band-gap yields a decreasing frequency and amplitude in the De Haas-van Alphen oscillations at $T=0$ K.

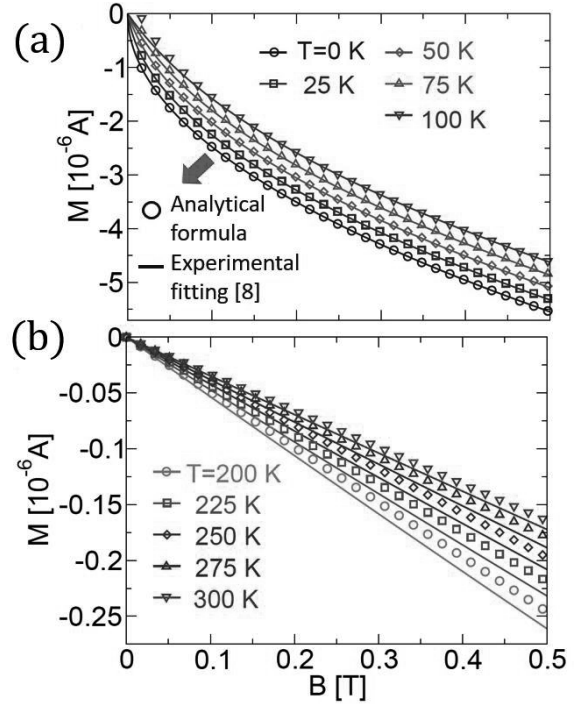


Fig 1. Magnetization of graphene M as a function of B and T for (a) strong- B /low- T and (b) weak- B /high- T limits. The analytical formula and the Langevin fitting of the experiment (from Ref. [8]) are depicted by symbols and lines, respectively.

- [1] J. W. McClure, Phys. Rev. **104**, 666 (1956).
- [2] M. Sepioni *et al.*, Phys. Rev. Lett. **105**, 207205 (2010).
- [3] L. Landau, Z. Phys. **64**, 629 (1930).
- [4] M. Koshino, T. Ando, Phys. Rev. B **81**, 195431 (2010).
- [5] T. Cai *et al.*, Phys. Rev. B **88**, 115140 (2013).
- [6] M. Koshino, I. F. Hizbullah, Phys. Rev. B **93**, 045201 (2016).
- [7] F. R. Pratama, M. S. Ukhtary, R. Saito, arXiv:2101.01367 (2021).
- [8] Z. Li *et al.*, Phys. Rev. B **91**, 094429 (2015).

Corresponding Author: F. R. Pratama
E-mail: pratama@flex.phys.tohoku.ac.jp

Synthesis of WTe₂ nanowires by tellurization of tungsten oxide nanowires and origin of non-formation of tubular structure

○Mai Nagano¹, Yohei Yomogida¹, Hiromu Hamasaki², Kaori Hirahara^{2,3}, Yasumitsu Miyata¹, Kazuhiro Yanagi¹

¹Department of Physics, Tokyo Metropolitan University, Hachioji, Tokyo 192-0372, Japan

²Department of Mechanical Engineering, Osaka University, Suita, Osaka 565-0871, Japan

³Center for Atomic and Molecular Technologies, Osaka University, Suita, Osaka 565-0871, Japan

Transition-metal dichalcogenides (TMDCs) MX₂ (M = Mo, W, Nb; X = S, Se, Te) have attracted much attention owing to their unique electronic and optical properties. TMDCs exhibit various physical properties depending on the constituent elements and their nano-structures, such as nanotube and nanowire structures. Among the TMDCs family, WTe₂ is a semi-metallic and attracts a lot of interest due to its topological properties, but no nanotube structure of WTe₂ has been reported. The physical properties of WTe₂ strongly depend on the morphology and the nano-structure, and thus its control is important for both basic science and applications. Typical methods to control nano-structures of TMDC is the chalcogenization of metal oxide nanowire precursors, which is used for nanotube synthesis [1]. However, successful report on nanotube formation is limited to sulfurization and selenization [2,3], and it is not clear whether we can get nanotube structure through tellurization. In this study, we performed various conditions of tellurization and investigated the effect on morphology and nano-structure of tellurized samples.

First, we investigated how supply of chalcogen influences the structure and composition of synthesized products. The tungsten oxide nanowire precursors obtained by solvothermal synthesis were used for tellurization. The nanowires were heated to 650-700 °C in Ar gas, and after reaching set temperature, Te powder was heated in Ar/H₂ gas to supply Te powder was heated at different temperatures (600, 620, 650, and 700°C) to investigate the conditions for effective tellurization.

The morphology and composition of the telluride sample were found to strongly depend on the Te supply and tellurization temperature, and through their optimization, Td-WTe₂ nanowires were finally synthesized successfully (Figure 1). Interestingly, the obtained WTe₂ has the planar layered nanowire structures. The result is different from those when we apply sulfurization and selenization on the same precursors. In the case of the WS₂ and WSe₂, we obtained the coaxial layered nanotube structures. This indicates that tellurization is very different from sulfurization and selenization. We assume that the volume of the compounds is also important for nanowire or nanotube formations, and the large volume change in WTe₂ will prohibit the nanotube formation [6].

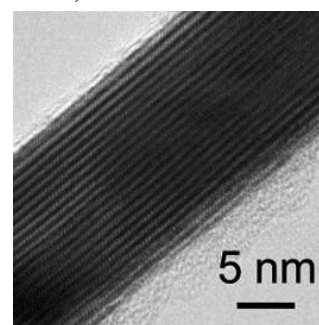


Fig.1 TEM image of synthesized WTe₂ nanowires.

- [1] G. H. Park et al., *Adv. Mater. Interfaces* **6**, (2019)
- [2] Y. Yomogida et al., *Appl. Phys. Express* **12**, 085001 (2019).
- [3] Y. Yomogida et al., *Appl. Phys. Lett.* **116**, 203106 (2020).
- [4] M. L. Hong et al., *Energy Fuels* **32**, 6371 (2018)
- [5] J. M. Woods et al., *ACS Nano* **13**, 6455 (2019)
- [6] Y. Yomogida, M. Nagano et al., *Jpn. J. Appl. Phys.* accepted (2021)

Electronic structures of MoS₂ nanotube bundles

○Kaoru Hisama¹, Mina Maruyama², Shohei Chiashi¹, Shigeo Maruyama¹
and Susumu Okada²

¹ Department of Mechanical Engineering, The University of Tokyo, Tokyo 113-8656, Japan

² Department of Physics, University of Tsukuba, Tsukuba 305-8571, Japan

Because of a chemically inert two-dimensional network, MoS₂ could be a constituent unit of nanomaterials with structural hierarchy. It can form van der Waals stacking structures with the other layer of MoS₂ or other layered materials. In addition to 2D MoS₂, a tubular form of MoS₂ is also the constituent material for the hierarchical structures. Coaxially arranged MoS₂ tubes have been synthesized, just as the multi-walled carbon nanotubes. In addition to the multi-walled tubes, bundles of MoS₂ nanotubes are also considered in analogy with the carbon nanotube bundles. However, in contrast to the carbon nanotube bundles, electronic structure of MoS₂ nanotube bundles is still unclear. Therefore, in this work we aim to investigate the electronic structure of those MoS₂ nanotube bundles in terms of their inter-tube spacing and mutual orientations using the density functional theory.

Figure 1(a) shows the electronic structure of (9,9) MoS₂ nanotube bundles in which each nanotube is separated by 0.3 nm vacuum spacing from its adjacent. The dispersion relation along the inter-tube direction of the three highest branches of the valence band exhibit unusual feature. The upper two branches of the valence band degenerated at the Γ point while the lower two crossed each other at the K point with linear dispersion relation. Thus, these three branches exhibit a Kagomé-like band structure comprising a little-dispersive band and a dispersive band with a conical structure at the K point. This Kagomé-like band structure is found to be robust against the inter-tube spacing and mutual orientations: The band width depends on the inter-tube spacing and orientation, owing to the S-S spacing between adjacent nanotubes. By analyzing the wave function distribution of these three branches, we found that the substantial overlap of wave functions between nanotubes causes the peculiar electronic structure [Fig. 1(b)].

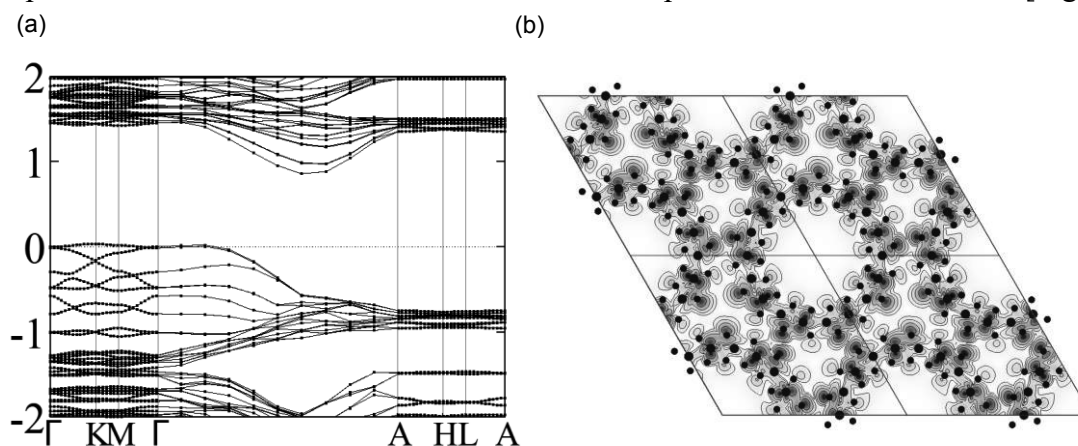


Figure 1 (a) The electronic structure of (9,9) MoS₂ nanotube bundle. (b) A contour plot of squared wavefunction of the highest branch of the valence band at the Γ point.

Corresponding Author: Susumu Okada E-mail: sokada@comas.frsc.tsukuba.ac.jp

Dispersion of single-walled carbon nanotubes with commodity plastics PMMA

○Ayaka Demise¹, Tsuyoshi Ando¹, Hiroharu Ajiro¹, Tsuyoshi Kawai¹, Yoshiyuki Nonoguchi^{1,2}

¹ Division of Materials Science, Nara Institute of Science and Technology, NAIST, Takayama, Ikoma, Nara 8916-5, Japan

² Faculty of Materials Science and Engineering, Kyoto Institute of Technology, Kyoto 606-8585, Japan

Single-walled carbon nanotubes (SWNTs) have superior physical properties (e.g. electric conductivity or mechanical strength) to other conventional filler materials. Due to their significant bundling, however, the solution processing of SWNTs has long been difficult, restricting the many application of SWNTs. Conventional approaches include the chemical functionalization of SWNTs' side walls to improve their interaction with the solvent, in which physical properties are unexpectedly harmed. Aqueous micellar solution was also studied for individual dispersion. However, these previous approaches are incompatible to the industrial plastics, which are soluble only in organic solvents. In this context, noncovalent wrapping to SWNTs with commodity polymers are highly desired for incorporating SWNTs to arbitrary organic matrix. Here we demonstrate the direct and efficient dispersion of SWNTs in the *theta* solvents containing poly methyl methacrylate (PMMA).

We used from good to *theta* solvents for PMMA to disperse SWNTs (**Table 1**). UV-Vis-NIR spectroscopy revealed that *theta* conditions for PMMA (ethyl acetate, DMSO, acetonitrile and 2-heptanone) allow for the individual isolation and the colloidal dispersion of SWNTs. We then demonstrated that the SWNTs' dispersibility is controlled by the PMMA solubility that can be tuned by the ratio of water to dry THF (*theta* condition: 6-25 w/w% water in dry THF [1]). **Fig 1** shows that good (dry THF) and poor solvents (30% H₂O in dry THF) lead to poor solubility, whereas the *theta* solvent (10% H₂O in dry THF) enables the efficient colloidal SWNT dispersion. We will further present the comprehensive assessments of dispersibility.

[1] I. Katime, L.C. Cesteros and J.R. Ochoa, *Polymer Bulletin*, **6**, 447-449 (1982).

Corresponding Author: Yoshiyuki Nonoguchi
Tel: +81-75-724-7515
E-mail: nonoguchi@kit.ac.jp

Table 1. List of solvents

solvents	<i>theta</i> temperature (PMMA)[K]
toluene	-
dry THF	-
ethyl acetate	318
DMSO	308
acetonitrile	303
2-heptanone	288

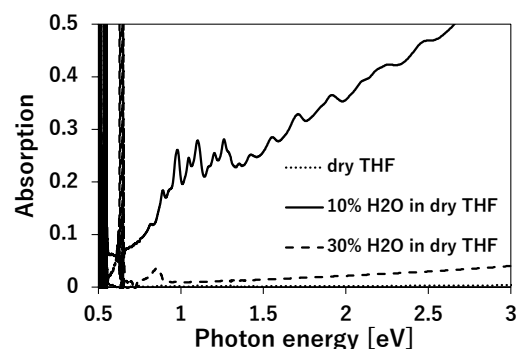


Fig 1. UV-Vis-NIR spectra of dispersions of Nopohipco in different composition of dry THF and water.

Cross-linking gelation of isomaltodextrin for the chromatographic separation of semiconducting carbon nanotubes

○Yuki Matsunaga¹, Jun Hirotsu², Yutaka Ohno^{2,3}, Haruka Omachi^{1,4}

¹ Department of Chemistry, Graduate School of Science, Nagoya University, Nagoya 464-8602, Japan

² Department of Electronics, Graduate School of Engineering, Nagoya University, Nagoya 464-8601, Japan

³ Institute of Materials and Systems for Sustainability, Nagoya University, Nagoya 464-8601, Japan

⁴ Research Center for Materials Science, Nagoya University, Nagoya, 464-8602, Japan

Semiconducting single-wall carbon nanotubes (s-SWCNTs) are promising materials with potential applications in thin-film transistors (TFTs). However, separation techniques are required to obtain highly enriched s-SWCNTs since conventional as-grown SWCNTs are a mixture of 70% semiconducting and 30% metallic SWCNTs. Gel column chromatographic separation is one of the most efficient separation methods. However, the well-used gel media such as Sephacryl, which is cross-linked polysaccharides of α -1,6-glycoses are not suitable for scale-up because of their high cost.

Recently, we have successfully separated s-SWCNTs in an aqueous two-phase extraction using Isomaltodextrin (IMD) [1]. It is a cost-efficient water-soluble dietary fiber and also contains continuous α -1,6-glycosidic bonds. Herein, we report the cross-linking gelation of IMD for the high-purity separation of s-SWCNTs by column chromatography [2]. IMD gels were synthesized using cross-linking reaction with epichlorohydrin (Fig. 1a). The reaction under precisely controlled basic conditions gave the sub-micrometer porous IMD gels. Gel column with the synthesized gels was achieved SWCNT separation with a high purity of up to 98.7% (Fig. 1b). After the gel column chromatographic separation, the fabrication of s-SWCNT-TFTs was demonstrated. The devices made using the separated s-SWCNTs exhibited excellent on/off ratios of about 10^5 .

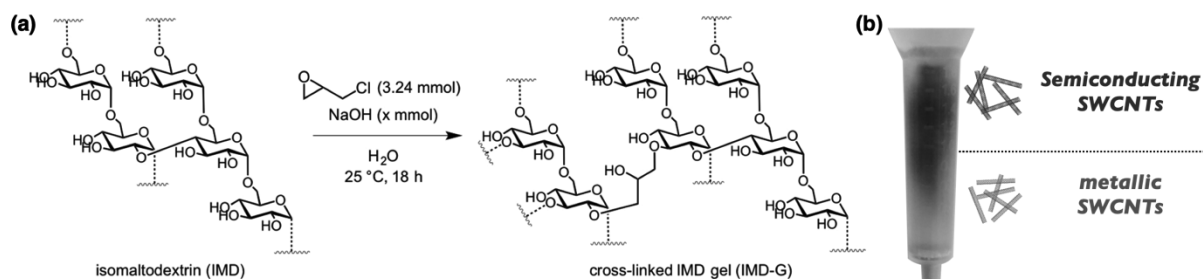


Fig. 1 (a) Schematic of IMD gel synthesis. (b) Photograph of IMD gel column.

[1] H. Omachi *et al.* Appl. Phys. Express, **12**, 097003 (2019).

[2] Y. Matsunaga, J. Hirotsu, Y. Ohno, H. Omachi, Appl. Phys. Express, **14**, 017001 (2021).

Corresponding Author: H. Omachi

Tel: +81-52-789-3660, Fax: +81-52-747-6442,

E-mail: omachi@chem.nagoya-u.ac.jp

Self-aligned hybrid quantum structure of diamond nitrogen-vacancy center and carbon nanotube for electrical control of quantum states

○Haruki Uchiyama¹, Shigeru Kishimoto¹, Junko Ishi-Hayase², and Yutaka Ohno^{1,3}

¹*Department of Electronics, Nagoya University, Nagoya 464-8603, Japan,*

²*School of Fundamental Science and Technology, Keio University, Yokohama 223-8522, Japan*

³*Institute of Materials and Systems for Sustainability, Nagoya University, Nagoya 464-8601, Japan*

The nitrogen-vacancy (NV) center in diamond is an attractive nanostructure for quantum technologies, including quantum metrology, information processing due to a long coherence time of \sim ms at room temperature. [1] The spin state is usually controlled by the laser light and microwave, which arises a difficulty in manipulate the coupled NV centers individually while quantum entanglement between NV centers can be achieved when they are closely placed within a distance of a few ten nanometers. [2] In this work, we propose a method to achieve the electrical and local control of the quantum state of NV centers, using a single-walled carbon nanotube (CNT), which can apply strong local magnetic field and microwave to NV centers due to the ultranarrow diameter and high ampacity.

The NV center-CNT hybrid structure was realized by a self-align process as described below. After depositing individualized CNTs on a fluorine-terminated (100) diamond substrate, contact electrodes (Au, 100 nm) were formed by electron beam lithography, electron beam evaporation, and lift-off process. To achieve self-align formation of NV centers along a CNT, nitrogen ion implantation was carried out through an organic film with a trench along the CNT. After depositing a $C_{29}H_{28}O_3$ film, a trench was formed in self-aligned manner by applying current through the CNT. [3] Then, ion implantation of $^{15}N_2^+$ ions at an acceleration energy of 15 keV and post annealing were carried out to form shallow NV centers.

The photoluminescence mapping (wavelength of 625-1000 nm) (Fig. 1(a)) clearly shows that NV centers were formed along the CNT. Optically-detected magnetic resonance (ODMR) measurements were carried out at the center of the hybrid structure with flowing current through the CNT. Figure 1(b) shows the ODMR spectra at CNT current of 0 and 12 μ A. The resonant frequency of NV center shifted by 0.9 MHz by the CNT current due to the generated magnetic field. This result indicates that the energy of the electron spin of the NV center can be controlled by the local current through a CNT.

[1] E. D. Herbschleb *et al.*, Nat. Commun. **10**, 3766 (2019).

[2] F. Dolde *et al.*, Nat. Phys. **9**, 139 (2013).

[3] S. H. Jin *et al.*, Nat. Nanotechnol. **8**, 347(2013).

Corresponding Author: Y. Ohno,

Phone: +81-52-789-5387, E-mail: yohno@nagoya-u.jp

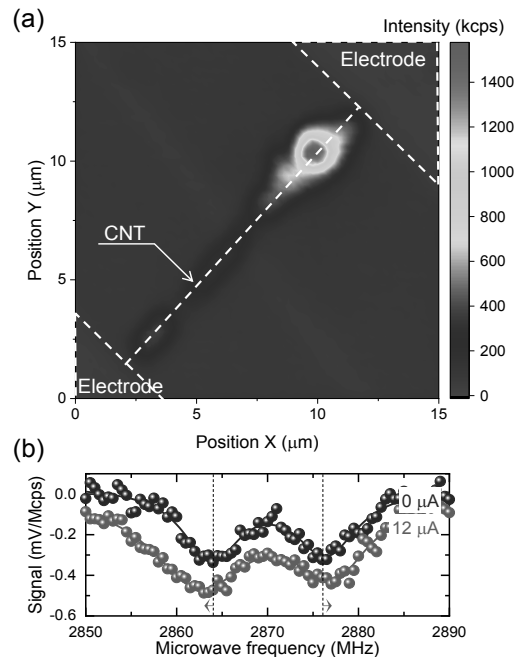


Fig. 1 Diamond NV center-CNT hybrid structure. (a) Photoluminescence mapping of NV centers, (b) ODMR spectra at CNT current of 0 and 12 μ A.

Preparation of twisted bilayers by folding monolayer WS₂

○Masahiko Kaneda, Yusuke Nakanishi, Hong En Lim, Takahiko Endo, Yasumitsu Miyata

Department of Physics, Tokyo Metropolitan University, Hachioji, 192-0397, Japan

Recently, twisted bilayers of two-dimensional (2D) materials have attracted much attention because of their unique physical properties and potential applications. Twisted bilayer graphene, for example, has been reported to show unprecedented superconducting and insulating states at specific twist angles [1,2]. For transition metal dichalcogenides (TMDCs), their photoluminescence (PL) intensity and peak energy change with the twist angle, rendering greater functional variety [3]. Such twisted bilayers are prepared either by transferring an atomic layer onto another or via direct growth in general. However, the control of twist angle usually requires a careful transfer process, and it is still difficult to grow bilayers with controlled twist angle directly. Herein, we report an origami-like way of folding a monolayer WS₂ grain into a bilayer structure with desired twist angle.

Monolayer WS₂ was grown on SiO₂/Si substrate by chemical vapor deposition [4]. To create a crease for subsequent folding, a layer of photoresist was first coated onto the isolated grain and exposed in desired pattern. Next, the unnecessary photoresist was removed in a developing solution. The sample was finally washed with pure water and blow dried. This process leads to the folding of the monolayer WS₂ grain, which takes place along the photoresist pattern prepared (Fig. 1a). Compared to that of un-folded monolayer site, a lower energy PL emission is observed at the folded bilayer region (Fig. 1b). This change can be explained by the interlayer coupling arose as reported in the CVD-grown twisted WS₂ bilayers [3]. Our method provides a facile way for not only fabricating twisted bilayers, but also manipulating the physical properties of 2D atomic layers by folding.

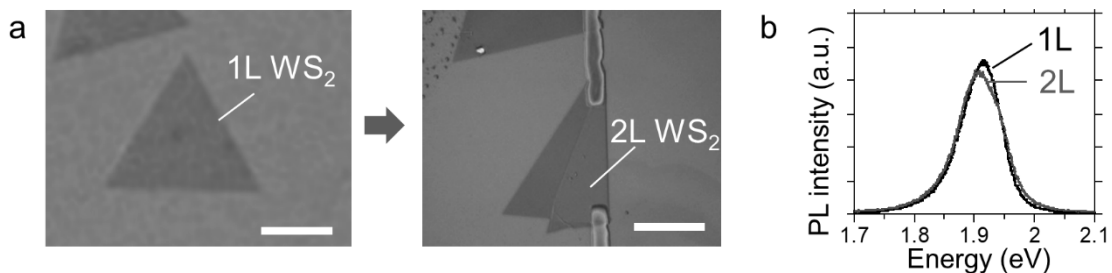


Fig. 1. (a) Optical images of a monolayer WS₂ grain before and after the folding process. Scale bars: 20 μm (b) Corresponding PL spectra taken at the monolayer and folded bilayer WS₂ regions.

[1] Y. Cao *et al.*, Nature **556**, 80-84 (2018). [2] Y. Cao *et al.*, Nature **556**, 43-50 (2018). [3] S. Zheng *et al.*, Adv. Opt. Mater. **3**, 1600-1605 (2015). [4] K. Kojima *et al.*, Nanoscale **11**, 12798-12803 (2019).

Corresponding Author: Y. Miyata, Tel: 042-677-2508, E-mail: ymiyata@tmu.ac.jp

First-principles study of impurity states induced by a carbon or oxygen atom in h-BN monolayer

○Taishi Haga¹, Shuaishuai Yuan², Kirk H. Bevan², and Susumu Saito^{1,3,4}

¹ *Department of Physics, Tokyo Institute of Technology, Tokyo 152-8551, Japan*

² *Division of Materials Engineering, McGill University, Montreal, QC H3A 0C5, Canada*

³ *Advanced Research Center for Quantum Physics and Nanoscience, Tokyo Institute of Technology, Tokyo 152-8551, Japan*

⁴ *Materials Research Center for Element Strategy, Tokyo Institute of Technology, Kanagawa 226-8503, Japan*

Hexagonal boron nitride (h-BN) has a honeycomb lattice structure in each layer similar to graphene. While it is known that h-BN is an ideal substrate for other two-dimensional materials, its thin layers as well as the bulk phase themselves attract much attention as wide-gap semiconductor materials for future device applications. It has been reported that carbon atoms as well as oxygen atoms are incorporated into the h-BN bulk during the synthesis [1]. Defects in semiconductors often play an important role in modifying the electronic properties of the system [2,3]. Therefore, it is important to theoretically investigate how an impurity in h-BN affects the electronic properties.

In this work, we study electronic properties of doped h-BN monolayer using first-principles electronic-structure calculations based on the hybrid functional approach. The mixing parameter between semi-local and non-local exchange in the Heyd-Scuseria-Ernzerhof (HSE) hybrid functional is optimized following the generalized Koopmans' theorem (gKT). It has been reported that the calculated defect levels can be accurate when the gKT is satisfied in the three-dimensional materials [4]. In this study, by applying the method to a two-dimensional system, we investigate the depth of impurity states induced by a carbon or oxygen atom in the h-BN monolayer.

[1] T. Taniguchi and K. Watanabe, *J. Cryst. Growth* **303**, 525, (2007).

[2] T. Haga, Y. Fujimoto, and S. Saito, *Phys. Rev. B* **100**, 125403 (2019).

[3] T. Haga, Y. Matsuura, Y. Fujimoto, and S. Saito, to be published.

[4] P. Deak, M. Lorke, B. Aradi, and T. Frauenheim, *J. Appl. Phys.* **126**, 130901 (2019).

Corresponding Author: T. Haga

E-mail: haga.t@stat.phys.titech.ac.jp

Air-Stable, Efficient Electron Doping of Monolayer MoS₂ by Salt-Crown Ether Treatment

○Hiroto Ogura¹, Masahiko Kaneda¹, Yusuke Nakanishi¹, Yoshiyuki Nonoguchi², Jiang Pu³, Mari Ohfuchi⁴, Toshifumi Irisawa⁵, Hong En Lim¹, Kazuhiro Yanagi¹, Takahiko Endo¹, Taishi Takenobu³, Yasumitsu Miyata¹

¹ Department of Physics, Tokyo Metropolitan University, Hachioji, 192-0397, Japan

² Kyoto Institute of Technology, Kyoto 606-8585, Japan

³ Department of Applied Physics, Nagoya University, Nagoya, 464-8603, Japan

⁴ Fujitsu Laboratories Ltd., Atsugi, 243-0197, Japan

⁵ Nanoelectronics Research Institute, AIST, Tsukuba, 305-8562, Japan

Two-dimensional (2D) transition metal dichalcogenides (TMDCs) have attracted much attention because of their unique physical properties and future device applications. To maximize their potential in device applications, it is essential to develop a sophisticated technique for stable and highly efficient carrier doping. For this purpose, surface charge transfer by chemical doping provides a powerful way to modulate the carrier density of TMDCs [1, 2]. However, current dopants used oftentimes suffer low doping efficiency or long-term stability, and thus a better alternative is strongly desired. Recently, an air-stable electron doping of carbon nanotubes has been demonstrated by Nonoguchi *et al.* using a series of potassium salts with crown ethers [3]. In this study, we have applied similar technique to achieve a stable, high electron doping of monolayer MoS₂.

Monolayer MoS₂ was grown on SiO₂/Si substrates by using chemical vapor deposition [4]. Electron doping was conducted by spin coating the butanol solution of KOH/benzo-18-crown-6 on MoS₂ (Fig. 1a). The transfer curves of MoS₂ field-effect transistors (FETs) change from a typical n-type semiconducting state to metallic one as the doping concentration increases (Fig. 1b). Such doping is found to be stable under ambient conditions, which lasts nearly even up to one month (Fig. 1c). The doped MoS₂ shows a high carrier density of $3.4 \times 10^{13} \text{cm}^{-2}$ and its resistance measurement revealed a metallic temperature dependence. These results indicate that the salt-based doping provides an effective way for the electron doping of MoS₂, benefiting its device applications.

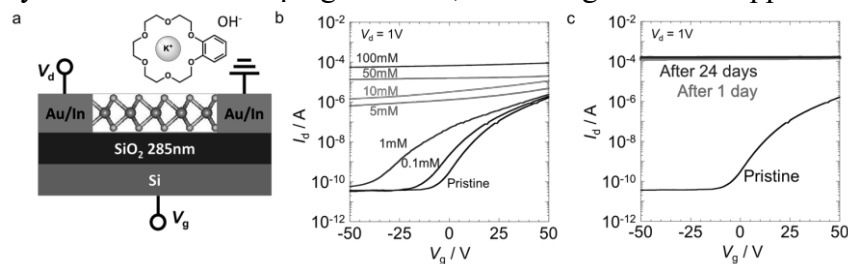


Figure 1 (a) Schematic illustration of the MoS₂ FET and benzo-18-crown-6 with K⁺ ion. (b) Transfer curves of the pristine and doped MoS₂ at different dopant concentrations. (c) Transfer curves of the device before and after doping at 100 mM monitored over 24 days. The doped device was kept in air throughout the period.

[1] D. Kiriya *et al.*, *J. Am. Chem. Soc.*, **139**, 7853 (2014). [2] H. G. Ji *et al.*, *Adv. Mater.*, **31**, 1903613 (2019). [3] Y. Nonoguchi *et al.*, *Adv. Funct. Mater.*, **26**, 3021 (2016). [4] K. Kojima *et al.*, *Nanoscale*, **11** 12798 (2019).

Corresponding Author: Y. Miyata, Tel: +81-042-677-2508, E-mail: miyata-yasumitsu@tmu.ac.jp

Detection of subband resonant tunneling in few-layer WSe₂/h-BN/p⁺-MoS₂ van der Waals junction

○Kei Takeyama¹, Rai Moriya¹, Shota Okazaki², Yijin Zhang¹, Satoru Masubuchi¹, Kenji Watanabe³, Takashi Taniguchi^{3,1}, Takao Sasagawa², Tomoki Machida^{1,4}

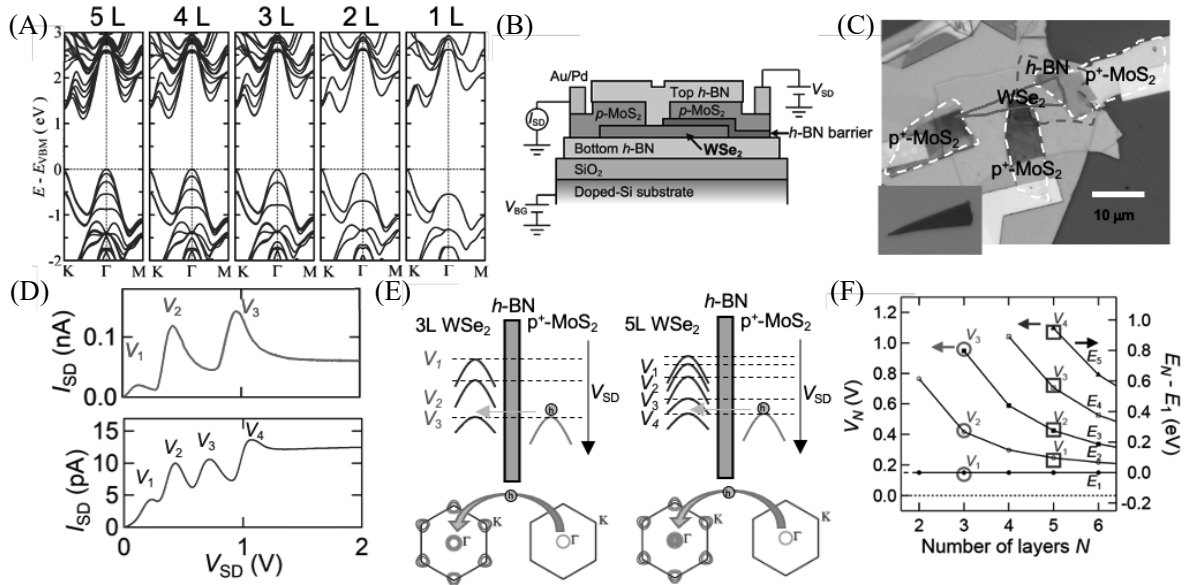
¹Institute of Industrial Science, University of Tokyo, Tokyo 153-8505, Japan

²Laboratory for Materials and Structures, Tokyo Institute of Technology, Kanagawa 226-8503, Japan

³National Institute for Materials Science, Tsukuba 305-0044, Japan

⁴CREST-JST

The few-layer WSe₂ exhibits subband quantization at Γ point of the valence band (VB) and the number of the subbands equals to the number of layers of WSe₂ (Fig. A). These subbands are induced by the out-of-plane confinement of wavefunction to form van der Waals quantum well states in analogue to the subband quantization in semiconductor quantum well. Here, we successfully probe these subbands in p⁺-MoS₂/h-BN tunnel barrier/few-layer WSe₂ vdW junction (Fig. B, C). A current–voltage (I_{SD} – V_{SD}) obtained from the device using three-layer (3L) WSe₂ demonstrates multiple peaks and negative differential conductance at ~ 2 K (Fig. D) [1]. Another device using 5L-WSe₂ showed similar peak structures, but the numbers of peaks and their positions are distinctly different from 3L device. We think results are demonstrated by the in-plane wave-vector conserved tunneling between p⁺-MoS₂ and few layer WSe₂ (Fig. E). When the Fermi level of p⁺-MoS₂ aligned to the subbands of WSe₂, resonant tunneling occurs at the VB Γ -point between p⁺-MoS₂ and few layer WSe₂. Here, the degenerately doped p⁺-MoS₂ plays a key role as an ideal metallic electrode [1] as well as hole injector with its Fermi level presented only at the VB Γ -point. The peak positions of these resonant tunneling exactly matched with theoretical calculation of subband energy levels (Fig. F). Since the separation of subband energies corresponds to infrared wavelength, these results demonstrate a new possibility of utilizing few layer TMD materials for infrared optoelectronics applications. [1] K. Takeyama, *et al.*, in preparation. [2] K. Takeyama, *et al.* *Appl. Phys. Lett.* **117**, 153101(2020).



Corresponding Author: K. Takeyama

Tel: +81-3-5452-6158, Fax: +81-3-5452-6157,

E-mail: takeyama@iis.u-tokyo.ac.jp

Fig. 1: (A) Band structure of WSe₂. (B,C) Device structure and optical micrograph. (D) I_{SD} – V_{SD} curve at ~ 2.0 K. (E) Resonant tunneling of hole between WSe₂ and p⁺-MoS₂. (F) Comparison with calculated subband energy spacings.

Optical induced Spin Current of Monolayer NbSe₂

Ren Habara¹, Katsunori Wakabayashi¹

¹*Department of Nanotechnology for Sustainable Energy, School of Science and Technology,
Kwansei Gakuin University, Gakuen 2-1, Sanda 669-1337, Japan*

Transition-metal dichalcogenide (TMDC) is a new class of two-dimensional (2D) electronic systems and provides a platform to design the new functional opt-electronic devices. In TMDC, electronic properties crucially depend on the combination of metal and chalcogen atoms. Monolayer NbSe₂ is known to show metallic behavior with superconducting phase transition at low temperature. Figure 1(a) shows the lattice structure of monolayer NbSe₂, which has no spatial inversion symmetry, but respects out-of-plane mirror symmetry. Owing to the strong atomic spin-orbit coupling (SOC) field, NbSe₂ possesses the Ising-type SOC [1], i.e., effective Zeeman field that locks electron spin to out-of-plane directions by in-plane momentums. In this work, we numerically calculate spin-dependent optical conductivity of NbSe₂ using Kubo formula based on an effective tight-binding model (TBM), and find the photo-induced generation of pure spin current [2].

We employ a multi-orbitals TBM which includes d_{z^2} , $d_{x^2-y^2}$ and d_{xy} orbitals of Nb atom to describe the electronic states of NbSe₂ [1, 3]. Figure 1(b) shows the energy band structure, where the red and blue lines indicate spin-up and spin-down states. NbSe₂ is metallic, but a large energy band gap between the partially filled valence bands and empty conduction bands. Figure 1(c) shows the numerically calculated angular frequency dependences of spin-dependent optical Hall conductivity for several SOC parameters. Since the up-spin and down-spin have opposite sign of Hall current, the pure spin Hall current can be induced in the NbSe₂. This indicates that we can generate the spin current by using the light irradiation. Our results will serve to design the opto-spintronics devices using 2D Materials.

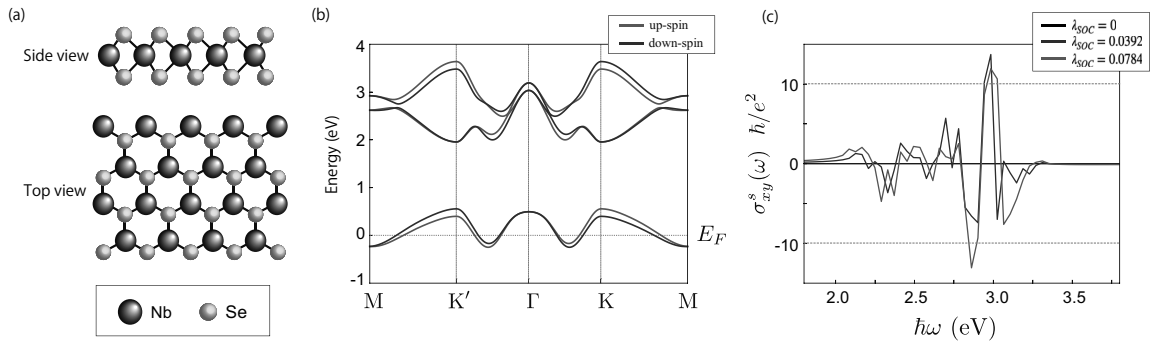


Figure 1 (a) Side and top views of crystal structure of monolayer NbSe₂. (b) Energy band structure of NbSe₂ with SOC parameter $\lambda_{SOC} = 0.0784$. (c) Optical angular frequency dependence of spin-dependent Hall conductivity $\sigma_{xy}^s(\omega)$ ($= \sigma_{xy}^{\uparrow}(\omega) - \sigma_{xy}^{\downarrow}(\omega)$) for several different SOC parameters.

[1] W.-Y. He, *et.al.*, Commun. Phys. **1**, 40 (2018). [2] R. Habara, *et.al.*, in preparation. [3] G.-B. Liu, *et.al.*, Phys. Rev. B. **88**, 085433 (2013). Corresponding Author: K. Wakabayashi (E-mail: waka@kwansei.ac.jp)

Intra-layer excitons trapped in moiré potential on monolayer-MoSe₂/NiPS₃ heterostructure

○ Yan Zhang, Keisuke Shinokita, Yuhei Miyauchi
and Kazunari Matsuda

Institute of Advanced Energy, Kyoto University, Uji, Kyoto 611-0011, Japan

Recently, the monolayer two-dimensional (2D) semiconductor and its artificial van der Waals (vdW) heterostructures have been attracted much attentions from the viewpoint of optical physics [1,2]. Moiré patterns in vdW heterostructures can be formed by stacking the same or different 2D semiconductors with lattice mismatch or stacking angle, offering a new platform to study novel optical phenomena [3]. It is well recognized that the moiré patterns would induce periodic distribution of the potential for optically generated electron-hole pair (exciton), which strongly modifies the optical properties of both intra- and inter-layer excitons in the vdW heterostructures [4].

In this study, we studied the influence of periodic moiré potential on intra-layer excitons of monolayer molybdenum diselenide (1L-MoSe₂) and nickel phosphorus trisulfides (NiPS₃) heterostructure with anti-ferromagnetic ordering. We fabricated a vdW heterostructure with the zigzag edge of 1L-MoSe₂ parallel to that of NiPS₃ (1L-MoSe₂/NiPS₃) using mechanical exfoliation, where the large lattice mismatch (11.2%) between the layers, introducing a short range of moiré period (~6.5 nm). Figure 1 shows photoluminescence (PL) spectra of 1L-MoSe₂ on SiO₂/Si substrate (grey) and 1L-MoSe₂/NiPS₃ (blue) at 10 K. The several sharp PL (X_M) peaks were observed in the vdW heterostructure, which might come from the recombination signals of intra-layer excitons in 1L-MoSe₂, trapped by the periodic moiré potential.

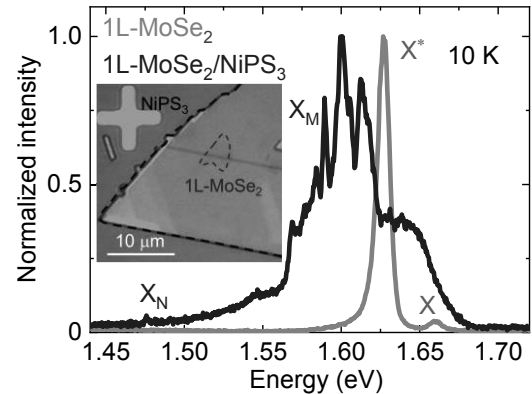


Figure 1. PL spectra of 1L-MoSe₂ and 1L-MoSe₂/NiPS₃ heterostructure at 10 K. X and X* are denoted as exciton and trion PL signals, respectively. X_M and X_N are assigned as PL from intra-layer excitons and NiPS₃ substrate, respectively.

- [1] Y. Miyauchi, K. Matsuda *et al. Nat. Commun.* **9**, 2598 (2018).
 [2] Y. Zhang, K. Matsuda *et al. Adv. Mat.* **32**, 2003501 (2020).
 [3] K. L. Seyler, P. Rivera, H. Yu, *et al. Nature*, **567**, 66 (2019).
 [4] E. M. Alexeev, D. A. Ruiz-Tijerina, M. Danovich, *et al. Nature*, **567**, 81 (2019).

Corresponding Author: Kazunari Matsuda
 Tel: +81-774-38-3460, Fax: +81-774-38-3460
 E-mail: matsuda@iae.kyoto-u.ac.jp

Tuning Heat Flow Across Two-dimensional Layered van der Waals Materials via Interfacial Mismatch and Coupling Engineering

○Wenyu Yuan¹, Kan Ueji¹, Takashi Yagi², Takahiko Endo¹, Hong En Lim¹, Yasumitsu Miyata¹, Yohei Yomogida¹, and Kazuhiro Yanagi¹

¹ Department of Physics, Tokyo Metropolitan University, Hachioji, Tokyo 192-0397, Japan

² National Metrology Institute of Japan, National Institute of Advanced Industrial Science and Technology, Tsukuba, Ibaraki 305-8563, Japan

The understanding of heat flow across solid interfaces and its control are extremely important for the applications of advanced electronics, thermal energy conversion, and thermal managements in devices. Two-dimensional (2D) material family with ultrathin thickness as a new rising star makes it possible to tune the thermal property at atomic-scale. [1] For instance, the stacking structure of graphene, MoS₂, and WSe₂ shows extremely high thermal isolator property on a sub-2-nm scale [2], and disordered WSe₂ exhibits very low thermal conductivity[3]. Therefore, experimental understanding on the heat flow across the 2D interfaces is of great

importance. Here, we provide a polyethylene glycol (PEG)-assisted TDTR method to evaluate thermal transport properties across four layered (4L)-transition metal dichalcogenides (TMDCs) with improved sensitivity. A series of 4L-TMDC materials were prepared via multi-step transfer process, and obvious TDTR

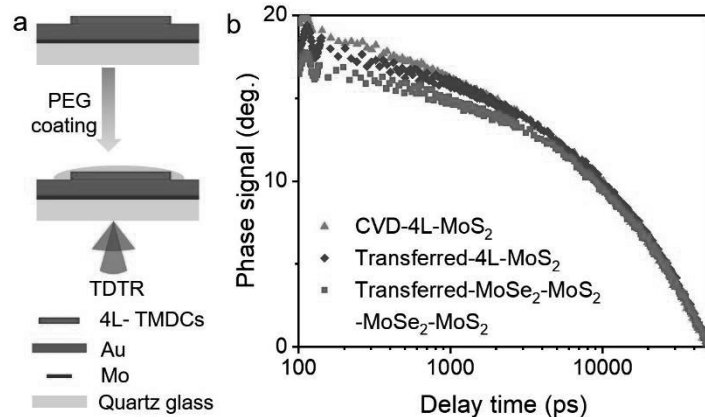


Figure 1. (a) Schematic for the PEG-assistant TDTR method. (b) The TDTR signals of CVD-4L-MoS₂, transferred 4L-MoS₂, and transferred MoSe₂-MoS₂-MoSe₂-MoS₂.

signal change can be observed in CVD-4L-MoS₂, transferred 4L-MoS₂, and transferred MoSe₂-MoS₂-MoSe₂-MoS₂ heterostructure, implying that the transfer and the heterostructure significantly affect the heat flow across the vdW materials due to the rich interfacial mismatch and weak interfacial coupling effect in transferred 2D vdW stacking materials.

[1] Y. Liu *et al.* Nature, **567**, 323(2019).

[2] S. Vaziri *et al.* Sci. Adv., **5**, eaax1325 (2019).

[3] C. Chiriac *et al.* Science, **315**, 351 (2007).

Corresponding Author: K. Yanagi

Tel: +81-(0)42-677-2494, Fax: +81-(0)42-677-2494,

E-mail: yanagi-kazuhiro@tmu.ac.jp

Photoreaction of C₇₀ with Disilirane: Electronic Properties of Silylated Adducts

○Shintaro Nishida¹, Masahiro Kako^{*1}, Michio Yamada², Yutaka Maeda²,
Makoto Furukawa³, Takeshi Akasaka^{2,3,4}

¹Department of Engineering Science, The University of Electro-Communications, Chofu,
Tokyo 182-8585, Japan

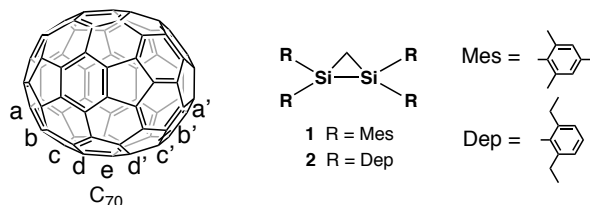
²Department of Chemistry, Tokyo Gakugei University, Koganei, Tokyo 184-8501, Japan

³Foundation for Advancement of International Science, Tsukuba, Ibaraki 305-0821, Japan

⁴School of Materials Science and Engineering, Huazhong University of Science and Technology,
Wuhan, Hubei 430074, P. R. China

Chemical derivatization of fullerenes has been intensively studied as useful methods to modify the physical and chemical properties of fullerenes for various applications such as molecular electronics, nanomaterial science, and biochemistry [1]. Introduction of heteroatoms such as electropositive silicon atoms has been reported to affect the electronic characteristics of fullerenes remarkably. Reactive organosilicon compounds such as silylenes, disiliranes, silyl radicals, and siliranes have been employed to derivatize of fullerenes to afford the corresponding silylated fullerene derivatives [2,3]. Electrochemical analyses and theoretical calculations have revealed that these silylated derivatives have more negative charge on the cage than the parent fullerenes. In our continuing studies, we reported that the photoreactions of hollow fullerenes and endohedral metallofullerenes with 1,1,2,2-tetramesityl-1,2-disilirane (**1**) as a versatile silylating reagent afforded the corresponding addition products [2,3]. Spectroscopic, electrochemical, and crystallographic techniques, as well as theoretical calculations disclosed the structural and electronic properties of the silylated adducts. Although the photoreaction of C₇₀ and disilirane **1** was also reported in the early stage of studies of the functionalization of fullerenes, the electronic properties of the corresponding photoadduct have not been characterized yet [4]. These results prompted us to investigate the reactivities of C₇₀ with 1,1,2,2-tetrakis(2,6-diethylphenyl)-1,2-disilirane (**2**), in which the regiochemistry of the photoaddition is expected to be affected by more bulky substituents on the silicon atoms. We now report the details of the photoaddition of C₇₀ with **2** indicating the structural and electronic properties of the photoproducts. The photoreaction of C₇₀ and **2** was conducted in toluene using two 500W halogen lamps with an aqueous sodium nitrite solution filter (cutoff < 400 nm) under an argon atmosphere. Separation of the reaction mixture afforded the two adducts, which were structurally assigned to 1,4-adduct at the [a,c] position and 1,4-adduct at the [d,d'] or [e,e] positions. The electron-donating effects of the silyl groups in these products are discussed in comparison with those of the related compounds.

Scheme 1.



[1] A. Hirsch *Angew. Chem. Int. Ed.*, **32**, 1138–1141 (1993).

[2] M. Yamada *et al.* *Bull. Chem. Soc. Jpn.*, **87**, 1289–1314 (2014).

[3] M. Kako *et al.* *Molecules*, **22**, 1179 (2017).

[4] T. Akasaka *et al.* *J. Am. Chem. Soc.*, **116**, 2627–2628 (1994).

Corresponding Author: M. Kako Tel: +81-42-442-5570 E-mail: kako@e-one.uec.ac.jp

Simulation and measurement of the infrared emission spectra of C₆₀

○Tomonari Wakabayashi¹, Yutaka Mukai¹, Kaito Tanka¹, Keisuke Fukumoto¹,
Miho Hatanaka², Takeshi Kodama³

¹Department of Chemistry, Kindai University, Higashi-Osaka 577-8502, Japan

²Department of Chemistry, Keio University, Yokohama 223-8522, Japan

³Department of Chemistry, Tokyo Metropolitan University, Hachioji 192-0397, Japan

High resolution infrared (IR) absorption spectra of fullerene C₆₀ molecules isolated in the cryogenic solid parahydrogen matrix host disentangled numerous narrow spectral lines of slightly different vibrational frequencies for a number of isotopomers stemming from substitution of the major ¹²C atom with the natural abundance of 1.1% ¹³C isotope [1]. The calculated absorption intensity of the four IR-active vibrational T_{1u} modes, which is proportional to the Einstein B coefficient, should be a necessary measure for the estimation of molecular abundance in space. Another factor to be considered for the analysis of IR emission intensity is the vibrational temperature or population in vibrationally excited states of the molecule. From the observed intensity ratio for the high-frequency T_{1u}(3) mode relative to those for the low-frequency T_{1u}(1) and T_{1u}(2) modes, the C₆₀ molecules in planetary nebulae are indeed gas-phase molecules at vibrational temperature of ≈300 K [2].

Taking Boltzmann distributions of the vibrationally excited v=1 level for each of the total 46 normal modes of C₆₀ having distinctly different vibrational frequencies into considerations, we simulated absolute intensities of the four IR-active emission bands as a function of the vibrational temperature (Fig. 1). It is compatible with the result of the previous report [2]. Further refinement is to be made by considerations on higher v levels and on overtones and combinations. We also plan to measure experimental IR emission spectra of C₆₀ molecules as reported previously [3], where the IR photons emitted from sublimed C₆₀ molecules at elevated temperatures up to 950°C are analyzed using an FTIR spectrometer.

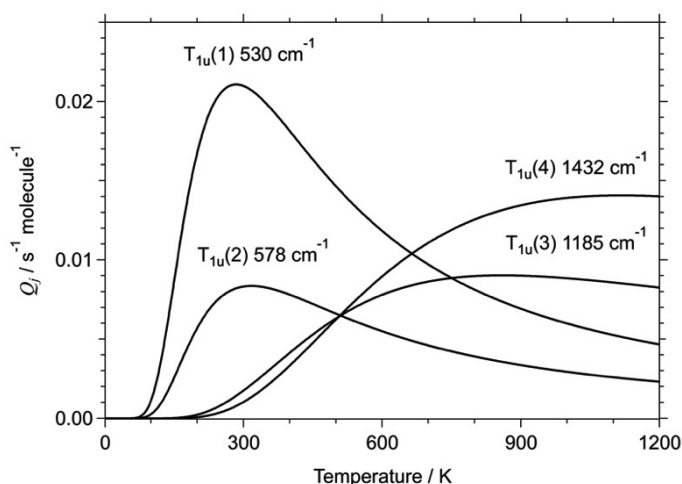


Fig. 1 Temperature dependence of the calculated emission intensity for the four IR-active vibrational T_{1u} modes of C₆₀.

[1] T. Wakabayashi, T. Momose, M. E. Fajardo, *J. Chem. Phys.* **151**, 224301 (2019).

[2] J. Bernard-Salas, J. Cami, A. P. Peeters, A. P. Jones, E. R. Micelotta, *Astrophys. J.* **757**, 41 (2012).

[3] C. I. Frum, R. Engleman Jr., H. G. Hedderich, P. F. Bernath, L. D. Lamb, and D. R. Huffman, *Chem. Phys. Lett.* **176**, 504 (1992).

Corresponding Author: T. Wakabayashi

Tel: +81-6-4307-3408, Fax: +81-6-6723-2721,

E-mail: wakaba@chem.kindai.ac.jp

Growth of single-walled carbon nanotubes on SiO₂/Si substrate and alumina buffer layer by alcohol catalytic CVD method using Ir catalyst

○Daiki Yamamoto¹, Shu Kondo¹, Kamal P Sharma¹, Takahiro Saida^{1,2},
Shigeo Naritsuka³, Takahiro Maruyama^{1,2}

¹Department of Applied Chemistry, Meijo University, Japan

²Nanomaterial Research Center, Meijo University, Japan

³Department of Materials Science and Engineering, Meijo University, Japan

1. Introduction

Single-walled carbon nanotubes (SWCNTs) are one-dimensional materials, having various potential for future nanoelectronics. So far, we have succeeded in growing vertically aligned small-diameter SWCNTs by alcohol catalytic chemical vapor deposition (ACCVD) with an Ir catalyst [1]. However, there are a few researches about SWCNTs growth using Ir catalysts, especially, using alumina buffer layer. In this study, to investigate the effect of alumina buffer layer, SWCNT growth was performed on SiO₂/Si substrates and those with alumina buffer layers by ACCVD using Ir catalysts, and compared the results.

2. Experimental procedure

After a 10 nm-alumina buffer layer was deposited on an SiO₂/Si substrate by rf-sputtering, an Ir catalyst was deposited on it by the pulsed arc deposition. The nominal thickness of the Ir catalyst was 0.3 nm. Then, the substrates were introduced into an ultra-high vacuum (UHV) CVD system, which was used for SWCNT growth. After the substrate was heated to a growth temperature in an H₂ atmosphere of $\sim 1 \times 10^{-3}$ Pa, ethanol gas was supplied through nozzle onto the substrates to grow SWCNTs [1]. The grown SWCNTs were analyzed by Raman spectroscopy.

3. Result and Discussion

Figs. 1 (a) and (b) show RBM regions of Raman spectra for SWCNTs grown at 800°C for 60 min under an ethanol pressure of 1×10^{-2} Pa with an Ir catalyst on a SiO₂ substrate and an alumina buffer layer, respectively. The SWCNTs on the alumina buffer layer were slightly larger than those on the SiO₂ substrate. Figs. 1 (c) and (d) show optical microscope images of SWCNT films grown on the SiO₂ and alumina/SiO₂ substrates, respectively. Morphology of grown SWCNTs were different between the two substrates, which suggests that the growth mechanism was different. We will discuss the effects of the alumina buffer layer on SWCNT growth.

This work was supported in part by Private University Research Branding Project from the Ministry of Education, Culture, Sports, Science and Technology (MEXT), Japan.

[1] T. Maruyama et al. Appl. Surf. Sci. 509 (2020) 145340.

Corresponding Author: T. Maruyama, Phone: +81-52-838-2386, Fax: +81-52-832-1179

E-mail: takamaru@meijo-u.ac.jp

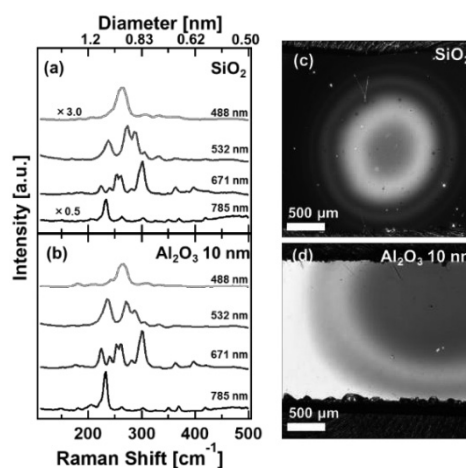


Fig. 1 (a, b) show the RBM regions of Raman spectra for SWCNTs from an Ir catalyst grown (a) on the SiO₂ substrate and (b) on the alumina buffer layer. (c, d) shows optical microscope images of the samples (a) and (b), respectively.

Analysis of acetylene-induced growth acceleration of single-walled carbon nanotubes by isotope labeling technique

○Akari Kobayashi¹, Ryoya Ishimaru¹, Keigo Otsuka¹, Taiki Inoue², Shohei Chiashi¹ and Shigeo Maruyama¹

¹Department of Mechanical Engineering, The University of Tokyo, Tokyo, 113-8656, Japan

²Department of Applied Physics, Osaka University, Osaka 565-0871, Japan

Single-walled carbon nanotubes (SWCNTs) are promising for various applications. Time-dependent growth analysis of SWCNTs has been conducted extensively for understanding the growth mechanism. However, most studies focused on growth of SWCNTs in bulk form and did not discuss individual difference of SWCNTs [1] and others observed only few and short individual SWCNTs [2]. There had been no method that could observe growth process of long, individual SWCNTs in large quantity. Recently, we have proposed a novel method, digital isotope labeling, which fulfills all these demands [3,4].

In this study we investigated effects of acetylene in addition to ethanol on individual SWCNT growth by the digital isotope labeling. We synthesized SWCNTs from ¹²C ethanol with addition of ¹³C ethanol as labels and obtained growth curves and growth rate by detecting the labels along each SWCNT with Raman mapping (Fig. 1(a)). We introduced ¹²C acetylene of 1/50 flow rate of ethanol in the middle of synthesis and calculated the composition ratio of ¹²C acetylene and ¹³C ethanol by observing Raman shift of SWCNTs (Fig. 1(b)). From Raman shift (1576 cm⁻¹), the SWCNT was composed of about 27 % of ¹³C ethanol and about 73 % of ¹²C acetylene at the point. When considering the flow rate, acetylene is easy to be used for grown 100 times or more than ethanol. Growth of most SWCNTs was accelerated by introducing of acetylene. Comparison of growth rate obtained by Raman mapping and incorporation frequency calculated by Raman spectrum reveals that more ethanol with acetylene is captured by catalysts than ethanol without acetylene.

[1] E. Einarsson, *et al.*, *Carbon*, **46**, 923 (2008).

[2] R. Rao *et al.*, *Nat. Mater.*, **11**, 213 (2012).

[3] K. Otsuka *et al.*, *ACS Nano*, **12**, 3994 (2018).

[4] B. Koyano *et al.*, *Carbon*, **155**, 635 (2019).

Corresponding Author: S. Maruyama Tel: +81-3-5841-6421, Fax: +81-3-5800-6983,

E-mail: maruyama@photon.t.u-tokyo.ac.jp

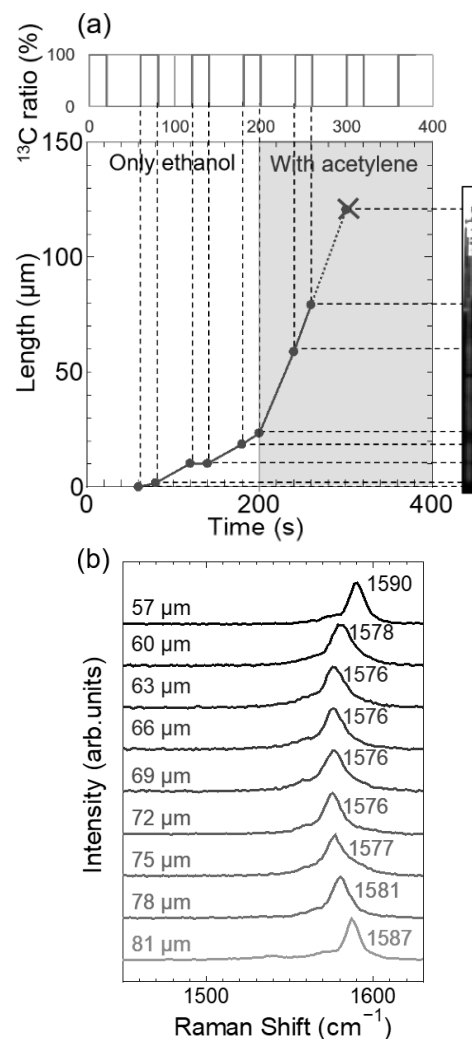


Fig. 1 (a) A typical growth curve of a SWCNT which is plotted based on an isotope introduction sequence (top panel) and a Raman mapping image (right panel). (b) Typical Raman spectra of the SWCNT grown by ¹³C ethanol with ¹²C acetylene at 57-81 μm from top of the SWCNT.

Fabrication and Efficiency Evaluation of Organic Photovoltaics using Single-walled CNT of the Transparent Conductive Electrode

○Riku Hatamoto,¹ Hao-Sheng Lin,¹ Takeshi Hashimoto,² Satoru Hashimoto,² Yutaka Matsuo¹

¹Department of Chemical System Engineering Graduate School of Engineering, Nagoya University, Furo-tyo, Chikusa-ku, Nagoya 464-8603, Japan

²Meijo Nano Carbon, Nagoya 463-0003, Japan

In organic photovoltaics (OPVs), indium tin oxide (ITO) substrates are mainly used for transparent conductive electrodes. Carbon nanotubes (CNTs) have been recognized as currently most promising alternative to ITO thanks to their remarkable flexibility and low-cost. However, the low conductivity and rough interfacial morphology of CNTs severely limited the up-layer fabrication in OPVs, such as hydrophilic hole-transport layer (HTL) fabrication, active layer fabrication *etc.*

Table.1 Photovoltaic parameters of OSCs

	I_{sc} (mA)	V_{oc} (V)	FF	PCE (%)
Ref (ITO)	0.48	0.61	0.51	1.61
HNO ₃ doped CNT	0.44	0.59	0.46	1.35
Nafion mixed PEDOT:PSS	0.52	0.54	0.36	1.12

This study focuses on solving the efficient fabrication of hydrophobic HTL by through modification of hydrophilicity of both CNTs and HTL materials. Nafion and HNO₃ were screened for altering the hydrophilicity of CNTs. Nafion and isopropanol in different doping ratio to HTL was investigated to modify the hydrophobicity of HTL. The results showed that HNO₃ can be an effective dopant to CNTs to achieve a power conversion efficiency (PCE) of 1.35%, and Nafion can effectively dope PEDOT:PSS to achieve a PCE of 1.12% compared to a reference PCE of 1.61%.

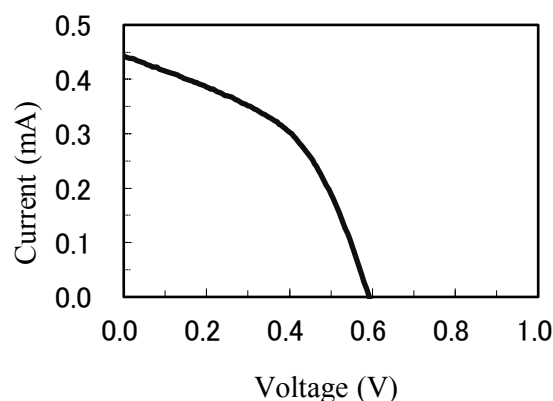


Fig.1 J-V curves of OSCs in HNO₃ doping

Corresponding Author: Y. Matsuo

Tel: +81-52-747-6722

E-mail: yutaka.matsuo@chem.material.nagoya-u.ac.jp

Thermoelectric properties of morphology-controlled single-walled carbon nanotube alloys

○Yota Ichinose, Rikuto Abe, Kan Ueji, Yohei Yomogida, Kazuhiro Yanagi

Department of Physics, Tokyo Metropolitan University, Tokyo, Japan

Thermoelectric performance of single-walled carbon nanotube (SWCNT) thin films attracts a lot of interest for both basic and application aspects [1]. The purity and the alloyed condition, *i.e.*, the ratio of metal to semiconducting types, of the thin films significantly influence their thermoelectric performance [2,3]. It is known that the network morphology of thin films also significantly influences various physical properties of the thin films, and thus it is important to clarify the relationships between the alloyed network morphology and thermoelectric performance. Here, in this study, we investigated how the difference of network connections of metallic and semiconducting SWCNTs influences thermoelectric performance although the alloyed condition, *i.e.*, the ratio of metallic to semiconducting types, was the same as a whole.

We prepared two kinds of devices; one is that metallic and semiconducting SWCNT films are connected in a series, and the other is that they are connected in a parallel manner (Fig.1). In both cases, the alloyed ratio is approx. 50% as a whole, but the network morphology is completely different. Subsequently, the Seebeck coefficient and electrical conductivity were measured while varying the Fermi level using the electrolyte double layer technique.

Comparing the thermoelectric performance of the parallel and series structures, the experimental results show that the parallel structure shows a larger performance (Fig.2), indicating the control of the alloyed morphology is very important for maximization of the thermoelectric performance. Furthermore, the theoretical analysis revealed that the parallel and series models can well reproduce the experimental results. In this presentation, we will discuss the detailed experimental results and the background.

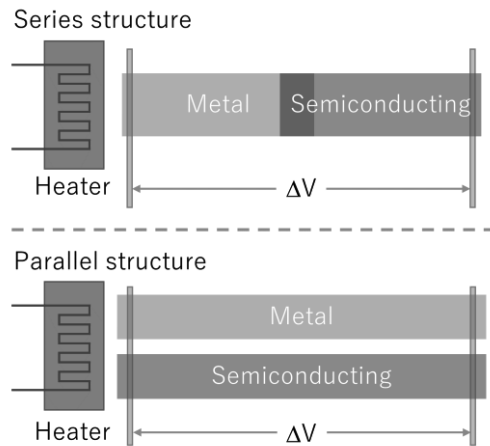


Fig. 1 Schematic diagram of the series and parallel structures.

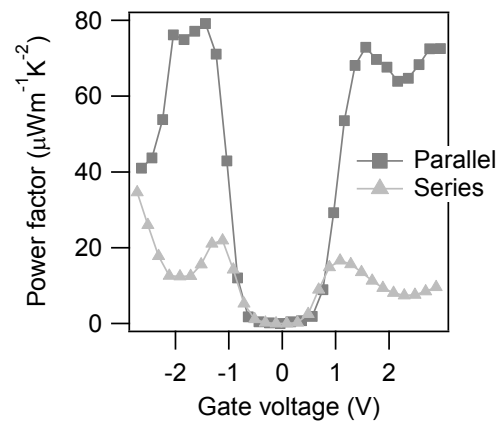


Fig. 2 Fermi level dependence of the power factor in parallel and series structure.

- [1] J. Blackburn et al., *Adv. Mater.* **30**, 1704386 (2018). [2] K. Yanagi et al., *Nano Letters* **14** (11), 6437 (2014). [3] Y. Ichinose et al., *Nano Letters* **19**, 7370 (2019).

Corresponding Author: K. Yanagi

Tel: +81-42-677-2494, Fax: +81-42-677-2483, E-mail: yanagi-kazuhiro@tmu.ac.jp

Gate-tuned high-harmonic generation in metallic single-walled carbon nanotubes and graphene

○Hiroyuki Nishidome¹, Kohei Nagai², Kent Uchida², Kenji Kawahara³, Junko Eda¹, Hitomi Okubo¹, Yohei Yomogida¹, Hiroki Ago^{3,4}, Koichiro Tanaka^{2,5}, Kazuhiro Yanagi¹

¹ Department of Physics, Tokyo Metropolitan University, Tokyo 192-0397, Japan

² Department of Physics, Kyoto University, Kyoto 606-8502, Japan

³ Global Innovation Center (GIC), Kyushu University, Fukuoka 816-8580, Japan

⁴ IGSES, Kyushu University, Fukuoka 816-8580, Japan

⁵ Institute for Integrated Cell-Material Sciences, Kyoto University, Kyoto 606-8501, Japan

High-harmonic generation (HHG), which is the generation of light with multiple optical harmonics, is an unconventional nonlinear optical phenomenon beyond the perturbation regime. HHG, which was initially observed in gaseous media, has recently been demonstrated in solid state materials. Determining how to control such extreme nonlinear optical phenomena is a challenging subject. It is expected that materials with large anharmonicity in the band dispersions would emit higher harmonics. Therefore, Dirac materials, like the graphene and the metallic single-walled carbon nanotubes (m-SWCNTs), which have linear dispersions are expected to emit higher harmonics. In previous work, however, m-SWCNTs generated lower-order harmonics than semiconducting ones[2], and graphene also generated lower order[3]. These low-order HHG might be caused by initially doping conditions. Certainly we have observed that carrier injection would suppress 5th harmonics and enhance 3rd in semiconducting SWCNTs[2]. Thus, in this study, we investigated Fermi-level dependence of HHG in the graphene and the m-SWCNTs by using electrolyte gating method.

We prepared monolayer graphene and aligned-m-SWCNT film and employed side-gating device using ionic liquid to tune Fermi-level through the gate voltage V_G . The samples were irradiated with 0.26 eV mid-infrared pulse laser, and we investigated the relations between HHG and carrier injection.

Figure 1 shows the HH intensities and source-drain current J_{SD} as a function of V_G in m-SWCNTs and insists carrier injection would suppress all HHG. In contrast, HHG in graphene was almost the same intensity through carrier injection, but we found unique ellipticity dependence. Figure 2 shows normalized HH intensity I_x and I_y in graphene with different V_G as a function of ellipticity ε of the laser. Here I_x (I_y) means intensity in the direction of major (minor) axis of elliptically polarized laser. This result suggests that V_G would tune only I_y . We will discuss experimental details and these backgrounds.

[1] S. Ghimire *et al.* Nat. Phys., **15**, 10 (2019).

[2] H. Nishidome *et al.* Nano Lett., **20**, 6215 (2020).

[3] N. Yoshikawa *et al.* Science, **356**, 736 (2017).

Corresponding Author: K. Yanagi, Tel: +81-42-677-2494, Fax: +81-42-677-2483, E-mail: yanagi-kazuhiro@tmu.ac.jp

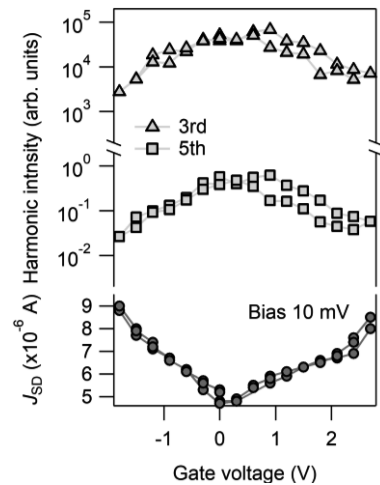


Fig.1 High-harmonic intensity (top) and source-drain current J_{SD} (bottom) with the shift of the gate voltage in m-SWCNTs.

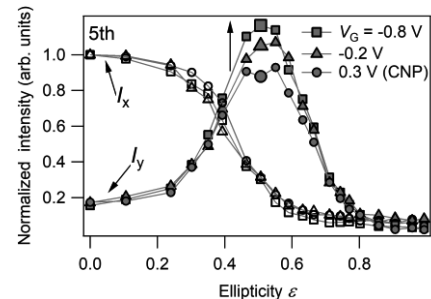


Fig. 2 Normalized harmonic intensity in graphene with different doping levels as a function of ellipticity ε of the laser. These intensities were normalized by I_x at $\varepsilon=0$.

Circular dichroism spectra on thin films of Helicity Selected Single-wall Carbon Nanotubes

○Yuuya Hosokawa, Yohei Yomogida, Kazuhiro Yanagi

Department of Physics, Tokyo Metropolitan University, Tokyo 192-0397, Japan

Chiral structure of nanotube materials can exhibit very unique physical properties such as bulk photovoltaic, unconventional super conductivity, and so on [1]. Regarding single walled carbon nanotubes (SWCNTs), theoretical studies suggest that their chiral structures will induce unique physical phenomena such as photo galvanic effect, gigantic circular dichroism, and so on [2]. However, those phenomena have not been experimentally verified yet. Recently, the advancement of purification techniques enables us to prepare helicity selected SWCNTs in a large scale [3], and then, as the first step, understanding of circular dichroism (CD) character of their thin films is required before the evaluation of their unique physical properties. It should be noted that, when we use CD spectrometer for thin films composed by nanomaterials with anisotropic structure, the presence of linear dichromic (LD) character induces “anomalous” CD signals [4]. Therefore, we need to carefully check whether we can detect “true” CD signals originating the helicity of nanotubes in SWCNT thin films. For that purpose, in this study, we prepared three types of thin films, (6,5), (11,-5) and their racemic mixture, and we intentionally prepared the thin films in which nanotubes are randomly oriented, and investigated the influence of LD component on their CD signals. Figures 1 and 2 show the LD and CD spectra of the three samples, respectively. In this study, since we intentionally prepared thin films where nanotubes are randomly oriented, the amount of LD in all the samples was suppressed to be less than 0.01. Then as shown in the fig. 2, in the racemic mixture, we could not observe anomalous CD signals. In contrast, in the case of (6,5) and (11,-5) thin films, we clearly observed asymmetrical CD signals as expected. These results indicate that the CD signals due to nanotube helical structure can be correctly detected when we prepare thin film form where the nanotubes were randomly oriented.

References:

- [1] Qin et al., nature comm. 8, 14465 (2017), Zhang et al., Nature 570, 349 (2019)
- [2] Ivchenko & Spivak, PRB 66, 155404 (2002), Satco et al., PRB 99, 075403 (2019)
- [3] X. Wei et al., Carbon 132, 1-7 (2018)
- [4] Y. Shindo, J. Spec. Soc. Jpn. 34, 215 (1985)

Corresponding Author: K. Yanagi

Tel: +81-42-677-2494 e-mail: yanagi-kazuhiro@tmu.ac.jp

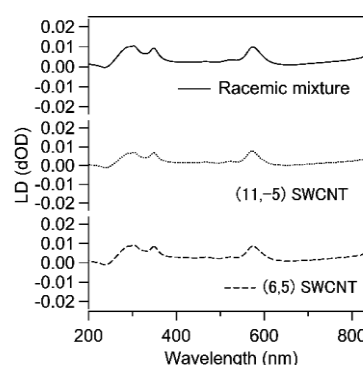


Figure 1 LD spectra of the thin film samples.

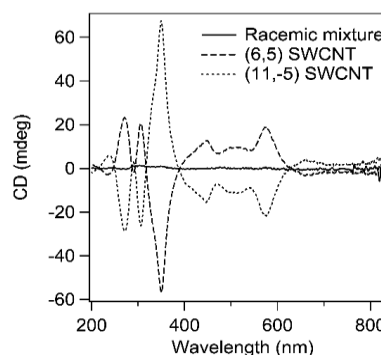


Figure 2 CD spectra of the thin film samples

Synthesis of Vertical-Aligned Carbon Nanotube / Al Composite Electrode for Li-ion Capacitor Cathode

○Masanori Hara, Ryo Kawachi, Takashi Banno, Masamichi Yoshimura

Toyota Technological Institute, Nagoya 468-8511, Japan

1. Introduction

Recently, expanding usage of mobile devices and renewable energies has demanded the development of a high performance rechargeable power sources with short charging time. Li-ion capacitor (LIC) [1] is a composite capacitor that consists of electric double layer capacitor (EDLC) cathode and Li-ion battery (LIB) anode [2]. LIC has both advantage of EDLC and LIB, high electron charged-discharge rate and high capacity. To improve performance of LIC, high surface area and highly-aligned structure are also required for the electrodes. In this research, we have synthesized vertical-aligned CNT on the Al substrate (CNT/Al) for cathode of LIC by alcohol catalytic chemical vapor deposition (ACCVD). The CNT/Al composite electrode was characterized and its performance was evaluated in Li ion containing organic solvent.

2. Experimental

Al substrate was covered with 2 nm Co layer as a catalyst for CNT growth by arc plasma deposition. Vertical-aligned CNT was grown on the Co deposited Al substrate by ACCVD using ethanol vapor as a carbon source [3] at 600°C for 10 min under 1 kPa condition. The CNT / Al electrode was characterized by scanning electron microscopy (SEM), Raman spectroscopy, and electrochemical methods (cyclic voltammetry (CV) and charge-discharge measurement (CDC)) in 1 M LiPF₆ and ethylene carbonate(EC) and diethyl carbonate (DEC) mixed solution (EC:DEC = 1:1) using a coin cell.

3. Results and discussion

Fig. 1 shows a SEM image of the CNT/Al electrode. The CNTs were grown vertically on the Al substrate and the length of CNT was around 10 μm. During the growth, the alumina layer formed on Al surface works as a passivation layer and suppresses aggregation of Co catalyst particles on the substrate during CNT growth. From Raman spectroscopy, we confirmed that the grown CNTs were multi-walled CNTs.

Fig. 2 shows a CV obtained on CNT/Al electrodes in the potential region between 2.5 and 4.0 V in 1 M LiPF₆ and EC:DEC solution. The CV curve without peaks suggests that no chemical reactions except for charging of double layer capacity take place and the electrode is stable in these potential region. The capacity of CNT/Al estimated from CDC measurements is 2.91 mC cm⁻², which is ca. 30 times higher than that on bare Al electrode. The electrochemical behavior demonstrates that the vertical-aligned CNT/Al electrode is a promising candidate of LIC capacitor cathode.

[1] P. Han, *Adv. Energy Mater.*, **8**, 1801243 (2018).

[2] C. de las Casas, *J. Power Sources*, **208**, 74 (2012).

[3] D. Yoneda, *et al.*, *Mater. Res. Express*, **6**, 086322 (2019).

Corresponding Author: M. Hara

Tel: +81-52-809-1850, E-mail: haram@toyota-ti.ac.jp

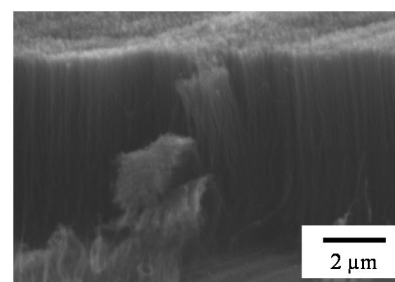


Fig. 1 Cross sectional SEM image of CNT/Al synthesized by ACCVD.

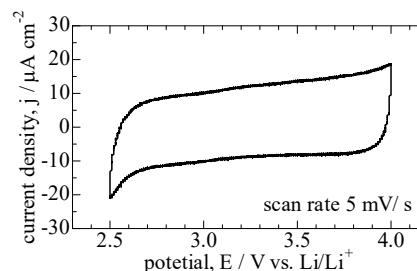


Fig. 2 CV obtained on the CNT/Al electrodes in 1 M LiPF₄ + EC:DEC (1:1) solution. Scan rate: 5 mV/s.

Observation of the UV-induced Photocurrent in PET sheet using CNT thin-film electrodes

○Satoru Suzuki¹, Taichi Nakamura¹, Takahiro Ishikawa², Teruaki Konishi²,
Tsuyoshi Hamano², Yutaka Ohno^{3,4}, Hiroshi Ajiki¹, Toshio Hirao², Satoshi Ishii¹

¹ Department of Physics, Tokyo Denki University, Saitama 350-0394, Japan

² National Institute for Radiological Sciences, National Institutes for Quantum and Radiological Science and Technology, Chiba 263-8555, Japan

³ Department of Electronics, Nagoya University, Nagoya 464-8602, Japan

⁴ Institute of Materials and Systems for Sustainability, Nagoya University, Nagoya 464-8601, Japan

The transparent real-time dosimeter with a visual field is required for the dosimetry of the curer's crystalline lens in radiation medicine. The electrical response to the X-ray irradiation has been investigated on the polymeric plastic sheet, and however, the detected current was due to the ionization of air in addition to the carrier generation inside the polymeric plastic. In this study, we have irradiated UV instead of X-ray to the polyethylene terephthalate (PET) sheets with the carbon nanotube (CNT) thin-film electrodes and observed the photocurrent by excluding the effect of air.

The circular electrodes were fabricated on the both sides of the PET sheet with the thickness of 50 μm [Fig. 1(a)]. The current path was confined vertically inside the PET to detect the current originated only from the sample [Fig. 1(b)]. The CNT thin-film electrodes were patterned on the sheet surface by spray coating of the CNT dispersion using the mask. The Au circular electrodes were also prepared by sputtering for comparisons. The sample was placed inside the cryostat under a vacuum of about 1.0×10^{-4} Pa. The photocurrent was measured for the UV irradiation (365 nm, $260 \mu\text{W}/\text{cm}^2$) at a bias voltage of 0V and at the temperatures of 173, 303 and 393 K.

The reverse current was observed for the both samples as shown in Fig. 2(a) and 2(b), which means that the hole carriers were injected from the main electrode. The activation energies were obtained as 27 and 50 meV from the peak current of the samples with CNT thin-film and Au electrodes, respectively, as shown in Fig. 2(c). These energies were about one or two orders of magnitude lower than the energy barriers between electrode and PET which were estimated from the work function differences of them. The injected holes were expected to be trapped at the interface becoming the space charges and limited the current.

This work was supported partially by JSPS KAKENHI Grant Number JP20K08036 and the joint usage/research program of the IMaSS, Nagoya University.

Corresponding Author: S. Ishii

Tel: +81-49-296-1926, Fax: +81-49-296-2915, E-mail: s.ishii@mail.dendai.ac.jp

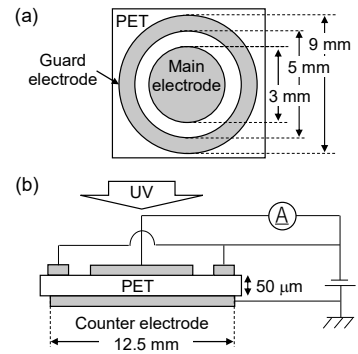


Fig. 1 (a) Surface and (b) sectional view of the sample.

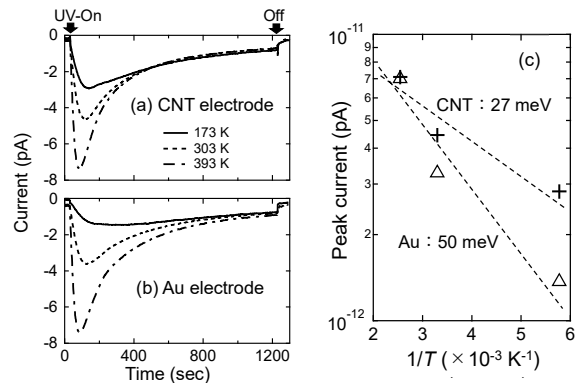


Fig. 2 Time dependence of the photocurrent at 0 V for the (a) CNT thin-film and (b) Au electrode samples. (c) Arrhenius plots of the peak current.

Relationship between van der Waals force and tensile strength of MWNT/polymer composites by Melt Blending

○Koichi Utsugi¹, Masaru Sekido²

¹ Division of Production System and design Engineering, National Institute of Technology, Sendai College, Natori 981-1239, Japan

² Department of Materials and Environmental Engineering, National Institute of Technology, Sendai College, Natori 981-1239, Japan

Interfacial properties are known to have a critical effect on the mechanical properties of a nanocomposite material system. Previously we have prepared CNT/high density polyethylene (HDPE) composites by melt blending and measured tensile strength to find that tensile strength of CNT/HDPE was not improved [1]. This is presumably due to the poor load transfer between the CNTs and HDPE. The van der Waals force between HDPE and CNT is small since HDPE is a non-polar polymer.

In this study, we investigated the effects of van der Waals force, such as dipole-induced dipole forces and π - π stacking at the interface between MWNT and polymer matrix on the tensile strength of MWNT/polymer composites.

MWNT/HDPE, MWNT/polyamide-6 (PA-6), MWNT/polyvinyl alcohol (PVA), MWNT/polystyrene (PS), and MWNT/polybutylene terephthalate (PBT) composites with 0.99wt.%, 2.9wt.%, and 4.8 wt.% MWNT content were prepared, screw speed of 100 rpm, and a recycle time of 10 minutes.

The tensile strength of MWNT/PA-6 and MWNT/PVA increased at all weight ratios. It is suggested in 0.99wt.% that the tensile strength is increased by the dipole-induced dipole force between the MWNT and the polymer matrix (Figure 1 and 2). The tensile strength may depend on the steric hindrance of polymer matrix rather than the van der Waals force between the CNTs and the polymer matrix at higher CNT weight ratios. In the case of MWNT/PS, it was expected that the interfacial properties would be improved by the π - π stacking at the interface between MWNT and aromatic rings of PS. But the tensile strength decreased at all weight ratios.

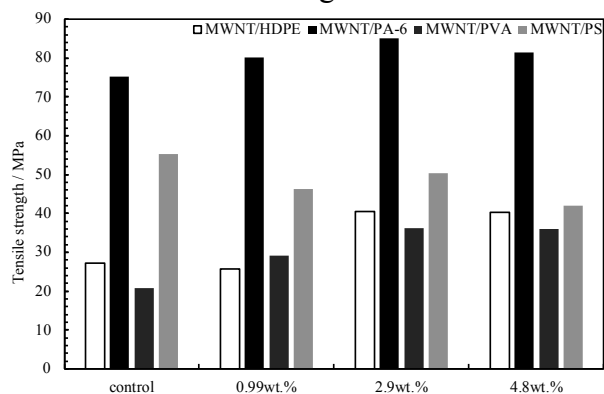


Fig. 1 Tensile strength of MWNT/polymer composite.

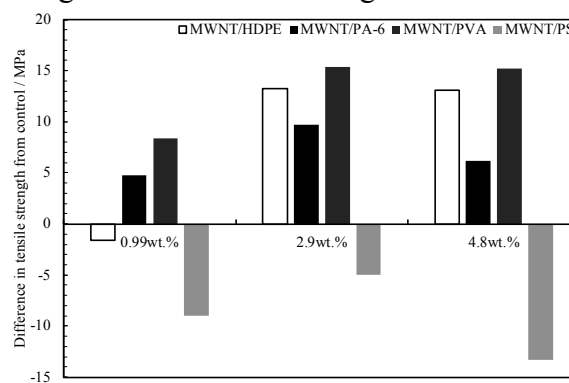


Fig. 2 Difference in tensile strength from control of MWNT/polymer composite.

[1] Atsushi Onodera et al., The 54th Fullerenes-Nanotubes-Graphene General Symposium, 1P-15 (2018)

Corresponding Author: K. Utsugi

Tel: +81-22-381-0329, Fax: +81-22-381-0329,

E-mail: a1912605@sendai-nct.jp

Direct Growth of Graphene on GaN using Alcohol CVD

○Shohei Yabuta, Shinichiro Mouri, Tsutomu Araki

*The Graduate School of Science and Engineering, Ritsumeikan University,
Nojihigashi 1-1-1, Kusatsu, Shiga, Japan*

GaN/graphene Schottky diodes have been studied recently towards applications in optical and electronic devices [1-3]. However, the current state of the art requires a process to transfer graphene crystals grown on metal foils onto compound semiconductor substrates, and there is concern that residues from this process deteriorate the device performance. In this study, to overcome this issue, we have attempted to grow graphene directly on GaN substrates using alcohol CVD [4].

Two types of substrates, a GaN (0001) template (GaN/sapphire) and a GaN template wrapped in a copper foil, were prepared and graphene was grown on them. Argon and nitrogen were used as the carrier gas and the etching gas, respectively. Ethanol was used as the carbon source. An optical microscope image of a sample grown at 950°C for 40 minutes is shown in Fig. 1. It can be seen that the film was grown on almost the entire surface of the substrate, and that there is a difference in contrast between the areas where the film was not grown and where the substrate is exposed. As shown in the Raman spectra for each substrate (Fig. 2), there are D, G and 2D bands, indicating the growth of graphene structures, and the G band wavenumber of 1601 cm^{-1} and the low 2D band intensity suggest the formation of multilayer graphene [5-7]. In addition, we found that the Raman intensity ratio of G-mode to D-mode (G/D ratio) of copper foil-wrapped GaN template was suppressed as compared with that of the unwrapped GaN template. We think that this is due to the catalytic effect of the copper evaporated from the copper foil, which suppresses the formation of amorphous structures on the substrate surface, resulting in a reduction of D-mode signal. The optimized growth condition towards the growth of few layer graphene will be discussed in the presentation.

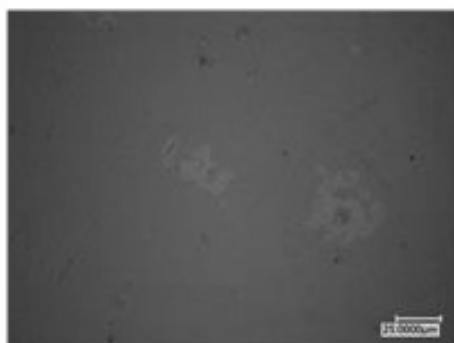


Fig.1 Optical microscope image of graphene grown on GaN

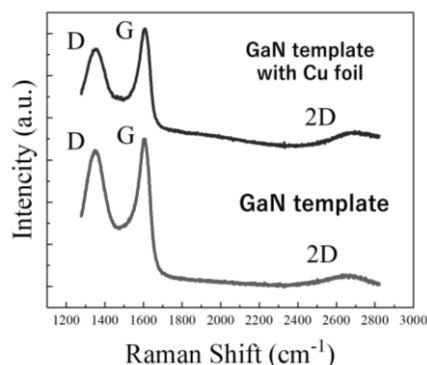


Fig.2 Raman spectrum after graphene growth

References

- [1] G Jo *et al.*, *Nanotechnology*.21,175201(2010)
- [2] S. Tongay *et al.*, *Appl. Phys. Lett.* 99, 102102 (2011)
- [3] Z.Yan *et al.*, *Nature Communications*.3, 827 (2012)
- [4] X. Chen *et al.*, *carbon*.94, 810 (2015)
- [5] A. C. Ferrari *et al.*, *Phys. Rev. Lett.* 97, 187401(2006)
- [6] D.L. Silva *et al.*, *Carbon*.161,181(2020)
- [7] F. Ghaemi *et al.*, *Chem Intermed*.43,4981 (2017)

Corresponding Author: S. Yabuta
E-mail: re0115px@ed.ritsumei.ac.jp

Elucidation of charge interactions between graphene and quantum dots

○Zen Inoue¹, Yasushi Ishiguro², Alexander Baranov³, Igor Nabiev⁴, Kazuyuki Takai^{1,2}

¹ Graduate school of Science and Engineering, Hosei University, Tokyo 184-8584, Japan

² Department of Chemical Science and Technology, Hosei University, Tokyo 184-8584, Japan

³ ITMO Univ, 49, Kronverksky, St. Petersburg, Russia

⁴ MEPHI Univ, 31, Kashirskoe, Moscow, Russia

Graphene as 2-dimensional material has attractive electronic properties, such as broad spectral bandwidth, high electron mobility. However, graphene has relatively low absorbance in spite of its extremely wide-band nature, which limits its application to photodevices [1]. Semiconductor nano-crystals in 0-dimension known as quantum dots (QDs) is promising for photonics applications due to their size-dependent tunable optical properties [2]. To realize a photodevices using graphene, a method of constructing hybrid structure combining graphene and QDs has been proposed. But, the mechanism of charge transfer at the interface between graphene and QDs is not yet understood [3]. In this study, we clarify the interactions of graphene with QDs and QD solvents (toluene and that containing water) at the interface.

Mono-layer (1L) Graphene was prepared by using mechanical exfoliation of highly oriented pyrolytic graphite (HOPG) followed by transferring on a SiO₂ (285 nm) / Si substrate. The electric conductivity was measured for a field effect transistor (FET) using 1L graphene as a channel material after annealing in vacuum chamber (<10⁻⁴ Pa), followed by dropping of CdSe-QDs and toluene, which are dehydrated, as stored, and water-saturated on graphene.

Fig.1 shows the transfer characteristics of the FET of graphene deposited with CdSe-QDs. The charge neutral point of the FET (V_{CNP}) shifted to the lower gate voltage (electron) side after deposition of CdSe-QDs on graphene, suggesting electron carrier transfer from QDs to graphene at the interface. Fig.2 shows the transfer characteristics of graphene deposited with Toluene dehydrated. V_{CNP} shifted to the higher gate voltage (hole) side. The water-containing toluenes show similar hole doping. On the contrary, previous studies have reported that adsorption of toluene vapor in vacuum chamber gives graphene electron carriers [4]. Toluene is expected to act as a catalyst and cause hole doping with oxygen and water in ambient.

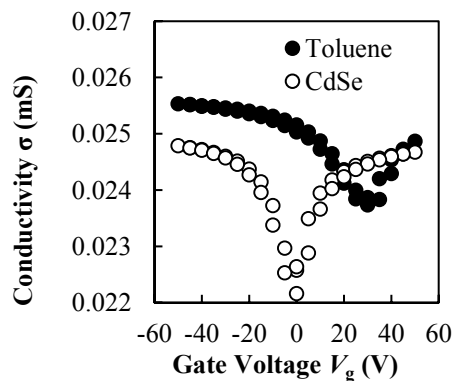


Fig. 1 Effects of CdSe QDs on FET

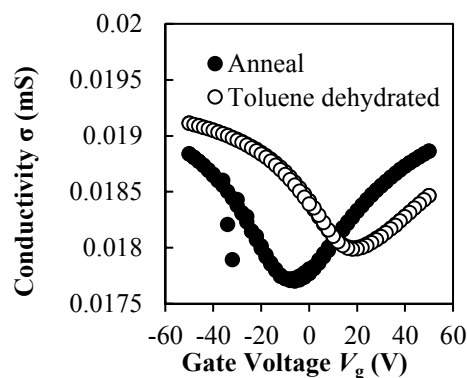


Fig. 2 Effects of solvent (Toluene) on FET

[1] K. Kim, et al. *Nature* **457**, 706–710 (2009). [2] Y. Sun, et al. *Scientific Reports* **8**, 5107(2018)

[3] R. Li, et al. *Scientific Reports* **6**, 28224(2016). [4] A.A. Kaverzin, et al. *CARBON* **49**, 3829-3834(2011)

Corresponding Author: K. Takai

E-mail: takai@hosei.ac.jp

Transport Properties of two-dimensional n/p-doped Transition Metal Dichalcogenides prepared through a post-doping method

○Shaochun Zhang¹, Yuya Murai¹, Toshinori Shirafuji¹, Ryo Kitaura¹

Department of Chemistry, Nagoya University, Nagoya 464-8602, Japan

Two-dimensional (2D) materials have been intensively studied since the discovery of graphene. In particular, 2D transition dichalcogenides (TMDs), such as MoS₂, WS₂, and WSe₂, are known as 2D semiconductors with sizable bandgap and excellent optical/electronic properties. 2D TMDs, therefore, have attracted significant attention as materials for the next generation optoelectronic device applications[1]. For this purpose, controlling of p/n type through introducing dopants plays an essential role. In this work, we prepared Nb/Re doped TMDs by injecting Nb/Re atoms into TMDs and investigated their transport properties in detail.

We performed doping by Nb/Re beams created with UHV e-beam evaporators. In this process, Nb/Re atoms were directly introduced into TMDs (monolayer WSe₂ and bilayer MoSe₂) on hexagonal boron nitrides flakes. Figure 1 shows a temperature dependence of the conductance of 5 % Nb-doped bilayer MoSe₂. As clearly seen in the figure, conductance (G) becomes small as temperature decreases. Plotting the natural logarithm of conductance against $T^{-1/3}$ gives a straight line, indicating that carrier transport occurs through hopping[2] between localized sites. In the presentation, in addition to the sample preparation, we will discuss more details on transport properties.

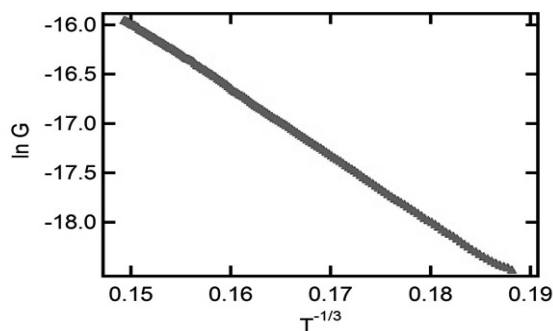


Fig.1 $\ln(G)$ of Nb-doped bilayer MoSe₂ plotted against $T^{-1/3}$

[1] M. Chhowalla, H. Shin et al. Nat. Chem. **5**, 263 (2013)

[2] H. Qiu, T. Xu, Z. et al. Nat. Commun. **4**, 2642 (2013)

Corresponding Author: Shaochun Zhang

Tel: +81-52-789-3660, Fax: +81-52-747-6442

E-mail: zhang.shaochun@f.mbox.nagoya-u.ac.jp

Optical properties of Zn-porphyrin covalently bounded to MoS₂ and WS₂.

Ruben Canton-Vitoria¹, Ryo Kitaura¹

¹ Department of Chemistry, Nagoya University, Nagoya 464-8602, Japan.

Two-dimensional transition metal dichalcogenides (TMDs) have attracted increased attention to develop donor-acceptor systems towards improved energy conversion applications. Optoelectronic properties of TMDs can be tuned by interaction with small organic chromophores, leading to versatile donor-acceptor systems. Herein we covalently functionalized MoS₂ and WS₂ with Zn-porphyrin towards 1,2-dithiolane additions. A reduced level of aggregations was confirmed by AFM in figure 1a-c, showing a pseudo-ideal system of a 0-dimensional emissive material (Zn-porphyrin) insolated on a 2D emissive-material (TMDs). EDX under high magnification STEM confirm the presence of Zn porphyrin at basal plane (figure 1d). Raman nodes of the porphyrin is only observed on the TMDs monolayers (figure 1e). UV spectra show a combination of absorption species from Zn-porphyrin and TMDs. Also, PL emission of ZnP-porphyrin-WS₂ evidenced a new band at the near-IR region. Power and temperature dependence reveals that such a new band was associated with a ZnP⁺-WS₂⁻ intermediate (figure f). Finally, the new hybrid materials show enhancement of the response in photo-sensors at the porphyrin absorption region.

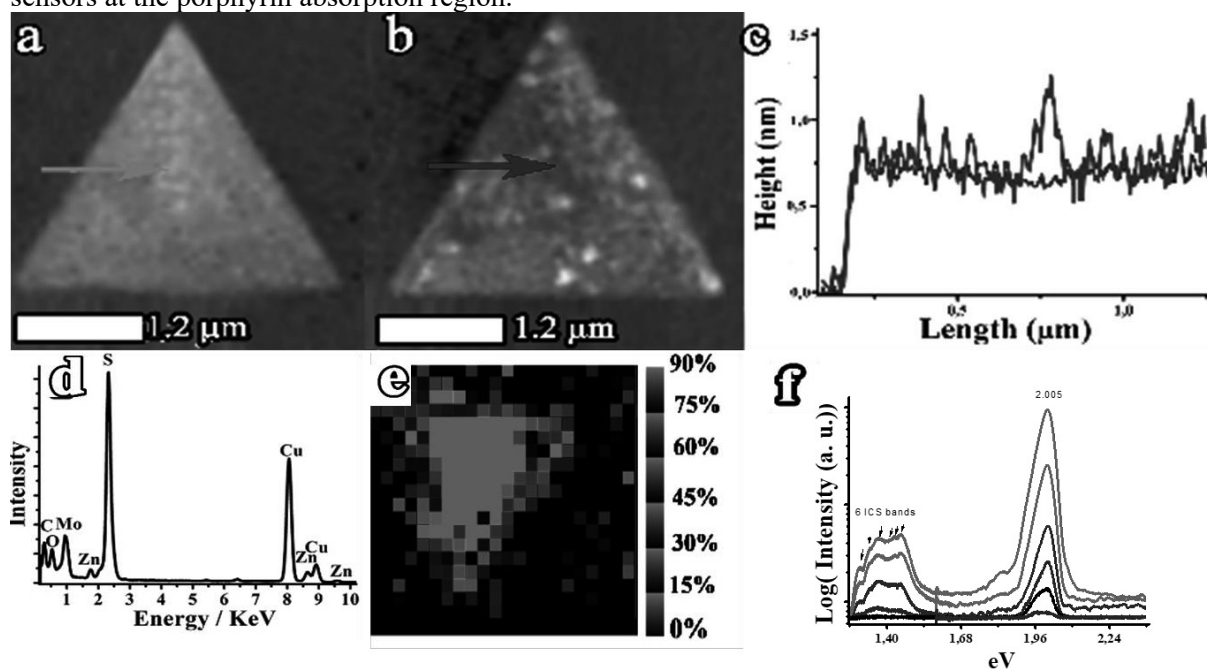


Figure 1. AFM of (a) CVD-WS₂ and (b) ZnP-WS₂. (c) Height line profile of AFM figures (a) and (b). (d) EDX, (e) Raman mapping of ZnP on WS₂ layer. (f) Power dependence of PL emission.

Cationic Nitrogen Doped Graphene as p-Type Dopant in PEDOT:PSS Hole-Transporters for Organic Solar Cells

○Takuhei Kaneko¹, Hao-Sheng Lin¹, Sangwoo Chae¹, Takumi Yana¹, Nagahiro Saito¹, and Yutaka Matsuo¹

¹ Department of Chemical System Engineering, Graduate School of Engineering, Nagoya University, Furo-cho, Chikusa-ku, Nagoya 464-8603, Japan

In this research, cationic nitrogen doped graphene (CNG) was designed as a p-type dopant in hole transport layer (HTL) for organic solar cells (OSCs). The CNG-doped poly(3,4-ethylenedioxythiophene)-poly(styrenesulfonate) (PEDOT:PSS) applied in OSCs as HTL showed an improved power conversion efficiency (PCE) of 2.76% with a PEDOT:PSS HTL reference in a PCE of 1.96%. The CNG applied device indicated higher short-circuit current (J_{sc}) and open-circuit voltage (V_{oc}). Increased J_{sc} value was majorly contributed by the improved conductivity of PEDOT:PSS. The promoted V_{oc} value was ascribed from the better interface that forming the active layer with a better morphology.

Table. 1 Photovoltaic parameters of OSCs

	J_{sc} (mA/cm ²)	V_{oc} (V)	FF	PCE (%)
PEDOT:PSS	5.13	0.603	0.634	1.96
CNG doped PEDOT:PSS	9.72	0.612	0.464	2.76

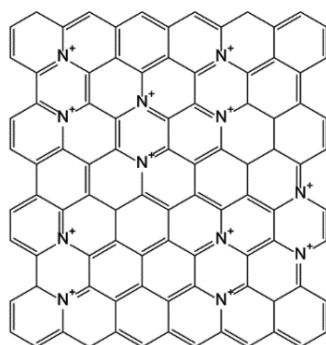


Fig. 1 The structure of CNG

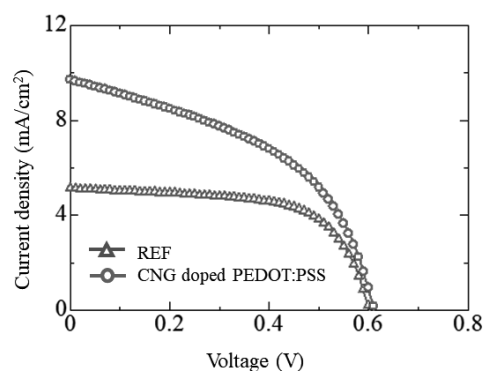


Fig. 2 J - V curves of OSCs

Corresponding Author: Y. Matsuo

Tel: +81-52-747-6722

E-mail: yutaka.matsuo@chem.material.nagoya-u.ac.jp

Micro-patterning of graphite by Lithographic method

○Jianwei Fu², Genki Hirobe¹, Yasushi Ishiguro¹, Kazuyuki Takai^{1,2}

¹ Department of Chemical Science and Technology, Hosei University, Tokyo 184-8584, Japan

² Graduate School of Science and Engineering, Hosei University, Tokyo 184-8584, Japan

Graphene has excellent properties such as high electron mobility and novel chemical reactivity, and is expected to be applied to next-generation semiconductor devices such as sensors and to catalysts. However, since graphite, which is the mother material of graphene, is difficult to microfabricate, there have been few studies using the sample of nano/micro-patterned graphite in well-defined manner so far, even though the size and shape have a great influence on the electrical properties and chemical activities of graphene. In this study, in order to achieve a large-scale production of micro/nano-graphene having well-defined geometry, we attempted to microfabricate graphite by using lithographic method for patterning on highly oriented pyrolytic graphite (HOPG).

By an ICP plasma etching system (RIE-101iPH, Samco), a HOPG plate (10×10×2 mm) was etched by using a micro-patterned siloxane islands and micro-patterned Au / Cr islands (3 μm circle) as masks, in the conditions of ICP power of 100 W, Bias power of 50 W, O₂ flow of 1.0 sccm, and process pressure of 0.05 Pa. AFM measurement was performed by using SPA400-DFM, Seiko Instruments Inc. with the Si cantilever. SEM images were acquired by using SU-8020, HITACHI High-Technologies in the condition of acceleration voltage of 15.0 kV.

As a result of etching with a siloxane mask, it was found that there was almost no change in the height and shape of the siloxane mask before and after etching, and that siloxane had high etching resistance. However, the lift-off process for miniaturization of siloxane mask was not successful on HOPG due to the weak interaction between siloxane and the graphite substrate. On the other hand, gold masks were found to be etched by oxygen plasmas in spite of their chemical inertness. Fig. 1 and 2 show the etching time dependence of the etched depth and surface composition of gold, respectively, for HOPG with micro-patterned gold masks (3 μm in diameter), where the patterned etching is practically ends when the gold mask is completely removed. After 10 h plasma etching, the array of micro-patterned graphites were finally obtained.

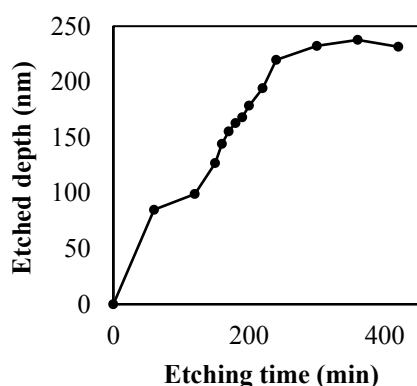


Fig. 1 Etching time dependence of the height of graphite pattern

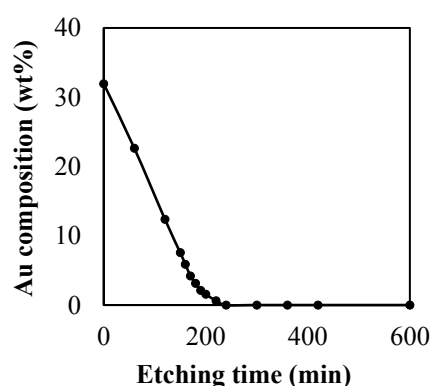


Fig. 2 Etching time dependence of Au composition

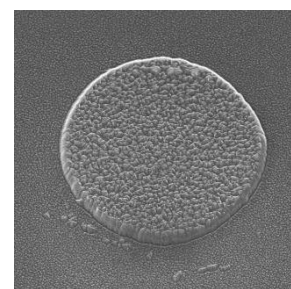


Fig. 3 SEM image of microfabricated graphite patterns (diameter : 3 μm)

Corresponding Author: Kazuyuki TAKAI
E-mail: takai@hosei.ac.jp

Phosphorescence excitation mapping of polyynic molecules isolated in solid acetonitrile at 20 K

○Kaito Tanaka, Aoi Mineyama, Riku Ohnishi, Keisuke Fukumoto, Tomonari Wakabayashi

Department of Chemistry, Kindai University, Higashi-Osaka 577-8502, Japan

We recently reported phosphorescence spectra of cyanopolyynes, HC₉N and HC₁₁N, isolated in solid acetonitrile at cryogenic temperature to discuss the energy level of the low-lying triplet state of the molecule and the influence of host molecules of acetonitrile on the electronic as well as the vibrational states of the guest molecule [1]. Phosphorescence excitation mapping is helpful to understand the overall feature of the vibronic excitation, thus to distinguish the series of transitions between different electronic states of the linear carbon molecule. We have applied the measurement to the series of hydrogen-capped polyynes such as C₁₀H₂, C₁₂H₂, and C₁₄H₂ using solid acetonitrile as a matrix host to compare the phosphorescence excitation spectrum with the UV absorption spectrum in a solution at ambient temperature.

Polyynic molecules were produced by laser ablation of graphite particles dispersed in liquid acetonitrile, CH₃CN at 0°C, using a nanosecond laser system (Nd:YAG 1064 nm, 5 W, 10 Hz). The mixture of polyynes, cyanopolyynes, and other byproducts was subjected to HPLC for separation and purification. The refined solution, e.g. C₁₀H₂/CH₃CN, was concentrated to a volume of a few milli-liters and sprayed on a copper slab cooled at 20 K in high vacuum. The droplets condensed immediately to become an opaque, milky white solid on the cold surface. The solid matrix sample was irradiated by photons from a tunable pulsed laser system (OPO-SHG/SFG 213–409 nm, 10 Hz) and dispersed phosphorescence spectra were recorded using a spectrometer equipped with a nitrogen-cooled CCD array detector (PI320-PyLoN256OE). The series of spectra were processed into a single 2D-mapping image.

Fig. 1 shows phosphorescence excitation mapping of polyynic C₁₀H₂ in solid acetonitrile at 20 K. Inset is the excitation curve of the phosphorescence peak at 601.2 nm. Salient features in the deep UV are comparable to the UV absorption bands of the allowed transition, $^1\Sigma_u^+ \leftarrow X^1\Sigma_g^+$, in solutions. Relatively weak signals in the near UV correspond to the vibronic transitions in the symmetry-forbidden electronic transitions, $^1\Delta_u \leftarrow X^1\Sigma_g^+$ and $^1\Sigma_u^- \leftarrow X^1\Sigma_g^+$ [2].

[1] U. Szczepaniak, K. Ozaki, K. Tanaka, Y. Ohnishi, Y. Wada, J.-C. Guillemin, C. Crépin, R. Kolos, Y. Morisawa, H. Suzuki, T. Wakabayashi, *J. Mol. Struct.* **1214**, 128201 (2020).

[2] T. Wakabayashi, H. Nagayama, K. Daigoku, Y. Kiyooka, K. Hashimoto, *Chem. Phys. Lett.* **446**, 65 (2007).

Corresponding Author: T. Wakabayashi

Tel: +81-6-4307-3408, Fax: +81-6-6723-2721,

E-mail: wakaba@chem.kindai.ac.jp

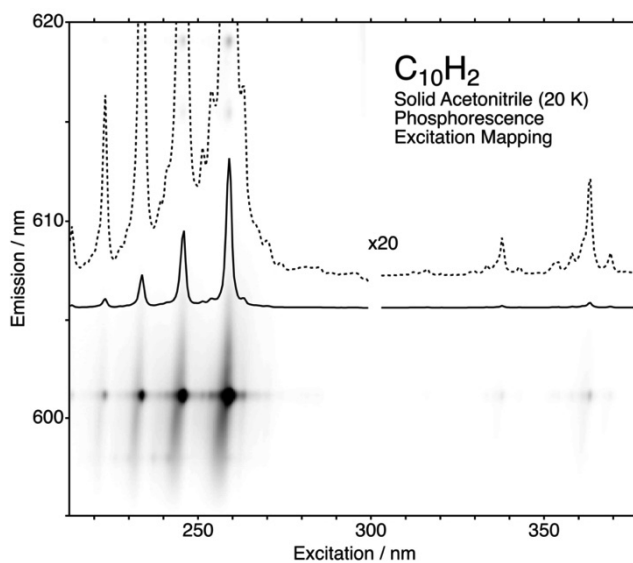


Fig. 1 Phosphorescence excitation mapping of C₁₀H₂.

Control of optical absorption property of PbPc donor film for development of full-spectra organic photovoltaic cells

○Hayato Yoshizawa, Masahiro Kato, Masato Nakaya, and Jun Onoe*

Department of Energy Science and Engineering, Nagoya University, Aichi 464-8603, Japan

Organic photovoltaic cells (OPVs) have been extensively investigated owing to their fascinating advantages such as flexibility, highly designability, and low fabrication cost. However, the energy conversion efficiency (η) of OPVs is still ca. 10%, which is much lower than those (ca. 25% at most) of the conventional Si solar cells. In order to improve the η of OPVs, it is indispensable to increase both the short-circuit current and open-circuit voltage simultaneously. In the former case, it is important to understand the elementary processes of photoelectric conversion [1-4]. In the present study, we examined the structural and optical properties of lead phthalocyanine (PbPc) used as a donor for C₆₀-based OPVs, because PbPc films exhibit absorption bands in a wide wavelength region of 400-1000 nm.

Heterojunction OPVs composed of indium-tin-oxide (ITO) electrode, PbPc film (40 nm thick), C₆₀ film (30 nm thick), and aluminum (Al) electrode (100 nm thick) were fabricated in the same ultrahigh vacuum chamber (base pressure: 2.0×10^{-6} Pa) without air exposure. Then, the external quantum efficiency (EQE) of the OPVs was measured *ex situ*. Fig. 1 shows (a) the EQE in a wavelength range of 400–1000 nm for the OPVs, UV-Vis-NIR spectra of (b) 40 nm-thick PbPc film (solid line) and 40 nm-thick C₆₀ film (dotted line), and of (c) 20 nm-thick PbPc film. As shown in Fig. 1a, three peaks appear at 450, 672, and 907 nm, which correspond to the optical absorption peaks for C₆₀ and PbPc films (Fig. 1b). Although the absorption peaks at 742 and 895 nm are mainly originated from the π - π^* transition, these absorption bands depend on the film thickness. For example, the absorption peak at 895 nm appearing for 40 nm-thick PbPc film (Fig. 1b) was not observed for 20 nm-thick PbPc film (Fig. 1c). This is explained by a mixture of two crystalline phases (monoclinic and triclinic phases) increasing with film thickness. We will discuss the optical characteristics of C₆₀/PbPc heterojunction before and after thermal-induced crystalline phases transition.

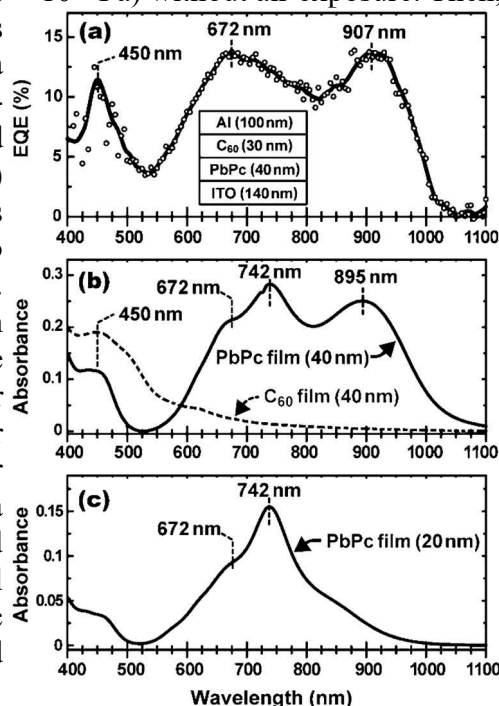


Fig. 1. EQE of C₆₀/PbPc OPV (a) and UV-Vis-NIR spectra of C₆₀ and PbPc films (b, c).

References

- [1] S. Ryuzaki and J. Onoe, *Nano Rev.* **4**, 21055 (2013).
- [2] S. Ryuzaki and J. Onoe, “*Solar Cell Materials, Devices, Interfaces, and Modeling*” (Q. Qiao ed.), CRC Press, Chap. 6, pp.143–166 (2015).
- [3] J. Onoe *et al.*, *J. Chem. Phys.* **147**, 2147018 (2017). [editor’s pick]
- [4] M. Kato *et al.* *J. Chem. Phys.* **153**, 144704 (2020).

*Corresponding Author: Jun Onoe

Tel/Fax: +81-52-789-3784, E-mail: j-onoe@energy.nagoya-u.ac.jp

Enhanced gas-phase synthesis of single-wall carbon nanotubes with methane as carbon source by preheating catalyst precursors

○ Zihao ZHANG [1], Itsuki CHIKAARASHI [1], Katsuya NAMIKI [1], Toshio OSAWA [1], Hisashi SUGIME [2], Suguru NODA [1,2]

¹ Department of Applied Chemistry, Waseda University, Tokyo 169-8555, Japan

² Waseda Research Institute for Science and Engineering, Waseda University, Tokyo 169-8555, Japan

Carbon nanotubes (CNTs) have been extensively researched owing to their unique one-dimensional nanostructure and properties. Floating catalyst chemical vapor deposition (FCCVD) yields high-quality single-wall CNTs (SWCNTs) [1,2]. Generally, catalyst precursors and carbon feedstock are fed to externally heated reactors. The mixture is gradually heated and thus catalyst particles gradually nucleate at low density, resulting in limited productivity.

In this work, we report the enhanced FCCVD method with a microheater for preheating of catalyst precursors (Fig. 1a). Ferrocene and sulfur vapors carried by Ar (Fig 1b) were overheated in the microheater, and then immediately mixed with CH₄/H₂/Ar to nucleate catalyst particles and initiate CNT growth.

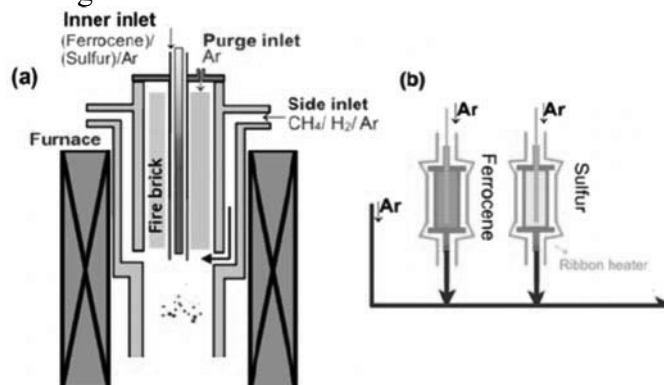


Fig 1. Schematic of (a) the FCCVD reactor, (b) sublimation of catalyst precursors with Argon.

This method yielded black smog of SWCNTs with few particles (Fig. 2a) with a Raman spectrum characteristic for high-quality SWCNTs (Fig. 2b). The thermogravimetry analysis showed a carbon purity >90 wt%. A productivity of 17.0 mg-CNT/min and carbon yield of 9.4% were achieved using a low-cost and less reactive carbon source of methane and a lab-scale reactor.

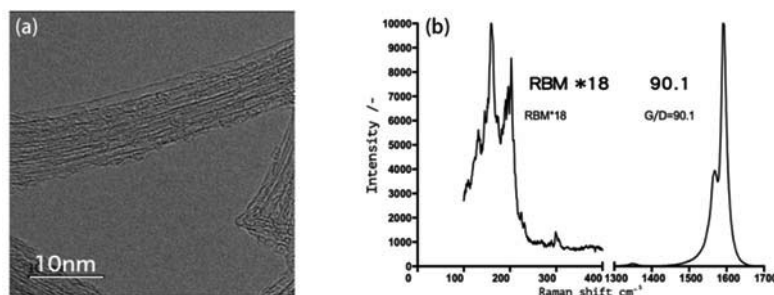


Fig. 2. (a) TEM images and (b) Raman spectrum of SWCNTs synthesized in this study.

[1] A.G. Nasibulin, et al., Chem. Phys. Lett. 402, 227 (2005).

[2] T. Saito, et al., J. Phys. Chem. B 110, 5849 (2006).

Corresponding Author: Suguru.NODA E-mail: noda@waseda.jp

Semiconducting carbon nanotube extraction enabled by cellulosic polymer wrapping

○Tomoko Yagi¹, Tsuyoshi Kawai¹, Yoshiyuki Nonoguchi^{1,2}

¹Division of Materials Science, Nara Institute of Science and Technology, NAIST, Takayama, Ikoma, Nara 8916-5, Japan

²Faculty of Materials Science and Engineering, Kyoto Institute of Technology, Kyoto 606-8585, Japan

The selective extraction of semiconducting carbon nanotubes (sc-SWNTs) is highly desired for the development of next-era electronic and energy devices. Conjugated polymers have mostly been used to selectively disperse sc-SWNTs [1]; however, these polymers are not suitable for large scale production due to their high production cost. Herein we demonstrate sc-SWNTs are selectively extracted by using alkyl cellulose. Alkyl cellulose is a sustainable, and environmentally friendly compound conformable to large-quantity production. By systematically investigating the separation condition such as the structure and concentration of alkyl celluloses, here we demonstrate successful selective extraction. The sc-SWNTs / alkyl cellulose film shows excellent thermoelectric power factor.

We dispersed SWNTs in tetrahydrofuran (THF) using alkyl cellulose (**Fig. 1(a)**). Obtained SWNTs dispersion was used to prepare semitransparent thin film on PET substrates. The doping level was modulated with a p-type doping reagent, silver bis(trifluoromethanesulfonyl)imide (AgTFSI). UV-Vis NIR spectra indicated that the selectivity of sc-SWNTs changes depending on the side chain length of alkyl cellulose. Particularly, hexyl cellulose selectively extracted sc-SWNTs in THF (**Fig. 1(b)**). This successful separation expectedly relies on the difference of the polarizability between sc- and m-SWNTs polymer complexes, which can be modulated by the side chain length of alkyl cellulose. We found that selectivity also depends on the solvent, polymer concentration and molecular weight, along with SWNT diameter. Successful sc-SWNTs extraction was also confirmed by thermoelectric transport measurements. Seebeck coefficient was as high as approximately $100 \mu\text{V K}^{-1}$ even in the heavy doping condition (**Fig. 1(c)**). The films sorted by alkyl cellulose showed ten times larger thermoelectric power factor than unsorted films.

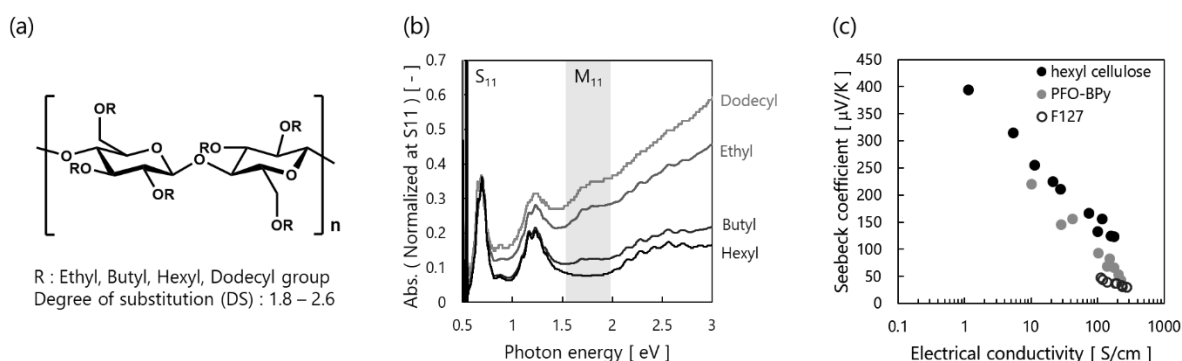


Figure 1. (a) A chemical structure of alkyl cellulose. (b) UV-Vis NIR spectra of dispersions normalized S_{11} using different alkyl cellulose as a dispersant. (c) Thermoelectric properties of film of sorted SWNTs by hexyl cellulose and conjugated polymer (PFO-BPy), along with unsorted SWNTs dispersed by pluronic F127.

[1] A. Nish *et al.* *Nat. Nanotech.*, **2**, 640-646 (2007).

Corresponding Author: Yoshiyuki Nonoguchi

Tel: +81-75-724-7515

E-mail: nonoguchi@kit.ac.jp

Investigation of water adsorption on vertically-aligned single-walled carbon nanotubes by Raman spectroscopy

○Masanori Bamba¹, Shu Sato¹, Taiki Inoue², Shigeo Maruyama¹, Shohei Chiashi¹

¹Department of Mechanical Engineering, the University of Tokyo, Tokyo 113-8654, Japan

²Department of Applied Physics, Osaka University, Osaka 565-0871, Japan

Previous study shows that water molecules physically adsorb on the surface of isolated and suspended single-walled carbon nanotubes (SWCNTs) [1] and the adsorbed water layer changes the SWCNT properties such as the optical transition energy and RBM peak frequency. However, the observation of the water adsorption layer has been limited in the SWCNT samples with the specific morphology. In this study, we investigated the vapor pressure and temperature dependence of water adsorption on the outer surface of vertically-aligned SWCNTs (VA-SWCNTs) by Raman scattering spectroscopy.

The VA-SWCNTs which were grown by ACCVD method using cobalt and molybdenum as the catalyst [2](Fig. 1) were put in a chamber where the pressure and temperature are controlled. Raman spectra measured with controlling water vapor pressure at room temperature (25°C) are shown in Fig. 2. With increasing pressure, RBM peaks from larger diameter tubes ($\omega_{\text{RBM}} \sim 145 \text{ cm}^{-1}$) up-shifted at $2.6 \times 10^2 \text{ Pa}$, while the peaks from smaller diameter tubes ($\omega_{\text{RBM}} \sim 181 \text{ cm}^{-1}$) shifted at $8.7 \times 10^2 \text{ Pa}$. This peak shift comes from the adsorption of water molecules on the surface of VA-SWCNTs, and it suggested that isolated and suspended SWCNTs with exposed outer surface existed in the VA-SWCNT samples [3]. In addition, the previously reported difference in the RBM spectra of VA-SWCNT samples [4][5] can be understood by considering the adsorption effects.

- [1] S. Chiashi *et al.* Phys. Rev. B, **91**, 155415 (2015).
- [2] Y. Murakami *et al.*, Chem. Phys. Lett., **377**, 49 (2003).
- [3] Z. Zhang *et al.*, Phys. Rev. B, **81**, 165442 (2010).
- [4] Y. Murakami *et al.*, Phys. Rev. B, **71**, 085403 (2005).
- [5] P. T. Araujo *et al.*, Phys. Rev. B, **77**, 241403 (2008).
- [6] P. T. Araujo *et al.*, Phys. Rev. Lett., **98**, 067401 (2007).

Corresponding Author: S. Chiashi

Tel: +81-3-5841-6407, Fax: +81-3-5841-6408,

E-mail: chiashi@photon.t.u-tokyo.ac.jp

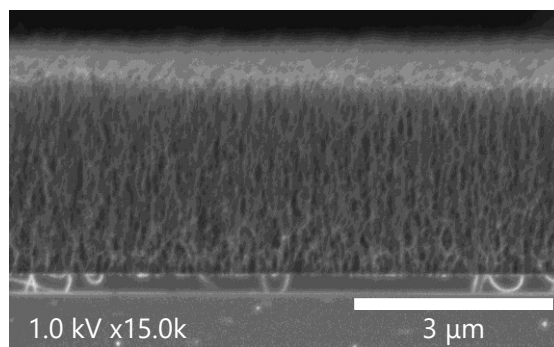


Fig. 1 SEM image of VA-SWCNTs.

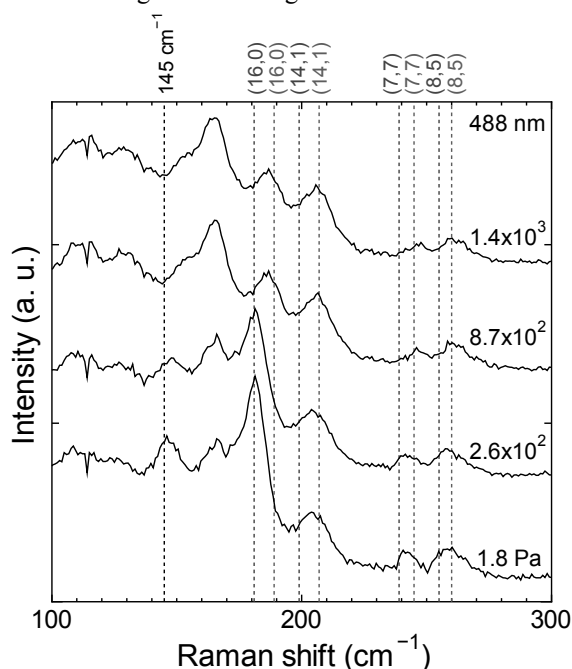


Fig. 2 RBM peaks at different water vapor pressures. The red and blue lines indicate Raman shift in vacuum [1][5] and ambient air [6], respectively.

Self-assembly of two-dimensional structures composed of tetrahedral molybdenum clusters

○Naoyuki Kanda^{1,2}, Zheng Liu³, Motoki Aizaki², Mina Maruyama⁴, Susumu Okada⁴, Yanlin Gao⁴, Hisanori Shinohara², Yasumitsu Miyata¹, and Yusuke Nakanishi^{1,*}

¹ Department of Physics, Tokyo Metropolitan University, Tokyo 192-0397, Japan.

² Department of Chemistry, Nagoya University, Nagoya 464-8603, Japan.

³ National Institute of Advanced Industrial Science and Technology (AIST), Nagoya 463-8560, Japan

⁴ Department of Physics, University of Tsukuba, Tsukuba 305-8571, Japan

The self-assembly of nanoscale elements into macroscopic structures offers a powerful strategy for the bottom-up synthesis of functional materials. Molecular clusters of transition metal chalcogenides (TMCs) are potential building blocks for such architectures. In particular, tetrahedral M_4 clusters of chalcogenides — whose generalized formula is M_4X_4 , where M is a transition metal and X is a chalcogen — form a variety of three-dimensional (3D) structures *via* chemical-cross linkages (Fig. 1a). Depending on their composition and morphology, 3D solids composed of M_4X_4 clusters exhibit versatile properties including ferromagnetism, Mott transition, and superconductivity [1]. The chemical and structural diversity of M_4X_4 clusters organized into such 3D structures would open new avenues of research in 2D materials. However, very few 2D structures are currently available due to the difficulty of preparing chemically uniform crystals.

Here we report the bottom-up synthesis of layered 2D structures consisting of Mo_4S_4 clusters bridged by Cl atoms (Fig. 1b). This methodology extends the vapor-phase reactions employed to fabricate 1D TMC nanowires [2]. Cross-sectional transmission electron microscopy revealed the layered structures, in which a plane of Cl atoms is sandwiched between planes comprising Mo_4S_4 and Cl_4 clusters (Fig. 1c). Significantly, we also demonstrate the isolation of monolayers inside carbon/boron-nitride nanotubes. Electronic structure calculations suggest that the monolayers should exhibit strong direct bandgap photoluminescence emission.

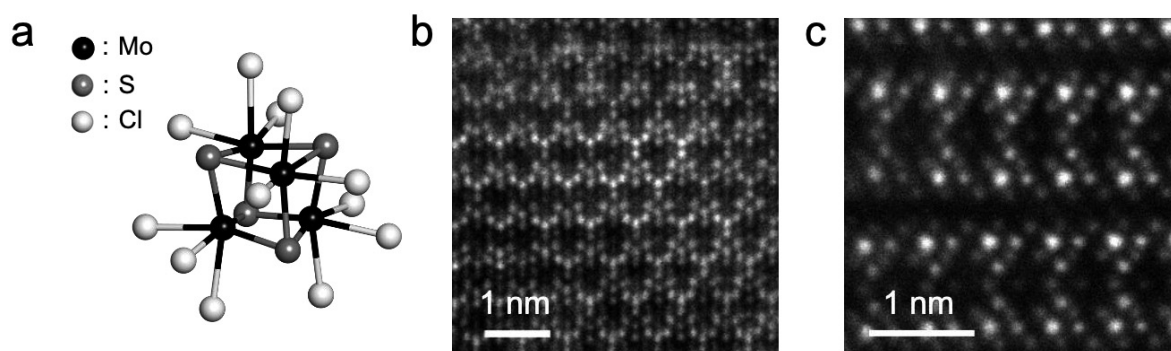


Fig. 1 a) A schematic of Mo_4S_4 cluster with 12 Cl ligands, HAADF-STEM images of Mo_4S_4 -based 2D structures viewed from b) surface and c) cross section.

[1] R. Pocha *et al.*, Chem. Mater. **12**, 2882 (2000); C. Vaju *et al.*, Microelectron. Eng. **85**, 2430 (2008); M. M. Abd-Elmeguid *et al.*, Phys. Rev. Lett. **93**, 126403 (2004)

[2] **N. Kanda** *et al.*, Nanoscale **12**, 17185 (2020); M. Nagata, **N. Kanda** *et al.*, Nano Lett. **19**, 4845 (2019)

Corresponding Author: Y. Nakanishi Tel: +81-42-677-2498 E-mail: naka24ysk@tmu.ac.jp

Theoretic Study on Raman Active Modes of SnS Thin Films

○Itsuki Yonemori¹, Sudipta Dutta², Kosuke Nagashio³, Katsunori Wakabayashi¹

¹ School of Science and Technology, Kwansei Gakuin University, Sanda 669-1337, Japan

² Indian Institute of Science Research and Education (IISER) Tirupati, India

³ Department of Materials Engineering, The University of Tokyo, Tokyo 113-8656, Japan

Tin sulfide (SnS) is recently attracting much attention as thermoelectric material due to its low crystal density. For the application to the transparent and flexible devices, the single layer growth and control of the number of layers are demanded. In addition, it has been reported that SnS thin film has ferroelectricity depending on the number of layers.^[1] In order to identify the number of layers using Raman spectroscopy, it is necessary to analyze the layer number dependence of phonon vibration mode. In this study, we investigate the phonon vibration modes of SnS thin films using first-principles calculations.

Figures 1(a) and (b) show the crystal structures of bulk SnS crystal in α and β' -phase, respectively. Both of them have orthorhombic structure and double layers in unit cell. The interaction between layers is van der Waals forces. In this study, we performed structure optimization and calculations of electronic states and phonon modes under Generalized Gradient Approximation (GGA-PBE)^[2] using VASP^[3] package. In addition, we use Heyd-Scuseria-Ernzerhof 2006 (HSE06)^[4] hybrid function in order to give reliable results for the energy band gap. α and β' -phase bulk SnS is an indirect transition semiconductor with a band gap about 1.33 eV and 1.09 eV. α -phase bulk SnS is slightly more thermodynamically stable than β' -phase. Figure 1 (c) shows the phonon vibration modes at Γ -point for each phase of bulk SnS. The filled circles and triangles indicate Raman active modes, and empty circles indicate Raman inactive modes. Phonon properties and decision of irreducible expression was using Phonopy code^[5]. As for the Raman active modes of α -phase bulk SnS in the range of 150 to 200 cm^{-1} , the in-plane frequency modes shift higher compared with the β' -phase bulk SnS. On the other hand, the out-of-plane Raman active modes of α -phase bulk SnS in the range of 200 to 250 cm^{-1} shifts toward lower frequency comparing with β' -phase bulk SnS. The difference in the appearance position of the vibration occurs due to the bond length. Thus, it is found that bulk SnS show the strong structure dependence in the Raman active modes in the range 150 cm^{-1} to 250 cm^{-1} .

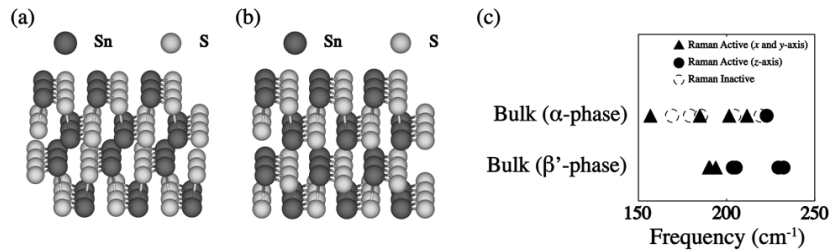


Figure 1: Crystal structure of bulk SnS in (a) α - and (b) β' -phase. (c) The phonon vibration mode for each phase of bulk. Closed (empty) objects indicate Raman active (inactive) modes.

[1] N. Higashitarumizu *et al.* *Nat. Commun.*, 11, 2428 (2020)

[2] J. P. Perdew, K. Burke, M. Ernzerhof, *Phys. Rev. Lett.* 77, 3865 (1996)

[3] G. Kresse and J. Furthmüller, *Phys. Rev. B*, 54, 11169 (1996)

[4] A. V. Krukau *et al.*, *J. Chem. Phys.*, 125, 224106 (2006)

[5] L. Chaput *et al.*, *Phys. Rev. B*, 84, 094302 (2011)

Corresponding Author: K. Wakabayashi, Tel: +81-79-565-9751, Fax: +81-79-565-9729, E-mail: waka@kwansei.ac.jp

Tuning electronic properties of graphene antidot lattices with truncated triangular holes: A First-principles study

○Yuta Taguchi, Susumu Saito

Department of Physics, Tokyo Institute of Technology, 2-12-1 Oh-okayama, Meguro-ku, Tokyo 152-8551, Japan

Graphene antidot lattices (GALs) have been studied theoretically. Previous theoretical studies indicate that GAL sometimes has a band gap and the size of band gap is sensitive to the shape and size of holes introduced into the graphene sheet periodically[1,2]. Furthermore, introducing holes with zigzag edges can change the magnetic property of pristine graphene. For example, GAL with triangular holes in the same direction has a ferromagnetic (FM) ground state and GAL with hexagonal holes has an antiferromagnetic (AFM) ground state[3,4]. Introducing holes into pristine graphene should be a promising method to expand the possibility of its application.

We investigate the electronic properties of graphene with holes in the shape of truncated triangles arranged periodically in the framework of the density-functional theory (DFT). There are two same holes in one supercell and sides of regular triangles face each other [Fig. 1(a)-1(c)]. We characterize the system studied by two integers: the hole side length l in units of pristine graphene lattice constant and subribbon width W in units of C-C bond length [Fig. 1(a)]. To investigate the spin-polarized state of system, the spin degree of freedom is taken into account. We find that the system has either a nonmagnetic (NM) ground state [Fig. 1(a)] or antiferromagnetic (AFM) ground state [Fig. 1(b),(c)] depending on l and W . We also find that the NM state and ferromagnetic (FM) state are energetically stable for (b) and (c), respectively. Their energy difference from the ground state is less than 5 meV/atom. These results show that the magnetic properties of the system can be controlled by changing l and W , being useful for spintronics applications. In this presentation, electronic structures and band gaps will be also discussed in detail.

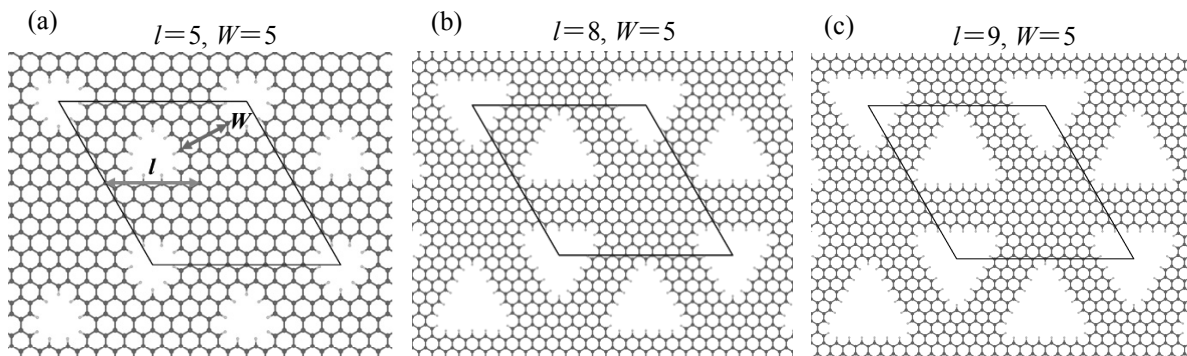


Fig. 1 Graphene antidot lattices with truncated triangular holes.

- [1] M. Sakurai, Y. Sakai and S. Saito, J. Phys: Conf. Ser. **302**, 012018 (2011)
- [2] G. Tang *et al.*, Carbon **76**, 348-356 (2014)
- [3] W. Liu *et al.*, Phys. Rev. B **80**, 233405 (2009)
- [4] M. L. Trolle, U. S. Møller, and T. G. Pedersen, Phys. Rev. B **88**, 195418 (2013)

Corresponding Author: Y. Taguchi

E-mail: taguchi.y@stat.phys.titech.ac.jp

Two-dimensional electron gas in laterally-assembled WTe atomic wires

○Hiroshi Shimizu¹, Jiang Pu², Zheng Liu³, Hong En Lim¹, Yusuke Nakanishi¹,
Takahiko Endo¹, Kazuhiro Yanagi¹, Taishi Takenobu², Yasumitsu Miyata¹

¹ Department of Physics, Tokyo Metropolitan University, Hachioji 192-0397, Japan

² Department of Applied Physics, Nagoya University, Nagoya 464-8603, Japan

³ Innovative Functional Materials Research Institute, AIST, Nagoya 463-8560, Japan

One-dimensional (1D) transition metal chalcogenides (TMCs) have attracted much attention lately due to their atomically-thin, wired structures and superior conducting properties. These wires interact via van der Waals forces, aggregating into 1D crystal of different shapes. By manipulating the assembled crystal structure, their physical properties can be possibly tuned. Indeed, metal-semiconductor transition and a crossover from 1D to 3D electronic states have been reported for single- to few-wires of WTe [1]. However, relevant studies remain limited. Recently, we had achieved a scalable growth of long, highly-crystalline 2D and 3D assemblies of WTe crystals using chemical vapor deposition (CVD) [2]. Such aggregates are expected to be an ideal system to realize a tunable wire-based electronic system. Using the high quality and long WTe prepared this way, herein we report the 2D electron gas of laterally-assembled WTe atomic wires.

The wires were grown on SiO₂/Si substrates with a typical length of more than 10 μm. In/Au electrodes were deposited onto an isolated WTe bundle by photolithography for measurements (Fig. 1a). Nanoribbon-shape, as-grown crystal comprises highly crystalline WTe wires can be clearly seen in the cross-sectional observation (Fig. 1b), forming thin aggregate with a width of 200~400 nm and 5~15 nm in thickness. Subjecting the sample to an applied magnetic field results in an oscillating behavior at 1.9 K (Fig. 1c). This corresponds to Shubnikov-de Haas oscillation due to oscillatory magnetoresistance. The oscillation period is determined to be 0.08 T⁻¹, yielding the estimated carrier density and mobility of 6.0×10¹¹ cm⁻² and 7000 cm² V⁻¹ s⁻¹, respectively. More importantly, although the oscillation period decreases as the sample is tilted with respect to the direction of the magnetic field, the MR curves at each tilt angle, θ , however show identical oscillations when plotted against $B\cos\theta$ (Fig. 1d). These serve a strong evidence for the realization of 2D electron gas in the laterally-assembled WTe wires, suggesting the use of TMC atomic wires as build blocks to create electronic systems of different dimensionality.

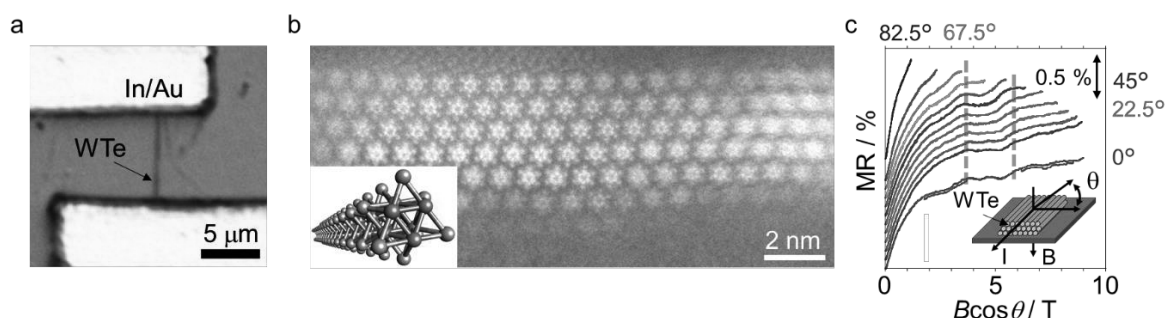


Figure 1 (a) Optical and (b) cross-section HAADF-STEM image of the WTe bundle. Inset: Structure model of a TMC atomic wire. (c) $B\cos\theta$ -dependent magnetoresistance of the WTe bundle at 1.9 K (B : Magnetic flux density).

[1] J. Deng *et al.*, Nano Lett., **20**, 12, 8866-8873 (2020).

[2] H. E. Lim *et al.*, Nano Lett., 10.1021/acs.nanolett.0c03456 (2020).

Corresponding Author: Y. Miyata, Tel: +81-42-677-2508, E-mail: miyata-yasumitsu@tmu.ac.jp

High-yield synthesis of MoS₂ and MoSe₂ nanotubes

○Ryoga Tanaka, Yohei Yomogida, Yasumitsu Miyata, Kazuhiro Yanagi

Department of Physics, Tokyo Metropolitan University, Tokyo 192-0397, Japan

Inorganic nanotubes (INTs) composed of transition-metal dichalcogenides (MX₂, M = Mo, W, Nb. X = S, Se) have unique physical properties that are different from 2D MX₂. Their physical properties depend on constituent elements, and thus, development of techniques to synthesize INTs with a variety of elements is important for both aspects of basic science and applications. In the case of W-based INTs (e.g., WS₂ and WSe₂ nanotubes), various synthesis methods including mass production have been developed [1,2,3]. In contrast, there are few reports on synthesis of Mo-based INTs (e.g., MoS₂ and MoSe₂ nanotubes). This may be due to instability of their precursor molybdenum oxide. Molybdenum oxide is known to be thermally and chemically unstable compared to tungsten oxide [4], which makes synthesis using the oxides as templates difficult. Thus, in this study, to obtain high-yield MoS₂ and MoSe₂ nanotubes, we developed efficient precursor synthesis and explored the appropriate condition of chalcogenization.

Molybdenum oxide nanowire precursors were synthesized on silicon substrates by thermal evaporation, according to the previous study [5]. Here, we adjusted supplied air gas and synthesis temperature to efficiently synthesize oxide nanowires. Thereafter, the obtained nanowire precursor was reacted with S or Se precursor in Ar/H₂ gas. The produced molybdenum oxide nanowires have a length of 3-10 μm and a diameter of about 10-200 nm. Then we applied chalcogenization on the oxide nanowires. To prevent the destruction of the nanowire structure during chalcogenization, the chalcogenization reaction was first carried out at low temperature 500 °C, followed by high temperature 600-700 °C.

Fig.1 shows typical TEM images of MoS₂ and MoSe₂ nanotubes produced through chalcogenization on the oxide nanowires. These nanotubes have layered walls and a hollow core. The nanotubes have similar morphology to the precursors, suggesting that chalcogenization took place without destruction of the nanowire structure. As shown in Raman spectra (Fig.2), the nanotubes show clear peaks of MoS₂ and MoSe₂, which is different from those of molybdenum oxide. This result indicates that molybdenum oxide nanowires are successfully converted to MoS₂ and MoSe₂ nanotubes. In the poster, we will discuss the detailed conditions of the synthesis.

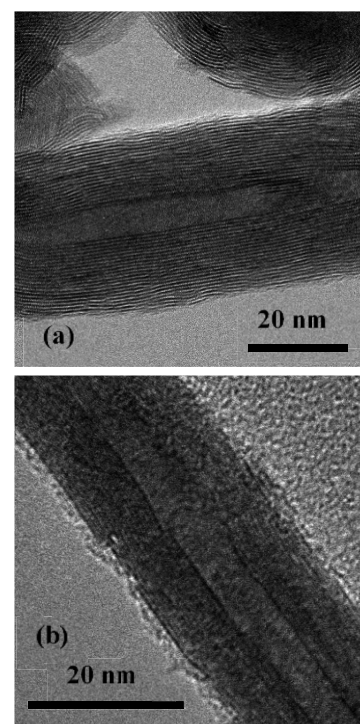


Fig. 1 TEM images of the MoS₂(a) and MoSe₂(b) nanotubes.

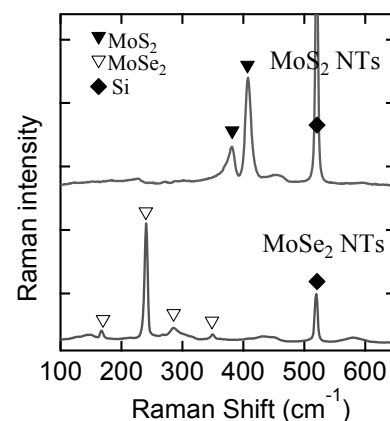


Fig. 2 Raman spectra of the MoS₂ and MoSe₂ nanotubes.

- [1] Y. Yomogida *et al.*, *Appl. Phys. Express* **12**, 085001 (2019).
- [2] Y. Yomogida *et al.*, *Appl. Phys. Lett.* **116**, 203106 (2020).
- [3] M.Serra *et al.*, *Nanoscale* **11**, 8073-8090 (2019).
- [4] P.Chithaiah *et al.*, *ACS Nano* **14**, 3004-3016 (2020).
- [5] K. Hong *et al.*, *Phys. Status Solidi RRL* **6**, No.2, 86-88 (2012).

Preparation of bipyramidal gold nanoparticle-[C₆₀]fullerene nanowhisker composites and kinetics study for reduction of 4-nitrophenol

○Jeong Won Ko¹, Yeon A Son¹, Se Hwan Park², Weon Bae Ko^{2,3,4}

¹ Department of Science Education, Graduate School, Dankook University, 152, Jukjeon-ro, Suji-gu, Yongin-si, Gyeonggi-do 16890, Republic of Korea, ² Department of Convergence Science, Graduate School, ³ Nanomaterials Research Institute, ⁴ Department of Chemistry, Sahmyook University, 815, Hwarang-ro, Nowon-gu, Seoul 01795, Republic of Korea

Bipyramidal gold nanoparticle-[C₆₀]fullerene nanowhisker composites were synthesized using C₆₀-saturated toluene, bipyramidal gold nanoparticle solution [1], and isopropyl alcohol by the liquid liquid interfacial precipitation (LLIP) method [2]. The product of bipyramidal gold nanoparticle-[C₆₀]fullerene nanowhisker composites was characterized by X-ray diffraction, Raman spectroscopy, scanning electron microscopy, and transmission electron microscopy.

The catalytic activity of bipyramidal gold nanoparticle-[C₆₀]fullerene nanowhisker composites for 4-nitrophenol reduction was evaluated with ultraviolet-visible (UV-vis) spectroscopy. The efficiency of reduction for 4-nitrophenol with bipyramidal gold nanoparticle-[C₆₀]fullerene nanowhisker composites increased in order of 288 K, 298 K, and 308 K. The kinetics study confirmed that the reduction of 4-nitrophenol using the bipyramidal gold nanoparticle-[C₆₀]fullerene nanowhisker composites at different temperatures followed a pseudo-first order reaction.

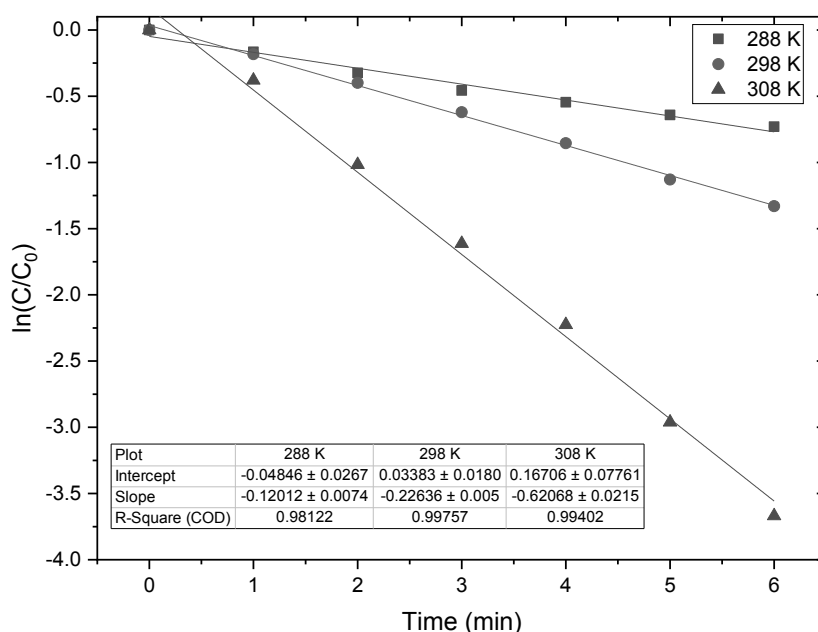


Fig.1 Graph of $\ln(C/C_0)$ vs. time at different temperatures for bipyramidal gold nanoparticle -[C₆₀]fullerene nanowhisker composites catalyzed reduction of 4-nitrophenol by NaBH₄.

[1] J. W. Ko *et al* Fuller. Nanotub. Car. N. **25**(12), 710 (2017).

[2] K. Miyazawa *et al*. Surf. Eng. doi.org/10.1080/02670844.2017.1396779 (2017).

Corresponding Author: W. B. Ko

Tel: +82-2-3399-1700, Fax: +82-2-979-5318,

E-mail: kowb@syu.ac.kr

Growth of single-walled carbon nanotubes using Ir catalyst prepared by dip-coating process

○Shu Kondo¹, Ai Misaki¹, Kamal P Sharma¹, Takahiro Saida¹, Shigeya Naritsuka¹, Takahiro Maruyama¹

¹ Department of Applied Chemistry, Meijo University, Nagoya 468-8502, Japan

1. Introduction

Single-walled carbon nanotubes (SWCNTs) are substances which are formed by rolling up graphene, and they are expected for various applications in future. Our group has succeeded in growing vertically aligned small-diameter SWCNTs on a SiO₂/Si substrate by the alcohol-catalytic CVD (ACCVD) method using an Ir catalyst, which was deposited by an arc plasma gun [1]. However, the deposition using the arc plasma gun is not suitable for mass production because it uses a vacuum system. Here, we have attempted to grow SWCNTs using Ir catalysts, which were prepared by the dip-coating technique containing Ir acetate.

2. Experimental Procedure

After immersing the SiO₂/Si substrates in a 0.01 M iridium acetate-containing ethanol solution, the Ir catalyst was deposited by the dip coating method, where the withdrawal speed was varied from 0.1 to 0.6 mm/sec. Then, the substrates were annealed at 250 °C for 15 min. SWCNT growth was carried out in a hot-wall CVD apparatus. The substrate temperature was raised to 850 °C in an Ar/H₂ atmosphere whose flow rate of 100 sccm. Then, ethanol of 500 sccm was supplied into the furnace to grown SWCNTs for 10 min. The samples were characterized by FE-SEM and Raman spectroscopy.

3. Results and discussion

Fig.1 shows the results for SWCNTs grown on a substrate of which the withdrawal speed was 0.1 mm/sec. Figs.1 (a) and (b) show the RBM region and the high-frequency region in the Raman spectra, respectively. These shows that SWCNTs with diameters between 0.8 and 1.0 nm were grown from Ir catalysts. Fig. 1 (c) shows a cross-sectional FE-SEM image, showing growth of an SWCNT forest. The thickness of the SWCNT forest was about 0.2 μm. We will discuss the dependence of the withdrawal speed in dip-coating on SWCNT growth.

Acknowledgments

Part of this research was supported by the private university research branding project "Meijo University Brand Building Program by Creating New Nanomaterials" and JSPS Bilateral International Joint Research Projects.

[1] T. Maruyama et al. Appl. Surf. Sci., **509** (2020) 145340.

Corresponding Author: S. Kondo

Tel: +81-80-9481-3507,

E-mail: 203429002@cmailg.meijo-u.ac.jp

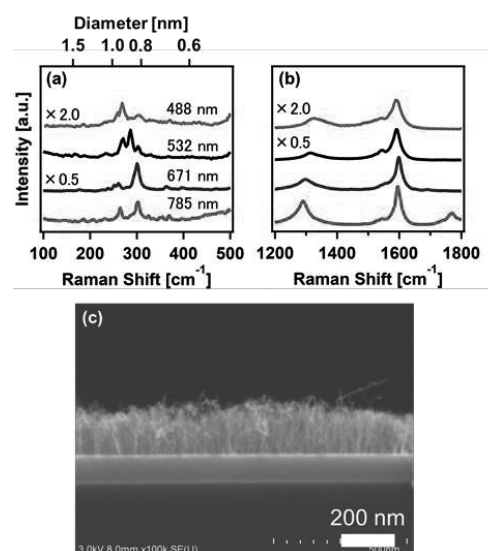


Fig. 1 Raman spectra in (a) the RBM region and (b) the high frequency region, and (c) FESEM image of SWCNTs grown from Ir catalysts prepared by the dip-coating.

Growth of hBN on CNT assemblies and their memristive behavior

○Misaki Kishibuchi, Kazuma Shimogami, Hiroataka Inoue, Kyohei Nasu, Tomohiro Nakagawa, Mitsuaki Maetani, Yuichiro Tanaka, Yasuhiko Hayashi and Hiroo Suzuki

Graduate school of Natural Science and Technology, Okayama University, Okayama 700-8530, Japan

Van-der-Waals (VdW) heterostructure is getting a lot of attention due to its potential to develop a new electronic device application. Recently, one-dimensional (1D) VdW heterostructure has been realized by direct growth of two-dimensional (2D) materials such as hexagonal boron nitride (hBN) and transition metal dichalcogenide (TMDC) on carbon nanotube (CNT) [1]. Because of its advantage in terms of higher integration density of heterojunctions than that of conventional 2D VdW hetero junctions owing to its extremely small size, assembling 1D VdW heterostructure is a reliable way for practical applications. One possible strategy for assembling a 1D VdW structure is the direct growth of homogeneous materials directory on CNT assemblies.

In our research group, we have developed the fabrication technique of bulk-size CNT assemblies [2]. The CNT sheet and yarn: one of the CNT assemblies, can be fabricated by a dry process with the drawable CNT forest grown by precisely tuned chemical vapor deposition (CVD) (Fig. 1(a)). In this research, we performed hBN growth directory on the CNT assemblies (sheet and yarn) by conventional powder CVD with a source of NH_3BH_3 . The heterogeneous growth of hBN on the CNT sheet was confirmed by UV-vis-NIR spectroscopy, Fourier transform infrared (FT-IR) spectroscopy, and transmittance electron microscopy (TEM).

From electrical transport measurements, we found the clear hysteresis in I - V curves, that is memristive behavior, with both hBN-grown CNT sheet and yarn (Fig. 1(b)). The strength of the hysteresis was evaluated with an area of hysteresis (S) as an indicator. The S showed the tunability with the growth conditions and device geometry. By the systematic experiments and structural observations, we proposed the possible mechanism of memristive behavior relating to the presence of the amorphous carbon (a-C) between hBN/CNT heterostructures and disordered structure of hBN layer. The a-C seemingly formed a conductive filament channel (CFC) in the disordered hBN layer under a high electric field, resulting in the memristive behavior.

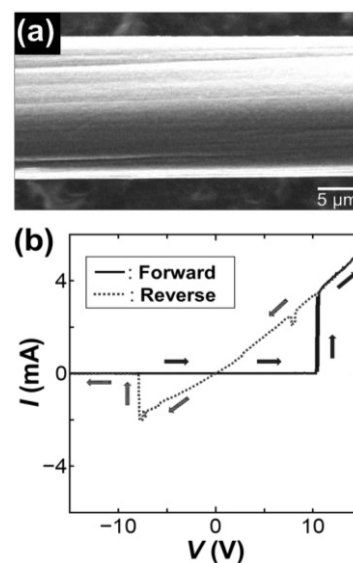


Fig. 1: (a) Scanning electron microscopy (SEM) image of CNT yarn. (b) I - V curve measured in hBN-grown CNT yarn.

[1] R. Xiang, *et al. Science* **367**, 537–542 (2020).

[2] H. Inoue, *et al. Carbon N. Y.* **158**, 662–671 (2020).

Corresponding Author: H. Suzuki

Tel: +81-86-251-8133

E-mail: hiroo.suzuki@okayama-u.ac.jp

Synthesis of high-density vertically aligned carbon nanotubes by suppressing migration of Fe using Fe/Mo_xO_y catalyst

○Mitsuaki Maetani, Hiroataka Inoue, Tomohiro Nakagawa, Kyohei Nasu, Takeshi Nishikawa, Hiroo Suzuki, Yasuhiko Hayashi

Graduate School of Natural Science and Technology, Okayama University, Okayama 700-8530, Japan

To realize the practical application of carbon nanotubes (CNTs) on the bulk scale, CNT yarns are fabricated from vertically aligned CNT (VACNT) on a substrate using the spinning process. Although single CNT has extraordinary physical properties, these are not fully reflected in those of the CNT yarn due to the presence of an interface between CNTs.

To improve the mechanical and electrical properties of the CNT yarns, high-temperature growth (>700°C) which can suppress the formation of kinks and defects is necessary. The use of bimetallic catalyst including Mo, having a high melting point, can suppress the migration, aggregation, and coarsening of the catalyst particles that occur during high-temperature growth, resulting in the synthesis of dense VACNT[1]. Increasing the density of VACNT with sustaining the long CNTs which can strengthen the fiber entanglement between CNT bundles is essential for its drawability[2].

In this study, we employed Fe/Mo_xO_y catalyst to achieve homogeneous dispersion of catalyst particles on a substrate leading to the high-density growth of VACNT. The melting point of Mo is 2623°C, while that of the typical oxide MoO₃ is 795°C. We presumed that the pre-oxidation of Mo would enhance the sufficient particle formation at the CNT growth temperature. Mo thin film was deposited on a silicon substrate with Al₂O₃/SiO₂ layers using electron beam evaporation. After being performed oxidization process by annealing the substrate in the air atmosphere, Fe thin film was deposited on the substrate. CNTs were grown by cold-wall CVD system in H₂/N₂ atmosphere with C₂H₂ as a precursor of CNT. To confirm the surface morphology of the substrate at the start point of CNT growth, atomic force microscope (AFM) images of the substrate were acquired after the annealing process in the H₂/N₂ atmosphere without C₂H₂ supply. This revealed that the pre-oxidation of Mo suppressed the coarsening of catalyst particles as shown in Fig. 1. The results of AFM analysis indicate that Mo_xO_y was reduced after forming the catalyst particles and produced pure Mo suppressed the coarsening of the catalyst particles with its high melting temperature. The Raman spectra of the CNTs grown with Fe/Mo_xO_y catalyst showed a high G/D band ratio (~15), indicating the high crystalline of the CNTs.

[1] E. R. Meshot *et al.*, *Carbon* **159**, 236-246 (2020).

[2] H. Inoue *et al.*, *Carbon* **158**, 662-671 (2020).

Corresponding Author: Yasuhiko HAYASHI

Tel: +81-86-251-8230

Email: hayashi.yasuhiko@okayama-u.ac.jp

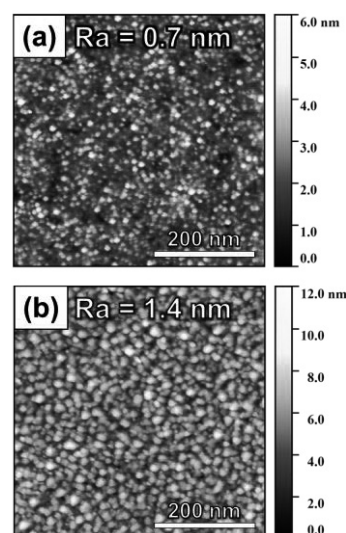


Fig. 1. AFM images of surface of substrate after annealing in H₂/N₂/nitrogen atmosphere (a) with and (b) without pre-oxidation of Mo.

Electrolyte effects on electrochemical doping of semiconducting carbon nanotube films

○Satoki Taniguchi¹, Tsuyoshi Kawai¹, Yoshiyuki Nonoguchi^{1,2}

¹ *Division of Materials Science, Nara Institute of Science and Technology, Nara 630-0192, Japan*

² *Faculty of Materials Science and Engineering, Kyoto Institute of Technology, Kyoto 606-8585, Japan*

Semiconducting single-walled carbon nanotubes (sc-SWNTs) are expected as a major material in next-generation electronics, and their doping is an essential technology for controlling charge transport properties. It is well known that p-type and n-type transport in SWNTs can be tuned by using oxidizing and reducing reagents, which is utilized in the fabrication of electronic and energy devices. Its reliability are current roadblocks to further applications involving practical requirements (e.g. precise control of electronic levels, and long-term stability). We have recently proposed that the stability of doped SWNTs depends on electrostatic interactions with counterions [1], while its quantitative verification using a high-purity sc-SWNTs has yet to be explored.

We apply the electrochemical quartz crystal microbalance (EQCM) in the analysis of chemical doping reactions. The mass change upon oxidation doping was investigated from the correspondence between the response current and the frequency by EQCM. sc-SWNT electrodes (purity $\geq 99\%$) allowed for reliable cyclic voltammetry about several organic electrolyte solution (e.g. tetrabutylammonium salts with BF_4^- , PF_6^-), where a bias sweep resulted in simultaneous increases in current and mass about +0.4 V corresponding to the valence band edge of sc-SWNTs. In addition, a comparison with counter anions showed that soft anions such as fluorinated salts are required for the observation of a capacitance and mass increase upon p-type doping (Fig.1). We will discuss effects of shape of counter anions, charge density and hydrophobicity of sc-SWNTs for turning electrochemical doping properties.

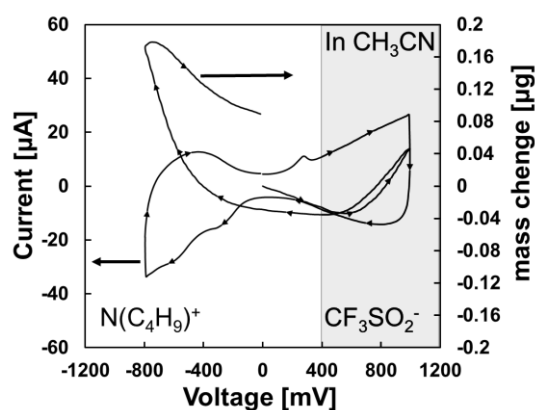


Fig. 1 Cyclic voltammogram (50 mV s^{-1}) and mass change of a sc-SWNTs.

[1] Y. Nonoguchi et al. *J. Mater. Chem. A*, **2018**, 6, 21896–2190

Corresponding Author: Y. Nonoguchi

Tel: +81-(75)-724-7515

E-mail: nonoguchi@kit.ac.jp

Visualization of thermal transports on bundled carbon nanotubes by monitoring phase transition of tin nanoparticles

○Hiromu Hamasaki¹, Takumi Kawase¹ and Kaori Hirahara²

¹ Dept. of Mechanical Engineering, Osaka University, Osaka 565-0871, Japan

² Dept. of Mechanical Engineering and Center for Atomic and Molecular Technologies, Osaka University, Osaka 565-0871, Japan

Thermal management based on carbon nanotubes (CNTs) is a fascinating topic because of their excellent thermal conductivity [1]. However, thermal conductivity of macroscopic assemblies of CNTs is significantly decayed mainly due to numerous interfaces between CNTs. In order to investigate the difference of the thermal conductivity between intra and inter CNTs, we focused on the bundles of single-walled carbon nanotubes (SWCNTs) and visualized thermal transport on it by monitoring the evaporation of gold nanoparticles as temperature markers [2]. However, this method cannot be applied to the metal nanoparticles forming surface oxide layer, and hence observable temperature range is limited. Moreover, the markers cannot be utilized repeatedly. We investigate the visualization of thermal transport by utilizing solid-liquid phase transition, instead of the evaporation.

Figure 1(a) shows a transmission electron microscope (TEM) dark-field image of the initial state of the bundle. Most of the particles show weak contrast, whereas several particles satisfying Bragg condition show strong white contrast. With increasing Joule heat generated at contact point, the particles near the contact point melted and showed intermediate contrast. As shown in Fig. 1(b), significant anisotropy for thermal transport between parallel and perpendicular direction to the bundle was successfully visualized.

This work was supported by JST CREST Grant Number JPMJCR17I5, Japan.

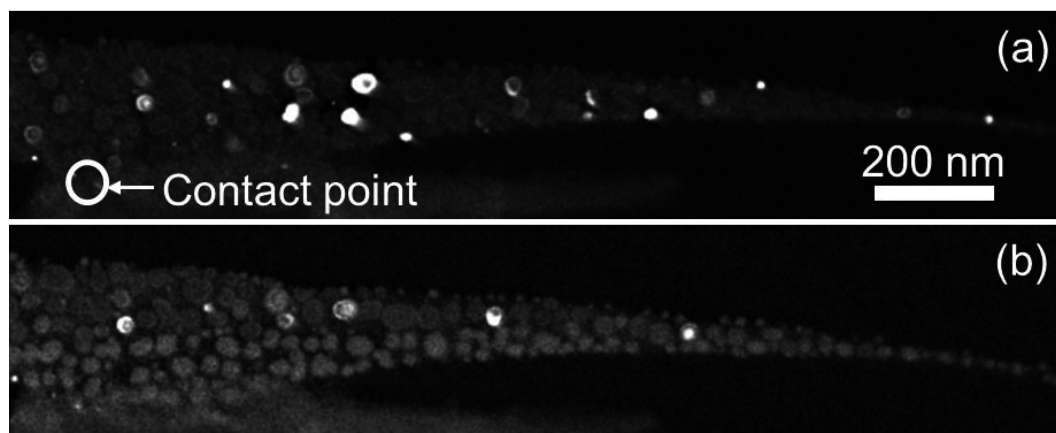


Figure 1 Dark field TEM images of a SWCNT bundle decorated with Sn particles. Applied voltage is increased (a) to (b).

[1] E. Pop *et al.*, Nano Lett. **6**, 96-100 (2006).

[2] H. Hamasaki *et al.* the 59th FNTG General Symposium, Sept. 16-18, 2020, online virtual symposium.

Corresponding Author: H. Hamasaki

Tel: +81-6-6879-7307

E-mail: hamasaki@ne.mech.eng.osaka-u.ac.jp

Excitonic photoluminescence properties of locally functionalized single-walled carbon nanotubes using cycloaddition modification

○ Tomohiro Shiraki^{1,2}, Keita Hayashi¹, Tsuyohiko Fujigaya^{1,2,3}

¹ Department of Applied Chemistry, Kyushu University, Fukuoka 819-0395, Japan

² WPI-I2CNER, Kyushu University, Fukuoka 819-0395, Japan

³ CMS, Kyushu University, Fukuoka 819-0395, Japan

Local chemical functionalization of single-walled carbon nanotubes (SWCNTs) has attracted great attention for enhancement of their photoluminescence (PL) properties in the near infrared (NIR) region.[1-4] This functionalization achieves doping of local defects such as sp^3 carbon to the semiconducting crystalline sp^2 carbon networks of SWCNTs. As a result, emissive doped sites that have narrower band gaps and exciton trapping features are created in the locally functionalized SWCNTs (lf-SWCNTs), and E_{11}^* PL appears with red-shifted wavelengths and increased PL quantum yields compared with original E_{11} PL of pristine SWCNTs. To date, various chemical functionalization methods including diazonium chemistry and reductive alkylation have been developed and E_{11}^* PL wavelength modulation has been observed depending on the molecular structure difference in the doped sites of the lf-SWCNTs.

Here, organic azide compounds are used to apply a [2+1] cycloaddition modification for the synthesis of lf-SWCNTs (lf-SWCNTs>N). The local chemical functionalization was conducted by mixing solubilized SWCNTs (CoMoCAT, (6,5) enriched) in an aqueous micelle solution and azide compounds under light irradiation conditions. Fig. 1 shows PL spectra of SWCNTs before and after the functionalization. For the lf-SWCNTs>N, a new PL peak appeared at 1116 nm that was observed in the longer wavelength region than E_{11} PL at 977 nm. In the XPS measurements of the lf-SWCNTs>N, N1s peak was clearly observed around 400 eV. These results indicate that defect doping to the SWCNTs occurs by the reaction with the azides to emit E_{11}^* PL from the lf-SWCNTs>N. As a control, lf-SWCNTs having the same aryl moiety (lf-SWCNTs-C) was synthesized by diazonium chemistry and its E_{11}^* PL was observed at 1140 nm that was red-shifted than that of lf-SWCNTs>N. In addition, temperature-dependent PL measurements revealed that the observed intensity changes of E_{11}^* PL by the thermal treatment also varied between lf-SWCNTs>N and lf-SWCNTs-C, indicating their different excitonic behaviors. Details will be discussed at the symposium.

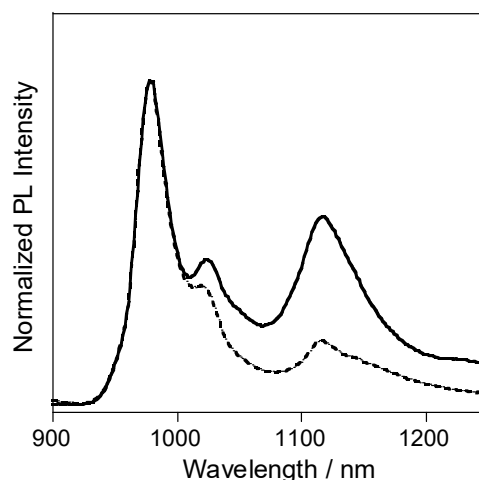


Fig. 1 Normalized PL spectra of lf-SWCNTs>N (solid line) and pristine SWCNTs (dashed line), λ_{ex} = 570 nm.

[1] T. Shiraki, Chem. Lett., in press (2021). DOI: 10.1246/cl.200776

[2] T. Shiraki *et al.*, Acc. Chem. Res., **53**, 1846 (2020).

[3] S. Tretiak *et al.*, Acc. Chem. Res., **53**, 1791 (2020).

[4] Y. Wang *et al.*, Nat. Rev. Chem., **3**, 375 (2019).

Corresponding Author: T. Shiraki

Tel/Fax: +81-92-802-2841,

E-mail: shiraki.tomohiro.992@m.kyushu-u.ac.jp

Reflection and Absorption Properties of Microwave Absorbers Made by SWNT-Cellulose Composite Paper

Weni Yulistia, Tetsu Mieno

Department of Physics, Shizuoka University, Shizuoka 422-8529, Japan

Recently, development of composite materials using CNTs and polymers is actively studied [1]. In this work, preparation of CNTs/cellulose composite papers and their electrical conductivity has been studied. And, good electromagnetic interference (EMI) shields have been developed. Singlewalled nanotubes (SWNTs) “ZEONANO” provided by Zeon Nano Company (average diameter = 3-5 nm, length in forest = 100-600 μm , and purity >99%), and multiwalled nanotubes (MWNTs, FT-9000) provided by CNano Technology Company (outer diameter = 10-20 nm, inner diameter = 3-10 nm, length = 10-30 μm , and purity >95%) are used to produce CNTs/cellulose composite papers (sample area 23 cm x 17.5 cm, thickness 0.2 mm) as shown in Fig. 1. For the eco-friendly process, NTs, pulp, and gelatin are mixed well to make the sheets [2]. The performance of the SWNTs and MWNTs cellulose-composite papers are studied for 8.9 w%, 13 w%, and 17 w% of CNTs. Their reflection and absorption of microwave properties are measured by a microwave transmitter of frequency 10.5 GHz ($\lambda \approx 3$ cm) and emission power $P_{\mu} = 10$ mW. Herein, it is found significant differences in EMI shielding effectiveness as shown in Fig. 2. The maximum values of EMI shielding by the MWNTs is 38.28 dB (1×10^{-4}) on 17 w% of MWNTs. On the other hand, SWNTs of 8.9 w% has shown EMI shielding of 52.56 dB (1×10^{-5}) and it is 75.15 dB (1×10^{-8}) by 17w% of SWNTs which are good as electromagnetic wave shieldings. Overall, the SWNTs composite shows much lower transmission and reflection properties than the MWNTs composite. The shields do not generate dusts and particles, have flexibility and toughness. Electric registers, electric heating sheets, electromagnetic wave (EMW) shields, EMW polarizers, pyramid type EMW absorbers as shown in Fig. 3 could be prepared.



Fig. 1 Photo of a SWNT composite paper.



Fig. 3 Photo of a pyramid type MW absorber made by NT composite paper.

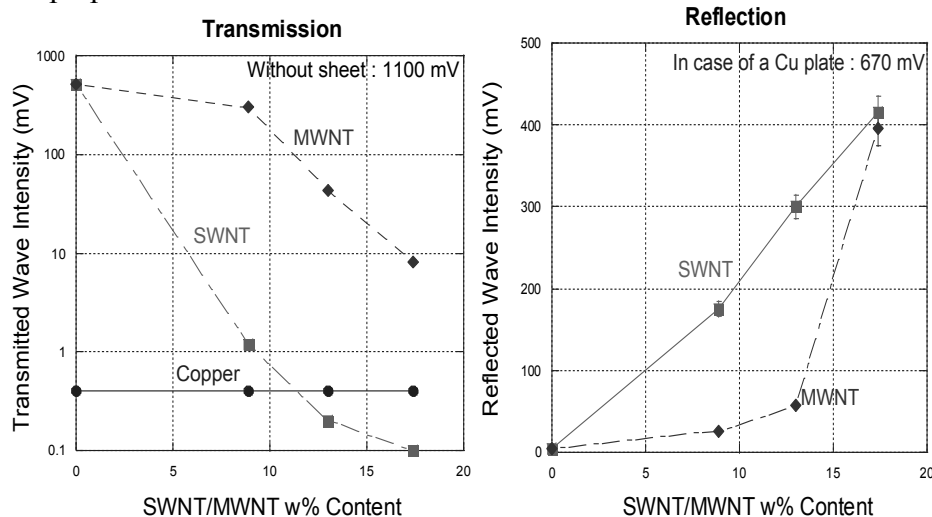


Fig. 2 The microwave absorption and reflection measurement of the SWNT composite papers and MWNT composite papers.

[1] M. Imai *et al.* “Highly strong and conductive carbon nanotube/cellulose composite paper”, *Composites*, **70** (2010).

[2] K. H. Maria, T. Mieno, “Production and Properties of Carbon Nanotube/Cellulose Composite Paper”, *J. Nanomaterials*, **2017**, 6745029 (2017).

Corresponding Author: Y. Weni E-mail: wenyulistia2@gmail.com

Preparation of carbon nanotube/organic-inorganic hybrid aerogel composites

○Taiyo Shimizu, Takeo Yamada, Kenji Hata

National Institute of Advanced Industrial Science and Technology (AIST), Tsukuba Central 5, 1-1-1 Higashi, Tsukuba, Ibaraki 305-8565, Japan

Aerogels are highly porous materials obtained by removing the solvent inside wet gels in a supercritical condition (so-called supercritical drying), where capillary force is substantially small and volume shrinkage of the gels caused during solvent evaporation is strongly suppressed. The characteristic properties of silica (SiO_2) aerogels, which are one of the most common aerogels, are lightweight, high specific surface area, good visible light transparency, low thermal conductivities and so forth. In particular, their thermal conductivities are the lowest among solid materials, and thus potential applications such as thermally insulating materials have been widely investigated. However, the poor mechanical properties are critical issues for aerogel applications, and numerous research on the reinforcement of aerogels has been conducted so far.

As one of the common strategies for improving their mechanical properties, organic-inorganic hybridization has been frequently adopted in the field of aerogels. Kanamori et al., reported that polymethylsilsesquioxane (PMSQ, $\text{CH}_3\text{SiO}_{3/2}$) aerogels exhibited superior flexibility and resilience against compressive deformation,[1] while retaining comparably low thermal conductivities to those of pure silica systems, achieved by precise control of formed pore structure. Incorporating organic moieties into pure inorganic matrix results in higher flexibilities. However, even for the above PMSQ aerogels, there are still a lot of problems concerning mechanical properties such as weakness against bending or tensile deformation.

In this study, our interest has been focused on the incorporation of the superior mechanical properties of carbon nanotubes (CNTs) into organic-inorganic hybrid aerogels. Using a surfactant as both a dispersant for single-walled CNTs and a control agent for pore structure of PMSQ matrix, we have successfully fabricated CNT/PMSQ aerogel composites (shown in Fig. 1). The obtained composite aerogels exhibited flexible but more resilient behavior than that of PMSQ.

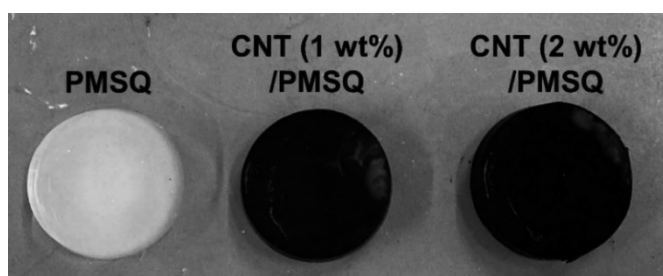


Fig. 1 Appearance of CNT/PMSQ composite aerogels.

Moreover, thermal stability in an air atmosphere has been improved by the incorporation of CNTs. Further detailed properties such as pore structure will be presented in this presentation.

[1] K. Kanamori, et al. *Adv. Mater.*, **19**, 1589 (2007).

Corresponding Author: T. Shimizu

Tel: +81-29-861-5712

E-mail: shimizu-t@aist.go.jp

CNT/HfO₂/CNT memristor with high on-off ratio for neuromorphic computing

○Adha Sukma Aji¹ and Yutaka Ohno^{1,2}

¹ Venture Business Laboratory, Nagoya University, Nagoya 464-8601, Japan

²Institute of Materials and Systems for Sustainability, Nagoya University, Nagoya 464-8601, Japan

Nowadays, the brain-inspired computing is one of promising next-gen computing paradigm because it enables self-learning process, low power consumption, and parallels calculation. To realize brain-inspired computing, one must overcome the bottlenecking in von-Neumann architecture where the processor and memory unit are separated [1]. The combination of many synaptic devices, where its memory and computing units are combined, could realize the brain-inspired computing at the hardware level [2]. The two-terminal memristors could be developed into a synaptic system if the conductivity of memristors can be trained by multiple input pulses. Carbon nanotubes (CNT) is a promising active material for brain-inspiring computing because of its excellent electrical properties and the similarity with biological neural network. We report the CNT/HfO₂/CNT stack as the memristors that exhibited a large on-off ratio and conductivity learning capability in this work.

Figure 1a shows the schematic view and the scanning electron microscopy (SEM) image of CNT/HfO₂/CNT stack. The memristor was realized by sandwiching HfO₂ with a thickness of 10 nm by bottom (left) and top (right) CNT films. The CNT films were synthesized by floating catalyst chemical vapor deposition and high-k HfO₂ insulator were deposited by atomic layer deposition system. Next, the electrical properties of CNT/HfO₂/CNT memristor is presented in Figure 1b. The I - V characteristic resembles “butterfly” curve which is a sign of memristive behavior. Moreover, our memristors exhibited high on/off ratios of $\sim 10^6$ with exceptionally low off current. We also observed that the memristor's conductivity increased with the number of voltage pulses applied as a learning process. This behavior suggests that our memristor is promising candidate for the brain-inspired computing.

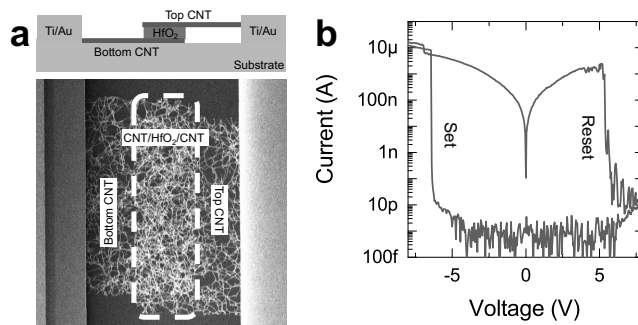


Figure 1. (a) Schematic and SEM images of CNT/HfO₂/CNT transistor. (b) I - V characteristic of memristors.

[1] D. Silver *et al. Nature*, **529**, 484 (2016).

[2] P. Merolla *et al. Science*, **345**, 668 (2014).

Corresponding Author: Y. Ohno

Tel&Fax: +81-52-789-5387,

E-mail: yohno@nagoya-u.jp

Synthesis and properties of carbon quantum dots using woody biomass.

○Takaki Yoda¹ and Hironori Ogata¹

¹ Department of Chem.Sci. and Technol., Hosei University, Tokyo 184-8584, Japan

² Research Center for Micro-Nano Technology, Hosei University, Tokyo 184-8584, Japan

Carbon quantum dots (C-QDs) are one of the nanomaterials that have attracted much attention in recent years. C-QDs have many advantages over conventional semiconductor quantum dots and organic dyes, including chemical stability, dispersibility, fluorescence properties, hydrophilicity, and high resistance to photodegradation [1]. Currently, there are two main synthesis approaches for the preparation of C-QDs; "top-down" and "bottom-up" approaches. In the top-down approach, large carbon materials are decomposed by arc discharge, laser ablation, or chemical oxidation [2]. On the other hand, the bottom-up approach is synthesis of C-QDs create carbon molecules via precursors such as the hydrothermal method [3], pyrolysis method, and the microwaves method [4]. These methods have been reported to have complicated procedures, relatively large particle sizes (30-50 nm), and low quantum yields of fluorescence.

Recently, biomass has been attracting attention as a material for C-QDs. It has been reported that C-QDs have been synthesized from organic materials such as soy milk[5] and plant seeds [6]. These studies use a simple process of heating only, and the synthesis can be done at a low cost.

In this study, C-QDs were synthesized by pyrolysis method using biomass such as lignin and cellulose Nano Fiber (CNF) as raw materials, and their structures and optical properties were investigated. Fig.1 shows TEM images of the C-QDs from lignin(a) and CNF(b).

Detailed results about their structures and optical properties will be reported at the meeting.

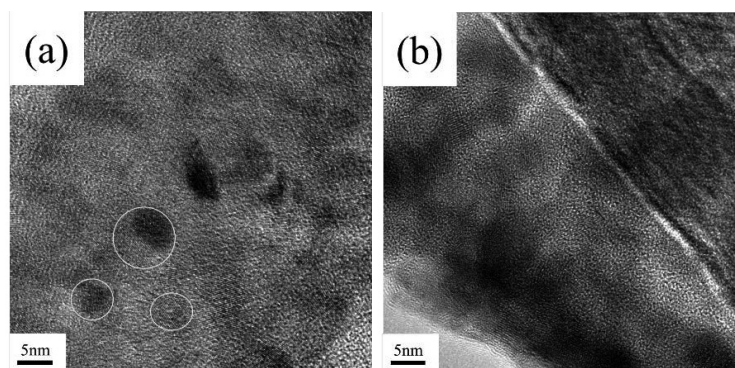


Fig.1 TEM images of C-QDs ((a) from lignin,(b) from CNF).

References:

- [1] Wang, Y. *et al.*, *J.Mater.Chem.C.* **2**,6921(2014).
- [2] Zhao, Q.L. *et al.*, *Chem.C.* **41**,5116(2008).
- [3] Pan, D. *et al.*, *Adv.Mater.* **22**,6,734(2010).
- [4] Liu, R. *et al.*, *J.Am.Chem.Soc.* ,**133**,39,15221(2011).
- [5] Chengzhou, Z. *et al.*, *Chem.C.* **48**,9367(2012).
- [6] Akansha, D. *et al.*, *Sci.Rep.* ,**9**,14004(2019).

Corresponding Author: H.Ogata

Tel: +81-42-387-6229, Fax: +81-42-387-6229,

E-mail: hogata@hosei.ac.jp

Effect of Defect Formation of Graphene on Proton Penetration Properties

○Tomohiro Fukushima, Takaha Komai, Kei Murakoshi

Department of Chemistry, Faculty of Science, Hokkaido University, Tokyo 123-4567, Japan

The electronic and chemical properties of graphene can be modulated through the interfacial structural control.[1] Recently, Geim *et al.*, reported that graphene can be uniquely used as proton permeable membrane.[2] The structural control of the proton permeability can be useful for the applications such as the separator for electrochemical systems. However, it is still difficult to control the structure of graphene including various defects. Recently, we reported that graphene/Au(111) electrode surface can show the unique Raman shift upon the hydrogen evolution reaction by intercalation of protons.[3] Here, we show that effect of defects formation of graphene surface can modulate the proton permeability from in-situ Raman spectroscopy under electrochemical potential control.

Graphene on Au surfaces (denoted as G/Au) were prepared by the chemical vapor deposition methods, and the crystallinity of graphene was characterized by confirmation of G band and 2D band from the Raman spectroscopy (excitation wavelength 514 nm, laser intensity 0.5 mW). All the electrochemical experiments were conducted by using HSV-110 potentiostat. Ag/AgCl and Pt electrodes were used as reference and counter electrodes, respectively. Molecular modification of graphene/Au(111) surface was by cyclic voltammogram by using 0.1 M NaClO₄ and 2 mM phenylhydrazine derivatives. The modified electrode was denoted as Ph-G/Au. In-situ electrochemical Raman spectroscopy was conducted by using 0.1 M KOH.

Molecular modification of graphene surface was conducted by electrochemical oxidation of phenylhydrazine. Electrochemical measurements were conducted in 0.1 M NaClO₄ in the presence of 2 mM phenylhydrazine. In the absence of phenylhydrazine, anodic current was not observed. On the other hand, in the presence of phenylhydrazine, anodic current was observed from -0.2 V vs. Ag/AgCl. The anodic feature was different from second cycle suggesting that deposition of phenyl groups on G/Au electrode (Ph-G/Au). Raman spectroscopy of as-prepared G/Au electrode revealed that high crystallinity of graphene by observation of G band (1580 cm⁻¹) and 2D band (2700 cm⁻¹). On the other hand, D band (1350 cm⁻¹) was additionally observed for Ph-G/Au. Additionally, underpotential deposition showed that the surface of electrode is still covered with graphene after electrochemical treatments.

Raman spectroscopy revealed that proton penetration potential was dependent on the molecular modification. G band and 2D band remains similar position upto -1 V. G band position, which suggests the electronic structure of graphene, suddenly shifts at -1.2 V. 2D band suddenly dropped at -1.2 V and -1.9 V and reversibly. Due to the electrochemical reaction, hydrogen evolution was spontaneously observed from cyclic voltammograms. The observed 2D band shift is due to the intercalation of H₂ molecules between graphene and Au through the proton tunneling. Importantly, these potential were modified through the surface modification. This study suggest that the modification of the graphene properties through the molecuels.

[1] T. Fukushima, K. Murakoshi, *Current Opinion in Electrochemistry*, **17**, 158 (2019).

[2] M. Lozada-Hidalgo, H. A. Wu, A. K. Geim *et al.*, *Nature* **516**, 227(2014).

[3] T. Fukushima, K. Murakoshi *et al.*, *J. Phys.: Conf. Ser.*, 1220(1), 012016 (2019)

Corresponding Author: T. Fukushima

Tel: +81-11-706-4811, Fax: +81-11-706-4810,

E-mail: tfuku@sci.hokudai.ac.jp

Electronic properties of 1D transition-metal chalcogenides nanowires

○ Nguyen T. Hung¹, Riichiro Saito²

¹*Frontier Research Institute for Interdisciplinary Sciences, Tohoku University, Sendai 980-8578, Japan*

²*Department of Physics, Tohoku University, Sendai 980-8578, Japan*

We discuss electronic properties of the one-dimensional (1D) transition-metal chalcogenides nanowire, in particular for WTe. A 1D structure of WTe consists of staggering triangular units of W_3Te_3 , as shown in Fig. 1 top [1]. Since the 1D WTe has van der Waals surface, the 1D WTe can have several geometries including, the single NW, bundle, or 2D layer. Therefore, it is essential to calculate the electronic properties of the 1D transition-metal chalcogenides nanowire with several geometries. Using the calculated results, we discuss the Raman spectra, or possible application based on the 1D transition-metal chalcogenides nanowire. Here, using the first-principles calculations with Quantum ESPRESSO, we found the bundle WTe is a metal, while the single nanowire is a semiconductor with a bandgap of about 0.3 eV (Fig. 1 bottom). We also perform the non-resonant Raman calculation, which shows two peaks at 156 cm^{-1} and 200 cm^{-1} and the calculated Raman peaks are consistent with the experiment. Since a 1D structure has a narrow bandgap of 0.3 eV, the single nanowire WTe shows potential for thermoelectric application. Therefore, we would like to discuss the possible thermoelectric application for the single nanowire WTe, too, in this work.

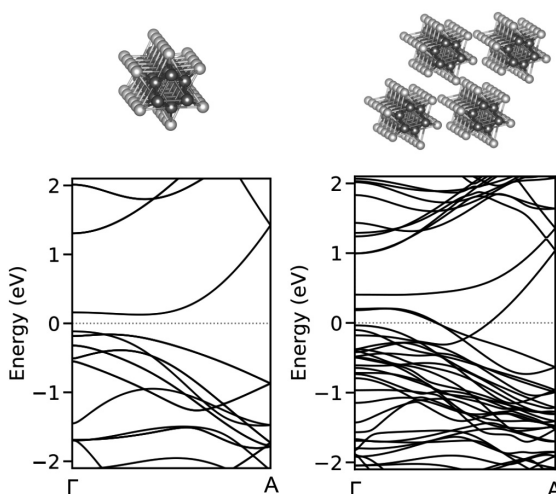


Figure 1: Geometries (top) and band structures (bottom) of the single nanowire WTe (left) and the bundle WTe (right).

Reference:

[1] H. E. Lim et al., *Nano Letter*, 21, 243-249 (2021)

Effect of iron ion beam irradiation on MoS₂ fluorescence

○Takumi Hidaka^{1,2}, Tomoaki Nishimura², Kazuyuki Takai^{1,2}

¹Graduate School of Science and Engineering, Hosei University, Tokyo 184-8584. Japan

²Research Center for Ion Beam Technology, Hosei University, Tokyo 184-8584. Japan

In 2D materials, defects and impurities significantly affect the electronic properties compared to 3D materials due to their low-dimensional structure. Meanwhile, ion beam implantation is one of the methods that can quantitatively and reproducibly introduce defects and impurities into materials. We can maintain the maximum implantation ion distribution on 2D materials by using a sacrificial layer [1]. The effect of the chemical properties of the implanted ion is not widely known yet in spite of many reports on the ion-dose dependence in of properties 2D materials. In this study, Fe⁺ which is a magnetic impurity that can cause spin scattering were introduced by ion beam irradiation into MoS₂ as a 2D material in which fluorescence strongly correlates with the degree of freedom of spin. The irradiation effects on structural and electronic properties were investigated using Raman spectroscopy and Photoluminescence (PL).

Cr / NaCl of 10 nm / 250 nm was deposited as a sacrificial layer on the single-layer MoS₂ obtained by the cleavage method on a SiO₂ / Si substrate. The film thickness of the sacrificial layer was optimized using Monte Carlo simulation for Fe⁺ distribution by SRIM2013. Fe⁺ irradiation to the sample was performed at an acceleration voltage of 200 keV with a dose of 10¹² cm⁻². Raman spectroscopy and PL were measured using a spectrometer (LabRAMHR, Horiba).

With Fe⁺ irradiation, no significant change in shape was observed on the E_{2g}¹ and A_{1g} peaks characteristic of the Raman spectrum of MoS₂ (Fig. 1). This confirms that MoS₂ maintains its fundamental crystal structure even after Fe⁺ irradiation. The PL spectra of MoS₂ consisting of A and B peaks, correspond to the transitions to two spin-subbands, showed a low energy shift of the A peak after Fe⁺ irradiation (Fig. 2). The low energy shift of the A peak indicates n-doping of MoS₂ by Fe⁺ irradiation [2], which was not observed in previous studies on Ar⁺ irradiation [3]. Moreover, A peak appears with a long tail in the lower energy side after the irradiation. This indicates that the introduction of defects in MoS₂ causes additional defect levels with various energy eigenvalues in the gap. In addition, the increasing of B peak intensity suggests that the introduced Fe⁺ caused spin-dependent relaxation in MoS₂.

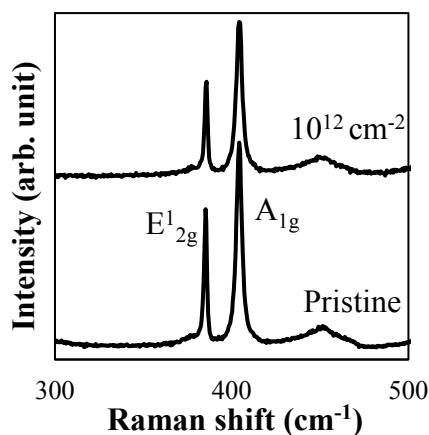


Fig. 1 Raman spectra for Fe⁺ irradiated MoS₂ before and after irradiation of Fe⁺ 10¹² cm⁻²

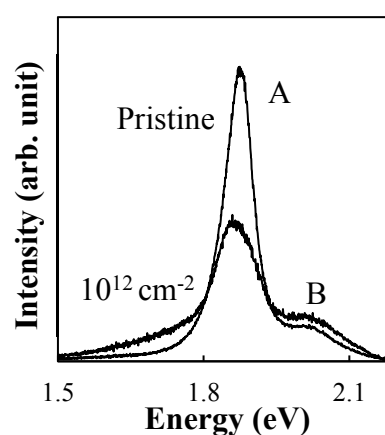


Fig. 2 PL spectra for Fe⁺ irradiated MoS₂ before and after irradiation of Fe⁺ 10¹² cm⁻²

[1] Y.Nakamura *et al*, FNTG Symposium (2019)

[2] S. Mouri *et al*, Nano Lett (2013)

[3] Y. Zhao *et al*, RPGR (2019)

Building of Platforms to Explore Transport Dynamics of Excitons and Trions in Monolayer Transition Metal Dichalcogenides

○Mengsong Xue¹, Yuya Murai¹, Shaochun Zhang¹, Toshinori Shirafuji¹, Ryo Kitaura¹

¹ Department of Chemistry, Nagoya University, Nagoya 464-8602, Japan

An exciton is a hydrogen-like quasi-particle, where the electrons in the conduction band and holes in the valence band bind together due to the Coulomb interaction. The exciton binding energies in monolayer transition metal dichalcogenides (TMDs) can reach hundreds of millielectronvolts due to reduced dielectric screening in the atomically thin limit—as much as two orders of magnitude larger than in conventional semiconductors such as silicon or GaAs [1]. On top of a neutral exciton, both trion (charged exciton) and biexciton (exciton molecule) states have been extensively studied both experimentally and theoretically in TMDs [2,3]. Besides, these excitonic states possess the information of valley degree of freedom. Therefore, monolayer TMDs provide an excellent platform to explore exciton physics and valley physics.

Understanding the spatial motion of optically generated carriers such as excitons and trions after generation and before recombination is of central importance for both fundamental research and optoelectrical applications. However, the environmental effects such as surface roughness, charged impurities and contaminants prohibit the exploration of the intrinsic properties of monolayer TMDs. It is essentially needed to build a high-quality material platform to exhibit intrinsic transport dynamics of excitons and trions. In this work, we fabricated hexagonal boron nitride (hBN)-encapsulated monolayer TMDs with super clean and flat surfaces and corresponding field-effect transistors (FETs) to explore the transport behaviors of excitonic carriers. The details will be discussed during the presentation.

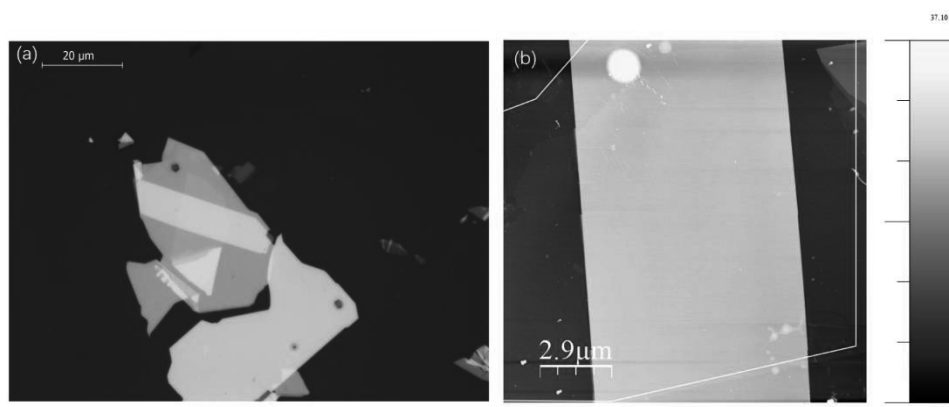


Fig. 1 Optical image (a) and AFM image (b) of a hBN/WSe₂/hBN heterostructure

[1] Chernikov, A *et al.* Phys. Rev. Lett. **113**, 076802 (2014).

[2] K. F. Mak *et al.* Nat. Mater. **12**, 207 (2013).

[3] You, Y *et al.* Nat. Phys. **11**, 477–482 (2015).

Corresponding Author: R. Kitaura

Tel: +81-52-789-2477, Fax: +81-52-747-6442

Web: <http://nano.chem.nagoya-u.ac.jp/>

E-mail: r.kitaura@nagoya-u.jp

Spin current induced by edge plasmon on two-dimensional materials

○Yuan Tian, M. Shoufie Ukhtary, Riichiro Saito

Department of Physics, Tohoku University, Sendai 980-8578, Japan

Manipulation of spin current is a novel technique in the field of spintronics, which promises new designs for memory storage and logic circuit ^[1,2]. It is expected that a device using spin current instead of electric current will have higher energy efficiency, since a pure spin current generates less heat than an electric current ^[2]. Although methods for generating spin current by on the either spin Hall effect ^[2], spin injection ^[3] or a spin valve ^[4] are well established, these conventional methods rely on either complicated structure or magnetic material, which makes the application difficult. If we can establish a method to generate spin currents via a simple two-dimensional (2D) structure with a light, many applications of spin devices are possible. Recently, Daigo Oue et.al.^[5] showed that surface plasmon can induce a spin current on metal. Due to the rotating electric field of the surface plasmon according to the inverse Faraday effect. We argue that an we can apply this effect to generate spin current on a 2D surface.

In this work, we investigate the spin current generated by an edge plasmon on a 2D material. Edge plasmon is an electromagnetic (EM) wave that propagates at the edge of the 2D surface. We start by giving an expression of the EM field of the edge plasmon by solving the Poisson equation. We found that the electric field of the edge plasmon is rotating as a function of time on the surface. According to the inverse Faraday effect, we therefore prove that the edge plasmon induces magnetization. As the edge plasmon is confined to the edge, the induced magnetization decays from the edge, which generates spin current on the surface ^[5].

We found the spin polarization of the spin current is perpendicular to the surface, while the flow of the spin current is in-plane and perpendicular to the edge. The magnitude of the spin current is enhanced resonantly by changing the frequency of the edge plasmon. Since the edge plasmon is excited by light, thus we can realize optical generation of the spin current on the 2D material.

Reference:

- [1] Huai, Yiming, et al.. AAPPS bulletin 18.6. 33-40. (2008).
- [2] Maekawa, Sadamichi, et al., eds. *Spin current*. Oxford University Press, (2017).
- [3] Vernier, Nicolas, et al. EPL (Europhysics Letters) 65.4. 526, (2004).
- [4] Yang, Tao, et al.. Nature Physics 4.11. 851-854. (2008).
- [5] Oue, Daigo, et al., Physical Review B 101.16, 161404, (2020).

Molecular orbital calculations of small carbon molecules in the singlet and triplet states

○Keisuke Fukumoto, Riku Ohnishi, Kaito Tanaka, Tomonari Wakabayashi

Department of Chemistry, Kindai University, Higashi-Osaka 577-8502, Japan

Small carbon molecules or clusters C_n have been thought as candidate carriers of spectral relevance to interstellar matter (ISM). Laboratory experiments, i.e. photoelectron spectroscopy (PES), electronic absorption spectroscopy (EAS), and ion chromatography (IC), revealed transitions of the stable structure from linear, monocyclic, polycyclic, to a caged form according to the molecular size n [1]. Among others, fullerene C_{60} as well as C_{70} has been detected in planetary nebulae in substantial abundance [2]. Cyanopolyynes molecules $H(C\equiv C)_n C\equiv N$ have been detected in asymptotic giant branch (AGB) or carbon stars and in dense molecular clouds by rotational emission spectra in radio waves, leading to a thorough discussion of their abundances in TMC-1 [3]. In contrast, nonpolar clusters C_n and symmetric hydrogen-capped polyynes $H(C\equiv C)_n H$ are missed in the astronomical observation in radio waves, but hopefully to be detected in the infrared or visible range.

For the measurement of laboratory spectra, we have developed an experimental setup for matrix isolation spectroscopy of highly reactive species trapped in solid rare-gas matrices at cryogenic temperature [4]. Prior to the measurement of phosphorescence spectra, we performed molecular orbital calculations of small carbon clusters and some polyyne molecules in their singlet and triplet states. Molecular orbital calculations were performed using Gaussian 16 program [5]. Theoretical models of density functional theory (DFT), namely RB3LYP and UB3LYP, were adopted with various basis sets, including 6-311++G(2d,p) as the largest one.

For linear C_n , the singlet (triplet) ground state was confirmed for n odd (even) species [1]. For monocyclic ones, contrary to the relatively symmetric singlet ground state [1], the triplet state was found deformed further into a structure of lower symmetry, revealing multiple minima having different bond angles for the planar form. We discuss about calculated transition energies for the singlet-triplet transition of linear- C_n and cyclic- C_n species in some details.

[1] A. Van Orden and R. J. Saykally, *Chem. Rev.* **98**, 2313 (1998), and references therein.

[2] J. Cami *et al.* *Science* **329**, 1180 (2010); E. K. Campbell *et al.* *Nature* **523**, 322 (2015).

[3] R. Loomis *et al.* *MNRAS* **463**, 4175 (2016).

[4] A. Endo *et al.* *Low Temp. Phys.* **45**, 689 (2019).

[5] M. J. Frisch *et al.* GAUSSIAN 16, Revision A.03/C.01, Gaussian Inc., Wallingford, CT (2016).

Corresponding Author: T. Wakabayashi

Tel: +81-6-4307-3408, Fax: +81-6-6723-2721,

E-mail: wakaba@chem.kindai.ac.jp

Effects of liquid phase oxidation of Nanodiamond surface on its water dispersibility and photo-absorption

○Takuma Tsuji¹, and Kazuyuki Takai^{1,2}

¹Graduate School of Science and Engineering, Hosei University, Tokyo 184-8584, Japan

²Research Center for Micro-Nano Technology, Hosei University, Tokyo 184-0003, Japan

Surface chemical modification of Nanodiamond (ND) is an important strategy to tune its electronic / chemical properties due to its large specific surface area. Especially, oxidation introduces the large electric polarization on the surface of ND, which could change electric screening of exciton in the photo absorption, carrier density, hydrophilicity, so on, depending on the chemical form of oxygen functional groups. Recently, selective introduction of oxygen-containing functional groups by using different oxidation reagent is reported for graphene in liquid phase [1]. In this study, effects of liquid phase oxidation of ND on its electronic and chemical properties are evaluated in terms of water dispersibility and photo absorption.

NDs repeatedly oxidized once to three times using the Brodie method [2] is labeled as **BND1**, **BND2**, **BND3**, respectively. UV-vis and the concentration of dispersed NDs are measured by a spectrometer (V-770, JASCO), and a total organic carbon (TOC) analyzer (TOC-V CSN, SHIMADZU), respectively.

Both of the absorbance shown in **Fig. 1** and the concentration of dispersed NDs show in **Fig. 2 (a)** increase as increasing in oxidation cycles. These results indicate that the graphene like shell on the ND surface was attached with oxygen-containing functional and / or removed by oxidation, resulting in enhancement of the dispersibility of NDs. The absorption coefficients for NDs show in **Fig. 2 (b)** were calculated from the absorbance at 660 nm and ND concentration. As the cycle of oxidation increases, the concentration of dispersed NDs increases and the absorption coefficient decreases.

From these results, the absorption at 660 nm is attributed to the plasmon excitation of the graphene like shell on the ND surface. As the destruction of π -conjugation or removing hydrophobic graphene by oxidation, the concentration of dispersed NDs increases but the photo absorption decreases.

[1] K. Tajima, *et. al*, *Polyhedron*, **136**, 155 (2017)

[2] M. R. Karim, *et. al*, *J.Phys.Chem. C* **120**, 21976 (2016)

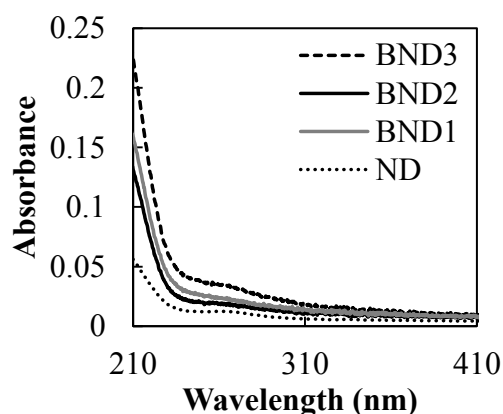


Fig. 1 UV-vis spectra for ND and BNDs

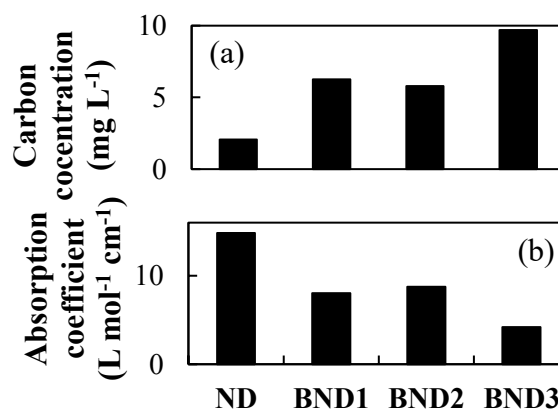


Fig. 2 Carbon concentration and Absorption coefficient of NDs

Do Elementary Diamond Nanoparticles Aggregate in their Aqueous Colloidal Solutions by just Diluting with Pure Water?

- Masaya Nemoto^{1,2}, Shusuke Ando¹, Yuho Itabashi¹, Tomohito Obata¹, Daiki Ayai¹, Nagito Haga¹, Kaito Hiruta¹, Toshihiko Tanaka^{1,2}, Yasuhiro F. Miura³, Tetsuya Aoyama², Kazunori Miyamoto⁴, Atsuya Muranaka², Masanobu Uchiyama^{2,4}, Eiji Osawa⁵

¹Department of Chemistry and Biochemistry, National Institute of Technology, Fukushima College, 30 Aza-nagao, Tairakamiarakawa, Iwaki, Fukushima, 970-8034, Japan

²Elements Chemistry Laboratory, RIKEN CPR, 2-1 Hirosawa, Wako, Saitama, Japan

³Hamamatsu University School of Medicine, 1-20-1 Handayama, Higashi-ku, Hamamatsu City, Shizuoka, Japan

⁴Graduate School of Pharmaceutical Sciences, the University of Tokyo, 7-3-1 Hongo, Bunkyo-ku, Tokyo, Japan

⁵Nano Carbon Research Institute Ltd., Asama Research Extension Center, Shinshu University, 3-15-1 Tokida, Ueda, Nagano, Japan

One enigmatic property of elementary diamond nanoparticles (EDIANs) is diluting aggregates in their aqueous solutions.¹ However EDIANs sediment with trace ions through strong interaction and we have to consider that trace carbonate or bicarbonate ions contaminate pure water and that they make them aggregate when diluting EDIANs solutions. So do EDIANs aggregate in their aqueous colloidal solutions just by diluting? We demonstrate here that our recent experiments under nitrogen atmosphere ($O_2 < 0.2\%$) show the diluting aggregation is unnoticeable.

One aspect of the interaction is that with the ions in biological organs with respect to their applications for drug delivery systems.² We consider that EDIANs should aggregate with ions in the organs and that the aggregates containing drug molecules will be delivered there.

We diluted nanodiamond(ND) solutions (NanoAmando[®], NanoCarbon Research Institute Ltd., containing EDIANs) from 2.5wt.% with ultrapure water in the atmosphere and their aggregation do not take place from 0.5 to 2.5wt.%, while it takes place from 1wt.% in air. Hence, the difference shows that the contaminants from air induce the diluting aggregation from 0.5 to 1 wt.%. Most probable contaminants are carbonate or bicarbonate ions from air; those from sodium carbonate induce sedimentation at lower concentration than sodium chlorides. We consider that the sensitive aggregation by trace ions can be attributed to the large multipolar electric charge³ of EDIANs.

[1]N.O. Mchedlov-Petrosyan, N. N. Kamneva, A. I. Marynin, A. P. Kryshnal, E. Osawa, *Phys. Chem. Chem. Phys.*, 17, 16186 (2015); [2]E.K.Chow, X.-Q. Zhang, M. Chen, R. Lam, E. Robinson, H. Huang, D. Schaffer, E. Osawa, A. Goga, D. Ho, *Sci. Trans. Med.*, 3, 73 (2011); [3]A. S. Barnard, E. Osawa; *Nanoscale* 6, 1188 (2014).
Corresponding Author: Toshihiko Tanaka / Tel: +81-246-46-0810 / E-mail: ttanaka@fukushima-nct.ac.jp

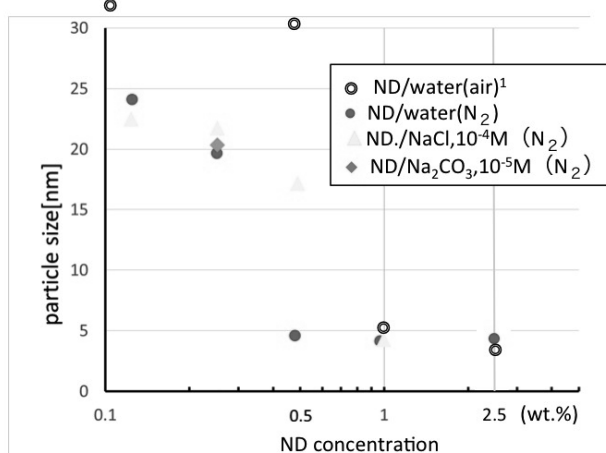


Figure 1. DLS size measurements of ND solutions diluted with water or aqueous salt solutions shown in the square. Samples are prepared in the N₂ atmosphere except ¹ cases.

発表索引
Author Index

Author index

A

Abe, Rikuto *1P-14, 2P-16
 Abe, Ryo 1-3
 Abe, Yuho *1P-18
 Adachi, Yusuke *1P-23
 Ago, Hiroki 2P-17
 Aizaki, Motoki 3-1, 3P-5
 Aji, Adha sukma 3P-19
 Ajiki, Hiroshi 2P-20
 Ajiro, Hiroharu 2P-1
 Akamatsu, Takatoshi 1P-6
 Akasaka, Takeshi 2P-11
 Akino, Kosuke 3-5
 Akita, Seiji 1P-23, 3-11
 Ando, Hideo *1-7
 Ando, Shusuke 3P-28
 Ando, Tsuyoshi 2P-1
 Anisimov, Anton 1P-12
 Aoyagi, Shinobu 1-8, 1P-11
 Aoyama, Tetsuya 3P-28
 Araki, Tsutomu 2P-22
 Arie, Takayuki 1P-23, 3-11
 Asaka, Koji 1-5
 Asaka, Toru 3-2
 Ayai, Daiki 3P-28

B

Bahramy, Mohammad saeed 1P-9
 Bamba, Masanori *3P-4
 Banno, Takashi 2P-19
 Baranov, Alexader 2P-23
 Barnard, Amanda 2-6
 Barnes, Stewart edward 1P-9
 Bevan, Kirk h. 2P-5
 Bhattacharya, Maireyee 1-3
 Bin mohd nasir, Mohd aidil amin 1P-24

C

Canton vitoria, Ruben 2P-25
 Chae, Sangwoo 2P-26
 Chen, Guohai 1P-13
 Cheng, Guoqing *1P-3
 Chiashi, Shohei 1P-4, 1P-12, 1P-28, 2P-14, 3P-4
 Chikaarashi, Itsuki 3P-2

D

Date, Hiroki *1P-4
 Demise, Ayaka *2P-1
 Dewey, Oliver S. 2I-1, 2I-2
 Dong, Yu 1P-6
 Dutta, Sudipta 3P-6

E

Eda, Junko 1P-15, 2P-17
 En lim, Hong 1P-10
 Endo, Takahiko 1P-8, 1P-10, 2P-4, 2P-6, 2P-10, 3P-8

F

F. miura, Yasuhiro 3P-28
 Fortner, Jacob 3-7
 Fu, Jianwei *2P-27
 Fujigaya, Tsuyohiko 1P-16, 3P-16
 Fujii, Takenori 1P-4
 Fukumoto, Keisuke 2P-12, 2P-28, *3P-26
 Fukushima, Tomohiro *3P-21
 Furukawa, Makoto 2P-11
 Futaba, Don 1P-13

G

Ganesan, Pandian 2-4
 Gao, Yanlin 2-2, 3-1, *3-3, 3P-5

H

Habara, Ren *2P-8
 Hada, Masaki 1-1
 Haga, Nagito 3P-28
 Haga, Taishi 2P-5
 Hamano, Ryo 3-8
 Hamano, Tsuyoshi 2P-20
 Hamasaki, Hiromu 1P-27, *3P-15
 Hanayama, Hiroki *2-7
 Hara, Masanori *2P-19
 Harano, Koji 2-7
 Hashimoto, Satoru 2P-15
 Hashimoto, Takeshi 2P-15
 Hata, Kenji 1P-13, 3P-18
 Hatanaka, Miho 2P-12
 Hatamoto, Riku *2P-15
 Hayamizu, Yuhei 1P-7, 3-9
 Hayashi, Keita 3P-16
 Hayashi, Tatsuhiro 1S-2
 Hayashi, Yasuhiko 1-1, 1P-20, 3P-12, 3P-13
 He, Xing *3-10
 Headrick, Robert j. 2I-1
 Hidaka, Takumi *3P-23
 Hirahara, Kaori 1P-27, 3P-15
 Hirao, Toshio 2P-20
 Hirobe, Genki 2P-27
 Hirota, Kazutoshi 2-5
 Hirotani, Jun 2P-2
 Hiruta, Kaito 3P-28
 Hisama, Kaoru 1P-12, *1P-28
 Honma, Chishu 1P-7, *3-9
 Hosokawa, Yuuya *2P-18
 Huang, Junwei 1P-6
 Hung, Nguyen T. 2-1, 3-12

I		Kishibuchi, Misaki	1P-20, *3P-12
Ichinose, Yota	1-2, 2I-2, *2P-16	Kishimoto, Shigeru	2P-3
Ideue, Toshiya	1P-6	Kitabatake, Daiki	*1P-11
Ieda, Jun	1P-9	Kitamura, Sota	1P-6
Iizumi, Yoko	2-5	Kitaura, Ryo	2P-24, 2P-25, 3P-24
Ikuhara, Yuichiro	1P-12	Ko, Jeong won	3P-10
Imamoglu, Atac	1I-2	Ko, Weon bae	3P-10
Inoue, Hirotaka	1-1, 1P-20, 3P-12, 3P-13	Kobashi, Kazufumi	*2-5, 2-8
Inoue, Taichi	3-11	Kobayashi, Akari	1P-4, *2P-14
Inoue, Taiki	1P-4, 1P-12, 2P-14, 3-7, 3P-4	Kodama, Takeshi	2P-12
Inoue, Yoku	1S-2	Koga, Yasumasa	2-5
Inoue, Zen	*2P-23	Komai, Takaha	3P-21
Irisawa, Toshifumi	2P-6	Komatsu, Naoki	1P-3
Ishi-hayase, Junko	2P-3	Komatsu, Natsumi	2I-1, 2I-2
Ishiguro, Yasushi	2P-23, 2P-27	Kondo, Riku	*1P-22
Ishii, Akihiro	3-6, 3-7	Kondo, Shu	2P-13, *3P-11
Ishii, Satoshi	2P-20	Kondo, Takahiro	*3S-1
Ishikawa, Takahiro	2P-20	Konishi, Teruaki	2P-20
Ishimaru, Ryoya	2P-14	Konno, Yui	*1P-2
Ishimaru, Saya	*1P-19	Kono, Junichiro	1-2, 1P-15, *2I-2
Ishizaka, Kyoko	1P-9	Kozawa, Daichi	*3-7
Islam, Md shafiqul	3-12	Kroner, Martin	1I-2
Itabashi, Yuho	3P-28	Kumamoto, Akihito	1P-12
Iwasa, Yoshihiro	1P-6, 1P-9, *1T-1	Kumari, Nikita	1-3
Izumi, Tatsuma	*1P-1	L	
J		Lee, Philip	3-4
Jarillo-herrero, Pablo	2I-3	Li, Mochen	*1-4
Jeon, Il	1-6, 3-4, 3-5	Li, Yan	*1I-1
Jiang, Hua	2I-5	Lim, Hong en	1P-8, 2P-4, 2P-6, 2P-10, 3P-8
K		Lin, Hao-sheng	1-6, 2P-15, 3-5
Kako, Masahiro	2P-11	Lin, Haosheng	2P-26
Kanda, Naoyuki	3-1, *3P-5	Lin, Yung-chang	2-3
Kaneda, Masahiko	*2P-4, 2P-6	Liu, Zheng	3-1, 3P-5, 3P-8
Kaneko, Takeshi	2-3	M	
Kaneko, Takuhei	*2P-26	Ma, Yue	1-6
Kaneko, Toshiro	3-10	Machida, Tomoki	2P-7
Kasama, Yasuhiko	1P-11	Machiya, Hidenori	3-6
Kashima, Taiga	1P-19	Maeda, Yutaka	1P-2, 2P-11
Katagiri, Atsuhiko	*1P-15	Maekawa, Sadamichi	1P-9
Kataura, Hiromichi	1P-19	Maetani, Mitsuaki	3P-12, *3P-13
Kato, Masahiro	3P-1	Manzhos, Sergei	1-6
Kato, Toshiaki	3-10	Maruyama, Mina	*1-10, 1P-28, 2-2, 3-1, 3P-5
Kato, Yuichiro k.	3-6, 3-7	Maruyama, Shigeo	1-6, 1P-4, 1P-12, 1P-28, 2P-14, 3-4, 3-5, 3-7, 3P-4
Kauppien, Esko	1P-4	Maruyama, Takahiro	2P-13, 3-2, 3P-11
Kauppinen, Esko	1P-12, *2I-5, 3-4	Masubuchi, Satoru	2P-7
Kauppinen, Esko.i.	3-5	Matsuda, Kazunari	2P-9
Kawachi, Kazuhiko	1P-11	Matsunaga, Yuki	*2P-2
Kawachi, Ryo	2P-19	Matsuo, Yoshiaki	1P-22
Kawahara, Kenji	2P-17	Matsuo, Yutaka	1-6, 2P-15, 2P-26, 3-5
Kawai, Tsuyoshi	2P-1, 3P-3, 3P-14	Matsuoka, Hideki	1P-9
Kawase, Takumi	3P-15	Matsuoka, Yuya	1-2, 1P-15
Khaniya sharma, Aliza	3-2	Mieno, Tetsu	3P-17
Kim, Jaeho	1P-13		

Mineyama, Aoi	2P-28	O	
Misaizu, Fuminori	1P-11	Obana, Daichi	1P-5
Misaki, Ai	3P-11	Obata, Tomohito	3P-28
Miwa, Kazuhira	*1-8	Ogata, Hironori	1P-18, 1P-25, 3P-20
Miyamoto, Kazunori	3P-28	Ogura, Hiroto	1P-10, *2P-6
Miyashiro, Daisuke	*3-8	Ohfuchi, Mari	2P-6
Miyata, Yasumitsu	1P-8, 1P-10, 1P-20, 1P-27, 2P-4, 2P-6, 2P-10, 3-1, 3P-5, 3P-8, 3P-9	Ohkubo, Kei	1-8
Miyauchi, Yuhei	2P-9	Ohnishi, Riku	2P-28, 3P-26
Morimoto, Takahiro	1P-6, 2-5, 2-8, *3S-2	Ohno, Yutaka	1P-19, 2P-2, 2P-3, 2P-20, 3P-19
Morishita, Shigeyuki	2-3	Ohshimo, Keijiro	1P-11
Moriya, Rai	2P-7	Okada, Hiroshi	1-8
Motai, Kazunori	1P-7	Okada, Susumu	1-10, 1P-28, *2-2, 3-1, 3-3, 3P-5
Mouri, Shinichiro	2P-22	Okamoto, Naofumi	1-3
Mukai, Yutaka	2P-12	Okazaki, Shota	2P-7
Murai, Yuya	2P-24, 3P-24	Okazaki, Toshiya	2-5, 2-8
Murakoshi, Kei	3P-21	Okoshi, Norihiro	2-3
Muranaka, Atsuya	3P-28	Okubo, Hitomi	1P-15, 2P-17
N		Omachi, Haruka	2P-2, *2S-2
Nabiev, Igor	2P-23	Onga, Masaru	1P-6
Nagai, Kohei	2P-17	Onoe, Jun	1-9, 1P-1, *1S-3, 3P-1
Nagai, Yukiko	*1P-16	Osawa, Eiji	*2-6, 3P-28
Nagano, Mai	*1P-27	Osawa, Toshio	3P-2
Nagashio, Kosuke	3P-6	Otsuka, Keigo	1P-12, 2P-14, 3-6, 3-7
Nagatomo, Mika	1P-4	Otsuki, Nao	*1P-17
Nagaya, Hiroki	3-5	P	
Naito, Hibiki	*1P-8	Pandey, Manish	1-3
Nakagawa, Rei	1S-2	Park, Se hwan	3P-10
Nakagawa, Tomohiro	1-1, 3P-12, 3P-13	Pasquali, Matteo	*2I-1, 2I-2
Nakagawa, Yuji	1P-6	Peraca, Nicolas marquez	2I-1
Nakajima, Hideaki	2-8	Pratama, Fenda rizky	1P-26
Nakamura, Eiichi	2-7	Pu, Jiang	2P-6, 3P-8
Nakamura, Kenta	1P-16	S	
Nakamura, Masakazu	1-3	Saida, Takahiro	2P-13, 3P-11
Nakamura, Taichi	2P-20	Saika, Bruno kenichi	1P-9
Nakamura, Yoshiki	1P-7	Saito, Nagahiro	2P-26
Nakanishi, Yusuke	1P-8, 1P-10, 2P-4, 2P-6, *3-1, 3P-5, 3P-8	Saito, Riichiro	1P-26, 2-1, 3-12, 3P-22, 3P-25
Nakano, Masaki	1P-9	Saito, Susumu	2P-5, 3P-7
Nakao, Yoshihide	1-7	Saito, Yahachi	*1-5
Nakashima, Naotoshi	*2-4	Saito, Yu	*2I-4
Nakaya, Masato	*1-9, 1P-1, 3P-1	Sakakita, Hajime	1P-13
Namiki, Katsuya	3P-2	Sakurai, Shunsuke	1P-13
Naritsuka, Shigeya	3P-11	Sasagawa, Takao	2P-7
Narituka, Shigeya	2P-13	Sasaki, Shuichi	2-6
Nasu, Kyohei	3P-12, 3P-13	Sasaki, Takeo	2-3
Nemoto, Masaya	*3P-28	Sasamori, Takahiro	1-8
Nishida, Shintaro	*2P-11	Sato, Shintaro	*1S-1
Nishidome, Hiroyuki	*2P-17	Sato, Shu	3P-4
Nishikawa, Takeshi	1-1, 3P-13	Sato, Toshihiro	1S-2
Nishimura, Tomoaki	3P-23	Sato, Yuta	1P-12
Noda, Suguru	1-4, 1S-2, 3P-2	Sawada, Hidetaka	2-3
Nonoguchi, Yoshiyuki	1P-8, 1P-10, 2P-1, 2P-6, 3P-3, 3P-14	Schwartz, Ido	1I-2
Nugraha, Ahmad r. t.	3-12	Sekido, Masaru	1P-17
Numata, Shunsuke	*1P-25	Senga, Ryosuke	*2-3

Seo, Seungju	*3-5	Tuan hung, Nguyen	3P-22
Sharma, Kamal	2P-13, 3P-11	U	
Sharma, Kamal prasad	3-2	Uchida, Kento	2P-17
Shawky, Ahmed	3-5	Uchiyama, Haruki	*2P-3
Shigeeda, Yuho	1-1	Uchiyama, Masanobu	3P-28
Shikata, Ryo	*1-1	Ueji, Kan	*1-2, 1P-14, 1P-15, 2P-10, 2P-16
Shimamoto, Kazuhiro	2-5	Uejima, Mitsugu	2-4
Shimazaki, Yuya	*1I-2	Ueno, Hiroshi	1-8, 1P-11
Shimizu, Hiroshi	*3P-8	Ukhtary, M. shoufie	1P-26, 2-1, 3P-25
Shimizu, Taiyo	*3P-18	Umemura, Kazuo	3-8
Shimogami, Kazuma	*1P-20, 3P-12	Utsugi, Koichi	*2P-21
Shinohara, Hisanori	3P-5	W	
Shinokita, Keisuke	2P-9	Wadati, Hiroki	1P-9
Shinomori, Naoki	2-5	Wakabayashi, Katsunori	1P-5, 2P-8, 3P-6
Shirafuji, Toshinori	2P-24, 3P-24	Wakabayashi, Tomonari	*2P-12, 2P-28, 3P-26
Shiraki, Tomohiro	*3P-16	Wang, Sake	*3-12
Shu, Hiroaki	2-4	Wang, Xirui	2I-3
Sideri, Ioanna	2-8	Wang, Yue	1P-9
Sinha, Sapna	2-3	Wang, Yuhuang	3-7
Skido, Masaru	2P-21	Warner, Jamie	*2S-1
Son, Yeon a	3P-10	Watanabe, Kenji	1I-2, 1P-6, 1P-8, 2I-3, 2P-7
Staykov, Aleksandar	2-4	Watanabe, Shinta	1-9, 1P-1
Suenaga, Kazu	1P-12, 2-3	Wehmeyer, Geoff	2I-1, 2I-2
Sugime, Hisashi	1-4, *1S-2, 3P-2	Wu, Xiaojian	3-7
Sukanta, Datta	2I-5	X	
Suzuki, Hiroo	1-1, 1P-20, 3P-12, 3P-13	Xiang, Rong	1-6, 1P-12, 3-5, 3-7
Suzuki, Satoru	*2P-20	Xue, Mengsong	*3P-24
Suzuki, Shunta	*1P-10	Y	
T		Yabuta, Shohei	*2P-22
Tagmatarchis, Nikos	2-8	Yagi, Takashi	1-2, 1P-15, 2P-10
Taguchi, Yuta	*3P-7	Yagi, Tomoko	*3P-3
Taira, Hisao	3-8	Yajima, Wataru	1-1
Takai, Kazuyuki	1P-21, 1P-22, 2P-23, 2P-27, 3P-23, 3P-27	Yamada, Junya	2-7
Takeda, Yukiharu	1P-9	Yamada, Michio	1P-2, 2P-11
Takei, Kuniharu	1P-23, 3-11	Yamada, Takeo	3P-18
Takenobu, Taishi	2P-6, 3P-8	Yamamoto, Daiki	*2P-13, 3-2
Takeyama, Kei	*2P-7	Yamanoi, Ryoko	2-6
Takizawa, Rio	*1P-7	Yamashita, Daiki	*3-6
Tanaka, Kaito	2P-12, *2P-28, 3P-26	Yamashita, Yoshifumi	1-1
Tanaka, Koichiro	2P-17	Yana, Takumi	2P-26
Tanaka, Ryoga	*3P-9	Yanagi, Kazuhiro	1-2, 1P-14, 1P-15, 1P-27, 2I-2, 2P-6, 2P-10, 2P-16, 2P-17, 2P-18, 3P-8, 3P-9
Tanaka, Toshihiko	3P-28	Yasoshima, Kazuki	*3-11
Tanaka, Yuichiro	3P-12	Yasuda, Kenji	*2I-3
Tang, Daiming	1P-12	Yoda, Takaki	*3P-20
Taniguchi, Satoki	*3P-14	Yomogida, Yohei	1-2, 1P-14, 1P-15, 1P-27, 2I-2, 2P-10, 2P-16, 2P-17, 2P-18, 3P-9
Taniguchi, Takahashi	2I-3	Yonemori, Itsuki	*3P-6
Taniguchi, Takashi	1I-2, 1P-6, 1P-8, 2P-7	Yoon, Jungjin	3-4
Taylor, Lauren w.	2I-1, 2I-2	Yoshida, Satoshi	1P-9
Thanh cuong, Nguyen	2-2		
Tian, Hongyu	3-12		
Tian, Yuan	*3P-25		
Trafford, Mitchell	2I-2		
Tsuji, Takashi	*1P-13		
Tsuji, Takuma	*3P-27		
Tsukiiwa, Mirano	1P-7, 3-9		

Yoshida, Takumi	*1P-21
Yoshii, Mao	1P-6
Yoshimura, Masamichi	2P-19
Yoshizawa, Hayato	*3P-1
Yuan, Hongtao	1P-6
Yuan, Shuaishuai	2P-5
Yuan, Wenyu	*2P-10
Yulistia, Weni	*3P-17
Z	
Zhang, Minfang	2-8
Zhang, Qiang	1P-12, 2I-5
Zhang, Shaochun	*2P-24, 3P-24
Zhang, Yan	*2P-9
Zhang, Yijin	2P-7
Zhang, Zihao	*3P-2
Zheng, Liu	1P-20
Zheng, Yongjia	1P-12
Zhou, Ling	1P-6
Zolotoukhina, Tatiana	1P-24

複写をご希望の方へ

フラーレン・ナノチューブ・グラフェン学会では、複写複製および転載複製に係る著作権を学術著作権協会に委託しています。当該利用をご希望の方は、学術著作権協会 (<https://www.jaacc.org/>) が提供している複製利用許諾システムもしくは転載許諾システムを通じて申請ください。

注意：著作物の引用、翻訳等に関しては、(社)学術著作権協会に委託致しておりません。直接、フラーレン・ナノチューブ・グラフェン学会へお問い合わせください。

Reprographic Reproduction outside Japan

Fullerenes, Nanotubes and Graphene Research Society authorized Japan Academic Association For Copyright Clearance (JAC) to license our reproduction rights and reuse rights of copyrighted works. If you wish to obtain permissions of these rights in the countries or regions outside Japan, please refer to the homepage of JAC (<http://www.jaacc.org/>) and confirm appropriate organizations to request permission.

In order to obtain permission to quote and/or translate, please contact the copyright holder directly.

2021年2月22日発行

第60回記念フラーレン・ナノチューブ・グラフェン総合シンポジウム 講演要旨集

《フラーレン・ナノチューブ・グラフェン学会》

〒464-8601 愛知県名古屋市千種区不老町

名古屋大学 未来材料・システム研究所

未来・エレクトロニクス集積研究センター 大野研究室内

Phone/Fax : 03-3830-4848

E-mail : secretariat@fntg.jp

URL : https://fntg.jp/jp_new/

印刷 / 製本 名古屋大学消費生活協同組合 印刷部

モデルチェンジ ～スマートなデザインに簡単操作～

BRANSON 超音波ホモジナイザー

長くご愛顧いただいておりますBRANSON超音波ホモジナイザーで新たなモデルが誕生しました。

主な特長

- 1.電気エネルギーから超音波振動への変換効率が95%以上
→ 無駄なエネルギーロスが小さく、安定した振幅が得られる。
- 2.通常では、液体の種類によって振幅が安定し難い。
→ 条件を変えても一定の振幅を保つ機能がついている。
- 3.ジュール (watt×sec) による発振制御が可能
→ Total何ジュールでこの処理が完了するという情報が論文に掲載できる。

20kHz超音波ホモジナイザー
BRANSON SONIFIER SFX250,550

40kHz超音波ホモジナイザー
BRANSON SONIFIER SFX150HH



主なアプリケーション

分散

カーボンナノチューブ 有機顔料 無機顔料 セラミック セメント 感光体 記録材料
磁性粉 粉末冶金 酸化鉄 金属酸化物 シリカ アルミナ カーボンブラック
ポリマー ラテックス 製紙 ファンデーション
研磨剤 電池 フィラー 光触媒 触媒 ワクチン 体外診断薬 歯磨き粉 シャンプー
半導体 電子基盤 液晶 貴金属 金属 宝石 タイヤ 発酵菌類 その他

乳化

エマルジョン製剤 農薬 トナー ラテックス 界面活性剤 クリーム 乳液 その他

日本国内販売総代理店



株式
会社

セントラル科学貿易

東京本社: 〒136-0071 東京都江東区亀戸1-28-6 タニビル3F

TEL 03-5627-8150 FAX 03-5627-8151

技術物流センター: 〒272-0146 千葉県市川市広尾2-1-9

TEL 047-701-6100 FAX 047-701-6116

大阪支店: 〒533-0031 大阪府大阪市東淀川区西淡路1-1-36 新大阪ビル

TEL 06-6325-3171 FAX 03-6325-5180

福岡営業所: 〒812-0016 福岡県福岡市博多区博多駅南1-2-15 事務機ビル

TEL 092-482-4000 FAX 092-482-3797

札幌出張所: 〒001-0911 北海道札幌市北区新琴似11条13-7-13-2

TEL 011-764-3611 FAX 011-764-3612

<https://www.cscjp.co.jp>



原子分解能分析電子顕微鏡
JEM-ARM300F2 GRAND ARM™2

40.5 pm

新しく開発された原子分解能分析電子顕微鏡 (GRAND ARM™2) では、
新ポールピース "FHP2" の導入に加え、防音・耐震・レンズ安定度の強化を行い、
世界最高峰の分解能を実現しています。
この世界最高峰の分解能とEDS性能を両立させ、さまざまな研究に対応できます。

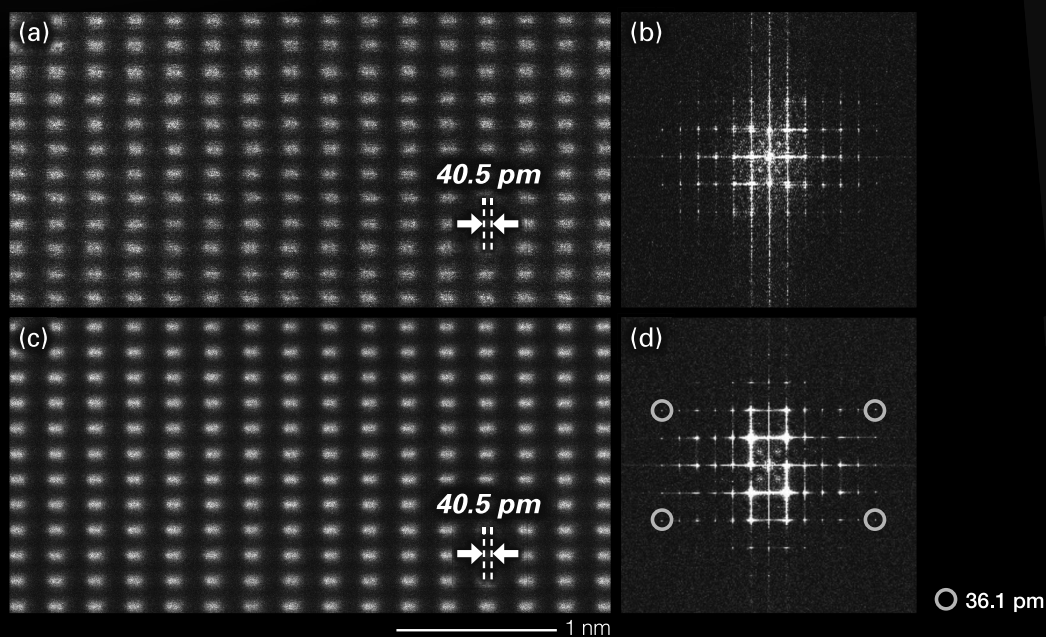


図1 (a) 1フレームで得られたGaN[212]のSTEM-HAADF像とそのFFTパターン(b)。
(c) 20フレーム積算で得られたGaN[212]のSTEM-HAADF像とそのFFTパターン(d)。

JEOL 日本電子株式会社

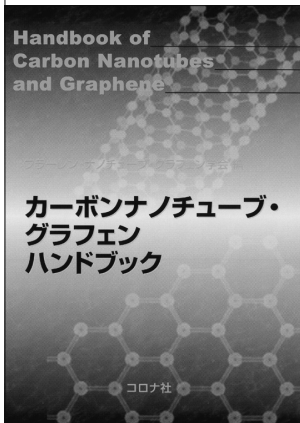
本社・昭島製作所 〒196-8558 東京都昭島市武蔵野3-1-2 TEL:(042)543-1111 (大代表) FAX:(042)546-3353
www.jeol.co.jp ISO 9001・ISO 14001 認証取得

JEOLグループは、「理科学・計測機器」「産業機器」「医用機器」の3つの事業ドメインにより事業を行っております。
「理科学・計測機器事業」電子光学機器・分析機器・計測検査機器 「産業機器事業」半導体関連機器・産業機器 「医用機器事業」医用機器

書籍のご案内

◆定価は本体価格+税です。

カーボンナノチューブ・ グラフェンハンドブック



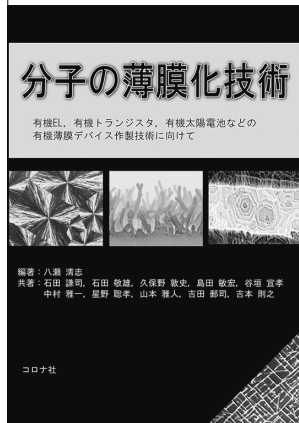
フラーレン・ナノチューブ・
グラフェン学会 編
B5判/368頁
本体10,000円



本ハンドブックでは、カーボンナノチューブの基本的事項を解説しながら、エレクトロニクスへの応用、近赤外発光と吸収によるナノチューブの評価と光通信への応用の可能性を概観。最近囁目のグラフェンやナノリスクについても触れた。

分子の薄膜化技術

—有機EL, 有機トランジスタ, 有機太陽電池などの
有機薄膜デバイス作製技術に向けて—



八瀬清志 編著
石田謙司・石田敬雄・
久保野敦史・島田敏宏・
谷垣宣孝・中村雅一・
星野聡孝・山本雅人・
吉田郵司・吉本則之 共著
A5判/288頁
本体4,200円



金属や無機物と多くの点で本質的に異なる有機分子の薄膜作製法、およびその素過程と成長機構の分子形状依存性について教育や研究に役立つよう記述した。また、有機EL, 有機トランジスタなどのデバイス応用についても記述した。

カーボンナノチューブの材料科学入門

齋藤弥八 編著/A5判/250頁/本体3,400円

物質科学を学ぶ人の 空間群練習帳

北條博彦 著/A5判/178頁/本体2,600円

ドライプロセスによる 表面処理・薄膜形成の基礎

表面技術協会 編/A5判/208頁/本体2,800円

ドライプロセスによる 表面処理・薄膜形成の応用

表面技術協会 編/A5判/318頁/本体4,600円

化学系学生にわかりやすい 平衡論・速度論

酒井健一・酒井秀樹・湯浅真 共著/A5判/2021年3月中旬刊行

ゼロからの最速理解 プラスチック材料化学

佐々木健夫 著/A5判/2021年3月下旬刊行

カーボンナノチューブの基礎

齋藤弥八・坂東俊治 共著/A5判/220頁/本体2,800円

基礎材料科学

伊藤公久・平田秋彦・山本知之 共著/A5判/200頁/本体2,600円

材料の熱力学 入門

正木匡彦 著/A5判/240頁/本体3,200円

ケミカルバイオロジー基礎

濱崎啓太 著/B5判/150頁/本体2,500円

真空科学ハンドブック

日本真空学会 編/B5判/590頁/本体20,000円

航空機設計法

—軽飛行機から超音速旅客機概念設計まで—
李家賢一 著/A5判/298頁/本体4,200円

航空機設計法 実践編

—小型ジェット旅客機からハイブリッド電動航空機概念設計まで—
李家賢一 著/A5判/204頁/本体2,700円



人と自然

のハーモニー。

卓越した技術が築く地球の未来。

CONTRIBUTION TO FUTURE SOCIETY

Life Science

Nano Technology

Electronics

Bio Technology

New Materials

Ecology

Energy Technology

科学機器・計測システムの技術・情報商社



オザワ科学株式会社



<http://www.ozawasc.co.jp>



高感度近赤外線
 2次元 InGaAs ハイスピードカメラ

NIRvana® HS

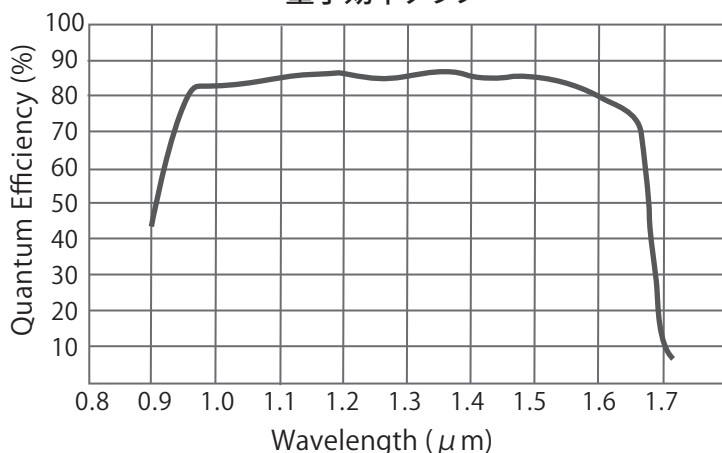
- **ハイスピード**
 250 fps (full 640x512 pixels)
 1200 fps (200x200 pixels)
- **多彩な読み出しモード**
 Integrate While Read (IWR) mode搭載
 マルチROI
- **低読み出しノイズ**
- **USB3.0接続**



アプリケーション例

- ・フォトリソ結晶PLイメージング及びスペクトル
- ・一重項酸素イメージング及びスペクトル
- ・太陽電池PLイメージング及びスペクトル
- ・天体観測微弱光イメージング
- ・食品断面イメージング
- ・In-Vivoイメージング など

量子効率グラフ



仕様

モデル	NIRvana HS	NIRvana:640	NIRvana:640LN
センサー	640 x 512 x InGaAs		
素子サイズ	20 μm x 20 μm		
波長範囲	0.9 ~ 1.7 μm		
冷却温度	-55°C (-50°C空冷)	-80°C	-190°C
ダークチャージ	700 e-/p/sec	300 e-/p/sec	<8 e-/p/sec
読み出しノイズ	<60 e-rms	<120 e-rms	15 e-rms
ダイナミックレンジ	16 Bit (>15Bit@1 素子)		
フレームレート	250 fps	110 fps	2.77 fps@250KHz
インターフェース	USB3.0	Gig E	

